CSMI Cooperative Science and Monitoring Initiative

LAKE MICHIGAN 2020 REPORT

Development of this document was supported by the Great Lakes Restoration Initiative via a cooperative agreement between the U.S. EPA Great Lakes National Program Office and National Oceanic and Atmospheric Administration. This is Illinois-Indiana Sea Grant publication number IISG24-HCE-TRP-001.

Cover page image by the Great Lakes Science Center, Buffalo State, The State University of New York. Cover page design by Joel Davenport. If there are issues with accessibility of this report, please email iisg@purdue.edu.

Recommended citation
Foley, C.J., Milanovich, J.M., TePas, K.M., Collingsworth, P.D. (Eds). 2024. Cooperative Science & Monitoring Initiative (CSMI) Lake Michigan 2020 Report. Prepared for the Great Lakes Water Quality Agreement Annex 2 Lake Michigan Partnership by Illinois-Indiana Sea Grant. 238 p.

Cooperative Science and Monitoring Initiative (CSMI) Lake Michigan 2020 Report

Table of Contents

Key Findings i

- Dreissenid mussel populations ii
- Fish populations and contaminants ii
- Effects of deeper light penetration ii
- Capitalizing on repeated CSMI cycles to understand patterns and inform sampling plans iii

Executive Summary iii

List of Tables xiii

List of Figures xv

USGS activities in support of 2020-2021 Lake Michigan CSMI 1

NOAA activities in support of Lake Michigan CSMI 2020/2021 72

Lake Michigan CSMI Lower Food Web Survey data summary 150

Lake Michigan CSMI phytoplankton and primary production 2021 168

Lake Michigan CSMI Benthic Survey 2021 176

Contaminants, stable isotopes, and fatty acids in the Lake Michigan food web 206

Key Findings

Dreissenid mussel populations

- Between 2010 and 2021, the population density of quagga mussels (*Dreissena r. bugensis*) has somewhat stabilized, although the spatial distribution of mussels is changing as the population continues to slowly expand into deeper areas of the lake.
- Lakewide, quagga mussels were found at 98% of all benthic stations and comprised 75% of benthos density and 99.7% of biomass.
- Dreissenid veliger densities and size distributions indicated two lakewide recruitment events occurred during the summer and fall of 2021, with the highest abundance of veligers detected at mid-depth (45 m) stations.
- Dreissenid veliger concentrations were high compared to other zooplankton taxa.
- Dreissenid mussel relative body mass (an indicator of physiological condition) was highest in shallow areas of the lake (< 30 m) and lowest in mid-depth areas (31–50 m).

Fish populations and contaminants

- Consumption of dreissenid mussel veligers by fish larvae reduces growth and survival.
- Comparisons of larval fish catches between 2015 and 2021 revealed Alewife densities to be 3.7 times lower in 2021 while Bloater densities were 2.2 times higher in 2021. Based on surveys of age-1 fishes in 2022, high larval Bloater catches correspond with a very strong 2021 year class.
- Warm, nearshore waters (depth < 15 m) were important spring habitat for adult Lake Whitefish in Lake Michigan. This finding contrasts with conceptual models, which are based on gill net and trawl survey data and predict that adult Lake Whitefish's use of shallow water reefs and shoal areas is limited to the fall-winter spawning season.
- Southern Green Bay is a key, year-round area of residency for Lake Whitefish.
- Per- and polyfluoroalkyl substances (PFAS) concentrations were higher in Spottail Shiner than Lake Trout even though Spottail Shiner feed at a much lower trophic level. Highly enriched $\delta^{13}C$ values for Spottail Shiner are consistent with a benthic energy source, which suggests that this species has potentially been exposed to a sediment repository of PFAS.
- In fish sampled near Saugatuck, Michigan, mercury concentrations were approximately 10 times higher in Lake Trout (230 ng/g) than in prey fish. These results demonstrate the expected pattern of hydrophobic chemical bioaccumulation increasing with trophic levels in Lake Michigan.

Effects of deeper light penetration

- Dreissenid mussels filter particles from the water column, which leads to deeper light penetration, and effects of this are seen throughout the food web. The extreme water clarity in Lake Michigan has shifted the vertical distribution of planktonic organisms lower in the water column as they avoid high ultraviolet radiation in the surface waters.

- The extreme clarity in Lake Michigan surface waters leads to decreased efficiency of and capacity for photosynthesis for phytoplankton in these waters. This action, termed photoinhibition, is leading to reduced primary productivity at the surface of the lake later in the year (i.e., into June and July).
- Generally, zooplankton densities were higher in the zero percent ultraviolet zone (deeper water layer) compared to the one percent ultraviolet zone (near-surface layer); this was likely observed because sampling was conducted during the day, when zooplankton often migrate to deeper depths in the water column (diel vertical migration).
- Mortality from ultraviolet exposure may be a bottleneck for fish larvae survival and potential recruitment in Lake Michigan.
- Higher pigmentation on Bloater larvae relative to Alewife larvae suggests that Bloater have the capacity to endure ultraviolet exposure.

Capitalizing on repeated CSMI cycles to understand patterns and inform sampling plans

- Seasonal zooplankton patterns were analyzed using data from previous CSMI studies in Lakes Michigan and Huron, which are hydrologically the same lake and have similar lower food web structure. Data were gathered from nearshore (11–27 m), mid-depth (40–51 m) and deep (64–112 m) stations from 2010 through 2017. Total zooplankton biomass was lowest in the nearshore stations, driven primarily by the relatively large catches of calanoid copepods in deeper, offshore waters.
- These data suggest that heterogeneity in primary production and zooplanktivory over space and time affects zooplankton community dynamics. Further, zooplankton population dynamics may not be fully understood without more frequent (i.e., monthly) sampling in nearshore (< 30 m) waters. Monitoring the zooplankton community in offshore waters with spring and summer cruises, as is currently undertaken, seems sufficient to capture interannual variation in zooplankton dynamics in the relatively stable offshore waters of Lake Michigan.

Executive Summary

The role of the Cooperative Science and Monitoring Initiative (CSMI) is to direct enhanced monitoring and research activities across each of the Laurentian Great Lakes to provide relevant information to address the science priorities of each Lake Partnership (established under the Lakewide Management Annex of the 2012 Great Lakes Water Quality Agreement). CSMI is an intensive effort to collect information on the health of one Great Lake each year, cycling through the lakes on a five-year period. The Lake Michigan Partnership (the Lake Partnership) is a collaborative team of natural resource managers led by the U.S. Environmental Protection Agency (EPA) with participation from federal, state, tribal, and local governments or agencies. The Lake Partnership uses the information collected through CSMI sampling of Lake Michigan to better develop long-term management strategies for protecting and restoring the Lake's ecosystem.

The 2020 Lake Michigan CSMI field year was significantly impacted by the COVID-19 pandemic. As many planned sampling activities were pushed to late 2020 or to 2021, we refer to this collective effort as the CSMI 2020/21 field year on Lake Michigan. Some of the samples analyzed in the reports provided by project investigators were collected in one year only (typically 2021). If patterns being discussed were only observed in one of the years, this is typically indicated in the text and, for clarity, the effort may not be referred to as 2020/21.

The CSMI 2020/21 field year on Lake Michigan targeted four broad science priorities identified by the Lake Partnership: 1) addressing nutrient-food web dynamics in a changing ecosystem, 2) addressing contaminants/bacteria, 3) addressing watershed/tributaries connections to lake water quality and 4) aiding in connecting with stakeholders. Specific field efforts were undertaken to collectively address the first, second, and third science priorities through a variety of focused projects, including: lake-wide sampling of the broad food web, focusing on lower trophic levels and smaller-bodied fishes; intensive sampling of all aspects of limnology and ecology along a transect off Muskegon, Michigan; Lake Whitefish (*Coregonus clupeaformis)* sampling in Green Bay and northern Lake Michigan; beach seining for fishes in new locations; and a highly spatially comprehensive larval fish survey. These research efforts were completed with contributions from a large number of groups, including the US Environmental Protection Agency Great Lakes National Program Office and Great Lakes Toxicology and Ecology Division Laboratory, the National Oceanographic and Atmospheric Administration Great Lakes Environmental Research Laboratory, the US Geological Survey Great Lakes Science Center, Buffalo State

University, Clarkson University, the University of Minnesota, Purdue University, and Wayne State University.

In recent decades, particularly since the introduction of invasive dreissenid mussels, the connections among nutrients, the lower food web, and fish populations have been identified as a key gap in understanding the Lake Michigan ecosystem. In direct response, these connections were studied in CSMI 2020/21 field year. Starting at the base of the food web, water chemistry and chlorophyll concentration data were collected through several CSMI field efforts in 2020 and 2021 to investigate spatial and temporal patterns along nearshore to offshore gradients. Total phosphorus concentrations were higher north of Manitowoc, Wisconsin, possibly influenced by the upwelling of colder, phosphorus-rich waters. The highest chlorophyll concentrations were measured at depths between 20 and 50 meters, consistent with the location of the deep chlorophyll layer. Chlorophyll concentrations were considerably lower closer to shore at stations less than 80 m deep. This likely indicates that mussel filtration is reducing phytoplankton biomass in nearshore areas with likely impacts on lower food web production in these habitats. There were no distinct nearshore-offshore gradients in cations and anions that are sometimes used as tracers of urban influence (e.g., Cl^-, Na^+). This indicates that the transect-based sampling design had poor resolution for urban influence; however, several water quality parameters, including NOx, TN, Chl a, and Si, exhibited a slightly positive correlation with depth in the water column.

Throughout the course of the 2021 growing season, Lake Michigan's algal load was diverse and composed of several species with no single algal division having an overwhelming dominance. Phytoplankton abundance was higher in summer when compared to spring, a phenomenon that is typical of all the Laurentian Great Lakes except Lake Erie. Nearshore and offshore waters differed negligibly in phytoplankton abundance and composition, an observation that differs from the distinct nearshore-offshore differences observed in the other lakes. In terms of cell density, small-celled cyanophytes strongly dominated community abundance but they comprised a very small portion of the total phytoplankton biovolume. Spring phytoplankton biovolume was dominated by flagellated chrysophytes and cryptophytes, with some contribution from centric diatoms. In contrast, summer phytoplankton were characterized by a more even and diverse community consisting of dinoflagellates, cyanophytes, chrysophytes, haptophytes, cryptophytes and centric diatoms. In 2021, along the Muskegon transect, peak occurrence in phytoplankton biomass was dominated by diatoms and dinoflagellates that generally grow in the spring or in the vicinity of the deep chlorophyll layer during the summer. The occurrence of these taxa in samples during early July and August 2021 corresponds with lower temperature and increased chlorophyll fluorescence values recorded in early July and August at the 20-m buoy.

Photoinhibition of phytoplankton productivity, a phenomenon in which a high light environment decreases efficiency of and capacity for photosynthesis, has previously been observed in the winter-spring period in Lake Michigan; however, in this CSMI 2020/21 field year, photoinhibition was measured later in the year (i.e., June-July) than previously documented. This may be attributed to the effects of deeper light penetration, as the sustained activity of dreissenid mussels filtering the water column continues to influence the physical properties of the ecosystem. Complementary long-term monitoring data for offshore pelagic waters from 2001 through 2021 indicate that spring phytoplankton abundance has stabilized at a relatively low level in recent years, after dropping rapidly following the quagga mussel invasion in the early 2000s. Though a statistically significant increase in phytoplankton abundance has been detected in summer, this change is subtle and subject to annual variability. While overall estimates of maximum rates of photosynthesis are comparable with previous results reported from Lake Michigan and other locations in the Great Lakes, future studies should focus on measuring water column production to evaluate if production levels have remained stable over time.

Several groups sampled lake wide zooplankton communities during the CSMI 2020/21 field year. Overall, zooplankton biomass was higher off Muskegon, Michigan in 2021 than in previous CSMI years (2010, 2015) and total zooplankton volumetric biomass was higher in offshore habitats than nearshore, with omnivorous copepods and herbivorous cladocerans comprising a significant fraction of the total zooplankton biomass in July and September. Lake wide, *Limnocalanus* copepod concentrations were low, and *Limnocalanus* were primarily captured at offshore stations. Rotifers had the highest density of all taxonomic groups. To take advantage of existing data sets, a synthesis of seasonal zooplankton sampling from previous CSMI studies that sampled nearshore (11–27 m), mid-depth (40–51 m) and deep (64–112 m) stations in Lakes Michigan and Huron between 2010 and 2017 was completed. The results indicate that total zooplankton biomass was lowest in the nearshore stations, driven primarily by several taxa of calanoid copepods. Because the nearshore typically has higher primary production, this result could arise from higher zooplanktivory in nearshore waters. Seasonally, zooplankton biomass in the nearshore declined in late-summer before increasing again in the fall, whereas the seasonal pattern at the middle and deep sites revealed no steep mid-summer decline. Future CSMI studies should consider building on these findings and emphasize more frequent sampling of zooplankton in nearshore waters.

The Lake Michigan benthic community was monitored through the CSMI 2020/21 effort and related annual agency monitoring activities. The bulk of the benthic community data analyzed in the current report was collected from surveys conducted in 2021. Lakewide, 106 species and higher taxa of benthic macroinvertebrates were found in the lake in 2021. The most diverse and most widely distributed taxa throughout the lake were oligochaetes, representing 20% of the total benthic density but only 0.2% of benthic biomass. The historically important amphipod *Diporeia* continued to decline even in the deepest parts of the lake. *Diporeia* were found at only 10 stations (9% of total stations sampled), and at very low densities. A similar lake wide decline was found in sphaeriid densities. In contrast, oligochaete abundance has progressively increased in shallow and intermediate depths over the last decade. The non-native New Zealand mud snail (*Potamopyrgus antipodarum*) first recorded in Lake Michigan in 2006, has increased in both abundance and distribution since 2015. In 2021, this species' density increased 25-fold compared to 2015, comprising 93% of the total gastropod density and 79% of the total gastropod biomass.

Lake wide, the quagga mussel population increased 30% between 2015 and 2021. This pattern was largely due to a threefold increase in density in the shallowest depth zone caused by recently settled, small mussels. A significant increase in both quagga mussel density and biomass was found only in the deepest zone (> 90 m). Over the last 10 years, the population density of quagga mussels has somewhat stabilized, although the spatial distribution is changing as mussel populations continue expanding to deeper parts of the lake. Additional monitoring of dreissenid mussels revealed depth-specific and region-specific differences in mussel body condition, where shallow depth (< 30 m) quagga mussels had the highest relative body mass and mid-depth mussels (31–50 m) had the lowest. Regional differences in quagga mussel body condition varied by depth zone, and, in all depth zones, body condition was higher in 2021 than in 2015. Mean dreissenid mussel density for a subset of southern stations was highest in the 31–50m depth zone, but not significantly so. Dreissenid density obtained using the benthic imaging system (videography) was only slightly lower than occurrence obtained using the Ponar grab (94% vs. 98%). The difference between average dreissenid densities estimated using videography and Ponar for mussels greater than 5 mm in length was within 10% and supports the use of underwater videography as a tool for rapid dreissenid population assessment. Dreissenid veliger densities and average length indicated two recruitment events that occurred in summer and fall. The density peaks in 2021 were synchronized across all three depths sampled with the mid-depth site (45 m) exhibiting the highest veliger abundance, but overall veliger densities were lower in 2021 than in earlier years.

In 2021, fish diet analysis indicated larval Alewife (*Alosa pseudoharengus)* and Bloater (*Coregonus hoyi)* mainly consumed copepods and ate few dreissenid veligers. For both species, larval growth was higher than in prior CSMI years (2010 and 2015); however, larval fish densities were relatively low compared to 2015. The zooplankton community in the beach nursery habitat of larval Lake Whitefish in northern Lake Michigan was dominated by copepod nauplii and adult calanoid copepods, while larvae selected for not only the abundant calanoid copepods but also the rarer cyclopoid copepods. Overall, less than 5% of Lake Whitefish larvae had empty stomachs. Future research will be required to determine whether declining lake productivity has led to reduced growth or survival of larval Lake Whitefish. However, laboratory studies indicate consumption of dreissenid mussel veligers by fish larvae will reduce larval growth and survival.

From a spatial perspective, CSMI researchers undertook the largest effort ever to sample the larval fish community in July of 2021. Larval Alewife and Bloater dominated the catches. Comparisons between 2015 and 2021 revealed Alewife densities to be 3.7 times lower in 2021, while Bloater densities were 2.2 times higher in 2021. By the time this report was finalized, agency staff had already begun analyzing their 2022 survey data. Based on surveys of age-1 fishes in 2022, the high larval Bloater catches correspond with a very strong 2021 year class for this native planktivore. Given the increasing depth to which visible light can be transmitted since 2004 when invasive dreissenid mussels began proliferating, current research is evaluating whether the depth of ultraviolet (UV) radiation has also concomitantly increased and what effects UV exposure has on larval fish. Alewife larvae generally avoided the surface waters during the daytime, perhaps to avoid UV exposure. Bloater larvae, however, were found at their greatest densities in the surface waters. Higher pigmentation on Bloater larvae relative to Alewife larvae suggests that Bloater have the capacity to endure UV exposure. Increased exposure to UV in Lake Michigan may contribute to a bottleneck for fish larvae survival, potentially limiting their recruitment to the adult fish population. In 2021, as in previous years, transect-based field surveys indicated that zooplankton and Alewife larvae avoided surface waters during day when UV effects were strongest, but migrated up to near surface at night. Bloater larvae, which are better able to tolerate UV exposure, were present at the surface and at mid-depths during the day.

A spatially extensive and temporally intensive data set on demersal temperature and dissolved oxygen from throughout Green Bay was conducted as part of the CSMI 2020/21 field year. These environmental data have manifold applications and are informing interpretation of seasonal movements and habitat use of Lake Whitefish that were tagged in conjunction with data logger deployments. Results from acoustic telemetry studies emphasized that southern Green Bay is a key area of residency for Lake Whitefish. Additionally, seasonal changes in vertical habitat use of this species highlight the need for a better understanding of pelagic trophic connections. Intensive Lake Whitefish sampling also occurred in northern Lake Michigan. Results from this location suggest that deep water likely constrains dispersal of adult Lake Whitefish in northern Lake Michigan, and that habitat(s) immediately adjacent to spawning reefs are “hotspots” for Lake Whitefish activity and production. In this area, acoustic-tagged Lake Whitefish were largely restricted to habitats with lake bottom depth less than 100 m, which suggests that deep water constrains adult dispersal. Because depth-habitat use is a phenotypic trait that is subject to selection in coregonines, between-population differences in depth-habitat use by acoustic-tagged Lake Whitefish in this study suggest the potential for local adaptation.

During the CSMI 2020/21 field year, beach sampling for larval and juvenile Lake Whitefish was extended into regions of relatively high productivity and farther south than any prior sampling to date. Relative to historical median catches at more central Lake Michigan sites, catches at South Haven, Michigan were higher whereas those at St. Joseph, Michigan were lower, indicating South Haven is a potentially important site for nursery habitat of Lake Whitefish. Future research could prioritize determining whether sampling larval Lake Whitefish with a neuston net and/or bag seine along beaches is predictive of recruitment to the fishery.

As part of this 2020/2021 CSMI field year effort, an intensive contaminant monitoring of the food web and trophodynamic markers was also performed. Due to the COVID-19 pandemic, a limited number of fish species were collected from the Saugatuck Great Lakes Fish Monitoring and Surveillance Program site. No water, sediments, or invertebrates were obtained for the CSMI 2020/21 field year. The forage and top predator fish were analyzed for stable isotopes of nitrogen, carbon, fatty acids, PFAS, and Hg. The fatty acid profiles showed that Rainbow Smelt (*Osmerus mordax)*, Alewife, and Lake Trout (*Salvelinus namaycush)* have elevated concentrations of the pelagic fatty acid marker (oleic acid) relative to cis-7-hexadecenoic acid, a benthic feeder fatty acid marker consistent with their pelagic feeding strategies. Spottail Shiner (*Notropis hudsonius)* had the highest PFAS concentrations followed by Lake Trout even though Spottail Shiner had significantly lower δ^{15}N values, indicating that it occupies a lower trophic position. The carbon source for Spottail Shiner was also significantly different than that of lake trout. The higher δ^{13}C values for Spottail Shiner are consistent with a benthic energy source. It is likely that the benthic feeding behavior of Spottail Shiner exposes this species to a potential sediment repository of PFAS. The observed Hg bioaccumulation provides an example of traditional hydrophobic chemical bioaccumulation increasing with trophic level. Future analysis will include development of predator-prey relationships to assess the bioaccumulation of PFAS in the lake.

In addition to knowledge gained via direct sampling, the CSMI field year often serves as an opportunity to expand on traditional long-term monitoring programs by testing new techniques and technologies. For example, previous CSMI studies have demonstrated that paleolimnological records from deepwater cores further enhance the phytoplankton and primary productivity record for Lake Michigan, and have assessed the effectiveness of different sampling methods for water quality or benthos. In 2020/21, monitoring efforts continued to support CSMI research in novel ways, including using models to predict larval fish locations, comparing laboratory and field methods for measuring ultraviolet light attenuation, and using cutting-edge laboratory spectrophotometry techniques to quantify the contribution of seston to visible and UV attenuation. Further, CSMI 2020/21 efforts were able to coordinate with multiple externally-supported academic efforts to study additional aspects of the identified science priorities. Scientists participating in CSMI 2020/21 field year sampling efforts were able to collect additional samples for academic partners to assess complementary questions as well as coordinate the timing and locations across various studies to address larger-scale questions. Through these contributions, the overall CSMI effort is providing a strong framework for continuing to improve understanding of the Lake Michigan ecosystem and inform resource management.

List of Tables

Coefficients in the equation ln(Weight) = a + b × ln(Length) relating zooplankton dry weight (µg) to body length (mm) 60

The first calendar date when surface water temperature reached 4 °C in each survey station......61

Summaries for patterns of zooplankton biomass and biomass seasonality from nearshore to offshore stations across transects in Lakes Michigan and Huron revealed in our generalized mixed models (GAMMs) 66

Table of stations sampled in Lake Michigan in 2021 to quantify dreissenid mussel density using Ponar grabs and assess quagga mussel body condition 79

GLERL sampling activities during the 2021 Lake Michigan CSMI field season 87

Photosynthetic parameters from all experiments......97

Parameters derived from photosynthesis versus irradiance experiments using ^{14}C uptake 105

Spearman rank correlation coefficients assessing covariation between chlorophyll concentrations in algal size categories and photosynthetic parameters derived for specific wavelengths of light (using PAM fluorometry) or water column kpar 105

Results of linear model testing whether slopes of Alewife length vs age relationships were significantly different among CSMI years (2010, 2015, 2021) 113

Average individual growth rate of Alewife larvae sampled off Muskegon in Lake Michigan CSMI years ...113

Results of linear model testing whether slopes of Bloater length vs age relationships were significantly different among CSMI years (2010, 2015, 2021) 114

Average individual growth rate of Bloater larvae sampled off Muskegon in Lake Michigan CSMI years....114

Archived Nowcast/Forecast biophysical models developed and run for CSMI 2020-21 Lake Michigan 139

Average (± standard error) density (ind. m^{-2}) and wet biomass (g m^{-2}) of major taxonomic groups of benthic invertebrates collected from 95 benthic stations in Lake Michigan in 2021 and averaged by depth zones, and lake-wide average (not stratified by depth) 186

Dynamics of mean (+ standard error) densities of major benthic macroinvertebrate taxa in Lake Michigan from 1930 to 2021 by depth zones 189

Long-term dynamics of Dreissena polymorpha and D. rostriformis bugensis density (m^{-2}) in Lake Michigan (excluding Green Bay)....................191

Dreissena population density (mussels per m^{-2}, average ± standard error) in four depth zones and lake-wide averages (weighted by depth zone) estimated using Ponar grab in 2010 and 2015, and BIS in 2021 198

Dreissena r. bugensis density (mussels per m^{-2}, average ± standard error) and sample size (in parenthesis) in four depth zones and lake-wide averages estimated using Ponar grab and BIS in Lake Michigan in 2021 199

The 99 CSMI stations sampled on Lake Michigan in July 2021 and 15 long-term monitoring stations with information on lake basins, location (decimal coordinates), water depth, taxa reported, and main substrates 202

Fish collected in September of 2020 by the GLFMSP at the Lake Michigan Saugatuck sampling site.........213

List of Figures

Great Lake Acoustic Telemetry Observation System (GLATOS) acoustic receiver (larger black cylinder) station equipped with a data logger (smaller white cylinders) prior to deployment (left picture), and a station being recovered with an ROV (Remotely Operated Vehicle) due to extreme fouling from dreissenid mussels (right picture) 8

Monthly mean demersal temperatures recorded by data loggers deployed on the Great Lakes Acoustic Telemetry Observation System (GLATOS) acoustic receiver network in Green Bay. Each panel is labeled by the first day of the month which it depicts 10

Monthly mean bottom dissolved oxygen recorded by data loggers deployed on the Great Lakes Acoustic Telemetry Observation System (GLATOS) acoustic receiver network in Green Bay 12

Monthly detections of acoustic-tagged Lake Whitefish (Coregonus clupeaformis) in Green Bay (June 2021 to July 2022) 14

Daily mean depths of Lake Whitefish (Coregonus clupeaformis) in Green Bay summarized by tag and receiver (circles) 16

Northern Lake Michigan study area and acoustic receiver arrays 23

Distribution of acoustic-tagged Grand Traverse Bay Lake Whitefish (Coregonus clupeaformis) in Lake Michigan during April, May, and June 2022. 26

Distribution of acoustic-tagged Good Harbor Bay Lake Whitefish (Coregonus clupeaformis) in Lake Michigan during April May, and June 2022 27

Seasonal thermal-habitat use by acoustic-tagged Lake Whitefish (Coregonus clupeaformis) from two Lake Michigan spawning populations, 2021-2022 28

Location of beach sampling sites in Lake Michigan that were sampled for Lake Whitefish and zooplankton between 2014 and 2021 34

Number of Lake Whitefish caught per net haul on the beaches of South Haven and St. Joseph MI 39

Sampling sites completed during the July 4-26, 2021 cruise targeting larval Alewife 44

Mean density of larval Alewife (Alosa pseudoharengus) estimated for each of 15 transects sampled once between July 4-26, 2021 in Lake Michigan 49

Mean density of larval Bloater (Coregonus hoyi) estimated for each of 15 transects sampled once between July 4-26, 2021 in Lake Michigan 50

Box-whisker plot of the median (center line), 25th and 75th percentile (as edges of the box), and 5th and 95th percentiles as error bars for the natural-log (LN) transformed density of larval a) Alewife (Alosa pseudoharengus), to b) Bloater (Coregonus hoyi), c) Burbot (Lota lota), d) Yellow Perch (Perca flavescens) for each daytime vertical habitat layer (ultraviolet = UV) sampled during July 2-26, 2021 in Lake Michigan…. 52

Size frequency distribution of Bloater (Coregonus hoyi) larvae caught in three different vertical layers of the water column during July 2-26, 2021 in Lake Michigan 53

Mean density of larval a) Alewife (Alosa pseudoharengus), b) Bloater (Corengonus hoyi), c) Burbot (Lota lota), d) Yellow Perch (Perca flavescens) estimated for each of the seven distance from shore sites across the transects sampled once between July 4-26, 2021 in Lake Michigan 54

Zooplankton sampling stations and transects in Lake Michigan in 2010 and 2015 and in Lake Huron in 2012 and 2017 60

Predicted mean biomass and biomass seasonality for (all) zooplankton and major zooplankton groups across sampling transects in Lakes Michigan and Huron 65

Five seasonality patterns revealed in out taxon-level generalized additive mixed models 66

Mean quagga mussel density (individuals/m^2 ± SD) for a quantitative Ponar survey conducted at a subset of 17 stations in southern Lake Michigan 80

Lake Michigan 2021 quagga mussel body condition by depth zone 80

Lake Michigan 2021 quagga mussel ln tissue ash-free dry weight (AFDW) as a function of ln shell length collected from three regions (North, Central, and South) and four depth zones, (<30 m, 31-50 m, 51-90 m, and >90 m) 81

Quagga mussel ash-free dry weight (mg AFDW), expressed as least square means (± SE) from a two- way ANCOVA with depth zone and year as the factors and shell length as the covariate 81

Mean dreissenid veliger density (top) and mean veliger length (bottom) at three sites in Lake Michigan near Muskegon, MI during 2021 82

Mean annual densities of dreissenid veligers sampled at the nearshore site (M15) in a 153-µm mesh net from 2007-2021 82

Sampling sites along the Muskegon transect in Lake Michigan 88

Near surface (2- 5 m) mean (±SD) TP concentrations at M15, M45, and M110 from May to September in 2021 89

TSS concentrations measured at 2m at M15, M45, and M110 in May, July and September 2021. 89
VSS concentrations measured at 2-m depth at M15, M45, and M110 in May, July and September 2021 .. 90

Secchi disk measurements at nearshore (M15), mid-depth (M45), and offshore (M110) sites off Muskegon in May, July and September 2021 90

Attenuation coefficients (A), and 1% attenuation depths (B) at three sites in Lake Michigan in 2021 for wavelengths of UV-B (320 nm), UV-A (380 nm), and PAR (400-700 nm) 91

Near surface (2-5 m) chlorophyll concentrations at the nearshore (M15), mid-depth (M45), and offshore station (M110) from May to September 2021 91

Concentration of chlorophyll-a greater or equal to each size fraction for five cruises along the Muskegon transect 92

Chlorophyll, temperature, and CDOM profiles from PSS and CTD profiles, paired with UV profiles for May (A), July (B), and September (C) 2021 at the M110 site in Lake Michigan 93

PI curves from all experiments for (TOP) the mid-depth site (M45); and (Bottom) the offshore site (M110). Points represent experimental values 98

Extinction coefficients from the laboratory method (blue line) and the UV radiometer profiles (squares)…. 99

Napierian absorbance (log scale) in the ultraviolet measured using the laboratory method 99
Predicted change in the 1% intensity depth of UV-A (380 nm), UV-B (310 nm), and PAR (400- 700 nm) due to change in abundance of seston as chlorophyll concentration 100

Size-specific chlorophyll measured in surface water for samples collected along the Muskegon transect in southern Lake Michigan (2021) 106

Relationship between phytoplankton carbon (from cell counts) and chlorophyll concentrations measured from samples collected along the Muskegon transect in southern Lake Michigan (2021) 106

Taxonomic composition of phytoplankton (as cellular carbon) in the surface waters along the Muskegon transect in southern Lake Michigan (2021) 107

Size-specific primary production estimates (measured as carbon uptake) for samples collected seasonally along the Muskegon transect in southern Lake Michigan (2021) 107

Wavelength-specific parameters derived from photosynthesis versus irradiance experiments using pulse amplitude modulated (PAM) fluorometry; samples were collected seasonally along the Muskegon transect in southern Lake Michigan (2021).......108

Estimated zooplankton biomass by month in 2021 sampled during the day at station M15 using the 64μm mesh net.......115

Estimated zooplankton biomass (dry wt.) by month in 2021 sampled at the offshore site (M110) during the day using the 64μm mesh net.......115

Estimated zooplankton biomass (dry wt.) by month at station M15 sampled using the 64 μm mesh net..116

Daytime vertical distribution of taxon-specific zooplankton biomass (dry wt.) at the offshore site (M110) sampled using the 64 μm mesh net in July 2021 116

Mean density (+ 1 s.e.) of Alewife, Bloater and Yellow Perch larvae by month in 2021 117

Alewife (Alosa pseudoharengus) larvae mean density (+1 s.e.) by month in CSMI years 2010, 2015 and 2021.......117

(A) July mean densities (± 1 s.e.) and vertical distributions of Alewife (Alosa pseudoharengus) larvae during the day at the 15m nearshore site (M15) of each CSMI year: 2010, 2015 and 2021; (B) Diel mean densities (± 1 s.e.) and vertical distributions of Alewife larvae at the 15 m nearshore site in July 2010 and 2015....118

Bloater (Coregonus hoyi) larvae mean density (+ 1 s.e.) by month for CSMI years 2010, 2015 and 2021..119

(A) July mean densities (± 1 s.e.) of Bloater (Coregonus hoyi) larvae by depth strata at offshore site M110 during the day for each CSMI year (2010, 2015, 2021). (B) Diel mean densities (± 1 s.e.) and vertical distributions of Bloater (Coregonus hoyi) larvae by depth strata at offshore site M110 in August of 2015 and 2021 120

Median lengths of (a) larval Alewife and (b) larval Bloater sampled off Muskegon in Lake Michigan CSMI years 2010, 2015 and 2021.......121

Alewife (Alosa pseudoharengus) larvae length at age (mm/day) in CSMI years 2010, 2015, and 2021......122

Bloater (Coregonus hoyi) larvae length at age in CSMI years 2010, 2015 and 2021.......122

Distributions of (TOP) Alewife and (BOTTOM) Bloater larvae hatch dates and capture dates off Muskegon in 2021 123

Percent biomass (dry weight) composition of Alewife (Alosa pseudoharengus) larvae diet items grouped by fish length during month of collection date 124

Percent biomass (dry weight) composition of Bloater (Coregonus hoyi) larvae diet items grouped by fish length during month of fish collection 124

(A) Mysis mean density (+1 s.e.) in vertical thermal strata offshore (site M110) at night in August 2021. (B) Mysis density (+1 s.e.) averaged over all thermal strata at nearshore, mid-depth and offshore sites at night in May and August, 2021. 125

Yellow perch survival by treatment for the duration of the 21-day experiment......................................127

Yellow perch growth rates (mm/d) fed different treatments of veligers and alternate prey after 21 days 127

Individual fish from treatment A (100% veligers) and the control treatment (0% veligers).......................128

Location of the thermistor mooring in southern Lake Michigan 129

Updated plot from Anderson, et al 2021 to include data through 2022..130

The Slocum buoyancy glider 133

Tracks of glider deployments in August (left) and September (right) 133

Surface chlorophyll (green) and temperature (blue) for the period from May 3 through November 10, 2021 134

Components of the Experimental Biophysical Nowcast/Forecast for Lake Michigan CSMI 2020…..........139

Graphics from the Experimental Biophysical Nowcast/Forecast for Lake Michigan CSMI 2020, paired with satellite-derived chlorophyll-a on the same dates...140

Graphics from the Experimental Biophysical Nowcast/Forecast for Lake Michigan CSMI 2020, paired with satellite-derived dissolved organic carbon (DOC) on the same date...140

Biophysical model graphics and paired satellite imagery showing elevated surface chlorophyll concentrations along the southeast Lake Michigan shore, associated with a period of elevated river discharge from approximately June 28 through July 9...141

Surface and cross-sectional view of the Muskegon transect region, showing modeled temperature and currents..142

Time series of wind speed, fluorescence chlorophyll, surface and bottom temperature from the Muskegon 20-m buoy, with modeled chlorophyll and temperature, and sampled chlorophyll 143

Graphics from the Experimental Larval Fish Dispersion Forecast for Lake Michigan CSMI 2020 on dates of larval fish sampling offshore of Muskegon, showing the expected spatial distribution of 15-16 day old larval fish hatched in nearshore areas (< 10 m) where spawning is assumed to occur 144

Comparison of simulated normalized density of larval fish from the Experimental Larval Fish Dispersion

Forecast for Lake Michigan CSMI 2021 to observed larval alewife density from sampling offshore of Muskegon at the 15, 45, and 110 m-depth stations 144

Backward trajectory simulations of aged larval fish collected offshore of Muskegon (yellow asterisk), showing the likely region of origin (blue dots), and a randomly selected example from the ensemble of 1000 simulated trajectories (red line) 145

Lake Michigan CSMI 2021 sampling locations 152

Spatial variability of analyte concentrations measured from epilimnion water samples: a) Soluble Reactive Phosphorus (SRP, µg L^{-1}), b) Total Phosphorus (TP, µg L^{-1}), c) Nitrate (NOx, µg L^{-1}), d) Total Nitrogen (TN, µg L^{-1}), e) Chlorophyll a (µg L^{-1}), f) Silica (Si, mg L^{-1}) 156

Metalimnion analyte concentration by depth at which the water was sampled (Collection Depth) 157

Fluorescence concentration by station depth (m) (top) and depth at which the deep chlorophyll maximum layer was observed by station depth (bottom) from the CTD at the stations sampled by USEPA ORD and USGS 158

Densities of a) Bosmina spp. (cladoceran) and b) Limnocalanus copepods in 1% UV exposure (left) and No UV exposure (right) 160

Densities of a) Dreissenid veligers and b) copepod nauplii in 1 % UV exposure (left) and No UV exposure (right) 161

Densities in 1% UV exposure and No UV exposure of zooplankton taxonomic groups a) adult cyclopoid copepods, b) adult calanoid copepods, c) adult cladocerans, d) rotifers 162

Location of the Rowley Bay transect (left) and location of transect stations (right) 163

Chlorophyll concentration at depth range 0-20m (top), 20-50m (middle), and greater than 50m, by station distance to shore 164

Chlorophyll concentration observed by the EPA glider during the Lake Michigan deployment July 2021 165

Map of Lake Michigan showing the standard set of pelagic (offshore) sampling locations (red squares, sampled twice a year) and nearshore CSMI stations (green circles, sampled twice a year during CSMI years) 172

Basin-wide sample averages of phytoplankton abundance in Lake Michigan in 2021 173

Basin-wide averages of offshore phytoplankton abundance in integrated (INT) isothermal layer samples from Lake Michigan 174

Temporal variation in geochemical proxies within sediment cores from Lake Erie 175
Non-parametric multidimentional (NMDS) ordination plots of Lake Michigan benthic community structure in 2021 (Stress = 0.16) 185

Non-parametric multidimentional (NMDS) ordination plots of Lake Michigan benthic community structure in 2021 (Stress = 0.16) 185

Shade plot grouping of benthic species and Lake Michigan stations where they were collected in 2021 .. 186

Spatial distribution of Diporeia sp. in Lake Michigan from 1994 to 2021, expressed as density (ind.m^{-2}) . 188

Spatial distribution of Dreissena rostriformis bugensis in Lake Michigan from 1994 to 2021, expressed as density (ind.m^{-2}) 191

Population dynamics of quagga mussels (densities, m^{-2} and biomass, re-calculated as g of ash free dry tissue weight per m^{-2}) at different depth zones in the main basin of Lake Michigan (excluding Green Bay, Thunder Bay, and Muskegon Bay) 192

Relationship between Dreissena estimation using the BIS and Ponar (without mussels <5 mm) in Lake Michigan in 2021 199

Locations of GLFMSP sampling sites in each Great Lake (U.S. EPA 2021a, 2021b) 212
Stable isotope summary of nitrogen and carbon in the Lake Michigan food web measured as part of the 2020 CSMI sampling effort 214

Summary of marker fatty acid concentrations in Lake Michigan sample types collected as part of the 2020 CSMI sampling effort. Error bars represent standard deviation among replicates 215

Summary of total PFAS concentrations in Lake Michigan sample types collected as part of the 2020 CSMI sampling effort. Error bars represent standard deviation among replicates 216

Summary of mercury concentrations in Lake Michigan sample types collected as part of the 2020 CSMI sampling effort 217

Report: USGS Activities in Support of 2020–2021 Lake Michigan CSMI

Lake and Year: Lake Michigan, 2020–2021

Lead Organization: U.S. Geological Survey Great Lakes Science Center

Lead authors of each subproject:
David B. Bunnell (dbunnell@usgs.gov), U.S. Geological Survey Great Lakes Science Center, Ann Arbor, MI
Richard Kraus (rkraus@usgs.gov), U.S. Geological Survey Great Lakes Science Center, Lake Erie Biological Station, Huron, OH
Darryl Hondorp (dhondorp@usgs.gov), U.S. Geological Survey Great Lakes Science Center, Ann Arbor, MI
Yu-Chun Kao (yuchun_kao@fws.gov), U.S. Geological Survey Great Lakes Science Center, Ann Arbor, MI (current address: U.S. Fish and Wildlife Service, La Crosse Fish and Wildlife Conservation Office, Onalaska, WI)

Project Overview

In support of the following three Lake Michigan science priorities from the Cooperative Science and Monitoring Initiative (CSMI) in 2020-2021 (see https://greatlakescsmi.org/publications/2021-csmi-lake-michigan-prospectus/), USGS conducted five subprojects:

1) Advance the understanding of nutrient dynamics (i.e., loading, transport, and cycling, spatial and temporal variability, and gradients) that directly influence lower trophic level productivity and offshore fish production (subproject E),

2) Identify and quantify the role of biological 'hot spots' (e.g., Green Bay, major tributaries/nearshore areas, reefs, and upwelling events) and substrate heterogeneity in supporting Lake Michigan productivity. Seek opportunities to leverage existing work in these areas, including the large array of acoustic receivers in Green Bay (subprojects A, B);

4) Investigate evidence for recruitment bottlenecks for key fish species such as Lake Whitefish (*Coregonus clupeaformis*) and Alewife (*Alosa pseudoharengus*). Seek opportunities to leverage the

ongoing multi-year nearshore larval Lake Whitefish sampling efforts by Lake Michigan Technical Committee agencies and tribes (subprojects C, D).

(CSMI Priorities #3, 5-14 were not addressed within these subprojects)

Subproject C benefited from a collaboration with Little Traverse Bay Band of Odawa Indians (LTTBOI- contact Kevin Donner- kdonner@ltbbodawa-nsn.gov) and Purdue University (contact Marissa Cubbage- mcubbage@idem.in.gov), neither of which received direct CSMI funding.

Study Highlights (for all subprojects)

- A spatially extensive and temporally intensive data set on demersal temperature and dissolved oxygen from throughout Green Bay was described. These environmental data have manifold applications and are informing interpretation of seasonal movements and habitat use of Lake Whitefish that were tagged in conjunction with data logger deployments. To date, results emphasized the dynamic characteristics of southern Green Bay as a key area of residency for Lake Whitefish. Additionally, seasonal changes in vertical habitat use of this species highlight the need to for a better understanding of pelagic trophic connections.
- Acoustic-tagged Lake Whitefish in northern Lake Michigan were largely restricted to habitats with lake bottom depth < 100 m, which suggests that deep water constrains adult dispersal. Limited extent of post-spawn dispersal by acoustic-tagged Lake Whitefish suggests that habitat(s) immediately adjacent to spawning reefs are “hotspots” for Lake Whitefish activity and production in Lake Michigan.
- Warm, nearshore waters (depth < 15 m) were important spring habitat for adult Lake Whitefish in Lake Michigan, in contrast to conceptual models based on gill net and trawl survey data that predict use of shallow water reefs and shoal areas is limited to the fall-winter spawning season.

- Because depth-habitat use is a phenotypic trait subject to selection in coregonines (Turgeon and Bernatchez 2003), between-population differences in depth-habitat use by acoustic-tagged Lake Whitefish in this study suggests the potential for local adaptation.
- The zooplankton community in the beach nursery habitat of larval Lake Whitefish in northern Lake Michigan was dominated by copepod nauplii and adult calanoid copepods, while larvae selected for not only the abundant calanoid copepods but also the rarer cyclopoid copepods. Less than 5% of Lake Whitefish larvae had empty stomachs. Future research will be required to determine whether declining lake productivity has led to reduced growth or survival of larval Lake Whitefish.
- Sampling along beaches for larval and juvenile Lake Whitefish was extended into regions of relatively high productivity for Lake Michigan and farther south than any prior sampling to date. Relative to the historical median catches observed at more central Lake Michigan sites by NOAA (National Oceanic and Atmospheric Administration), catches at South Haven, MI were higher whereas those at St. Joseph, MI were lower, indicating South Haven is a potentially important site for nursery habitat. Future research could prioritize determining whether sampling larval Lake Whitefish with a neuston net or bag seine along the beaches is predictive of recruitment to the fishery.
- From a spatial perspective, we undertook the largest effort ever to sample the larval fish community in July 2021. Larval Alewife and Bloater (*Coregonus hoyi*) dominated the catches. Comparisons between 2015 and 2021 revealed Alewife densities to be 3.7 times lower in 2021 while Bloater densities were 2.2 times higher in 2021. Based on surveys of age-1 fishes in 2022, the high larval Bloater catches correspond with a very strong 2021 year-class.
- Given the increasing depth to which visible light has transmitted since 2004 when invasive dreissenid mussels began proliferating, current research is evaluating whether the depth of

ultraviolet (UV) radiation has also concomitantly increased. Alewife larvae generally avoided the surface waters during the daytime, perhaps to avoid UV exposure. Bloater larvae, however, attained their greatest densities in the surface waters. Higher pigmentation on Bloater larvae relative to Alewife larvae suggests that Bloater have evolved the capacity to endure UV exposure.

- A synthesis of seasonal zooplankton sampling was undertaken from previous CSMI transects that have sampled nearshore (11–27 m), middle (40–51 m) and deep (64–112 m) stations in Lakes Michigan and Huron between 2010 and 2017. Total zooplankton biomass was lowest in the nearshore stations, driven primarily by several taxa of calanoid copepods. Because the nearshore has higher primary production, this result could arise from higher zooplanktivory. Furthermore, the seasonal pattern for zooplankton in the nearshore declined in late-summer before increasing again in the fall, whereas the seasonal pattern at the middle and deep sites revealed no steep mid-summer decline.
- How the heterogeneity in primary production and zooplanktivory over space and time affects zooplankton community dynamics may not be understood without more monthly sampling conducted in nearshore (<30 m) waters. In contrast, monitoring the zooplankton community in the more offshore waters with one summer cruise, as is currently undertaken by Environmental Protection Agency (EPA), could capture interannual variation in zooplankton owing to less seasonal variation. Future CSMI studies could consider building on these findings and emphasize more frequent sampling of zooplankton in nearshore waters.

Subproject A: Lake whitefish habitat selection in Green Bay

[a]Kraus, R.K, [b]Dembkowski, D., [b]Izzo, L., [b]Isermann, D., [c]Treska, T., and [d]Binder, T.

[a]U.S. Geological Survey Great Lakes Science Center, Ann Arbor, MI 48105 USA

[b]Wisconsin Cooperative Fishery Research Unit, College of Natural Resources, University of Wisconsin–Stevens Point, Stevens Point, Wisconsin 54481 USA

[c]U.S. Fish and Wildlife Service, Green Bay Fish and Wildlife Conservation Office, New Franken, WI 54229 USA

[d]Michigan State University, Department of Fisheries and Wildlife, Hammond Bay Biological Station, Millersburg, MI 49759 USA

Overview

Green Bay is an important area of human activity in Lake Michigan, providing manifold ecosystem services such as municipal water, shipping routes to key ports, and fisheries (both commercial and recreation). It has a longitudinal trophic gradient with the highest nutrient levels in the southern most portion of the bay. Like other hypereutrophic areas in the Great Lakes (e.g., Saginaw Bay, Lake Huron; Bay of Quinte, Lake Ontario; western Lake Erie), seasonal algal blooms and hypoxia in southern Green Bay are significant concerns for water quality (LaBuhn & Klump 2016, Klump et al. 2018). Typically point or profile sampling has provided data for understanding nutrient and water quality dynamics; however, recent observations (Kraus et al. 2015) and modeling efforts (Rowe et al. 2019) from Lake Erie have revealed the spatially and temporally dynamic characteristics of hypoxia. Similar dynamics are likely present in Green Bay, with implications for treating municipal water and elucidating fish movements relevant to conservation and management.

Lake Whitefish are a native fish that supports important interjurisdictional fisheries in Green Bay (Ransom et al. 2021). Movements across jurisdictional boundaries influence stock mixing to an unknown degree in Green Bay, and recent efforts to understand seasonal habitat use relevant to mixed stocks provided evidence of north-south segregations in Green Bay (Dan Dembkowski, University of Wisconsin-

Stevens Point, personal communication, 4/5/2023). This initial work raised questions about habitat use in large areas of Green Bay that were unmonitored, and preferred habitats throughout the year.

This study was responsive to CSMI Priority #2 ((see https://greatlakescsmi.org/publications/2021-csmi-lake-michigan-prospectus/), listed at the beginning of this report, focusing on examining and characterizing biological hotspots such as southern Green Bay and developing an approach for leveraging an existing acoustic telemetry monitoring network in Green Bay (Great Lakes Telemetry Observation System, GLATOS; www. glatos.glos.us).

Methods

Through cooperation with fishery stakeholders, U. S. Fish and Wildlife Service (USFWS) and U.S. Geological Survey Wisconsin Cooperative Fishery Research Unit and University of Wisconsin Stevens Point researchers, Lake Whitefish were tracked using the GLATOS network to understand seasonal movements and habitat use in Green Bay. By leveraging GLATOS stations as a platform for distributing temperature and dissolved oxygen loggers throughout Green Bay, we developed data sets that support manifold inquiries to understand fish behavior and environmental variability.

GLATOS acoustic telemetry receivers (model VR2-AR; Innovasea, Halifax, Nova Scotia) were equipped with data loggers (model: miniDOT logger; PME, Inc., Vista, California; n=52) that were factory calibrated and programmed to record at 10-minute intervals (temperature accuracy = +/- 0.1C; optical dissolved oxygen accuracy = 0.3 mg/L). To mitigate biofouling, the devices were equipped with a copper antifouling collar around the dissolved oxygen sensor and a mechanical wiper to clean the sensor throughout deployment. The acoustic telemetry receivers were moored to small granite boulders and suspended with floats approximately 2.5 m above the bottom. Moorings were deployed by hand from a small vessel and retrieved via an acoustic release system which was triggered by a coded signal from the surface vessel. As soon as possible after retrieval and maintenance, the logger was placed in a solution of sodium metabisulfate to assess instrument drift with a zero-oxygen point calibration. Retrieval endpoint calibrations deviated from the known value by less than the reported instrument accuracy. Data were downloaded and processed according to manufacturer instructions, prior to maintenance, battery installation, and redeployment.

Three loggers malfunctioned during deployment and ceased to record. One of these was traced to a faulty battery, and the others have not been diagnosed. Two other loggers were set to calibration mode, which we learned later can only be initiated by the manufacturer. No data were available from these loggers, and they were returned to the manufacturer for diagnostic evaluation. Two of the loggers could not be retrieved using the acoustic release mechanism. Assistance to retrieve these manually was provided by Wisconsin law enforcement, who located the moorings with a remotely operated vehicle and attached a surface line to the units for retrieval. These two units were extremely fouled with dreissenid mussels (Fig. A1) which affected either the mechanical release from the mooring or transmission of the release code. Several stations, limited to southern Green Bay, were heavily fouled with mussels, which is suspected to have impacted results for dissolved oxygen as described below.

Figure A1. Great Lake Acoustic Telemetry Observation System (GLATOS) acoustic receiver (larger black cylinder) station equipped with a data logger (smaller white cylinders) prior to deployment (left picture), and a station being recovered with an ROV (Remotely Operated Vehicle) due to extreme fouling from dreissenid mussels (right picture). Photo credit: Wisconsin Department of Natural Resources.

To understand habitat-use of a native fish using the revised sampling design of receivers in Green Bay, Lake Whitefish were implanted with acoustic telemetry transmitters (VEMCO Model V13-TP, depth range = 68 m; Innovasea, Inc., Nova Scotia, Canada). Tags broadcasted data on temperature and depth from onboard sensors (thermistor and pressure sensors). Fish were obtained in the fall of 2020 from spawning aggregations, primarily in the Menominee and Peshtigo Rivers of Wisconsin (Marinette County) with the aid of Wisconsin Department of Natural Resources. A total of n=100 fish were successfully released, but during the first winter at-large, the GLATOS array had highly limited coverage with some receivers unable to decode tag transmissions per the issue described above. Here we censored the data to detections that occurred after the implementation of the revised GLATOS sampling design, which was coincident with the data logger deployments. As some of the fish were not detected after this event, our synopsis represents only those fish (n=63) that survived to be detected after June of 2021.

Results and Discussion

Monthly means of logger data illustrated the spatial and temporal variation in temperature and dissolved oxygen across demersal habitats of Green Bay. As expected, demersal temperatures followed typical patterns of seasonal change with greater spatial variability during warmer months. Mean temperatures ranged from 0.07 to 0.8 C in January 2022 and 7.1 to 23.5 C in July 2021. The warmest temperatures were observed at the most southern and the most northern stations (Fig. A2). These areas represented the shallowest deployments (<45 m). Additional analyses of these temperature data will include examination of the high-frequency (10-minute) time-series to understand short-term variability that may be related to internal hydrography, such as with internal waves along the thermocline.

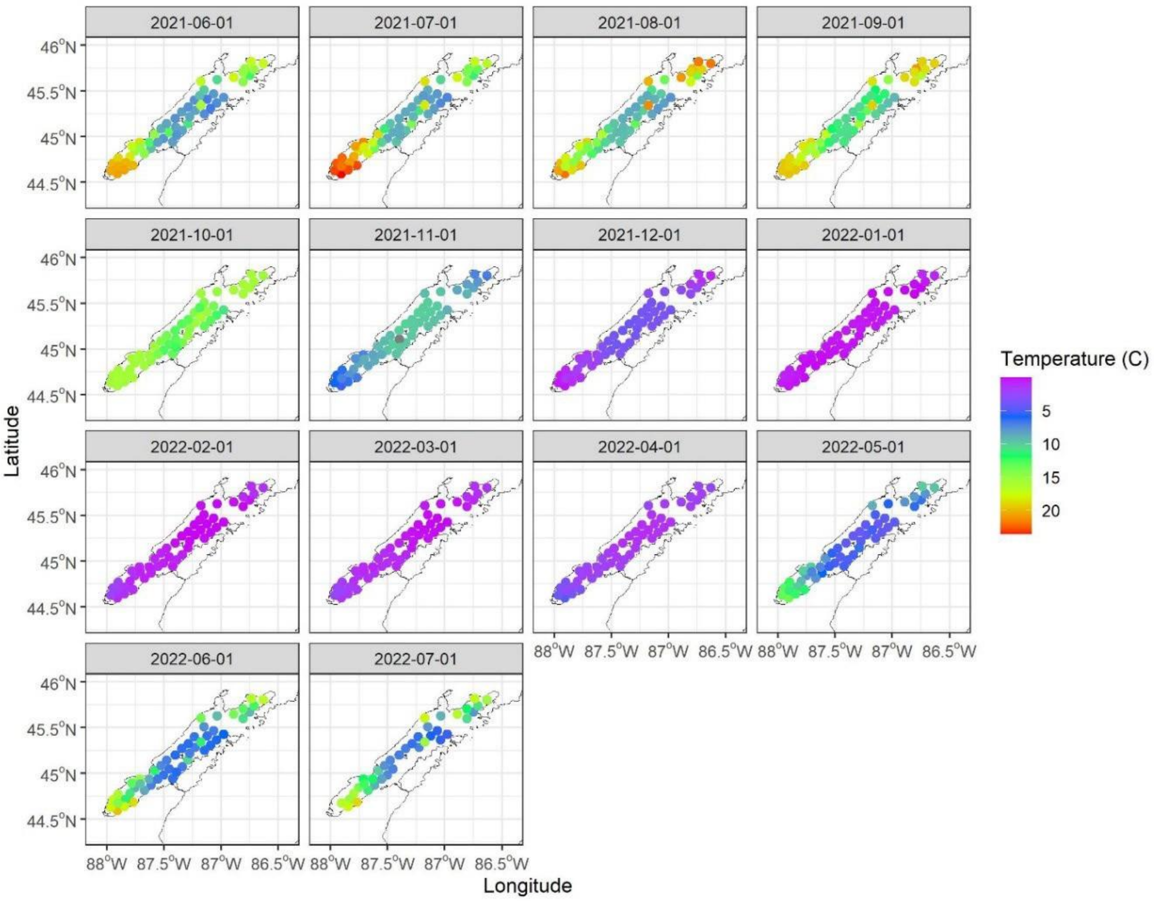

Figure A2. Monthly mean demersal temperatures recorded by data loggers deployed on the Great Lakes Acoustic Telemetry Observation System (GLATOS) acoustic receiver network in Green Bay. Each panel is labeled by the first day of the month which it depicts.

While most of the data loggers from Green Bay had little or no biofouling from mussels at the end of the first deployment, several stations in southern Green Bay were heavily encrusted with dreissenid mussels. The fouling was substantial enough that it appears to have affected the dissolved oxygen measurements during the deployment, leading to prolonged periods with hypoxia from fall of 2021 through winter and summer of 2022 (Fig. A3). Preliminary inspection of these data did not indicate a malfunction of the devices, but rather encrusting of Quagga mussels around the dissolved oxygen sensor appeared to have created an area of stagnate water. Quagga mussel fouling was most severe in southern Green Bay, but not observed to interfere with data loggers in middle and northern parts of the array. Once this stagnate water became depleted of oxygen, it remained hypoxic until the logger was retrieved. In addition, some stations fluctuated between normoxia and hypoxia (<2.0 mg/L), and these were spread out to the margins of the southern portion of the network (Fig. A3).

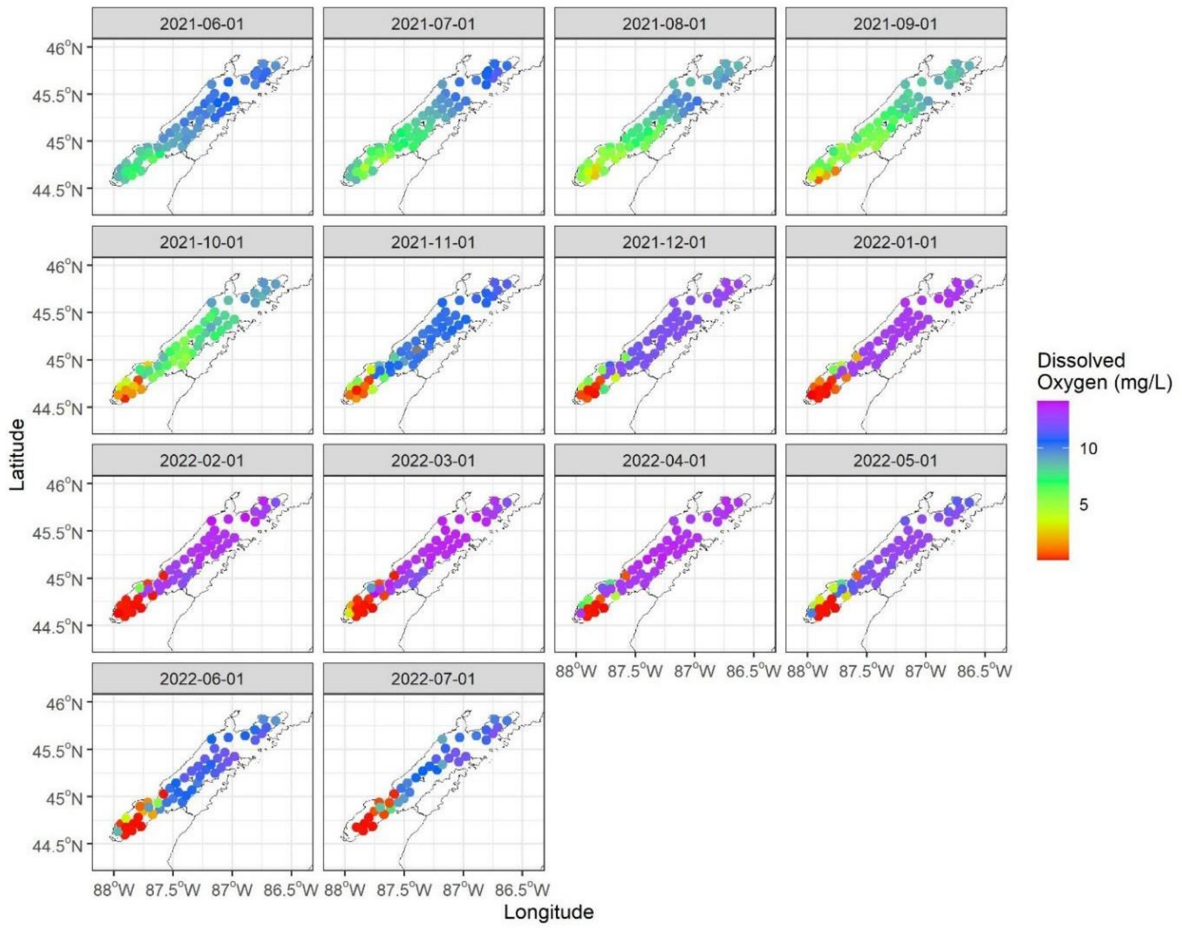

Figure A3. Monthly mean bottom dissolved oxygen recorded by data loggers deployed on the Great Lakes Acoustic Telemetry Observation System (GLATOS) acoustic receiver network in Green Bay. Each panel is labeled by the first day of the month which it depicts. Fewer stations in July of 2022 are a result of the receiver tending schedule that started in June 2022.

Although disappointing, the interference of southern Green Bay data loggers by mussels is still potentially informative to two different questions. First, as evidenced by the lack of fouling in other areas of Green Bay, mussel recruitment is spatially heterogenous and enhanced by warmer temperatures and eutrophy (Karatayev et al. 2018). The new surfaces provided by moorings in southern Green Bay obviously provided favorable substrate for mussel colonization, whereas elsewhere moorings were in habitats that were colder, deeper, and presumably lacking in food (Karatayev et al 2018). Second, our experiences in environments of Lake Erie with similar depths, temperatures, and trophic status have not produced similar fouling issues. Rather, in Lake Erie, our moorings are much shorter – rising no more than a meter above the bottom in most cases – but otherwise constructed according to the same template. Comparative investigation would be needed to reveal factors that might mitigate biofouling on these moorings, but for temperature (which would not be affected by biofouling) and dissolved oxygen, the majority of these data loggers represent a high-resolution data set with many potential applications beyond this CSMI study.

In general, Lake Whitefish utilized southern Green Bay throughout the year (Fig. A4), none of these fish were observed moving into northern embayments or outside of Green Bay into Lake Michigan. This result supported the hypothesis that Lake Whitefish that spawn in major tributaries of southern Green Bay remain resident there. These results also supported the widely accepted notion that, despite lack of detection on receiver gates in the previous study, Lake Whitefish are utilizing (previously) unmonitored, open-water habitats. Detection of fish in this study also demonstrated seasonal shifts in the areas of southern Green Bay that were most heavily occupied. For example, in July, August, and September, fish avoided the southern-most portions of Green Bay (Fig. A4). More fine-scale examination of the data will help to resolve the timing and associations of Lake Whitefish movements in response to environmental correlates. Warmer temperatures at the southern-most stations during summer (Fig. A4) approached the generally accepted upper thermal limit of 19.5°C for lake whitefish (Jacobsen et al. 2010); therefore, tagged fish movements may have been partially in response to avoidance of supra-optimal temperatures. Although, fish primarily remained in southern Green Bay (<45.2°N) year-round, October represented one month when fish were more widely dispersed, with detections spread throughout Green Bay as far north as latitude 45.6°N (Fig. A4). The most geographically restricted months were January, February, and March (Fig. A4).

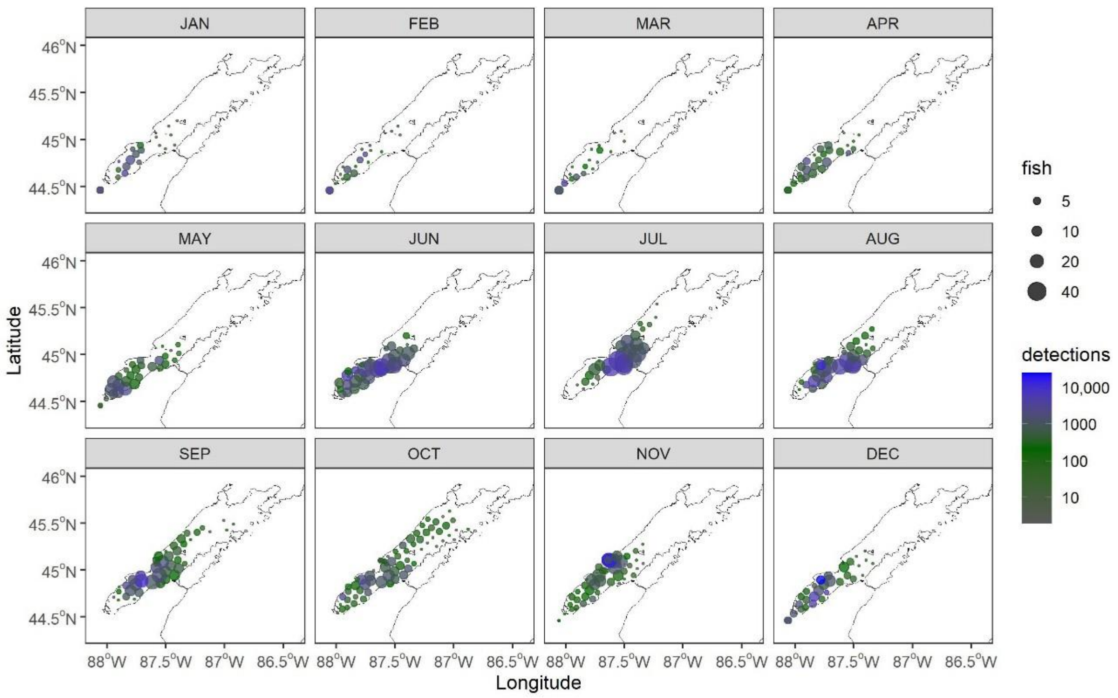

Figure A4. Monthly detections of acoustic-tagged Lake Whitefish (C*oregonus clupeaformis*) in Green Bay (June 2021 to July 2022). Total detections (color gradient) and number of unique tags (size graded circles) are depicted by calendar month in each panel.

Additional aspects of Lake Whitefish habitat use were examined through the onboard tag sensors. For this synopsis, tag temperature and depth were examined relative to moored data loggers and lake depth when fish were detected. Examination of dissolved oxygen as a correlate of fish behavior (e.g., Kraus et al. 2023) will require additional processing and quality checking of logger data to identify erroneous values and is not included in this report. Tag depths and temperatures provided a complementary view of fish behavior, with insights to commercial fishery catchability in open waters of Green Bay. Tag data from this project revealed that Lake Whitefish associations with demersal habitats varied greatly by season (Fig. A5). The deepest mean daily depth of any tagged lake whitefish was ca. 30 m across a range of bottom depths while most depths were <25 m (Fig. A5). Factors such as lake level and tag pressure sensor accuracy (+/- 0.9 m) in part can account for tag depths that were greater than the lake depth, but in areas where detection ranges overlapped steep bathymetry gradients, fish may have been present at depths greater than the depth of the receiver. A pattern of high association with the bottom was seen from December through April, with few detections in mid-water (Fig. A5). By comparison, detections at mid-water depths were more frequent during May through August, especially at deeper stations (lake depth >20m; Fig. A5). Interestingly, during September, October, and November, fish utilized the entire water column, including the surface (Fig. A5). The suspension of Lake Whitefish in Green Bay was unexpected and will require additional research beyond the scope of this project to understand this behavior.

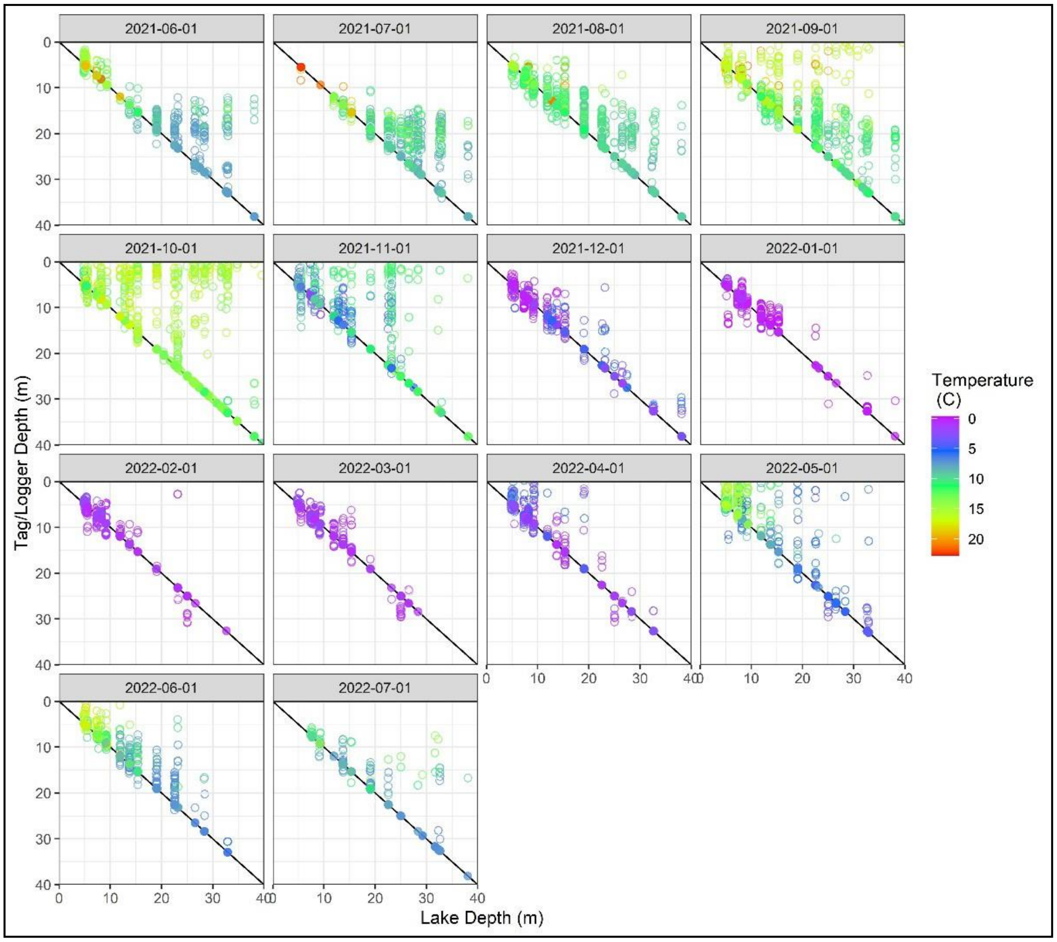

Figure A5. Daily mean depths of Lake Whitefish(*Coregonus clupeaformis*) in Green Bay summarized by tag and receiver (circles). Corresponding mean monthly temperatures recorded by data loggers (dots) are plotted along the diagonal line representing the bottom of the lake. Colors indicate temperature as shown in the key, while each panel is labeled by the first day of the month which it depicts.

For the Green Bay Lake Whitefish, an obvious question is whether suspended fish were in the hypolimnion or epilimnion during stratified months (typically July, August, and September). Mean daily tag temperatures were nearly identical to data logger values in all months: 90th percentile of differences <1.9°C, 95th percentile of absolute difference <3.2°C, and the maximum absolute difference was 10.2°C. Isothermal similarity in temperature between tag and data logger emphasized that fish spent large portions of time in demersal habitats or at depths that were isothermal with near bottom habitats where data loggers were deployed. Additionally, 95% of tag temperatures were <16.7°C, which is well within the range of preferred temperatures reported in the literature (Jacobson et al. 2010).

Although Lake Whitefish have morphological adaptations for demersal feeding and are generally considered to be a demersal coldwater species (Eshenroder et al. 2016), these results highlight questions about the position of this species in the southern Green Bay ecosystem. Recent analysis of Lake Whitefish diets from southern Green Bay showed predominately invertebrates, including pelagic items such as *Bythotrephes* sp. and chironomids and demersal mollusks (Dembkowski et al. 2022). This recent study provided only coarse taxonomic resolution of invertebrate prey, and samples were captured by methods that targeted demersal or shallow habitats (e.g., trawls, electrofishing). We posit that Lake Whitefish switch to pelagic feeding in the open waters of Green Bay, and that a better understanding of trophic interactions from pelagic waters (obtained with different sampling gears) could better resolve an accurate understanding of the Green Bay ecosystem.

This synopsis highlighted novel information on the behavior of a key native fish species of considerable economic importance in Green Bay. In addition, data from this effort will become publicly released through a data release (R. Kraus, USGS, personal communication, 4/4/2023) to provide a resource for addressing resource management issues that range from municipal water treatment to fisheries. Ongoing efforts may address the uncertainties described above.

Acknowledgements

We are especially grateful for the efforts of USFWS, the USGS Wisconsin Cooperative Fishery Research Unit (Stevens Point), and commercial fishers who provided various in-kind contributions to the deployment and maintenance of data loggers, acoustic telemetry receivers, and fish tagging. The protocol for fish handling and tag implantation followed each agency's approved animal care policies, American Fisheries Society policies (Jenkins et al. 2014) and previous successful studies in Green Bay (e.g., Dembkowski et al. 2021).

References

Dembkowski, D.J., Isermann, D.A., Vandergoot, C.S., Hansen, S.P., and Binder, T.R. 2021. Short-term survival of lake whitefish following surgical implantation of acoustic transmitters using chemical anesthesia and electroimmobilization. Adv. Limnol. **66**: 173-187.

Eshenroder, R.L., Vecsei, P., Gorman, O.T., Yule, D., Pratt, T.C., Mandrak, N.E., Bunnell, D., Muir, A.M., 2016. Ciscoes (Coregonus, subgenus Leucichthys) of the Laurentian Great Lakes and Lake Nipigon. Great Lakes Fishery Commission.

Koenig, L.D., Dembkowski, D.J., Hansen, S.P., Tsehaye, I., Paoli, T.J., Zorn, T.G., and Isermann, D.A. 2022. Diet composition and overlap for adult walleye, lake whitefish, and yellow perch in Green Bay, Lake Michigan. J. Great Lakes Res. **48:** 1681-1695.

Jacobson, P.C., Stefan, H.G., and Pereira, D.L. 2010. Coldwater fish oxythermal habitat in Minnesota lakes: influence of total phosphorus, July air temperature, and relative depth. Can. J. Fish. Aquat. Sci. **67**: 2002-2013.

Jenkins, J.A., Bart Jr, H.L., Bowker, J.D., Bowser, P.R., MacMillan, J.R., Nickum, J.G., Rachlin, J.W., Rose, J.D., Sorensen, P.W., and Warkentine, B.E. 2014. Guidelines for Use of Fishes in Research—Revised and Expanded, 2014. Fisheries **39**: 415-416.

Karatayev, A.Y., Karatayev, V.A., Burlakova, L.E., Rowe, M.D., Mehler, K., and Clapsadl, M.D., 2018. Food depletion regulates the demography of invasive dreissenid mussels in a stratified lake. Limnol. Oceanogr. **63**: 2065-2079.

Klump, J.V., Brunner, S.L., Grunert, B.K., Kaster, J.L., Weckerly, K., Houghton, E.M., Kennedy, J.A., and Valenta, T.J. 2018. Evidence of persistent, recurring summertime hypoxia in Green Bay, Lake Michigan. J Great Lakes Res. **44:** 841-850.

Kraus, R.T., Knight, C.T., Farmer, T.M., Gorman, A.M., Collingsworth, P.D., Warren, G.J., Kocovsky, P.M., and Conroy, J.D. 2015. Dynamic hypoxic zones in Lake Erie compress fish habitat, altering vulnerability to fishing gears. Can. J. Fish. Aquat. Sci. **72:** 797-806.

Kraus, R.T., Cook, H.A., Faust, M.D., Schmitt, J.D., Rowe, M.D., and Vandergoot, C.S. 2023. Habitat selection of a migratory freshwater fish in response to seasonal hypoxia as revealed by acoustic telemetry. J. Great Lakes Res. DOI: 10.1016/j.jglr.2023.01.004

LaBuhn, S., and Klump, J.V. 2016. Estimating summertime epilimnetic primary production via in situ monitoring in an eutrophic freshwater embayment, Green Bay, Lake Michigan. J. Great Lakes Res. **42:** 1026-1035.

Ransom, A.L., Houghton, C.J., Hanson, S.D., Hansen, S.P., Doerr, L.R., Forsythe, and P.S., 2021. Recolonization of lake whitefish river spawning ecotypes and estimates of riverine larval production in Green Bay, Lake Michigan. J. Great Lakes Res. **47**: 213–225

Rowe, M.D., Anderson, E.J., Beletsky, D., Stow, C.A., Moegling, S.D., Chaffin, J.D., May, J.C., Collingsworth, P.D., Jabbari, A., and Ackerman, J.D. 2019. Coastal Upwelling Influences Hypoxia Spatial Patterns and Nearshore Dynamics in Lake Erie. J. Geophys. Res.: Oceans **124:** 6154-6175.

Subproject B: Lake whitefish habitat selection in Grand Traverse Bay

[a]Hondorp, D., [b]Smith, J., [c]Olsen, E., [d]Turschak, B.A., [e]Donner, K., and [d]Jonas, J.L.

[a]U.S. Geological Survey Great Lakes Science Center, Ann Arbor, MI 48105 USA

[b]Sault Ste. Marie Tribe of Chippewa Indians, Sault Ste. Marie, MI 49783

[c]Grand Traverse Band of Ottawa and Chippewa Indians, Peshawbestown, MI 49682 USA

[d]Michigan Department of Natural Resources, Charlevoix Fisheries Research Station, Charlevoix, MI 49720 USA

[e]Little Traverse Bay Band of Odawa Indians, Harbor Springs, MI 49740 USA

Overview

The U.S. Geological Survey, in partnership with the Great Lakes Acoustic Observation System (GLATOS), is a world leader in the application of acoustic telemetry to problems in fish management and conservation. Acoustic telemetry is an ideal tool for examining how the response of fish communities to oligotrophication may depend on the movement ecology and behavior of individual species. In Lake Michigan, for example, populations of Cisco (*Coregonus artedi*) are thriving amid declining lake productivity whereas numbers of Lake Whitefish are decreasing. In this project, we used acoustic telemetry to compare movements and seasonal habitat use of adult Cisco and Lake Whitefish in Grand Traverse Bay (GTB) with the goal of relating differences in species status to variation in their spatial ecology. Our project leverages existing acoustic receiver networks and acoustic-tagged Cisco already present in GTB and will generate information that can be compared with results of an ongoing acoustic telemetry study of Lake Whitefish in Green Bay.

Lake Whitefish were not tagged in GTB until 2021, as the COVID pandemic resulted in the cancellation of tagging plans for 2020. Instead of comparing within-bay habitat use between Cisco and Lake Whitefish, we opted to compare habitat use of the GTB population with a second population that spawns in Good Harbor Bay (GHB; Fig. B1) located west of GTB. This change in focus was made to leverage expansion of acoustic receiver arrays in northern Lake Michigan in 2021 as well as subsequent funding from the Great Lakes Fish and Wildlife Restoration Act Grant Program and the Great Lakes Fishery Trust that enabled us to tag Lake Whitefish from additional populations. Moreover, a Lake Whitefish focus is more relevant to fishery managers who currently are under pressure to prevent collapse of Lake Whitefish fisheries in northern lakes Michigan and Huron (Ebener et al. 2021, Rook et al. 2022). The goal of this project is to use acoustic telemetry to describe and compare bathythermal habitat used by adult Lake Whitefish sampled from west GTB (near Ingalls Pt.) and GHB, Lake Michigan (Fig. B1). Study objectives are to determine 1) if depth-habitat use by Lake Whitefish varies seasonally, between populations (GTB vs. GHB), and/or their interaction; 2) whether lake bottom depth constrains Lake Whitefish movements; 3) if seasonal trends in thermal habitat use differ between populations (GTB vs. GHB); and 4) whether thermal habitat use by one or both populations during stratified periods differs from the preferred range (10-15 °C).

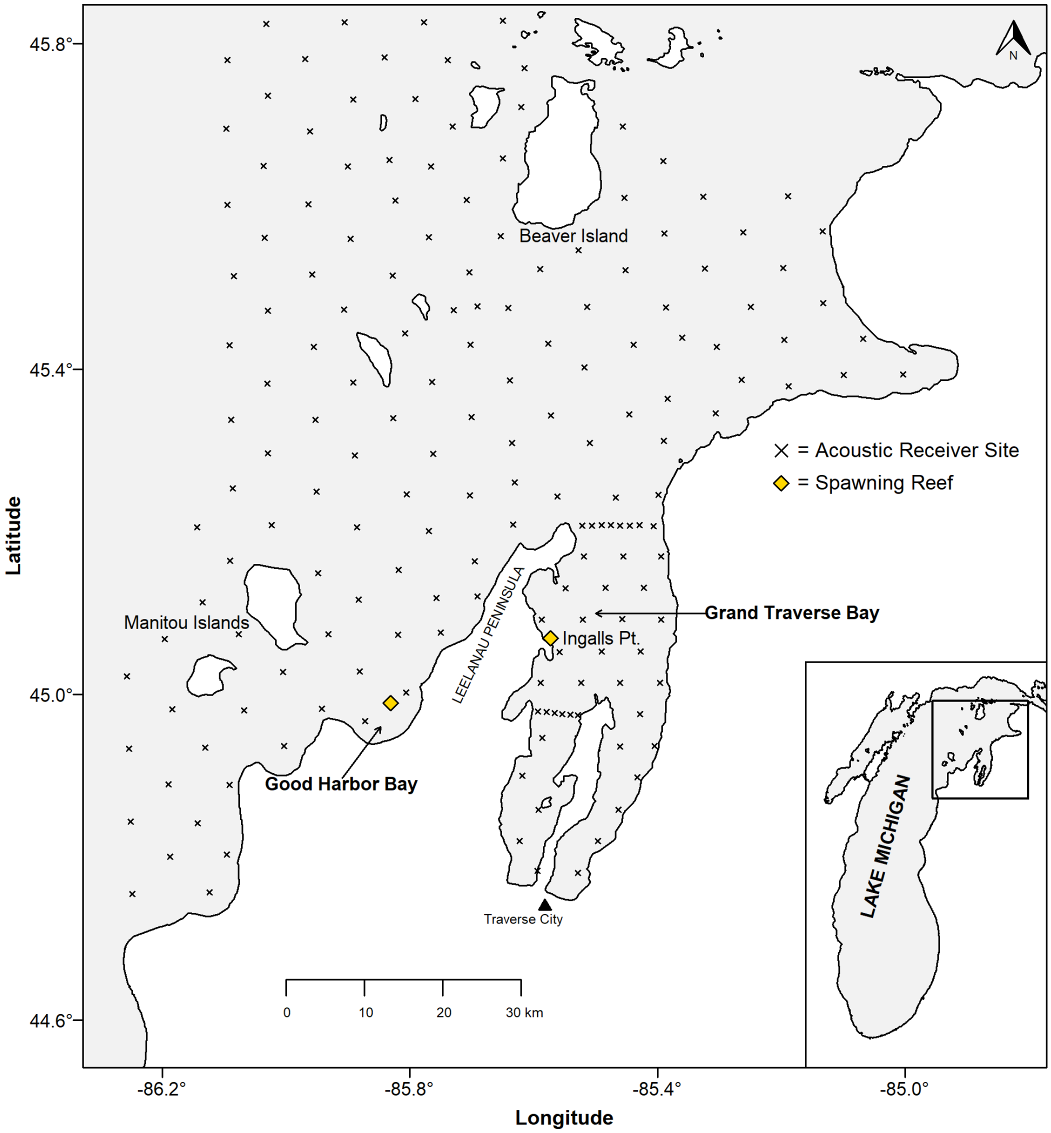

Figure B1. **Northern Lake Michigan study area and acoustic receiver arrays.**

Methods

In acoustic telemetry, individual fish are captured, marked with coded ultrasonic transmitters or “tags,” and then released back into the environment. Networks of autonomous, stationary receivers then are used to track the movements of tagged individuals over large areas and long periods of time (> 1 year). Unlike conventional net sampling, mark-recapture methods, passive integrated transponder (PIT) tags, or radio tags, acoustic tags can be detected and identified from great distances (usually hundreds of meters), resulting in high detection (i.e., encounter) rates. Each acoustic receiver records the date, time, and unique ID code for each acoustic tag detection.

Lake Whitefish in this study were collected in trap nets set adjacent to spawning areas during April 2021 (GHB only) and November-December 2021 (GHB, GTB). A total 43 Lake Whitefish were tagged and released at the Ingalls Pt. spawning reef in west GTB, and another 33 were tagged and released at an offshore reef site in GHB. Acoustic tags (Vemco-InnovaSea® V13) configured with depth (0.60 m resolution) and temperature (0.15 °C resolution) sensors were surgically implanted in the abdominal cavity via laparotomy. Customization of acoustic tags with pressure and temperature sensors also allows for testing hypotheses about fish bathythermal habitat use.

Results and Discussion

A total of 333,167 depth measurements and 332,590 temperature measurements were made by temperature- and depth-sensor tags in acoustic-tagged Lake Whitefish between April 2021 and early July 2022, when most receivers were last downloaded. A few isolated receivers were recovered and downloaded in August and September 2022. Most acoustic-tagged individuals have not yet been observed for a full year, so the focus of this report is on post-spawn movements and habitat use that occurred between January and June 2022

Depth-habitat use by acoustic-tagged Lake Whitefish during 2021-2022 varied considerably within individual months, yet statistically significant seasonal trends and differences between populations still were observed. For example, acoustic-tagged individuals from both populations moved from deeper over-wintering habitat (median depth = 24-27 m) into shallower water (median depth = 11-15 m) during the late spring or early summer (Fig. B2). This shift occurred one month earlier in GHB than in GTB (May vs. June) but was ephemeral as individuals from both populations returned to deeper water (median depth ~ 20 m) the following month (Fig. B2). Use of shallow areas (depth < 15 m) by Lake Whitefish previously has been linked only to spawning (Ebener et al. 2008), but movements of telemetered individuals in this study suggest that warming, nearshore waters are important spring foraging habitats for adult Lake Whitefish.

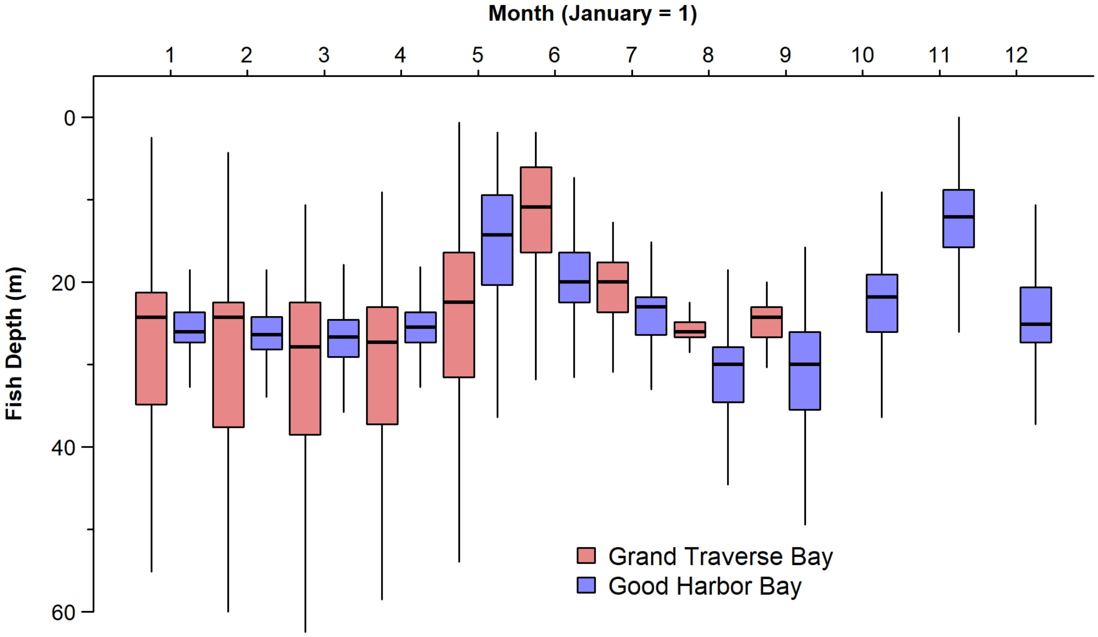

Figure B2. Seasonal depth-habitat use by acoustic-tagged Lake Whitefish (*Coregonus clupeaformis*) from two Lake Michigan spawning populations, 2021-2022. Heavy dark line represents the median value; boxes denote the interquartile range, while the whiskers represent the 10th and 90th percentiles.

The return to deeper water that occurred during the summer stratified period (July-September) undoubtedly is the result of Lake Whitefish seeking lake bottom habitat within the preferred temperature range of 10-15 °C (Christie and Regier 1988, Gorsky et al. 2012). However, depths occupied during summer were greater for acoustic-tagged individuals from the GHB population (median depth = 23-30 m) than for conspecifics from GTB (median depth = 20-26 m; Fig. B2). Consistent with known reproductive behaviors, acoustic-tagged Lake Whitefish again moved into shallower water to spawn during October and/or November (Fig. B2). Median depth occupied during November was ca. 12-m for Lake Whitefish from the GHB population (spring-tagged fish only), but over 18% of detections occurred at depths ≤ 7-m, the depth range that defines Lake Whitefish spawning habitat (Ebener et al. 2021). We lack detection data for the GHB population during October and November because receivers deployed on the west GTB spawning site (Ingalls Pt.) in September 2022 have not yet been recovered and downloaded.

Adult dispersal during spring (April, May, June) was primarily limited to areas within 6-20 km of spawning reefs where lake bottom depth was less than 100 m (Figs. B3, B4). Indeed, only 25 depth sensor readings (< 0.01 % of all detections) occurred at depths ≥ 100 m. These observations are consistent with the hypothesis that depth constrains Lake Whitefish movement. Acoustic-tagged Lake Whitefish from the GTB population mainly dispersed along corridors bounded by shorelines and deep-water trenches (Fig. B3), whereas conspecifics from GHB also dispersed to offshore islands (Fig. B4). Limited dispersal by both populations suggests that complex habitats immediately adjacent to spawning reefs are activity “hotspots” for Lake Whitefish in Lake Michigan.

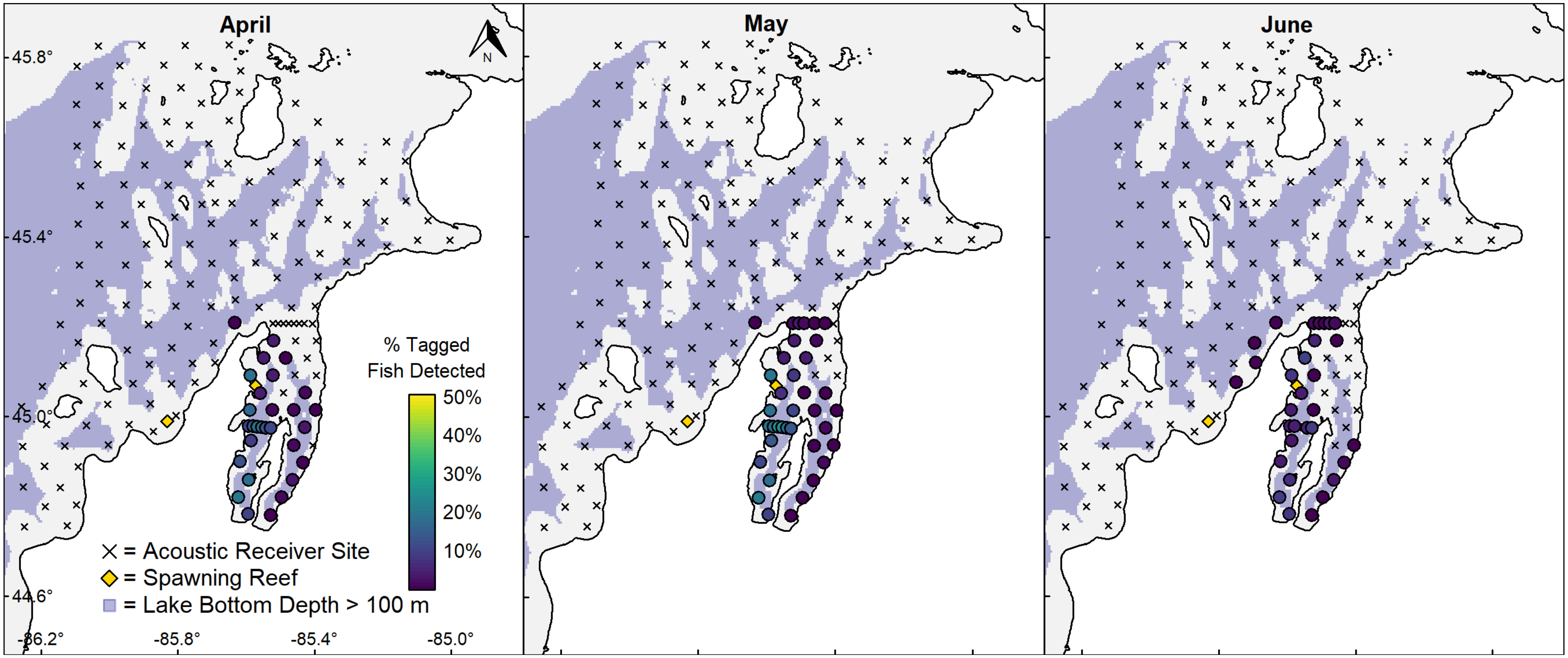

Figure B3. Distribution of acoustic-tagged Grand Traverse Bay Lake Whitefish (*Coregonus clupeaformis*) in Lake Michigan during April, May, and June 2022.

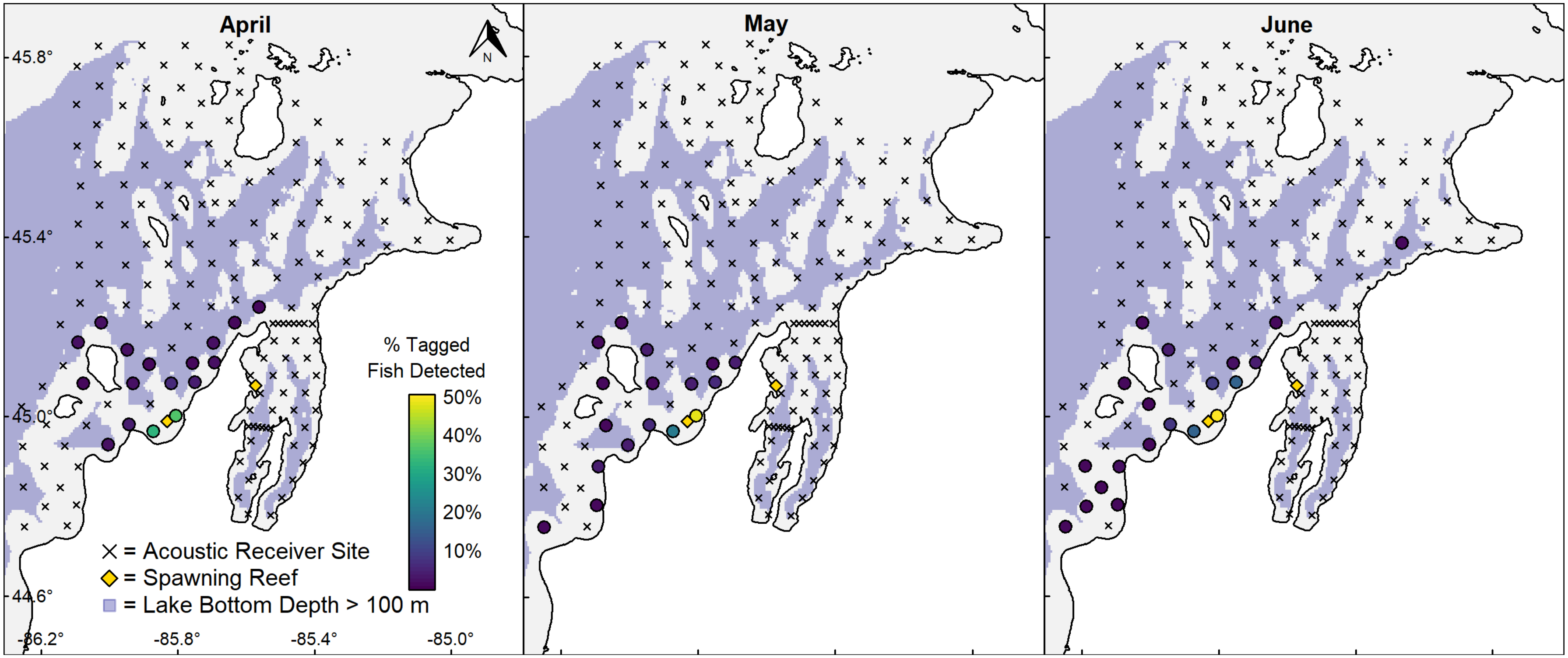

Figure B4. Distribution of acoustic-tagged Good Harbor Bay Lake Whitefish (*Coregonus clupeaformis*) in Lake Michigan during April May, and June 2022.

Thermal habitat use by acoustic-tagged Lake Whitefish in Lake Michigan during 2021-22 varied seasonally and between populations. Both populations exhibited a shift to warmer waters starting in May, but temperatures occupied by acoustic-tagged Lake Whitefish during the May-to-August period were consistently 1-2 °C higher for adults from the GHB population (median temperature = 6.2-11.7 °C) than for conspecifics from GTB (median temperature = 3.5-10.6 °C; Fig. B5). During the summer-fall stratified period (July-September), temperatures occupied by acoustic-tagged Lake Whitefish from both populations generally were within the preferred ranges (Fig. B5).

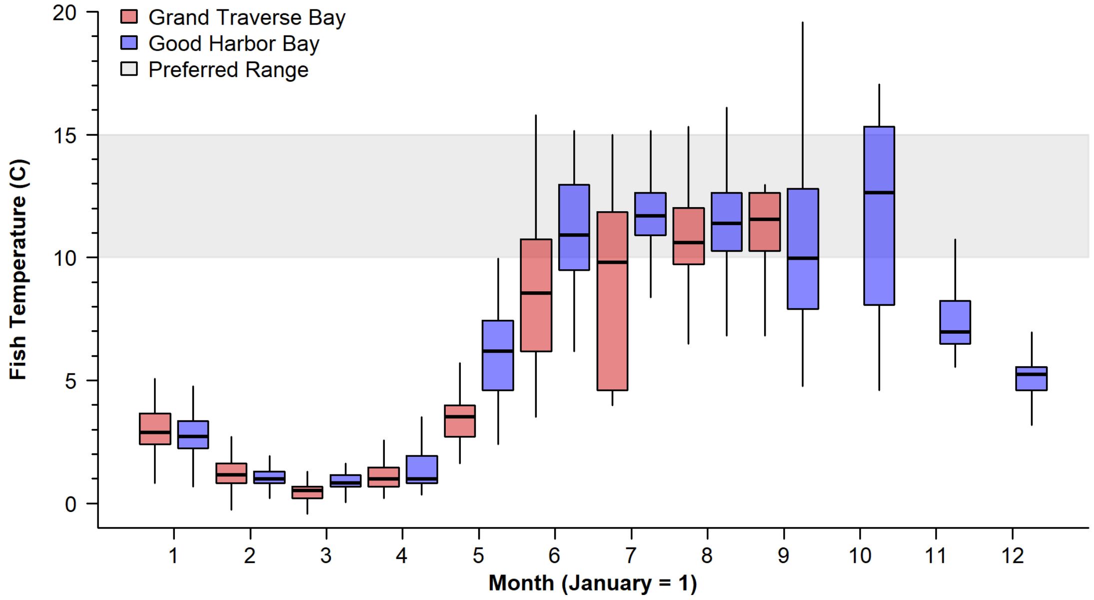

Figure B5. Seasonal thermal-habitat use by acoustic-tagged Lake Whitefish (*Coregonus clupeaformis*) from two Lake Michigan spawning populations, 2021-2022. Heavy dark line represents the median value; boxes denote the interquartile range, while the whiskers represent the 10th and 90th percentiles.

Project Highlights:

- Rapid seasonal changes in the depth and temperature of acoustic-tagged Lake Whitefish suggest that high-resolution sampling techniques such as acoustic telemetry are necessary to characterize the bathythermal habitat niche of Lake Whitefish.
- Warm, nearshore waters were important spring habitats for adult Lake Whitefish in Lake Michigan. This is in direct contrast to existing conceptual models based on gill net and trawl survey data that predict use of shallow water reefs and shoal areas is limited to the fall-winter spawning season (Ebener et al. 2021; Ebener et al. 2008).
- Depth-habitat use is a phenotypic trait subject to selection in Coregonines (Turgeon and Bernatchez 2003), so differences in the depths occupied by Lake Whitefish in Grand Traverse Bay and Good Harbor Bay may be indicative of local adaptation.
- Acoustic-tagged Lake Whitefish in northern Lake Michigan were largely restricted to habitats with lake bottom depth < 100 m, which suggests that deep water constrains adult dispersal.
- Limited extent of post-spawn dispersal by acoustic-tagged Lake Whitefish suggests that habitat(s) immediately adjacent to spawning reefs are “hotspots” for Lake Whitefish activity and production in Lake Michigan.

Potential topics for further research:

- Combine habitat use with habitat availability to determine if Lake Whitefish actively choose or avoid specific depth ranges and/or temperatures.
- Determine whether Lake Whitefish populations consist of multiple groups that exhibit distinct patterns of bathythermal habitat use (i.e., determine evidence for the existence of cryptic behavioral diversity in Lake Whitefish populations).

- Sex specific movement patterns exist in other Great Lakes fish species (e.g., Binder et al. 2018, Raby et al. 2018), so determine if depth-habitat use differs between male and female Lake Whitefish.

Acknowledgements

We are especially grateful to the crew of the USGS research vessel Arcticus who assisted with receiver recovery and maintenance in open waters of the main basin. The protocol for fish handling and tag implantation followed each agency's approved animal care policies, American Fisheries Society policies (Jenkins et al. 2014) and previous successful studies in Green Bay (e.g., Dembkowski et al. 2021).

References

Binder, T.R., Farha, S.A., Thompson, H.T., Holbrook, C.M., Bergstedt, R.A., Riley, S.C., Bronte, C.R., He, J., and Krueger, C.C. 2018. Fine-scale acoustic telemetry reveals unexpected lake trout, *Salvelinus namaycush*, spawning habitats in northern Lake Huron, North America. Ecol. Freshw. Fish **27**(2): 594-605.

Christie, G.C., and Regier, H.A. 1988. Measures of Optimal Thermal Habitat and Their Relationship to Yields for Four Commercial Fish Species. Can. J. Fish. Sci. **45**(2): 301-314.

Dembkowski, D.J., Isermann, D.A., Vandergoot, C.S., Hansen, S.P., and Binder, T.R. 2021. Short-term survival of lake whitefish following surgical implantation of acoustic transmitters using chemical anesthesia and electroimmobilization. Adv. Limnol. **66**: 173-187.

Ebener, M.P., Dunlop, E.S., and Muir, A.M. 2021. Declining Recruitment of Lake Whitefish to Fisheries in the Laurentian Great Lakes: Management Considerations and Research Priorities. Great Lakes Fish. Comm. Misc. Pub. 2021-01 1553-8087 (online).

Ebener, M.P., Kinnunen, R.E., Schneeberger, P.J., Mohr, L.C., Hoyle, J.A., and Peeters, P.J. 2008. Management of commercial fisheries for Lake Whitefish in the Laurentian Great Lakes of North America. In International Governance of Fisheries Ecosystems. American Fish. Soc., Bethesda, MD. pp. 99–143.

Gorsky, D., Zydlewski, J., and Basley, D. 2012. Characterizing seasonal habitat use and diel vertical activity of Lake Whitefish in Clear Lake, Maine, as determined with acoustic telemetry. Trans. Am. Fish. Soc. **141**(3): 761-771.

Jenkins, J.A., Bart Jr, H.L., Bowker, J.D., Bowser, P.R., MacMillan, J.R., Nickum, J.G., Rachlin, J.W., Rose, J.D., Sorensen, P.W., and Warkentine, B.E. 2014. Guidelines for Use of Fishes in Research—Revised and Expanded, 2014. Fisheries **39**: 415-416.

Raby, G.D., Vandergoot, C.S., Hayden, T.A., Faust, M.D., Kraus, R.T., Dettmers, J.M., Cooke, S.J., Zhao, Y., Fisk, A.T., and Krueger, C.C. 2018. Does behavioural thermoregulation underlie seasonal movements in Lake Erie walleye? Can. J. Fish. Sci. **75**(3): 488-496.

Rook, B.J., Lenart, S.J., Caroffino, D.C., Muir, A.M., and Bronte, C.R. 2022. A 90-year record of lake whitefish *Coregonus clupeaformis* abundances in Michigan waters of the upper Laurentian Great Lakes. J. Great Lakes Res. **48**(6): 1618-1635.

Turgeon, J., and Bernatchez, L. 2003. Reticulate evolution and phenotypic diversity in North American ciscoes, *Coregonus* ssp. (Teleostei: Salmonidae): implications for the conservation of an evolutionary legacy. Cons. Gen. **4**(1): 67-81.

Subproject C: Exploring the bottleneck for larval lake whitefish

[a]Bunnell, D.B., [b]Donner, K., [c]Cubbage, M., [c]Collingsworth, P.D., [c]Höök, T.O., and [d]Pothoven, S.A.

[a]U.S. Geological Survey Great Lakes Science Center, Ann Arbor, MI 48105 USA

[b]Little Traverse Bay Band of Odawa Indians, Harbor Springs, MI 49740 USA

[c]Purdue University, Department of Forestry and Natural Resources, West Lafayette, IN 47907 USA

[d]NOAA Great Lakes Environmental Research Laboratory, Lake Michigan Field Station, Muskegon, MI 49441 USA

Overview

Lake Whitefish are a key native species in the Great Lakes given the many key services they provide within the ecosystem. First, they are of high cultural value within the Great Lakes especially to the Tribes and First Nations (Gobin et al. 2022), in which they are named 'Adikameg' or 'dikameg'. Second, Lake Whitefish have high economic value given that they are the most important commercial fishery across Lakes Superior, Michigan, and Huron (Baldwin et al. 2018). Third, they play a key role in the benthic food-webs of the Great Lakes given their ability to consume invasive dreissenid mussels and thereby convert this abundant resource to consumable fish biomass. Because relatively few native fish species in the Great Lakes consume dreissenid mussels, Lake Whitefish prevent dreissenid mussels from becoming a "dead-end" in Great Lakes food webs (see Madenjian et al. 2010).

Given declining Lake Whitefish biomass and harvest over the past 15 years in Lakes Michigan and Huron, management agencies have prioritized research to determine what mechanisms are limiting recruitment (i.e., the production of new fish each year, see Ebener et al. 2021). One factor limiting our understanding of recruitment dynamics for Lake Whitefish is the lack of a fishery independent survey that can predict recruitment success within the first year of life. As a result, the Little Traverse Bay Band of Odawa Indians (LTBBOI) initiated a beach-seining survey in 2014 that was ultimately adopted by other Tribes and agencies over the next several years throughout lakes Michigan, Huron, and Superior (K.

Donner, LTBBOI, personnel communication). Although it is too soon to determine whether the catch per unit effort of larval and juvenile fishes sampled on the beaches can provide the elusive index of recruitment success, the collection of these fishes has already increased our knowledge of the growth and food habitats at a potentially critical life stage (e.g., Pothoven 2020; Pothoven and Olds 2020).

One original goal of the 2020 CSMI was to expand the sampling of the beach-seining surveys in Lake Michigan. Given that Ann Arbor was most closely located to the southeastern region of the lake, our original intent was to expand this beach-seining effort southward - to St. Joseph and South Haven, Michigan (Fig. C1). For those Lake Whitefish that were collected, the intent was for them to be processed to evaluate the diets and prevalence of empty stomachs. Increased understanding of larval feeding during a potential critical period will help test the hypothesis that lake whitefish recruitment is declining due to declining spring zooplankton availability in the very nearshore waters (i.e., < 10 m) since the proliferation of dreissenid mussels. We were able to collect only two early March 2020 samples before the COVID pandemic ended spring 2020 field work, and so we altered our plans to result in two objectives that we carried out between 2020 and 2021.

Objective 1: Describe the understudied nearshore zooplankton community and assess prey selectivity by Lake Whitefish and Cisco (C. artedi) larvae across four sites in northeastern Lake Michigan (Big Stone Bay, Elk Rapids, Petoskey State Park, Bliss Beach- see Fig. C1). We developed a collaborative study between LTTBOI and Purdue University (West Lafayette, IN) that could exploit archived and unprocessed putative larval Lake Whitefish and zooplankton samples collected between 2015 and 2019. This information will inform the hypothesis that declining productivity in Lake Michigan over the past 20 years has led to reduced growth and survival of Lake Whitefish larvae (see Ebener et al. 2021; Cunningham and Dunlop 2023).

Objective 2: Conduct field sampling in 2021 at St. Joseph and South Haven. With densities in hand, we then sought to compare them to densities estimated by Steve Pothoven (NOAA Great Lakes Environmental Research Laboratory) on the beaches of Muskegon and nearby Grand Haven, Pentwater, and White Lake (Fig. C1), some of which dated back to 2014.

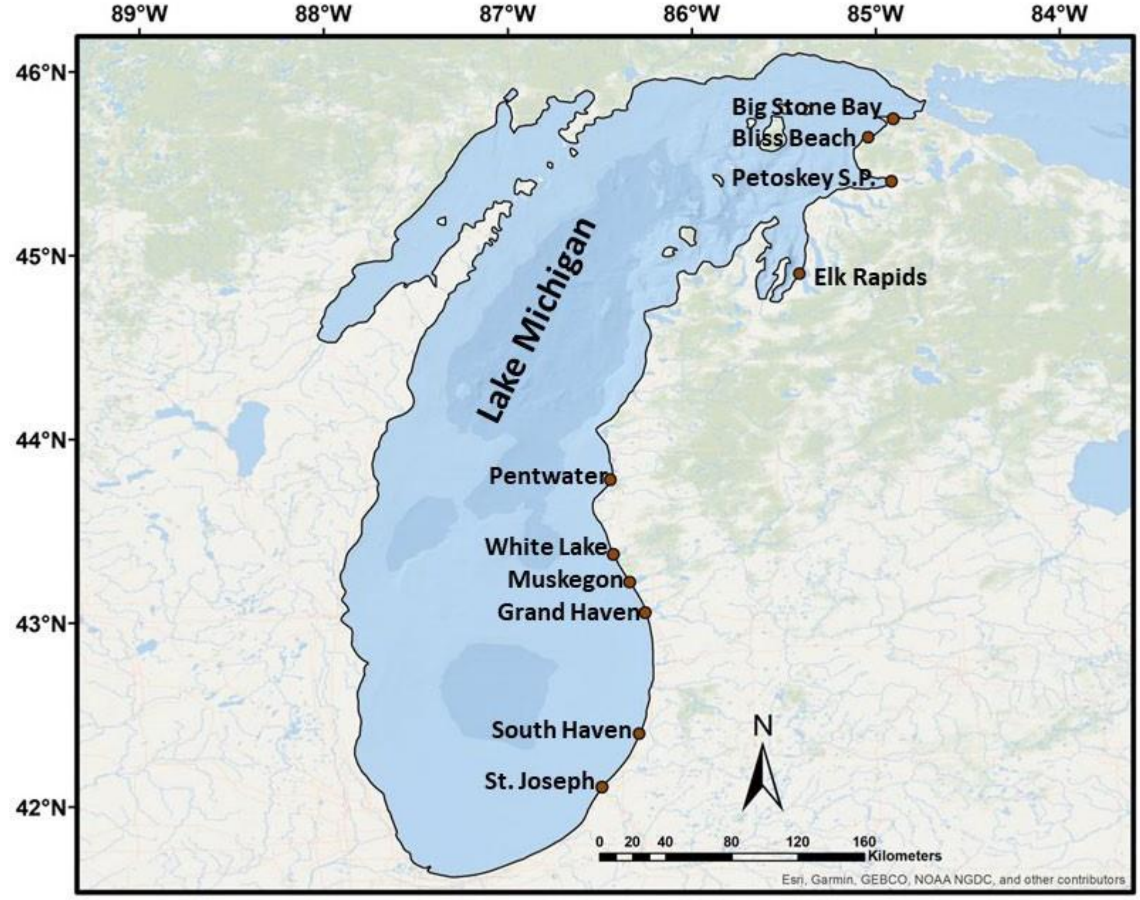

Fig. C1. Location of beach sampling sites in Lake Michigan that were sampled for Lake Whitefish and zooplankton between 2014 and 2021.

Methods

Objective 1: Using archived samples collected by LTBBOI between 2015 and 2019, USGS processed zooplankton samples while diet analyses of larval coregonines (subsequently identified to species with genetics) were completed by Purdue University. The methods are fully described in the 2nd chapter of Cubbage (2021), but are briefly described below.

Larval fish were sampled up to five times between March and June at each site and year, with the exception of Elk Rapids not being sampled in 2019. Larvae were sampled using a 1 x 2 m, 1000-µm mesh neuston net that was pulled by hand parallel to shore in depths between 0.5 and 1 m. Although larval sampling effort varied across sites and years, the primary intent of our analysis was to identify investigate the diet contents of the larval coregonines that were collected and to compare their diets to concomitant collections of zooplankton collected on the same day and location. In total, 753 larval coregonines were available for diet analyses and subsequent genetic determination of Lake Whitefish versus Cisco. These two species that co-occur in beach nursery habitats are not reliably morphologically distinguished (George et al. 2018). A protocol adapted from George et al. (2018) was used that relies on unique banding patterns of restriction fragment length polymorphisms of the mitochondrial cytochrome c oxidase I (COI) digested with a restriction enzyme (EcoO109I; New England BioLabs).

Zooplankton were sampled using a 0.3-m diameter, 1.5-m long, 60-µm mesh net that was pulled horizontally for 30 m in the water column in about 1 m of water alongside the beach. Exactly where the zooplankton were sampled within the water column varied across years: maintained in the middle during 2015-2017, near the surface in 2018 (paired samples near the bottom were unable to be processed owing to high levels of sedimentation), and in a sinusoidal pattern in 2019. Despite these differences, we assume that the zooplankton distribution is relatively uniform within the water column within this shallow depth.

The key analysis was diet selectivity for five major prey groups [copepod nauplii, cyclopoid copepod adults, cyclopoid copepodites, calanoid copepods (included copepedite and adult stages), and cladocerans] using Chesson’s Alpha (Chesson 1978), which ranges between 0 (complete avoidance) and 1 (complete preference).

Objective 2: USGS sampled larval coregonines on beaches by using two different gears. From 16 March 2021 to 21 April 2021, we used a 500-µm mesh neuston net (1 m x 2 m opening) pulled by two people in ~0.5 m of water for 61 m. Two replicate neuston tows were collected on each date. Larvae were preserved with ethanol upon capture and subsequently identified as coregonine, enumerated, and measured using a dissecting microscope. In between each tow, the concomitant zooplankton community was sampled by one person pulling a 0.3-m diameter, 0.9-m long, 60-µm mesh net for 15 m (50 feet).

From 29 April 2021 to 27 May 2021, we used a 45.7 m (150 foot) bag seine (height = 1.83 m; mesh = 3.18 mm) that was extended in an arc out from the shoreline. Specifically, we 1) anchored one end of the seine to the shoreline, 2) extended the net to its full length perpendicular to the shoreline, and 3) swept the offshore end of the net back to the shoreline in an arc. Up to two samples were collected at each beach site each week. Larval and juvenile coregonines were preserved in ethanol, and subsequently identified as coregonine, enumerated, and measured using a dissecting microscope. Zooplankton samples were collected in the same way as previously described.

On each day of sampling, water temperature, conductivity (us/cm), and pH were also measured at each site.

In the laboratory, larval fish were sorted out from other zooplankton or sediments. Under a dissecting microscope, larvae were identified to genus using Auer (1982) and enumerated. The same genetic protocol as in Objective 1 (adapted George et al. 2018) was used to determine whether coregonine larvae were Lake Whitefish or Cisco.

Results and Discussion

Objective 1 (Derived from Cubbage 2021):

The zooplankton community composition on the beaches where larval coregonines were sampled did not markedly vary among years, but showed some differences across the four sites. Copepod nauplii and adult calanoid copepods were generally most abundant. Interestingly, this community composition was different than what was described along southern Lake Michigan beaches concomitant with larval coregonine seining: copepod nauplii were still abundant, but other numerically dominant zooplankters were cyclopoid copepods and cladocerans (Pothoven 2020). In general, cyclopoid copepods have declined in the offshore waters of Lake Michigan (Barbiero et al. 2019) and while they still may be abundant in nearshore areas of southern Lake Michigan (see Pothoven 2020), they appear to be rare in nearshore regions of northern Lake Michigan.

Larval coregonine densities peaked in May in most years, associated with water temperatures ranging 8-11°C. For the 583 larvae that still had sufficient genetic material to be able to assign species, 74% were Lake Whitefish, 25% were Cisco, and <1% were putative hybrids between Cisco and Lake Whitefish. The Ciscoes tended to be captured at its highest densities at the Elk Rapids site and, from a temporal perspective, earlier in the spring than Lake Whitefish. Notably, Cisco larvae were present at all sites in at least one year.

Once yolk-sacs were absorbed, very few coregonine larvae had empty stomachs: <5% of Lake Whitefish and 3% of Cisco. The amount of food in the stomachs increased with increased larval size for both species. Selectivity did not vary between the species when data were pooled across sites and years. The highest selectivity (>0.4) for both species were calanoid copepods (adults and copepodites) and adult cyclopoid copepods. This result is consistent with what Pothoven and Olds (2020) reported for larval and juvenile Lake Whitefish in Lake Huron. For the other three prey types (e.g., cyclopoid copepodites, cladocerans, copepod nauplii), the selectivity was very close to 0 (i.e., <0.03). Several studies, even some outside the Great Lakes, have reported high diet consumption, or even selectivity, for cyclopoid copepods by larval whitefishes (e.g., Johnson et al. 2009; Anneville et al. 2011; Hoyle et al. 2011; Pothoven 2020).

With regards to the hypothesis that declining lake productivity is reducing growth and survival of Lake Whitefish larvae, support from recent work has been somewhat equivocal. In support of this hypothesis, cyclopoid copepods appear to be important prey items for Lake Whitefish larvae, yet cyclopoid copepod densities have generally been declining with lake productivity (Barbiero et al. 2019). The extremely low frequency of empty stomachs reported by Cubbage (2021), however, is not consistent with reduced growth or survival as a key mechanism. Additional work that can estimate daily growth rates at sites along gradients of primary and secondary production could help clarify whether larval Lake Whitefish have been affected by declining lake productivity in Lakes Michigan and Huron. One recent study in Lake Huron reported slower growth rates in 2017-2021 than in 1976-1986, consistent with reduced productivity in the 2000s following the establishment of dreissenid mussels (Cunningham and Dunlop 2023).

For Objective 2, all sampled coregonines were genetically confirmed to be Lake Whitefish. Catch per net haul of Lake Whitefish larvae sampled in both net types was always higher at South Haven than at St. Joseph (Fig. C2). Whether this difference was due to the more northerly latitude of South Haven (~ 37 km farther north) or due to other spawning habitat characteristics in the nearby areas is not clear. The most southern beach routinely sampled by Pothoven is Grand Haven, which is about another 70 km north of South Haven. When comparing our catches in 2021 to the median catches of all of Pothoven's data from 2014-2021 for a given 10-day period, it appears that South Haven could provide above average catches of Lake Whitefish along its beaches. Conversely, the catches in St. Joseph generally fell below the median (Fig. C2).

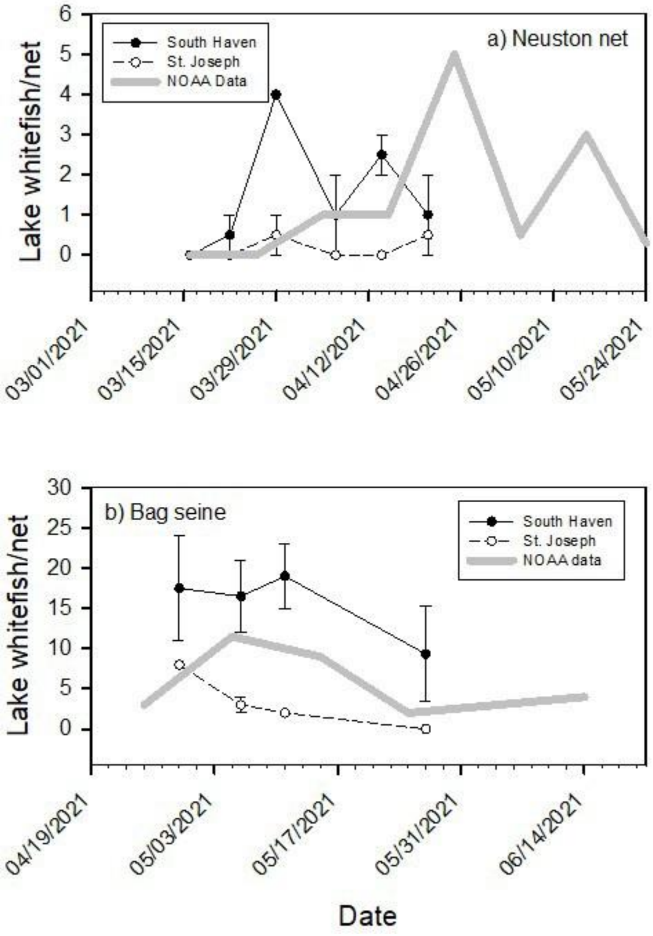

Fig. C2. Number of Lake Whitefish caught per net haul on the beaches of South Haven and St. Joseph MI. Panel a) shows the catches in a neuston net in the early spring. Panel b) shows the catches in a bag seine in later spring. In both plots, the median catches from NOAA in south-central Michigan from 2014-2021 are shown to provide context (Pothoven, unpublished data).

The usefulness of towing a neuston net in the shallow beaches to index Lake Whitefish recruitment is uncertain. On the one hand, it is much easier to sample than the large and sometimes unwieldy bag seine. Furthermore, in our very limited sampling, there was some suggestion that higher larval densities in the neuston net at South Haven could predict higher juvenile densities in the bag seine. On the other hand, catches in the neuston net were very low in 2021, with the highest average catch being only 4. In fact, in the 23 neuston samples, we only caught 20 putative Lake Whitefish larvae. Likewise, Pothoven only captured 9 putative Lake Whitefish larvae in 24 neuston samples at Muskegon in 2021. We recommend comparisons of neuston vs bag seine data collected by other agencies (e.g., LTBBOI, Michigan Department of Natural Resources) in other years to determine whether this easier sampling method is predictive of at least bag seine densities.

The greatest usefulness of the bag seine in 2021 is that is provided far more putative Lake Whitefish larvae for subsequent laboratory evaluation of key parameters, such as diets or growth rate. For example, in 14 seine hauls, we caught 150 putative Lake Whitefish in 2021. Whether the higher number of fish (and non-zero tows) is predictive of relative year-class strength within a given Lake Whitefish management unit also will require analysis of longer time series of data that could be coupled with fishery-dependent indices of year-class strength.

Acknowledgements

We are grateful for the efforts of Lindsie Egedy, Darren Kirkendall, and Josh Hug in both the field collections and in the laboratory in 2020-2022. Thanks to Patty Dieter for creating Figure C1.

References

Anneville, O., Berthon, V., Glippa, O., Mahjoub, M-S, Molinero, JC, and Souissi, S. 2011. Ontogenetic dietary changes of whitefish larvae: insights from field and experimental observations. Env. Biol. Fishes **91**:27–38.

Auer, N.A. 1982. Identification of larval fishes of the Great Lakes basin with emphasis on the Lake Michigan drainage. Great Lakes Fish. Comm. Spec. Pub. 82-3.

Baldwin, N.A., Saalfeld, R.W., Dochoda, M.R., Buettner, H.J., Eshenroder, R.L., and O’Gorman, R. 2018. Commercial fish production in the Great Lakes 1867–2015. Great Lakes Fishery Commission, Ann Arbor, Michigan

Barbiero, R.P., Rudstam, L.G., Watkins, J.M., and Lesht, B.M. 2019. A cross-lake comparison of crustacean zooplankton communities in the Laurentian Great Lakes, 1997–2016. J. Gt. Lakes Res. **45**(3): 672–690

Chesson, J. 1978. Measuring preference in selective predation. Ecology **59**: 211-215.

Cubbage, M.L. 2021. Impacts of zooplankton abundance and community composition on larval fish habitat quality and larval coregonid diets. Master’s thesis. Purdue University.

Cunningham K.E., and Dunlop, E.S. 2023. Declines in lake whitefish larval densities after dreissenid mussel establishment in Lake Huron. J. Great Lakes Res. https://doi.org/10.1016/j.jglr.2022.12.015

Gobin, J., Duncan, A.T., and Lauzon, R. 2022. Saugeen Ojibway Nation community input and action: Initiating a Two-Eyed Seeing approach for dikameg (*Coregonus clupeaformis*) in Lake Huron. J. Gt. Lakes Res. https://doi.org/10.1016/j.jglr.2022.10.010

Ebener, M., Dunlop, E.S., and Muir, A. 2021. Declining recruitment of lake whitefish to fisheries in the Laurentian Great Lakes: Management Considerations and Research Priorities. Great Lakes Fish. Comm. Misc. Pub. 2021-01. http://www.glfc.org/pubs/misc/2021-01.pdf

George, E.M., Hare, M.P., Crabtree, D.L., Lantry, B.F., and Rudstam, L.G. 2018. Comparison of genetic and visual identification of cisco and lake whitefish larvae from Chaumont Bay, Lake Ontario. Can. J. Fish. Aquat. Sci. 75: 1329–1336.

Hoyle J.A., Johannsson O.E., and Bowen K.L. 2011. Larval lake whitefish abundance, diet and growth and their zooplankton prey abundance during a period of ecosystem change on the Bay of Quinte, Lake Ontario. Aquat. Ecosyst. Health Manage. **14**: 66–74.

Johnson J.H., McKenna J.E., Chalupnicki M.A., Wallbridge T., and Chiavelli R. 2009. Feeding ecology of lake whitefish larvae in eastern Lake Ontario. J. Gt. Lakes Res. **35**: 603–607.

Madenjian, C.P., Pothoven, S.A., Schneeberger, P.J., Ebener, M.P., Mohr, L.C., Nalepa, T.F., and Bence, J.R. 2010. Dreissenid mussels are not a “dead end” in Great Lakes food webs. J. Gt. Lakes Res. J. Gt. Lakes Res. **36**: 73–77.

Pothoven, S.A. 2020. The influence of ontogeny and prey abundance on feeding ecology of age-0 Lake Whitefish (*Coregonus clupeaformis*) in southeastern Lake Michigan. Ecol. Freshw. Fish **29**: 103-111.

Pothoven, S.A., and Olds, C. 2020. Spatial variation in feeding ecology of age-0 lake whitefish *Coregonus clupeaformis* in Lake Huron J. Freshw. Ecol. **35**: 349-366.

Subproject D: Exploring the bottleneck for larval alewife

[a]Bunnell, D.B., [a]Dieter, P.M., [b]Hoffman, J.C, [b]Lepak, R.F., [a]Ackiss, A.S., and [c]Berry, N.L.

[a]U.S. Geological Survey Great Lakes Science Center, Ann Arbor, MI 48105 USA

[b]U.S. Environmental Protection Agency Office of Research and Development, Duluth, MN 55804 USA

[c]Miami University, Department of Biology, Oxford, OH 45056 USA

Overview

Alewife (*Alosa pseudoharengus*) are the most consumed prey fish by salmonines in Lake Michigan (Jacobs et al. 2013). Following the collapse of Alewife in Lake Huron in the early 2000s, owing to both excessive predation and declining lake productivity (Kao et al. 2016), fishery managers in Lake Michigan have sought to adjust salmonine stocking to prevent a similar collapse in their lake (Tsehaye et al. 2014). Furthermore, for 2020 CSMI, managers prioritized improved understanding of a potential bottleneck that limits survival of Alewife at the larval stage (see https://greatlakescsmi.org/publications/2021-csmi-lake-michigan-prospectus/). Mortality due to starvation has been hypothesized as a key driver of this potential bottleneck given their relatively small size after hatching and declining lake productivity (Miller et al. 1988; Bunnell et al. 2018).

The proposed 2020 CSMI research built upon the 2015 CSMI results that revealed larval alewife growth rates were at least 40% lower than rates measured in 1989-1992, 2001-2002, and 2006 (Eppehimer et al. 2019). Consistent with slower growth, 67% of the alewife larvae whose diets were analyzed in 2015 were empty; when prey items were observed, the larvae of invasive dreissenid mussels (known as veligers) were the most frequent diet item and its nutritional value remains unknown (Eppehimer et al. 2019). Since 2015, a new hypothesized mechanism has emerged that could affect the vertical distribution and survival of larval alewife- UV radiation exposure (Bunnell et al. 2021). In their native range along the Atlantic coast, alewife spawn in tributaries that likely have low water transparency and limited UV exposure for incubating eggs and emerging larvae. In their introduced range in Lake Michigan, spawning occurs in the tributaries but also along the beaches of Lake Michigan. Larvae born in Lake Michigan can be advected into offshore waters, where UV exposure may have increased in the last 20 years concomitant with the doubling of water transparency as measured by Secchi disk depth. Given that alewife larvae have limited pigmentation to offer protection, detrimental UV effects could be contributing to reduced larval survival in this changing ecosystem.

Hence for 2020 (delayed until July 2021), USGS Great Lakes Science Center and EPA Great Lakes Toxicology and Ecology Division (GLTED) designed and completed a lakewide larval fish survey that expanded the 2015 spatial coverage and added new vertical sampling to investigate the UV hypothesis. The survey focused on maximizing spatial coverage during July when alewife larvae are present, but because sampling was not repeated through time it is likely that some of the larval hatch could have been earlier or later.

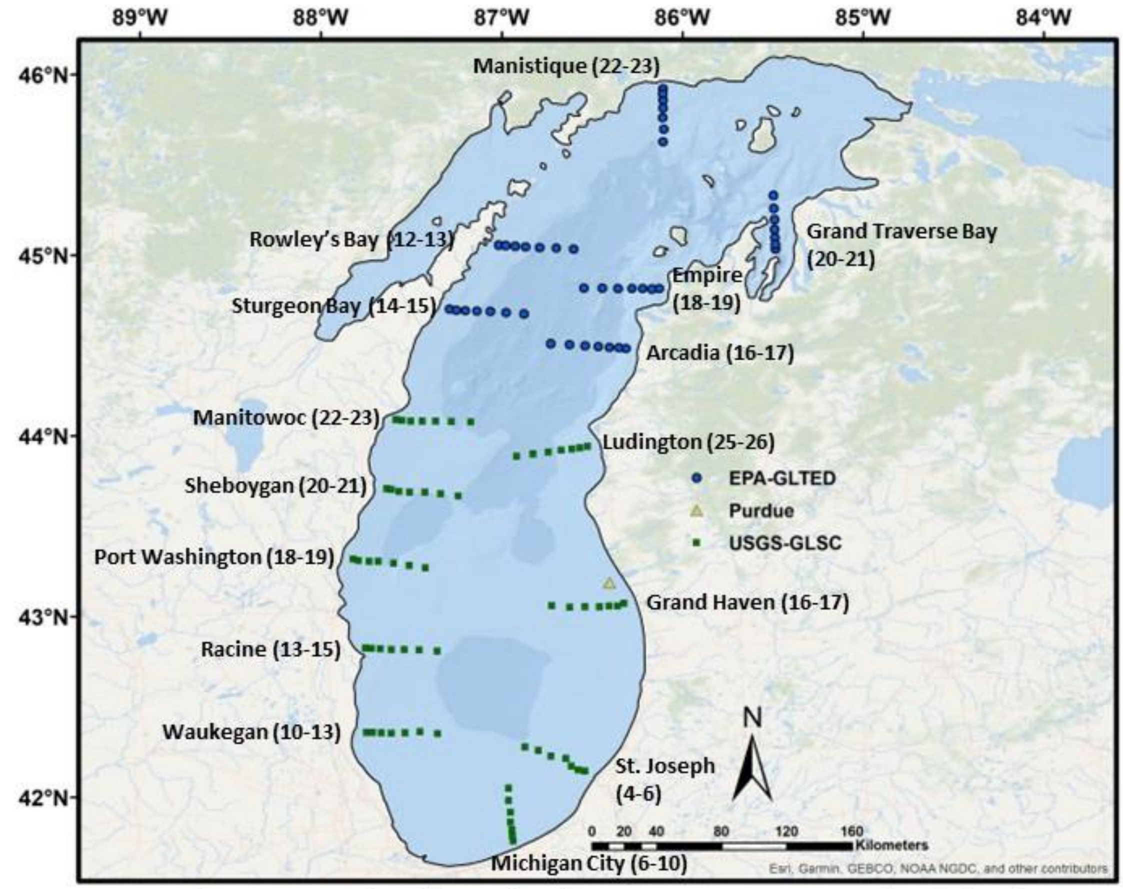

Figure D1. Sampling sites completed during the July 4-26, 2021 cruise targeting larval Alewife. U.S. Geological Survey Great Lakes Science Center (USGS-GLSC) sampling occurred July 4-26 along the 9 transects indicated by green squares. Environmental Protection Agency Great Lakes Toxicology and Ecology Division (EPA-GLTED) occurred July 12-23 along the 6 transects indicated by blue circles. The yellow triangle just north of the Grand Haven transect represents the area sampled weekly (June-August) by Purdue University for a complementary research project funded by the Great Lakes Fishery Trust. Each transect is labeled with the July dates of sampling indicated within the parentheses.

Methods

From 4-26 July 2021 during daytime hours, 15 transects around Lake Michigan were sampled by the R/V Lake Explorer 2 and R/V Sturgeon. Specifically, nine of the transects in the southern half of the lake were completed by the R/V Sturgeon from July 4-26, while the other six transects in the northern half were completed by the R/V Lake Explorer 2 from July 12-23 (Fig D1). Seven sites were sampled along each transect based on distance from shore: 5, 8, 12, 17, 23, 30, and 38 km. At each site, vertical profiles were recorded to estimate temperature, UV, and fluorescence at 1 m intervals. The profiles were analyzed upon retrieval to estimate the depth of 1% UV (i.e., the depth at which the UV radiation was 1% of the value measured at the surface) and the thermocline.

Larval fish were sampled in three vertical layers at each site- first, a surface tow representing the highest UV exposure; second, a 1% UV tow targeting a region of lower UV exposure; third, an oblique tow targeting a region of putatively no UV exposure. The surface tow was sampled with a neuston net (500-µm mesh, 1 m x 2 m opening) for 10 min, outfitted with a flowmeter to calculate distance of the tow. The 1% UV tow sampled from the 1% UV depth up to 2 m below the surface using a rectangular ichthyoplankton net (500-µm mesh, 1.4 m X 1.85 m opening) equipped with a flowmeter; the duration of this tow ranged 10-12 min and was fished obliquely targeting 3-4 depths within this vertical layer. The third, final oblique tow (herein “no UV”) targeted a region from 20 m below the thermocline up to the 1% depth with the same net that was used for the 1% UV tow; the duration of this tow was 12-14 min and targeted layers at ~5 m increments. We note that the oblique tow was not a closing net so that some fish from the upper layers could have been collected during the ~30 seconds that the nets was retrieved from its final targeted layer.

Zooplankton were also sampled to coincide with two of the vertical layers with a 0.5 m diameter, 64-µm mesh net. Unlike the oblique larval fish tow, this zooplankton net could be closed at discrete depths by deploying a messenger. One sample covered the no UV region whereas the other sample began at the 1% UV layer and continued to the surface. No surface zooplankton tow was collected, so we had to assume that the 1% UV layer was representative of the surface zooplankton. These samples were transferred to GLTED where they oversaw processing.

In the laboratory, larval fish were first sorted from all other plankton preserved in the sample. Individual fish were then identified into one of the following categories based on characteristics of the anal location and the number of pre- and post-anal myomeres as described in Auer (1982): Alewife, Rainbow Smelt (*Osmerus mordax*), Burbot (*Lota lota*), Yellow Perch (*Perca flavescens*), Deepwater Sculpin (*Myoxocephalus thompsonii*), Three-spined Stickleback (*Gasterosteus aculeatus*), Common Carp (*Cyprinus carpio*), unidentified coregonine, unidentified clupeid, unidentified minnow, or unidentified (due to deterioration). The unidentified clupeid category stems from overlap in pre- and post-anal myomere counts for Gizzard Shad (*Dorosoma cepedianum*) and Alewife at smaller, post yolk-sac sizes (e.g., 4-9 mm) and for other sized clupeids whose anal position could not be identified due to damage in the net. For this report, we assume that all unidentified clupeids are Alewife, but to be confirmed one a genetic assay is developed.

From a given sample, the first 30 individuals randomly encountered in each taxon were measured for total length (TL) using imaging software that could account for the common non-linear orientation. Coregonine, Alewife, and unidentified clupeid taxa were individually preserved in small vials for subsequent processing. All other individuals were pooled by taxon in larger vials and archived for future scientists given that delays due to the COVID pandemic resulted in insufficient resources to estimate growth rates or conduct diet analyses to make a complete comparison to 2015 (i.e., Eppehimer et al. 2019).

Genetic analyses were completed to determine species (e.g., Bloater, Cisco, Lake Whitefish, Round Whitefish) for the Coregonine taxon. A total of 816 coregonine larvae were sub-sampled (up to 30 per tow) and dissected to remove tissue for genetic amplification while preserving the stomach and head for potential future diet and growth analyses. A total of 825 samples were run with Gt-seq panel markers (Weidel et al. 2022) mined from restriction site-associated DNA sequencing (Ackiss et al. 2020).

Larval densities for each taxon and tow were estimated by dividing the total count by the volume sampled (m^3), which was calculated as the distance towed (using the flowmeter) and multiplying by the area of the net opening. Larval densities for each taxon at a given site were averaged across the three vertical layers (including zero values where relevant). Larval densities by taxon could then be averaged across sites (N = 7) for a transect average. Likewise, lakewide averages equaled the average of the larval densities across sites (N = 105). Values were always multiplied by 100, such that densities equaled number per $100m^3$. When densities were compared across vertical layers, we first transformed the data by adding the smallest non-zero value ($0.0247/100m^3$) to all density estimates and then calculated a natural log transformation. We then ran a generalized linear model and when densities differed across habitats, we applied the Tukey's Studentized Range test to compare densities in the surface, 1% UV, and no UV habitats.

Results and Discussion

A total of 314 larval fish tows distributed across the 15 transects were completed: 105 surface tows, 104 1% UV tows, and 105 no UV tows. Of the 6367 larval fish counted, 4463 could be identified to species. Of the remaining 1904, 1443 were unidentified coregonines, 195 were unidentified clupeids, 262 were unidentifiable, and 4 were unidentified minnows. Genetic identification was possible for 804 of the 825 individuals that were processed and all of them were Bloater. Hence, we assume that all coregonines are Bloater and note that no Cisco were collected.

Excluding the 262 unidentifiable larvae, the species composition for the July 2021 survey was 64% Alewife, 24% Bloater, 8% Burbot, and 3% Yellow Perch (with the other species summing up to 1%). This composition differed from the July 2015 CSMI survey where Alewife and Bloater were 89% and 4% of the catch, respectively, while Burbot were 3% and Yellow Perch were 2%. The lake wide average larval density for Alewife in 2021 equaled 1.47/100m^3 [standard error (SE) = 0.35], which was more than 3.7 times lower than the 5.45/100m^3 (SE = 2.12) lake wide 2015 average. Conversely, the lake wide average larval density for Bloater in 2021 equaled 0.47/100m^3 (SE = 0.11), which was 2.2 times greater than the 0.21/100m^3 (SE = 0.07) lake wide 2015 average. Below, we focus our results on describing the distribution of Alewife and Bloater given they comprised more than 88% of the identifiable fishes.

Among transects, the two highest mean densities of Alewife were in the northern half of the lake (Fig. D2)- Sturgeon Bay (6.85/100m^3) and Manistique (4.02/100m^3). Mean densities were surprisingly low (i.e., <0.35/100m^3) in the southern half of the lake, especially at Ludington, Racine, St. Joseph, Sheboygan, Port Washington, and Grand Haven; it was notable that densities at Arcadia and Empire were also <0.35/100m^3. In contrast, mean Alewife densities in 2015 were highest in the southeast region of Lake Michigan, with mean density being highest at St. Joseph (26.6/100m^3) when it was sampled July 16-19. One possible explanation for lower densities in the southern basin in 2021 was that Alewife hatched in mid-late June and were no longer vulnerable to the sampling net when we sampled them July 4th (St. Joseph) through the 26th (Ludington). In support of this hypothesis, weekly sampling by Purdue University along a Muskegon transect just north of Grand Haven (Fig D1) revealed the peak density of Alewife were collected June 26-30, 2021 (Les Warren, Purdue University, personal communication, Dec 13, 2022).

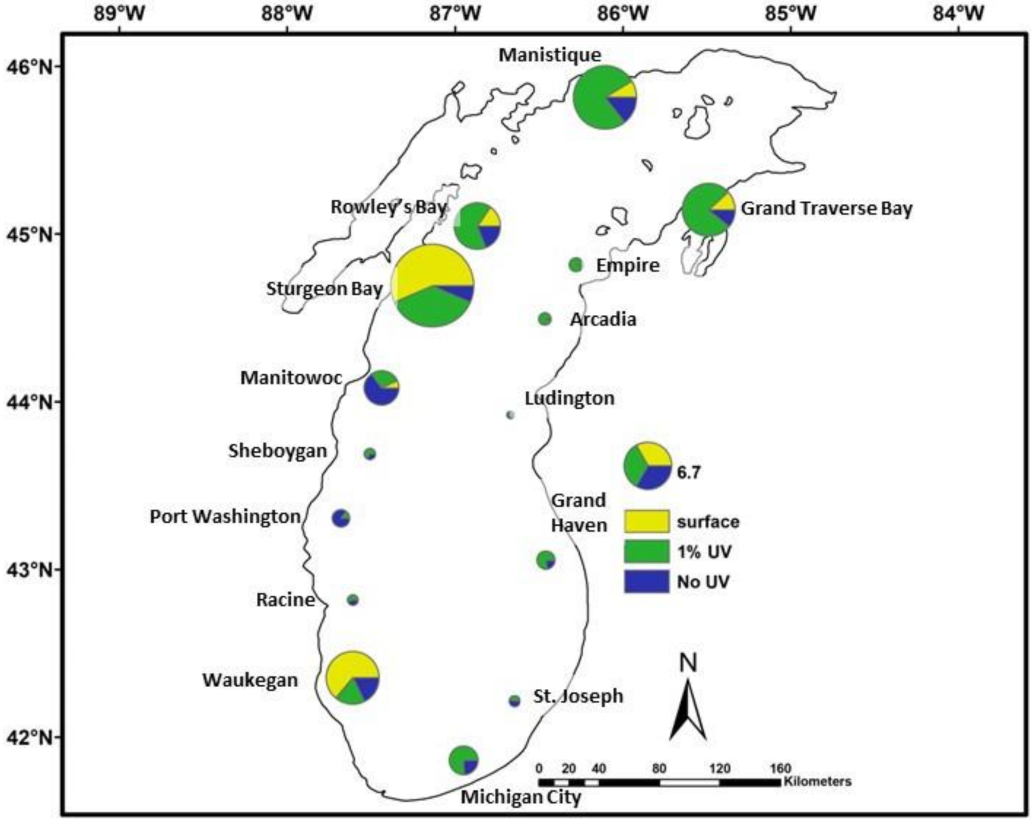

Fig. D2. Mean density of larval Alewife (*Alosa pseudoharengus*) estimated for each of 15 transects sampled once between July 4-26, 2021 in Lake Michigan. The size of the circle is scaled by the mean density (legend size = 6.7/100m^3). The composition of the circle represents the contribution of the density from each of the vertical layers- surface as yellow, 1% ultraviolet (UV) as green, and no UV as blue.

Mean densities of Bloater were more similar across transects (Fig. D3) compared to Alewife. The three highest densities (i.e., > 0.80/100m^3) were throughout the lake- at Arcadia, Manitowoc, and St. Joseph. The transects with the lowest densities (i.e., < 0.05/100m^3) were Grand Traverse Bay (0 caught), Manistique, Empire, and Michigan City. In 2015, when the lake wide average was 2.2 times lower than what we measured in 2021, the only sites with mean densities > 0.30/100m^3 were Saugatuck, St. Joseph, and Racine, but no sites north of Arcadia and Sturgeon Bay were sampled in 2015. Weekly nearshore sampling near Muskegon by Purdue University sampled very few Bloater, but those that were caught were mostly in July (Les Warren, Purdue University, personal communication, Dec 13, 2022).

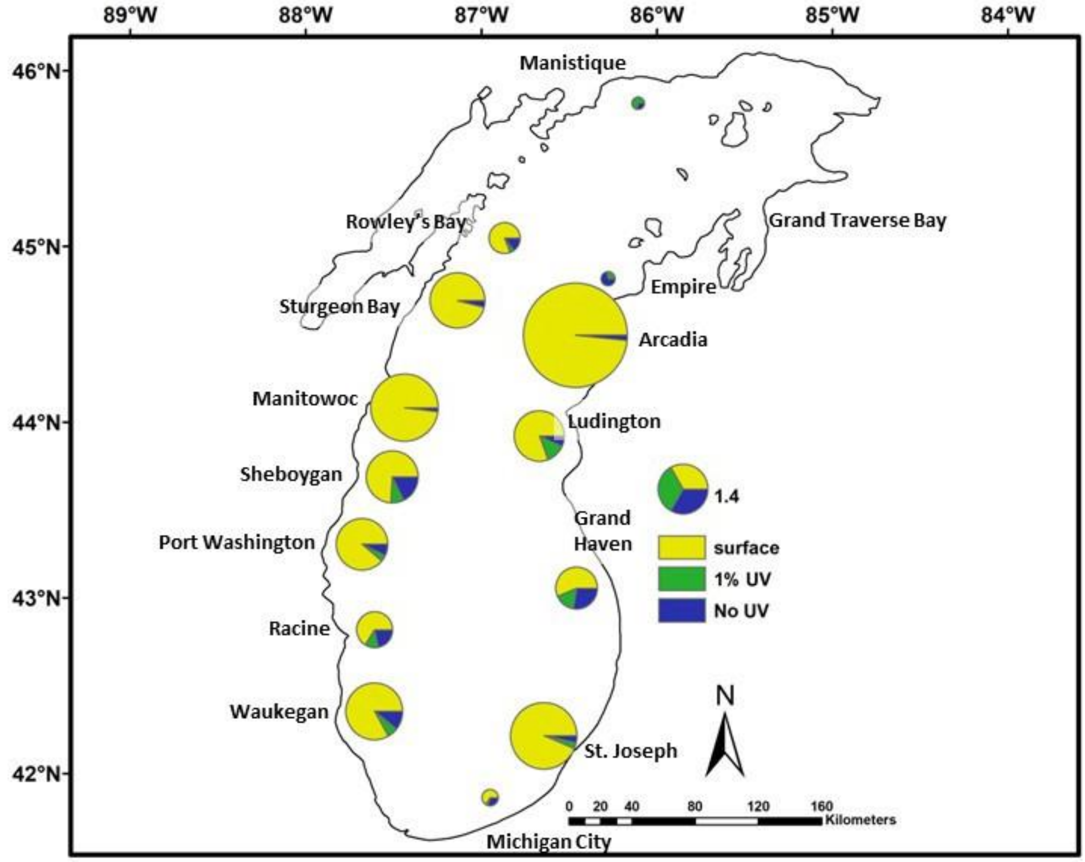

Fig. D3. Mean density of larval Bloater (*Coregonus hoyi*) estimated for each of 15 transects sampled once between July 4-26, 2021 in Lake Michigan. The size of the circle is scaled by the mean density (legend size = 1.4/100m^3). The composition of the circle represents the contribution of the density from each of the vertical layers- surface as yellow, 1% ultraviolet (UV) as green, and no UV as blue.

From a vertical perspective, Alewife densities were highest in 1% UV waters, the next highest in the no UV layer, and the lowest in the surface waters (Fig D4a). In the only comparable published study that sampled larvae in different vertical layers, Nash and Geffen (1991) reported that Alewife larvae in August (when Alewife densities were highest) 1983 in southeast Lake Michigan were more abundant in the epilimnion than in the surface tows. Figure D2 also shows a relatively low proportion of densities from the surface tows (yellow) contributing to the transect averages- with two major exceptions. Among all of the tows, the two with the highest larval Alewife densities were actually at the surface layer for the 17 km site at Sturgeon Bay (68.7/100m^3) and the 5 km site at Waukegan (37.3/100m^3). Examination of the UV irradiance measured at the 1 m depth for these two surface tows revealed them to be among the lowest five irradiance values measured during the survey (Nicole Berry, Miami University, personal communication, January 19, 2023), likely owing to the overcast (Sturgeon Bay) or foggy (Waukegan) weather. The remaining 4 tows with larval Alewife densities exceeding 15/100m^3 were all captured in the 1% UV layers. For Alewife, we had hypothesized that their limited exposure to UV in their native range and their low pigmentation could cause their larvae to either avoid areas in the water column with the highest UV exposure (i.e., the surface) or suffer mortality if they remained in surface waters (Bunnell et al. 2021). Our data were somewhat consistent with this hypothesis, as the Tukey's Multiple Comparison test revealed densities in the surface layer to be the lowest among the three layers. The potentially confounding data, however, were the two surface tows with the highest larval densities. When we investigated the sizes of Alewife larvae caught in the different layers, the modal size was 5 mm TL for all three layers. Mean sizes differed, however, across the three layers with the surface layer having the smallest larvae (7.1 mm TL), no UV larvae being of intermediate size (8.1 mm TL), and 1% UV layer larvae being the largest (9.9 mm TL). Why these mean sizes vary among layers is unclear, but if UV is found to cause mortality it would make sense that only the larger (and older) animals would be below the UV exposure.

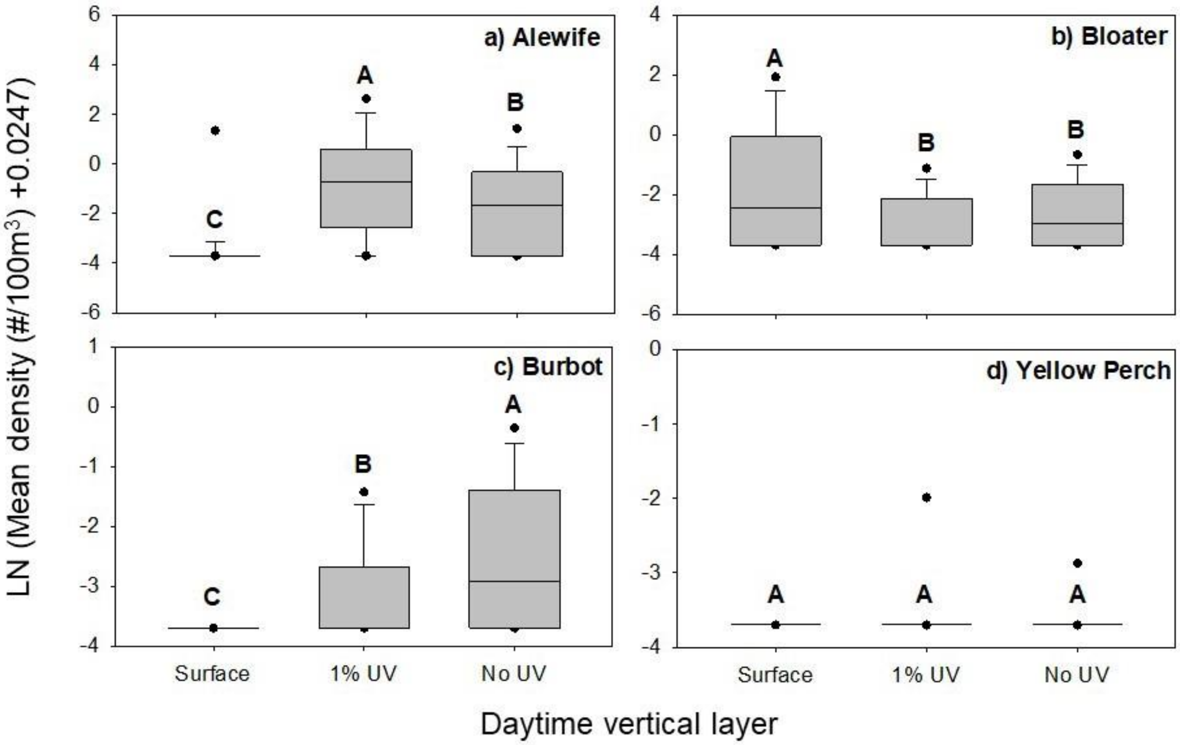

Fig. D4. **Box-whisker plot of the median (center line), 25th and 75th percentiles (as edges of the box), and 5th and 95th percentiles as error bars for the natural-log (LN) transformed density of larval a) Alewife (*Alosa pseudoharengus*), b) Bloater (*Coregonus hoyi*), c) Burbot (*Lota lota*), d) Yellow Perch (*Perca flavescens*) for each daytime vertical habitat layer (ultraviolet = UV) sampled during July 2-26, 2021 in Lake Michigan. Note the scale of the y-axis varies across plots. Letters indicate the results of Tukey's Multiple Comparison test for differences between habitats- different letters indicate differences in mean densities.**

Bloater vertical distribution was opposite (Fig. D4b) from what we observed for Alewife: the densities at the surface were higher than what was measured in the 1% and no UV layers (which did not differ from one another). This pattern is also evident in Fig. D3 with densities from the surface tows (yellow) consistently dominating the proportions in most transects. Our pattern of the highest Bloater densities in the surface matches what was observed in southeastern Lake Michigan in May-September monthly sampling of different layers of the water column in 1983 (Nash and Geffen 1991).

When investigating the size distributions of Bloater that we caught in the different layers, the largest Bloater were caught near the surface and mean size decreased with deeper layers sampled (Fig. D5). The Bloater at the surface were generally at least 20 mm TL and some likely already had metamorphosed to the juvenile stage. The size distributions at the surface were similar to what Rice et al. (1987) reported for surface dwelling Bloater larvae in July 1982 and 1983 offshore of Racine, WI in bottom depths ranging 40-100 m. Likewise, Rice et al. (1987) sampled the smallest larvae (i.e., 8-12 mm TL) only 5-10 m above the bottom during June 1983. Although we did not sample as deep as Rice et al. (1987) our "No UV" samples extended into the upper hypolimnion. Taken together, these patterns indicate that after hatching from the profundal waters, Bloater larvae increasingly achieve greater depths in the water column through ontogeny, up the juvenile stage.

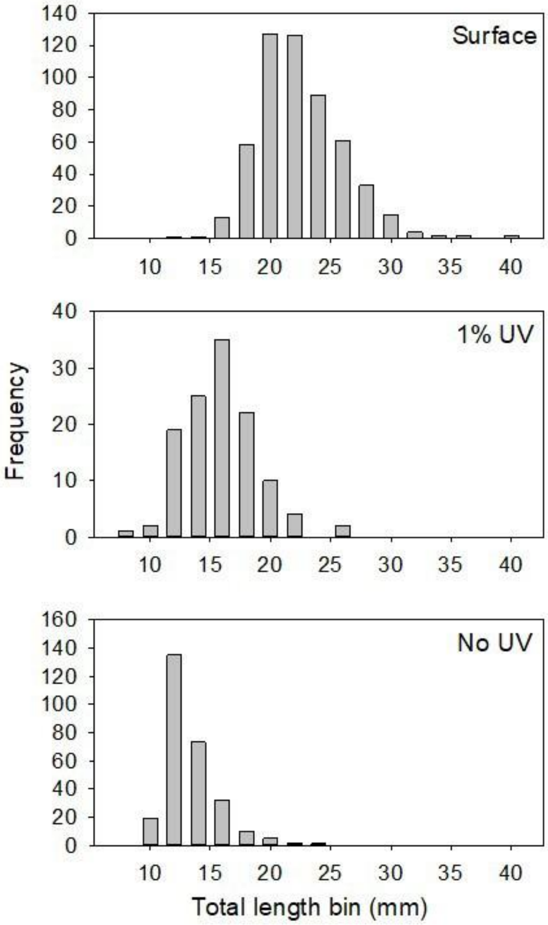

Fig. D5. Size frequency distribution of Bloater (*Coregonus hoyi*) larvae caught in three different vertical layers of the water column during July 2-26, 2021 in Lake Michigan. Note the scale of the y-axis varies across plots.

In terms of horizontal distribution (i.e., distance offshore), the largest mean densities of Alewife were sampled at 5 km from shore, but mean densities remained >1/100m^3 for all sites out to 23 km offshore (Fig. D6a). The highest density among all Alewife samples was at the 17 km Sturgeon Bay surface collection, which increased the variation around the mean at the 17 km site. As found in other studies

(Weber et al. 2015; Eppehimer et al. 2019), some Alewife larvae were advected to even the most offshore sites (mean at 38 km = 0.32/100m^3). The Bloater distribution pattern was generally opposite from Alewife (Fig D6b): the highest densities were sampled at sites ranging from 17-38 km, with the highest mean density occurring at 38 km. The Bloater horizontal distribution was similar to what was reported in Wells (1966) and Rice et al. (1987), and likely a result of Bloater spawning in the deeper regions of Lake Michigan (40 – 110 m depth, Wells 1966; Emery and Brown 1978; Rice et al. 1987).

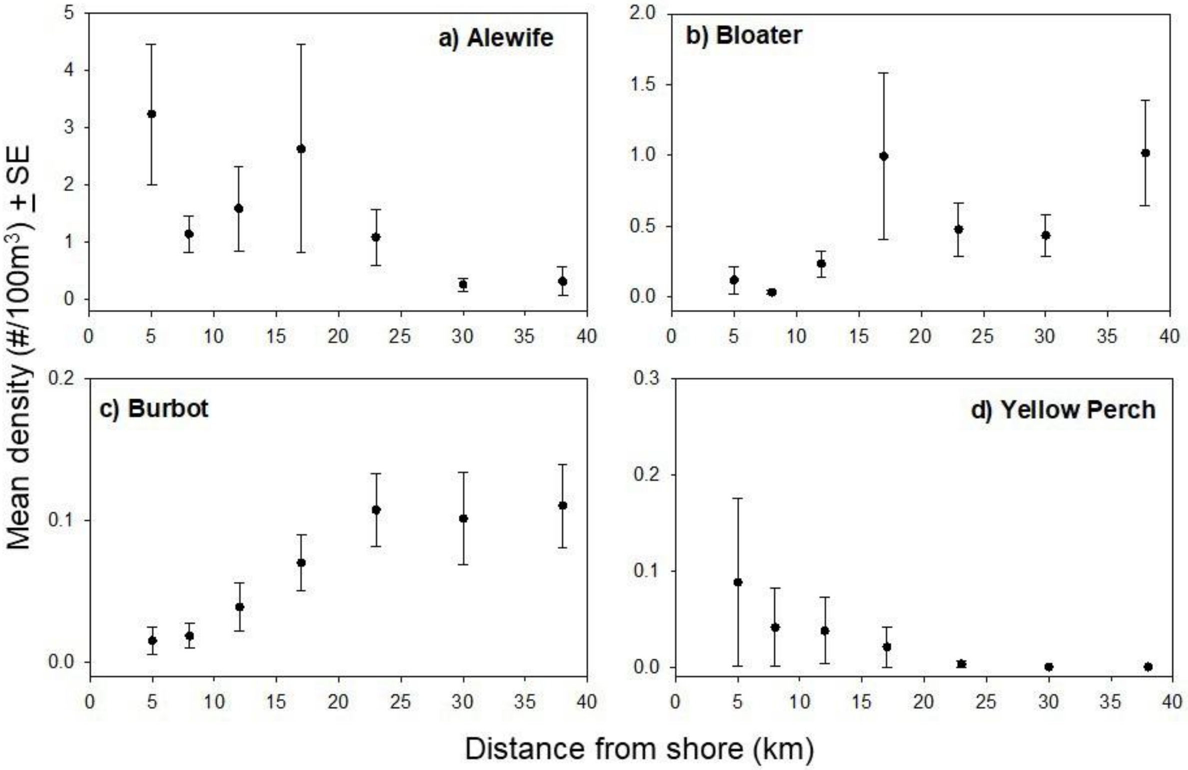

Fig. D6. Mean density of larval a) Alewife (*Alosa pseudoharengus*), b) Bloater (*Coregonus hoyi*), c) Burbot (*Lota lota*), d) Yellow Perch (*Perca flavescens*) estimated for each of the seven distance from shore sites across the 15 transects sampled once between July 4-26, 2021 in Lake Michigan. Note the scale of the y-axis varies across plots.

Finally, we provide a brief summary of the distributions of Burbot and Yellow Perch, the 3rd and 4th most abundant larval species caught. With respect to distance from shore, the distribution of Burbot was similar to what was observed with Bloater- highest densities at the three sites that were sampled farthest from shore (Fig. D6c). Burbot were rarely captured at the sites 5 or 8 km offshore. When

Burbot were captured, their highest densities were in the no UV layer, with the 2nd highest densities in the 1% UV layer and the lowest densities at the surface (Fig. D4c). Hence this pattern was completely opposite from Bloater. For Yellow Perch, their highest densities were sampled closest to shore (Fig. D6d) and the larvae were not advected as far offshore as Alewife (the farthest yellow perch larvae were sampled at 23 km offshore). Had we sampled in June, when Yellow Perch larvae were smaller given that they hatch in May, we may have detected greater offshore advection. When Yellow Perch were captured, their densities were not different among the three vertical layers (Fig. D4d), perhaps as a function of relatively low sample size and limited power to detect potential differences.

In conclusion, our July 2021 lakewide sampling effort provided a snapshot of the distribution primarily for Alewife and Bloater larvae. Key patterns included differences in horizontal (Bloater more offshore and Alewife more nearshore) and vertical (Bloater more concentrated at surface and Alewife more concentrated below the surface where UV exposure was lower) distributions. Compared to July 2015 CSMI, mean densities of July 2021 Alewife were 3.7 times lower. In contrast, compared to July 2015 CSMI, mean densities of Bloater were 2.2 times higher. Whether higher larval densities correspond to higher recruitment success remains to be determined. The high larval Bloater densities in 2021 found in this study were consistent with unusually high densities of putative yearling Bloater sampled during the lakewide 2022 bottom trawl and age-0 Bloater in the 2021 acoustic survey (Tingley et al. 2023). Complementary and ongoing research also suggests Alewife larvae are far less tolerant to UV radiation in the laboratory relative to Bloater and other native coregonine species (Nicole Berry, Miami University, personal communication, April 4, 2023). Whether UV radiation in Lake Michigan has actually increased over the past decade (concomitant with increased water clarity) and could underlie reduced larval Alewife survival in Lake Michigan is not yet known (Bunnell et al. 2021). Furthermore, future research to estimate the diets and growth rates of larval Alewife from 2021 could shed more light on whether the reduced growth rates that were measured in 2015 is reflective of a longer-term shift to slower growth that could reduce larval Alewife survival in an era of reduced pelagic productivity. Finally, for future larval fish surveys, we recommend a design that focuses more on capturing the temporal dynamics (i.e., weekly intervals), even at the expense of reduced spatial coverage. Coupling our results with complementary research by Purdue University revealed that our sampling design likely missed a pulse of earlier hatched Alewife larvae in southern Lake Michigan. Ideally, to best understand recruitment dynamics from an early life history perspective, a multi-agency survey could be developed that would sample larvae weekly between mid-June and the end of July at up to six sites distributed between the western and eastern coastlines of Lake Michigan.

Acknowledgements

We are extremely grateful for the efforts of Lindsie Egedy, Darren Kirkendall, Josh Hug, and Katie Anweiler in either field collections or in the laboratory. We appreciate the excellent seamanship from the vessel crews of the R/V Sturgeon (Joe Bergan, Lyle Grivicich, and Kris Bunce) and R/V Lake Explorer 2.

References

Ackiss, A.S., Larson, W.A., and Stott, W. 2020. Genotyping-by-sequencing illuminates high levels of divergence among sympatric forms of coregonines in the Laurentian Great Lakes. Evol. App. **13**: 1037-1054.

Auer, N.A. 1982. Identification of larval fishes of the Great Lakes basin with emphasis on the Lake Michigan drainage. Great Lakes Fishery Commission Special Publication 82-3.

Bunnell, D.B., Carrick, H.J., Madenjian, C.P., Rutherford, E.S., Vanderploeg, H.A., Barbiero, R.P., Hinchey-Malloy, E., Pothoven, S.A., Riseng, C.M., Claramunt, R.M., Bootsma, H.A., Elgin, A.K., Rowe, M.D., Thomas, S.M., Turschak, B.A., Czesny, S., Pangle, K.L., Warner, D.M., and Warren, G.J. 2018. Are changes in lower trophic levels limiting the capacity of prey fish biomass in Lake Michigan? Great Lakes Fishery Commission Special Publication 2018-01.

Bunnell, D.B., Ludsin, S.A., Knight, R.L., Rudstam, L.G., Williamson, C.E., Höök, T.O., Collingsworth, P.D., Lesht, B.M., Barbiero, R.P., Scofield, A.E., Rutherford, E.S., Gaynor, L., Vanderploeg, H.A., and Koops, M.A. 2021. Consequences of changing water clarity on the fish and fisheries of the Laurentian Great Lakes. Can. J. Fish. Aquat. Sci. **78**: 1524-1542.

Emery, L., and Brown, E.H. 1978. Fecundity of the bloater (*Coregonus hoyi*) in Lake Michigan. Trans. Am. Fish. Soc. **107**: 785– 789.

Eppehimer D.E., Bunnell D.B., Armenio P.M., Warner D.M., Eaton L., Wells D.J., and Rutherford E.S. 2019. Densities, diets, and growth rates of larval Alewife and Bloater in a changing Lake Michigan ecosystem. Trans. Am. Fish. Soc. **148**: 755–770.

Jacobs, G.R., Madenjian, C.P., Bunnell, D.B., Warner, D.M., and Claramunt, R.M. 2013. Chinook salmon foraging patterns in a changing Lake Michigan. Trans. Am. Fish. Soc. **142**: 362–372

Miller T.J., Crowder L.B., Rice J.A., and Marschall E.A. 1988. Larval size and recruitment mechanisms in fishes: toward a conceptual framework. Can. J. Fish. Aquat. Sci. **45**(9): 1657–1670.

Nash R.D.M. and Geffen A.J. 1991. Spatial and temporal changes in the offshore larval fish assemblage in southeastern Lake Michigan. J. Gt. Lakes Res. **17**(1): 25–32.

Kao Y.C., Adlerstein S.A., and Rutherford E.S. 2016. Assessment of top-down and bottom-up controls on the collapse of alewives (*Alosa pseudoharengus*) in Lake Huron. Ecosystems, **19**: 803–831.

Rice, J.A., Crowder, L.B., and Holey, M.E. 1987. Exploration of mechanisms regulating larval survival in Lake Michigan bloater: a recruitment analysis based on characteristics of individual larvae. Trans. Am. Fish. Soc. **116**: 703–718.

Tingley III, R.W., Warner, D.M., Madenjian, C.P., Dieter P.M., Turschak, B., and Hanson, D. 2023. Status and trends of pelagic and benthic prey fish populations in Lake Michigan, 2022. Great Lakes Fishery Commission, Ypsilanti, MI.

Tsehaye, I., Jones, M.L., Brenden, T.O., Bence, J.R., and Claramunt, R.M. 2014. Changes in the salmonine community of Lake Michigan and their implications for predator–prey balance. Trans. Am. Fish. Soc. **143**: 420– 437

Weber M.J., Ruebush B.C., Creque S.M., Redman R.A., Czesny S.J., Wahl D.H., and Dettmers J.M. 2015. Early life history of Alewife *Alosa pseudoharengus* in southwestern Lake Michigan. J. Gt. Lakes Res. **41**: 436–447.

Weidel, B. C., Ackiss, A. S., Chalupnicki, M. A., Connerton, M. J., Davis, S., Dettmers, J. M., ... & LaPan, S. R. (2022). Results of the collaborative Lake Ontario bloater restoration stocking and assessment, 2012–2020. Journal of Great Lakes Research, **48**(2), 371-380.

Wells, L. 1966. Seasonal and depth distributions of larval bloaters (*Coregonus hoyi*) in southeastern Lake Michigan. Trans. Am. Fish. Soc. **95**: 388–396.

Subproject E: Synthesizing nearshore to offshore transect data from previous CSMI efforts

Kao, Y-C., Bunnell, D.B., and Dieter, P.M.

U.S. Geological Survey Great Lakes Science Center, Ann Arbor, MI 48105 USA

Overview

Zooplankton surveys conducted by the EPA Great Lakes National Program Office in Lakes Michigan and Huron have been spatially limited to the offshore waters, at stations with (bottom) depths of 89–256 m in Lake Michigan and 52–139 m in Lake Huron (Barbiero et al. 2018a). Data from these surveys showed decreases in the biomass of all major zooplankton groups since the late 1990s (Barbiero et al. 2018b) and these decreases have been attributed to the engineering effects of invasive zebra and quagga mussels (*Dreissena polymorpha* and *D. bugensis*; collectively dreissenid mussels) that have established large colonies during the same period (Mehler et al. 2020, Nalepa et al. 2007). Previous studies have shown that the large biomass and strong filter-feeding ability of the dreissenid mussels could have allowed them to sequester much of the terrestrial nutrient inputs in the nearshore waters, which, in turn, limited the primary productivity in the offshore waters (Cha et al. 2011, Fishman et al. 2009, Hecky et al. 2004, Rowe et al. 2017, Shen et al. 2020). Therefore, although our understanding is still limited, it is generally expected that zooplankton in the nearshore waters (i.e., < 30 m) could be less limited by primary productivity than their offshore counterpart.

In this subproject, our goal is to better understand the nearshore–offshore differences in zooplankton assemblages in Lakes Michigan and Huron. We hypothesized that zooplankton in nearshore and offshore waters are different in biomass and biomass seasonality (i.e., phenology). To evaluate this hypothesis, we used generalized additive mixed models (GAMMs; Wood 2017) to analyze zooplankton data collected from CSMI surveys for Lake Michigan in 2010 and 2015 and for Lake Huron in 2012 and 2017 (Kao et al. 2022). The extensive spatiotemporal coverage of this dataset allowed us to describe the seasonal changes in zooplankton biomass from nearshore to offshore waters and examine the differences. These results can help us better understand the ecosystems of Lakes Michigan and Huron and inform whether stations in nearshore waters (<30 m in depth) should be included in GLNPO surveys to monitor the changes in lower trophic levels.

Methods

Zooplankton data

We used data for 396 zooplankton samples collected by vertical, whole water-column tows in CSMI surveys conducted during the growing season, from late April to early November, in Lake Michigan in 2010 and 2015 and in Lake Huron in 2012 and 2017. These surveys covered a total of 18 transects (Fig. E1). Each transect included two or three stations from nearshore to offshore waters in different depth categories, namely shallow, middle, and deep. The shallow and middle stations have depths of 11–27 m and 40–51 m, respectively, in both lakes. The Lake Huron transects off Thessalon and Spanish did not include a deep station because of the bathymetry. For the other transects, the deep stations have depths of 85–112 m in Lake Michigan and 64–90 m in Lake Huron due to the difference in bathymetry between these two lakes. Details for field sample collection, laboratory sample processing, and quality control and quality assurance of the data are given in a USGS data release (Kao et al. 2022).

For each sample in our data, we estimated zooplankton biomass in dry weight per cubic meter (mg/m^3) by the lowest taxonomic level and life stage as the volumetric density of the organism multiplied by the mean organism weight. The organism density was calculated following the GLNPO standard operating procedures LG403 (EPA 2003) for samples collected in 2010 and the methods described in Eppehimer et al. (2019) for samples collected in 2012, 2015, and 2017. The mean organism weight was calculated based on body length data and published weight–length relationships given in Table E1.

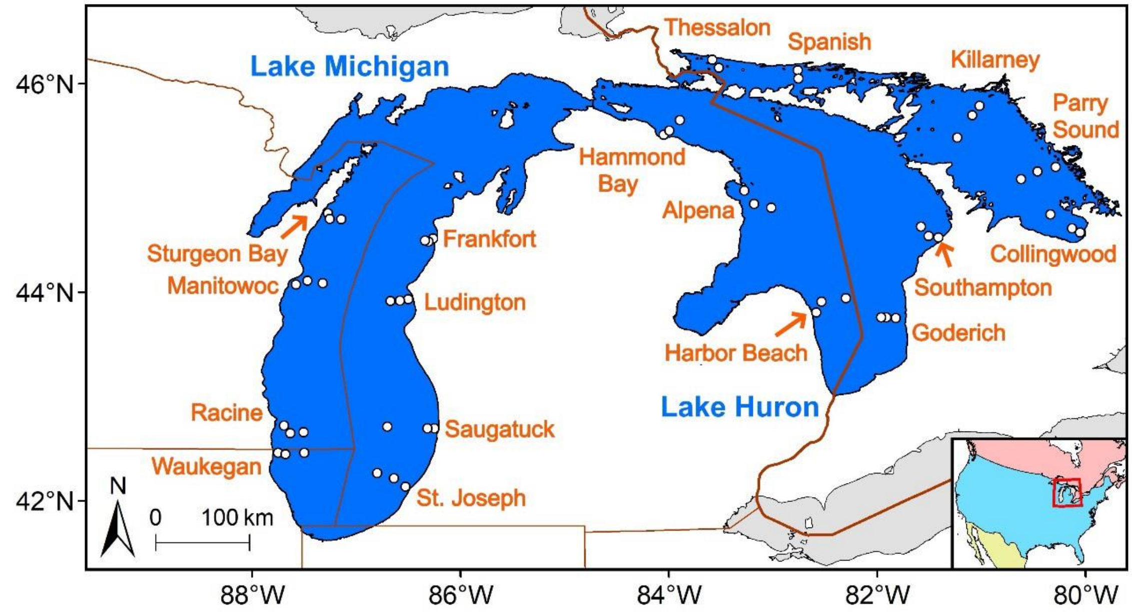

Fig. E1. Zooplankton sampling stations and transects in Lake Michigan in 2010 and 2015 and in Lake Huron in 2012 and 2017.

Table E1. Coefficients in the equation ln(*Weight*) = *a* + *b* × ln(*Length*) relating zooplankton dry weight *Weight* (µg) to body length *Length* (mm).

Group/taxon	*a*	*b*	Source
Non-predatory cladocerans			
Acroperus harpae	1.167	0.85	Dumont et al. (1975)
Alona spp.	2.768	3.84	Dumont et al. (1975)
Bosmina spp.	2.712	2.53	Bottrell et al. (1976)
Chydorus sphaericus	4.543	3.64	Rosen (1981)
Daphnia spp.	1.603	2.84	Dumont et al. (1975)
Diaphanosoma spp.	1.289	3.04	Rosen (1981)
Eubosmina spp.	2.712	2.53	Bottrell et al. (1976)
Eurycercus spp.	2.096	2.26	Dumont et al. (1975)
Holopedium gibberum	2.073	3.19	Persson and Ekbohm (1980)
Macrothrix spp.	2.768	3.84	Dumont et al. (1975)
Predatory cladocerans			
Bythotrephes longimanus	2.83	2.09	Makarewicz and Jones (1990)
Cercopagis pengoi	0.488	2.98	Ojaveer et al. (2001)
Leptodora kindtii	−0.822	2.67	Rosen (1981)
Polyphemus pediculus	2.779	2.15	Rosen (1981)
Calanoids (all taxa)	1.59	2.59	Burgess et al. (2015)
Cyclopoids (all taxa)	1.66	3.97	Rosen (1981)

Days after 4 °C

We used the first (calendar) date when surface water temperature reached 4 °C as a proxy for the peak of spring turnover and the beginning of growing season in Lakes Michigan and Huron. Accordingly, we derived a metric “days after surface water temperature reached 4 °C”, namely D4C, as a measure of time into the growing season. To derive D4C for each sample, we obtained the first date when surface water temperature reached 4 °C (Table E2) from a spatially-explicit database generated by National Oceanic and Atmospheric Administration (NOAA) Great Lakes Environmental Research Laboratory (GLERL) under the program Great Lakes Surface Environmental Analysis (https://coastwatch.glerl.noaa.gov/erddap/griddap/GLSEA_GCS.html). D4C was included in our statistical analysis as a predictor variable to account for the seasonality of zooplankton biomass.

Table E2. The first calendar date when surface water temperature reached 4 °C in each survey station. Data were generated by Great Lakes Surface Environmental Analysis (GLSEA) program and available at https://coastwatch.glerl.noaa.gov/erddap/griddap/GLSEA_GCS.html.

		First calendar date when surface water temperature reached 4 °C		
Year	Transect	Shallow station	Middle station	Deep station
2010	Frankfort	Apr 6	Apr 6	Apr 6
2010	Sturgeon Bay	Apr 6	Apr 6	Apr 6
2012	Hammond Bay	Apr 15	Apr 19	Apr 30
2012	Alpena	Apr 2	Apr 14	Apr 14
2015	Frankfort	May 2	May 7	May 6
2015	Ludington	May 2	May 4	May 5
2015	Saugatuck	Apr 19	Apr 21	May 5
2015	St. Joseph	Apr 11	Apr 25	May 6
2015	Waukegan	Apr 16	Apr 17	Apr 17
2015	Racine	Apr 16	Apr 17	May 9
2015	Manitowoc	May 2	May 6	May 8
2015	Sturgeon Bay	May 9	May 15	May 15
2017	Hammond Bay	Apr 26	Apr 30	May 13
2017	Harbor Beach	Apr 27	Apr 30	May 10
2017	Goderich	Apr 14	Apr 27	Apr 27
2017	Southampton	Apr 13	Apr 21	Apr 26
2017	Collingwood	Apr 25	Apr 25	Apr 26
2017	Parry Sound	Apr 26	Apr 27	May 15
2017	Killarney	Apr 27	May 11	May 16
2017	Spanish	May 2	May 12	–
2017	Thessalon	Apr 25	Apr 28	–

Statistical analysis

In our GAMMs, we used zooplankton biomass as the response variable and included survey year (2010, 2012, 2015, and 2017), station depth (shallow, middle, and deep), and *D4C* as fixed effects, which accounted for the extrinsic drivers associated with climate that could vary across years, the gradient of nutrients from shallow to deep waters, and the seasonality of zooplankton biomass, respectively. To account for their differences in tributary nutrient inputs and bathymetry, we included transects as random effects that could modify the intercepts in our GAMMs.

The GAMMs were fitted to our biomass data of (1) all zooplankton, (2) three major zooplankton groups, and (3) 14 zooplankton taxa of interests. The three major zooplankton groups were cladocerans, calanoids, and cyclopoids. Our 14 taxa of interests included subspecies, species, and species groups that were present in at least 25% of samples. The cladoceran taxa of interests included *Bosmina* spp. (present in 72% of samples), *Bythotrephes longimanus* (59%), *Daphnia galeata mendotae* (52%), and nearshore predatory cladocerans (*Cercopagis pengoi*, *Leptodora kindtii*, and *Polyphemus pediculus*; 28%). The biomass of each cladoceran taxon of interest was of all life stages combined. The calanoid taxa of interests included calanoid copepodites (present in 100% of samples) and adult *Leptodiaptomus minutus* (97%), *L. ashlandi* (96%), *L. sicilis* (82%), *Limnocalanus macrurus* (63%), *Skistodiaptomus oregonensis* (55%), and *Epischura lacustris* (47%). The cyclopoid taxa of interests included cyclopoid copepodites (present in 100% of samples) and adult *Diacyclops thomasi* (91%) and *Tropocyclops prasinus mexicanus* (32%).

We used statistical software (the package “gamm4” version 0.2-6 (Wood and Scheipl 2022) in R version 4.2.2 (R Core Team 2022) for our GAMM fitting. The package used a panelized maximum-likelihood method to estimate parameters. We used the cubic regression spline as the smoothing basis, instead of the default thin plate regression spline in the package, because it less likely overfits the model to the abrupt changes in zooplankton biomass that are unlikely part of annual seasonal cycle. Refer to Wood (2017) for more details about GAMM in practice.

Results and Discussion

Big pictures

Our GAMM revealed remarkable differences in zooplankton biomass and biomass seasonality from nearshore to offshore waters (Fig. E2A; Table E3). With adjustments for interannual differences, the predicted total zooplankton biomass was significantly higher in middle and deep stations than in shallow stations. The predicted total zooplankton biomass in the shallow stations increased after the growing season began until reaching a first peak after around 70 days into the growing season. Then the biomass started to decrease, reached a minimum near day 140, and then started to increase again until the end of the growing season. In the middle and deep stations, however, the biomass increased gradually as the growing season progressed and plateaued after around 100 days into the growing season.

With respect to group-level GAMMs, calanoids showed similar trends of biomass and biomass seasonality from near to offshore waters (Fig. E2; Table E3) as total zooplankton, which was not surprising given that 83% total zooplankton biomass was comprised of calanoids across our samples. Our GAMMs showed that the mean biomass of cladocerans and cyclopoids did not significantly differ across stations from nearshore to offshore waters. However, the predicted biomass seasonality of cladocerans and cyclopoids was similar to that of calanoids, except that no clear seasonal trends of cyclopoid biomass were predicted in middle and deep stations.

For a basis of comparison, we referred to the overall pattern of biomass trends and biomass seasonality of calanoids from nearshore to offshore waters as the “calanoid pattern” (Fig. E2C). This basis was chosen because the majority of zooplankton biomass was comprised of calanoids and the same overall pattern was also revealed in the GAMM of total zooplankton biomass. This overall pattern highlights that (1) predicted mean standing biomass would be higher in offshore waters than in nearshore waters, (2) a “late-summer minimum” of biomass would occur in the nearshore waters when D4C was around 140 days, and (3) the biomass would increase and become “plateaued” in offshore waters until the end of the growing season. As shown in Fig. E3, the biomass seasonality revealed in our group- and taxon-level GAMMs could be categorized into five major patterns. In addition to “late-summer minimum” and “plateaued” described earlier, these five major patterns of biomass seasonality also included “decreasing” which means that the biomass was decreasing throughout the growing season, “summer maximum” which means that a unimodal biomass maximum occurred in summer, and “no trend” which means that the biomass varied little throughout the growing season. In the following sections, we examined whether the calanoid pattern was revealed in each taxon-level GAMM.

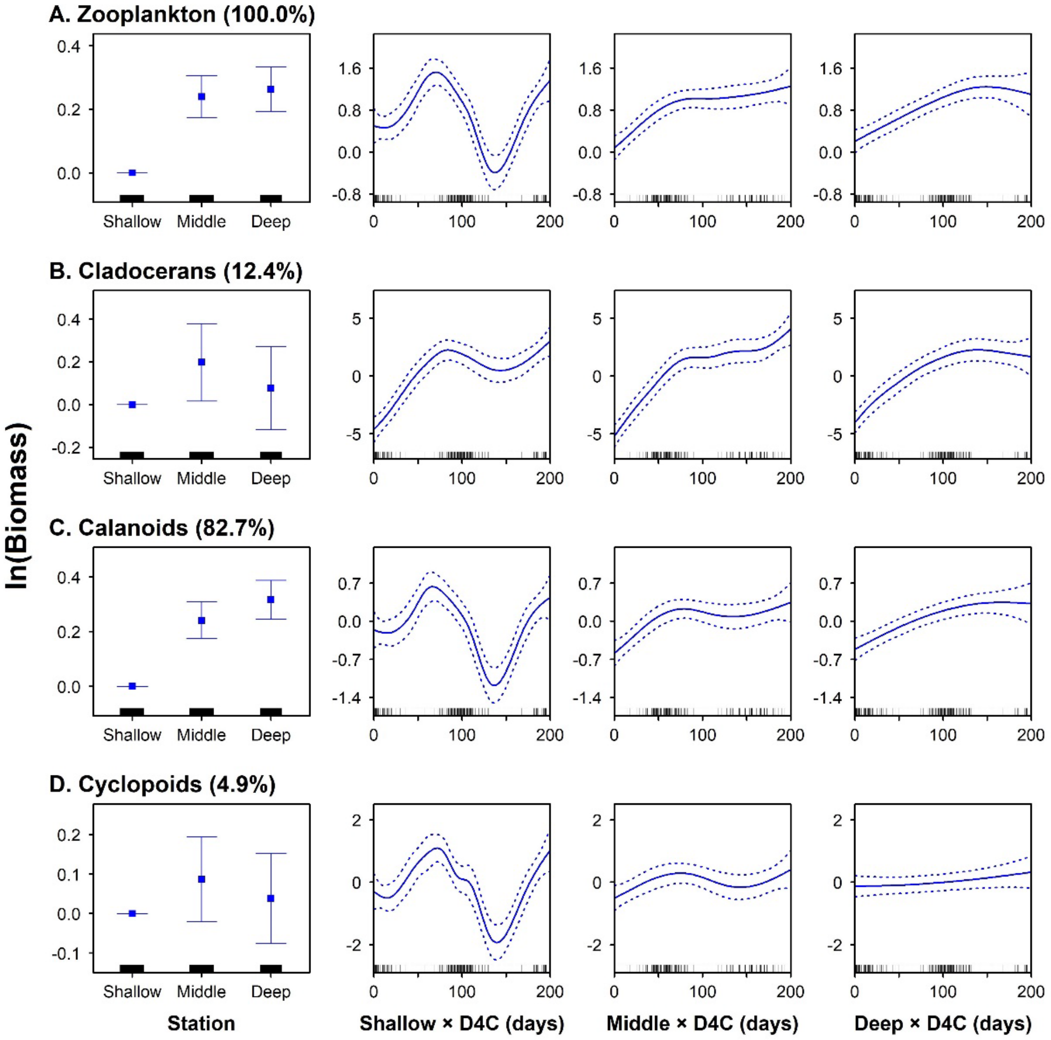

Fig. E2. Predicted mean biomass and biomass seasonality for (all) zooplankton and major zooplankton groups across sampling transects in Lakes Michigan and Huron. These predictions are based on generalized additive mixed models and have been adjusted for interannual variability. The percentage in parentheses is the proportion of biomass in total zooplankton biomass across samples. Biomass represents zooplankton biomass, Station represents sampling station in different depth categories, including shallow (11–27 m in depth), middle (40–51 m), and deep (64–112), and D4C represents days after surface water temperature reached 4 °C, which was used as a proxy for time into the growing season. In the panel of Station, square points represent the predicted values, error bars represent +/− one standard error, and the width of each short bar above the horizontal axis represents the relative sample size. In the panels of D4C, the solid line represents the predicted values, the dotted lines cover +/− one standard error, and ticks above the horizontal axis represent the distribution of data points.

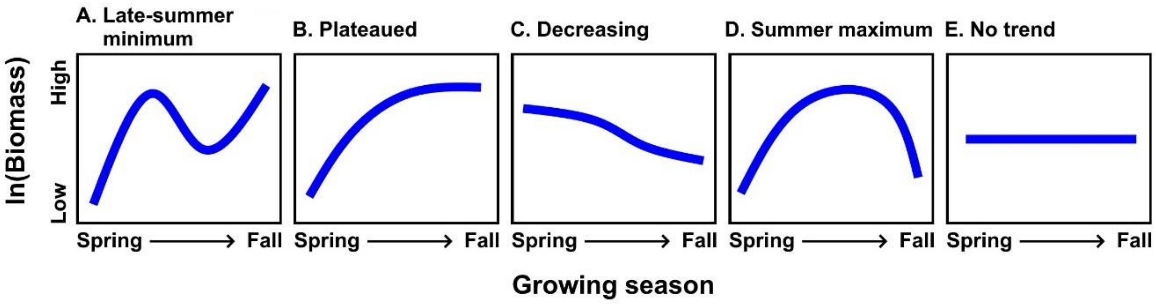

Fig. E3. Five seasonality patterns revealed in out taxon-level generalized additive mixed models.

Table E3. Summaries for patterns of zooplankton biomass and biomass seasonality from nearshore to offshore stations across transects in Lakes Michigan and Huron revealed in our generalized mixed models (GAMMs). Taxa within each major zooplankton group are ordered by the proportion of biomass (%) in total zooplankton biomass across samples. Relative biomass was compared between stations in different categories, namely shallow (S; 11–27 m in depth), middle (M; 40–51 m in depth), and deep (D; 64–112 m in depth). For example, "S < M ~ D" means that GAMM-predicted biomass was lower in shallow stations than in middle and deep stations, where the predicted biomass was about the same. Five major seasonality patterns were revealed in our GAMMs, including late-summer minimum (LSM), plateaued, decreasing, summer maximum, and no trend, which are explained in Fig. E3. The * indicates that the calanoid pattern was revealed in the GAMM.

Group/taxon (biomass %)	Relative biomass between stations	Seasonality across stations		
		Shallow	Middle	Deep
Zooplankton (100.0%)	**S < M ~ D**	**LSM**	**Plateaued**	
Cladocerans (12.4%)	**S ~ M ~ D**	**LSM**	**Plateaued**	
Daphnia galeata mendotae (7.5%)*	S < M ~ D	LSM	Plateaued	
Bosmina spp. (2.4%)	S ~ M > D	Plateaued		
Bythotrephes longimanus (1.0%)	S ~ M ~ D	Plateaued		
Nearshore predatory cladocerans (0.3%)	S > M ~ D	Summer maximum		
Calanoids (82.7%)	**S < M ~ D**	**LSM**	**Plateaued**	
Calanoid copepodites (39.2%)*	S < M ~ D	LSM	Plateaued	
Limnocalanus macrurus (15.0%)*	S < M ~ D	LSM	Plateaued	
Leptodiaptomus sicilis (10.4%)	S < M ~ D	LSM	No trend	
Leptodiaptomus ashlandi (7.8%)	M > S ~ D	LSM	Decreasing	No trend
Leptodiaptomus minutus (6.8%)	S ~ M > D	LSM	No trend	Decreasing
Epischura lacustris (1.8%)	S ~ M ~ D	LSM	Plateaued	
Skistodiaptomus oregonensis (1.1%)	S ~ M > D	LSM	No trend	
Cyclopoids (4.9%)	**S ~ M ~ D**	**LSM**	**No trend**	
Diacyclops thomasi (2.4%)	S < M ~ D	LSM	No trend	
Cyclopoids copepodites (2.2%)	S ~ M ~ D	LSM	Plateaued	
Tropocyclops prasinus mexicanus (0.03%)	S > M ~ D	Plateaued		

Cladocerans

Our GAMMs also showed remarkable differences in biomass and biomass seasonality between nearshore and offshore stations across cladoceran taxa (Table E3). The calanoid pattern was only revealed in the GAMM of *Daphnia galeata mendotae*. The biomass of *Bosmina* spp. and nearshore predatory cladocerans were significantly higher in the nearshore than offshore stations while the biomass *Bythotrephes longimanus* were not significantly different between nearshore and offshore stations. In terms of biomass seasonality, the plateaued pattern was revealed in the GAMMs of *Bosmina* spp. and *Bythotrephes longimanus* while the unique summer maximum pattern was revealed in the GAMM of nearshore predatory cladocerans across all stations from nearshore to offshore waters.

Calanoids

The calanoid pattern was revealed in the GAMMs of calanoid copepodites and *Limnocalanus macrurus*, which comprised more than half (54%) of total zooplankton biomass in our samples (Table E3). However, the late-summer biomass minimum in shallow stations was revealed in all seven GAMMs of calanoid taxa. For *L. sicillis* and *L. ashlandi*, the predicted biomass was also significantly higher in offshore than nearshore stations, but the opposite was predicted for *L. minutus* and *Skistodiaptomus oregonensis*. For these four taxa, the predicted biomass was decreasing or had no trend throughout the growing season. For *Epischura lacustris*, the GAMM showed that the biomass was not significantly different between nearshore and offshore stations and a plateaued seasonality pattern in offshore waters.

Cyclopoids

Interestingly, the calanoid pattern was not revealed in any cyclopoid GAMMs but the late-summer biomass minimum was revealed in the GAMMs of *Diacyclops thomasi* and cyclopoid copepodites (Table

E3). The GAMM of *Diacyclops thomasi*, the most dominant taxon in biomass of cyclopoids (2.4% of total zooplankton biomass across our samples), showed a pattern similar to the calanoid pattern but the biomass showed no trend in the offshore stations as the growing season progressed. The GAMM of cyclopoid copepodites, another dominant taxon in biomass of cyclopoids (2.2% of total zooplankton biomass across our samples), also showed a pattern similar to the calanoid pattern but the predicted biomass was not significantly different from nearshore to offshore stations. The GAMM of *Tropocyclops prasinus mexicanus* showed that biomass decreased from nearshore to offshore stations and the biomass increased and plateaued as the growing season progressed in all stations, quite different from the calanoid pattern.

Implications for future monitoring surveys

Our results showed clear differences in the dynamics of zooplankton in the nearshore (shallow stations <30 m in depth) waters relative to those in deeper waters (stations with bottom depths ≥ 46 m). For example, total zooplankton biomass was lowest in the nearshore waters where the primary productivity is generally the highest (Stadig et al. 2020), implying that zooplankton could be under higher predation pressure in nearshore than in offshore waters. How this heterogeneity in primary production and intensity of zooplanktivory over space and time affects zooplankton community dynamics may not be understood without surveys conducted in nearshore waters. We also frequently documented a late-summer biomass minimum of zooplankton in nearshore waters: in all three group-level GAMMs and in 10 of 14 taxon-level GAMMs. Given these unusual dynamics in the nearshore waters, an ideal nearshore monitoring survey would need to be at least monthly, from August to October, to best capture potential differences in interannual variability in the nearshore zooplankton community. This monthly monitoring already occurs by NOAA, offshore of Muskegon MI (see Pothoven and Vanderploeg 2022), but whether those local patterns are reflective of dynamics in other nearshore regions of the lake will require additional research. In contrast, the more offshore waters (bottom depths ≥45 m) revealed less seasonal variation: the group level GAMMs were all either plateaued or no trend, and most of the taxon level GAMM trends were also plateaued (16) or no trend (8), with a few summer maximum (2) and decreasing (2). Hence, monitoring the zooplankton community in the more offshore waters with one summer cruise, as is currently undertaken by EPA, should better capture interannual variation in zooplankton owing to less seasonal variation.

Acknowledgements

We are grateful for the efforts of numerous scientists that contributed to either the collection of these data or the processing of the zooplankton samples in the laboratory: Lynn Benes, Margret Chriscinske, Bruce Davis, Drew Eppehimer, Lauren Eaton, Kevin Keeler, Brendan Nee, Eric Nelson, Brian O'Malley, Betsy Puchala, Amelia Runco, Nicole Watson. Lynn Benes also carried out a final quality control for the data. We also acknowledge the vessel crew from the R/V *Arcticus* and R/V *Sturgeon* from 2010–2017.

References

Barbiero, R.P., Lesht, B.M., Hinchey, E.K., and Nettesheim, T.G. 2018a. A brief history of the U.S. EPA Great Lakes National Program Office's water quality survey. Journal of Great Lakes Research **44**(4): 539–546.

Barbiero, R.P., Lesht, B.M., Warren, G.J., Rudstam, L.G., Watkins, J.M., Reavie, E.D., Kovalenko, K.E., and Karatayev, A.Y. 2018b. A comparative examination of recent changes in nutrients and lower food web structure in Lake Michigan and Lake Huron. Journal of Great Lakes Research **44**(4): 573–589.

Bottrell, H.H., Duncan, A., Gliwicz, Z.M., Grygierek, E., Herzig, A., Hillbricht-Ilkowska, A., Kurasawa, H., Larsson, P., and Weglenska, T. 1976. A review of some problems in zooplankton production studies. Norwegian Journal of Zoology **24**: 419–456.

Burgess, S., Jackson, E.W., Schwarzman, L., Gezon, N., and Lehman, J.T. 2015. Improved estimates of calanoid copepod biomass in the St. Lawrence Great Lakes. Journal of Great Lakes Research **41**(2): 484–491.

Cha, Y., Stow, C.A., Nalepa, T.F., and Reckhowt, K.H. 2011. Do invasive mussels restrict offshore phosphorus transport in Lake Huron? Environmental Science & Technology **45**(17): 7226–7231.

Dumont, H.J., Van de Velde, I., and Dumont, S. 1975. The dry weight estimate of biomass in a selection of Cladocera, Copepoda and Rotifera from the plankton, periphyton and benthos of continental waters. Oecologia **19**(1): 75–97.

EPA. 2003. Standard operating procedure for zooplankton analysis, LG 403 revision 03. U.S. EPA Great Lakes National Program Office, Chicago.

Eppehimer, D.E., Bunnell, D.B., Armenio, P.M., Warner, D.M., Eaton, L.A., Wells, D.J., and Rutherford, E.S. 2019. Densities, diets, and growth rates of larval alewife and bloater in a changing Lake Michigan ecosystem. Transactions of the American Fisheries Society **148**(4): 755–770.

Fishman, D.B., Adlerstein, S.A., Vanderploeg, H.A., Fahnenstiel, G.L., and Scavia, D. 2009. Causes of phytoplankton changes in Saginaw Bay, Lake Huron, during the zebra mussel invasion. Journal of Great Lakes Research **35**(4): 482–495.

Hecky, R.E., Smith, R.E.H., Barton, D.R., Guildford, S.J., Taylor, W.D., Charlton, M.N., and Howell, T. 2004. The nearshore phosphorus shunt: a consequence of ecosystem engineering by dreissenids in the Laurentian Great Lakes. Canadian Journal of Fisheries and Aquatic Sciences **61**(7): 1285–1293.

Kao, Y-C., Dieter, P.M., Watson, N.M., Keeler, K.M., Eaton, L.A., Chriscinske, M.A., Davis, B.M., and Bunnell, D.B. 2022. 2010–2017 zooplankton data from whole water-column tows in Lakes Michigan and Huron. U.S. Geological Survey data release, https://doi.org/10.5066/P9UCG8Q0.

Makarewicz, J.C., and Jones, H.D. 1990. Occurrence of *Bythotrephes Cederstroemi* in Lake Ontario offshore waters. Journal of Great Lakes Research **16**(1): 143–147.

Mehler, K., Burlakova, L.E., Karatayev, A.Y., Elgin, A.K., Nalepa, T.F., Madenjian, C.P., and Hinchey, E. 2020. Long-term trends of Lake Michigan benthos with emphasis on the southern basin. Journal of Great Lakes Research **46**(3): 528–537.

Nalepa, T.F., Fanslow, D.L., Pothoven, S.A., Foley III, A.J., and Lang, G.A. 2007. Long-term trends in benthic macroinvertebrate populations in Lake Huron over the past four decades. J. Great Lakes Res. **33**(2): 421–436.

Ojaveer, H., Kuhns, L.A., Barbiero, R.P., and Tuchman, M.L. 2001. Distribution and population characteristics of *Cercopagis pengoi* in Lake Ontario. Journal of Great Lakes Research **27**(1): 10–18.

Persson, G., and Ekbohm, G. 1980. Estimation of dry weight in zooplankton populations: Methods applied to crustacean populations from lakes in the Kuokkel area, northern Sweden. Archiv für Hydrobiologie **89**: 225–246.

Pothoven, S.A., and Vanderploeg, H.A. 2022. Variable changes in zooplankton phenology associated with the disappearance of the spring phytoplankton bloom in Lake Michigan. Freshw. Biol. **67**: 365-377.

R Core Team. 2022. R: a language and environment for statistical computing. R Foundation for Statistical Computing, Vienna.

Rosen, R.A. 1981. Length–dry weight relationships of some freshwater zooplankton. Journal of Freshwater Ecology **1**(2): 225–229.

Rowe, M.D., Anderson, E.J., Vanderploeg, H.A., Pothoven, S.A., Elgin, A.K., Wang, J., and Yousef, F. 2017. Influence of invasive quagga mussels, phosphorus loads, and climate on spatial and temporal patterns of productivity in Lake Michigan: A biophysical modeling study. Limnology and Oceanography **62**(6): 2629–2649.

Shen, C., Liao, Q., and Bootsma, H.A. 2020. Modelling the influence of invasive mussels on phosphorus cycling in Lake Michigan. Ecological Modelling **416**: 108920.

Stadig, M.H., Collingsworth, P.D., Lesht, B.M., and Höök, T.O. 2020. Spatially heterogeneous trends in nearshore and offshore chlorophyll *a* concentrations in lakes Michigan and Huron (1998–2013). Freshwater Biology **65**(3): 366–378.

Wood, S., and Scheipl, F. 2022. Package 'gamm4': Generalized additive mixed models using 'mgcv' and 'lme4'. R package version 0.2-6.

Wood, S.N. 2017. Generalized additive models: an introduction with R. CRC Press, Boca Raton, Florida.

Acknowledgements

For all subprojects, any use of trade, product, or firm names is for descriptive purposes only and does not imply endorsement by the U.S. Government. We are grateful for the reviews by Ralph Tingley and Michael Lowe that helped improve this report.

Report: NOAA Support of Lake Michigan CSMI 2020/2021

Lake and Year: Lake Michigan 2020/2021
Lead Organization: NOAA Great Lakes Environmental Research Laboratory

Authors of This Report: Ashley Elgin[1], Edward Rutherford[1], Paul Glyshaw[1], Doran Mason[1], Steve Pothoven[1], Mark Rowe[1], Steve Ruberg[1], Madeline Tomczak[2], Peter Alsip[2], Casey Godwin[2], Andrew Camilleri[2], Russ Miller[2], Hunter Carrick[3], Katrina Lewandowski[4], Mike Sayers[5], Eric J. Anderson[6]

[1]NOAA Great Lakes Environmental Research Laboratory
[2]University of Michigan Cooperative Institute for Great Lakes Research
[3]Central Michigan University
[4]Wayne State University
[5]Michigan Tech Research Institute
[6]Colorado School of Mines

Contacts for Questions About this Report:
ashley.elgin@noaa.gov, 616-414-1059
ed.rutherford@noaa.gov, 734-717-0885

The projects address the following Lake Michigan 2020 science priorities and research questions:

1. Advance the understanding of nutrient dynamics (i.e. loading, transport, and cycling, spatial and temporal variability, and gradients) that directly influence lower trophic level productivity and offshore fish production.
2. Identify and quantify the role of biological ‘hot spots’ (e.g., Green Bay, major tributaries/nearshore areas, reefs, and upwelling events) and substrate heterogeneity in supporting Lake Michigan productivity. Seek opportunities to leverage existing work in these areas, including the large array of acoustic receivers in Green Bay.
3. Investigate understudied but potentially important components of the food web, including: fall/winter/early spring and nearshore (including shallow shoreline areas) community structure, dreissenid veligers (including their nutrition as a prey for larval fish), *Limnocalanus* copepods, *Mysis*, the microbial loop (bacteria and microzooplankton), and round gobies (which are undersampled by traditional gears).
4. Investigate evidence for recruitment bottlenecks for key fish species such as lake whitefish and alewife. Seek opportunities to leverage the ongoing multi-year nearshore

larval lake whitefish sampling efforts by Lake Michigan Technical Committee agencies and tribes.

5. Further understanding of the current and future impacts of terrestrial and aquatic invasive species upon the health of the Lake Michigan ecosystem.
6. Continue nearshore to offshore monitoring of key food web components (e.g., phytoplankton, zooplankton, *Diporeia* and dreissenid mussels)

Study Highlights (for all subprojects)

- A biophysical model nowcast and 5-day forecast provided field researchers with predicted surface chlorophyll and dissolved organic carbon (river water tracer) during the 2020 and 2021 field season, giving field researchers awareness of broad-scale phenomena such as coastal upwelling and river plume events (Priorities 1 & 2). Model predictions were assessed in comparison by grab samples of chlorophyll. Future studies should focus on additional assessment and improvement of models of tributary phosphorus loading, nearshore concentrations, regions of influence, and transport phenomena with ecological impacts.

- Observing systems (satellite, moored and autonomous) provided high-resolution data on physico-chemical variables over long time periods and between cruises. (Priorities 1 and 2)

- We compared laboratory and field methods for measuring ultraviolet light attenuation, and used cutting-edge laboratory spectrophotometry techniques to quantify the contribution of seston to visible and ultraviolet light (UV) attenuation. (Priorities 4 and 6)

- Phytoplankton were more efficient at using low light levels earlier in the season. A significant proportion of chlorophyll and primary production came from pico and nanoplankton (2-20 µm). (Priority 6)

- Photoinhibition of phytoplankton productivity is a phenomenon previously observed in the winter-spring period in Lake Michigan; however, we measured photoinhibition later in the year during 7 of the 8 experiments done in June-July. We believe the extension of photoinhibition later in the year is likely due to increased light penetration in Lake Michigan. (Priority 6)

- Our estimates for maximum rates of photosynthesis (P_{max}) are comparable with previous results reported from Lake Michigan and other locations in the Great Lakes. Future studies should focus on measuring water column production to evaluate if levels of production have remained stable over time. (Priority 6)

- Interestingly, peak occurrence in phytoplankton biomass was dominated by diatoms and dinoflagellates species that generally grow in the spring or in the vicinity of the deep chlorophyll layer in summer. Their occurrence in our samples during early July and

August corresponds nicely with lower temperature and increased chlorophyll fluorescence values recorded in early July and August at the 20-m buoy. (Priority 6)

- Zooplankton biomass was higher off Muskegon in 2021 compared to biomass in earlier CSMI years (2010, 2015). Total biomass was higher offshore than nearshore, with omnivorous copepods and herbivorous cladocerans comprising a significant fraction of the total in July and September. (Priority 6)
- Monitoring of dreissenid mussels revealed depth-specific and region-specific differences in mussel body condition, where shallow depth (<30 m) quagga mussels had the highest relative body mass and mid-depth mussels (31-50 m) had the lowest. Regional differences in quagga mussel body condition varied by depth zone and body condition was lower in 2021 than in 2015 in all depth zones. (Priority 6)
- Mean dreissenid mussel density for a subset of southern Lake Michigan stations was highest in the 31-50m depth zone, but not significantly so. (Priority 6)
- Dreissenid veliger densities and average length indicated two recruitment events that occurred in summer and fall. The density peaks in 2021 were synchronized across all three depths sampled, with the mid-depth site (45 m) exhibiting the highest abundance. Veliger densities were lower in 2021 compared to earlier years. (Priority 3)
- Laboratory studies by Wayne State University scientists indicate consumption of dreissenid mussel veligers by fish larvae will reduce larval growth and survival. Diet analysis in 2021 indicated larval Alewife and Bloater mainly consumed copepods and ate few *Dreissena* veligers, and larval growth was higher than in prior CSMI years. However, larval fish densities were relatively low compared to 2015. (Priorities 3, 4, 5)
- UV wavelengths also may be a bottleneck to fish larvae survival and potential recruitment in Lake Michigan. In 2021, as in previous years, NOAA surveys indicated zooplankton and Alewife larvae avoided surface waters during the day when UV effects were strongest, but migrated up to near surface at night. Bloater larvae, which are better able to tolerate UV exposure, were present at surface and at mid-depths. (Priority 4)

Subproject A: Benthic Surveys

Overview

We helped to monitor dreissenid mussel populations in Lake Michigan by collecting and processing samples in the southern region to supplement the whole lake benthic survey and by conducting repeated surveys of mussel veligers along the NOAA Long-term Research transect near Muskegon, MI. We also determined lake-wide mussel length-weight relationships with quagga mussels collected during the whole lake benthic survey. Due to repeated delays related to Covid-19, we were not able to establish the long term (5+ year) series of moorings in the Muskegon region as originally proposed in 2020/2021. However, we were able to initiate the study in 2022 and will start gathering the first data on mussel growth and mortality in 2023.

Methods

During the CSMI whole lake benthic survey on board the USEPA R/V Lake Guardian and during NOAA GLERL benthic surveys conducted on board the NOAA GLERL R/V Laurentian and R/V 5501, GLERL researchers collected quagga mussels from 26 stations for length-weight analysis and quantitative Ponar grabs at 17 stations to assess *Dreissena* abundance. (Table A-1). Depth was recorded upon arrival at each station.

The whole lake benthic survey was led by Buffalo State University and conducted on board the R/V Lake Guardian. The sites selected for the 2021 whole lake survey did not include all GLERL stations historically sampled in southern Lake Michigan, so GLERL conducted supplemental surveys for 15 of these stations and the R/V Lake Guardian collected Ponar grabs at two additional stations for GLERL to process. Triplicate Ponar grab samples were collected at each station, with the exception of station B4 in the middle of the lake, where we collected 12 replicates to intensify the search for *Diporeia*. Each sample was placed into an elutriation device and washed through a nitex sleeve having mesh openings of 500-µm. Samples were preserved with a 10% solution of neutral buffered formalin containing rose bengal stain. In the lab, samples were washed using a 500-µm sieve and gently rinsed to remove formalin. All dreissenid mussels and amphipods were picked, sorted, and placed into labeled vials. Accurate counts of the number placed in each vial was kept (laboratory counter) and recorded on a bench sheet after all organisms had been removed from the sample. Length was measured for all mussels (to the nearest 1 mm).

For quagga mussel length-weight analysis, the overall goal was to collect mussels from sites that represented different depth zones and basin regions. Mussels were collected from the lake bottom using either a Ponar grab sampler or a benthic sled. Multiple samples were taken at each station to obtain a sufficient number and size range of individuals, which was 25 individuals between shell length 10-25 mm. Mussels were then hand-picked from the sediments or rinsed over a 500-3000 µm sieve to remove sediments. The mussels were wrapped in paper towels and placed in petri dishes or plastic totes and stored immediately in a cooler with ice packs and then as soon as possible in a 4 ℃ incubator.

In the lab, the mussels for length-weight were processed as described by Nalepa et al. (2020). Briefly, the soft tissue was removed from 25 individuals (target shell length: 10 mm-25 mm), dried at 60 C for at least 48 h, then ashed at 550 C for 1 h. Ash-free dry weight (AFDW) was calculated as the difference between dry weight and post-ashed weight. Overall, a total of 645 individual *D. r. bugensis* from 26 sites were weighed and measured. Measured AFDWs and shell lengths (SL) were used to develop length-weight relationships according to the allometric equation: $\log_e$AFDW (mg) = b + m*$\log_e$SL (mm). Relationships were developed for pooled sites within four different depth intervals: < 30 m, 31-50 m, 51-90 m, and > 90 m. We used ANCOVA (response variable: ln AFDW; covariate: ln shell length) to analyze differences in length weight relationships: (1) among depth zones in 2021; and (2) temporal differences between 2015 (data from Nalepa et al. 2020) and 2021, analyzing each depth zone separately. Post-hoc pairwise comparisons of least square means were completed using Tukey's HSD. All statistical analysis was completed using the R statistical package (R Core Team, 2022); post-hoc tests were calculated with the lsmeans package (Lenth, 2016).

Sampling for dreissenid veligers took place at a nearshore site (M15; 17 m depth; 43° 11.29' N, 086° 20.64' W), a transitional-depth site (M45; 45 m depth; 43° 12.37' N, 086° 26.98' W) and an offshore site (M110; 113 m depth; 43° 11.99' N, 086° 34.19' W) near Muskegon, Michigan during March-December 2021. Veligers were collected using duplicate whole water column tows with a 50-cm diameter, 3-m long, 64-µm mesh, conical net. To determine veliger abundance, an aliquot was taken from a known sample volume with a Hensen–Stempel pipette so that a minimum of 100 veligers were counted for each sample, or if veligers were rare, up to 10% of the sample volume was counted. Length of at least 100 veligers (if available) was measured for each sample site and date.

Results and Discussion

The survey of 17 southern Lake Michigan stations that focused on dreissenid mussels and amphipods found only quagga and no zebra mussels. Deep station B4 (129 m) has been the only southern station to consistently have *Diporeia* in the last decade, but no *Diporeia* have been collected there since 2018. We collected additional Ponar grabs at this station in 2021 to increase the probability of detecting *Diporeia*, but none were found. Quagga mussel density was relatively variable in the sites <50 m and so despite higher mean densities at 31-50 m, there was no significant difference among depth zones ($F_{3,16}$ = 0.488, p = 0.70; Figure A-1). The data from this subset will be better to interpret when combined with other data from the whole-lake survey and compared to past annual surveys.

Quagga mussels from Lake Michigan exhibited significant depth- and region-specific length-weight patterns. There were significant differences when examining depth (ANCOVA:$F_{3,621}$ = 130.6, p < 0.001; Figure A-2) and regional (region, $F_{2,621}$ = 4.2, p = 0.016; Figure A-3) length-weight patterns. There was a significant interaction between shell length and depth zone ($F_{3,621}$= 3.4, p = 0.018), but not region ($F_{2,621}$= 1.3, p = 0.275), and a significant interaction between depth zone and region ($F_{6,261}$= 36.7, $p < 0.001$). The trend of highest body condition at <30 m stations and lowest condition at depths between 31-90 m is consistent with previous surveys in Lake Michigan (Nalepa et al. 2020).

Pairwise comparisons across depth zones (pooling regions) and among regions within each depth zone revealed additional insights. Mussels were relatively heaviest at sites <30 m, followed by sites >90 m and 51-90 m, and lightest at 31-50 m (all post-hoc pairwise comparisons $p < 0.05$) (Figure A-2 inset). In the < 30 m depth zone mussels in the northern region were significantly lighter than those in both the central and south regions ($p <0.001$; Figure A-3). No significant differences were found among regions in the 31-50 and 51-90 m depth zones. In the >90 m depth zone all regions were significantly different from each other ($p<0.001$), where northern mussels were heaviest, central mussels were intermediate, and southern mussels were lightest.

There were also depth-specific changes in relative tissue weight over time. The effects of depth and year were both significant, and there was an interaction between shell length and depth zone (ANCOVA: depth, $F_{3,1205}$ = 191.9, $p < 0.001$; year, $F_{1,1205}$= 36.9, $p < 0.001$; shell length * depth interaction, $F_{3,1205}$= 2.66, $p < 0.047$; Figure A-4). Pairwise comparisons between years within each depth zone revealed significant decreases between 2015 and 2021 in tissue AFDW within all depth zones ($p <0.0001$ for all pairwise comparisons). Looking back to samples collected from Lake Michigan since 2004, mussels at 31-50 m have consistently declined over time and mussels <30 m have been highly variable (Nalepa et al. 2020). Since 2010, body condition of mussels from 51-90 m has declined slightly and at >90 m, body condition has been relatively steady (Nalepa et al. 2020). Declines in body condition can be an indication of nutritional stress (Glyshaw et al. 2015).

Veliger abundance at the three Muskegon sites peaked in late June 2021, with a secondary peak in late September 2021 (Figure A-5). Overall annual abundance (based on areal density) was highest at the 45 m site during 2021, averaging 189,822/m^2 across all sampling dates, and lowest at the 110 m site, averaging 94,711/m^2. The average size of veligers also provided support for multiple periods of recruitment. Veligers were present during late winter and early spring, but as those veligers settled out, a new cohort of small veligers was evident in sampling by May (Figure A-5). This cohort grew through August, when it appeared to settle out of the water column, and a new cohort of small veligers was evident in late September, especially at the 15 and 45 m sites. To put the 2021 veliger densities into context, we looked to past data collected from these stations. Based on the overall annual average veliger density at the 15 m site from a 153-µm mesh net sampling, veliger density has been cyclical over time since 2007, with annual densities quite low in 2021 (Pothoven unpub. data, Figure A-6). Pothoven and Elgin

(2019) also showed inter-annual variation for these stations. Thus, seasonal and length/growth patterns of veligers from 2021 are likely reflective of veligers during a period of relatively low abundance in the environment.

Tables and Figures

Table A-1: Table of stations sampled in Lake Michigan in 2021 to quantify dreissenid mussel density using Ponar grabs and assess quagga mussel body condition.

Region	Station	Date Sampled	Depth (m)	Latitude	Longitude	Quantitative	Mussel Body
South	A1	2021-07-20	18	42.1083	-86.5333	X (n = 3)	
	A2	2021-07-20	35	42.1	-86.6167	X (n = 3)	
	B2	2021-07-15	50.0	42.3999	-86.4507		X
	B4	2021-07-19	129	42.3917	-87.0167	X (n = 12)	
	B5	2021-07-14	103.7	42.3750	-87.3493		X
	B7	2021-07-14	45.3	42.3662	-87.6660		X
	B8	2021-07-19	122	42.3792	-87.25	X (n = 3)	
	C10	2021-07-19	103	42.7983	-87.3708	X (n = 3)	
	C8	2021-07-19	150	42.8167	-87.00	X (n = 3)	
	C9	2021-07-19	132	42.8083	-87.20	X (n = 3)	
	EG14	2021-07-15	92.6	42.3776	-86.7737		X
	EG22	2021-07-21	45	43.1033	-86.3667	X (n = 3)	
	H13	2021-07-14	19	41.9265	-87.4903	X (n = 3)	
	H14	2021-07-14	37	42.0722	-87.4528	X (n = 3)	
	H21	2021-07-15	72.8	42.0403	-86.8834		X
	H22	2021-07-20	46	42.1392	-86.6638	X (n = 3)	
	H28	2021-07-20	19	42.63	-86.2653	X (n = 3)	
	H29	2021-07-20	37	42.63	-86.3058	X (n = 3)	
	H30	2021-07-20	73	42.63	-86.4333	X (n = 3)	
	M25	2021-07-13	27.0	43.2002	-86.3779	X (n = 3)	X
	M45	2021-07-13	45.7	43.2062	-86.4497	X (n = 3)	X
	X2	2021-07-13	103.0	43.2000	-86.5171	X (n = 3)	X
Central	9561	2021-07-16	130.7	43.4709	-86.7841		X
	9574	2021-07-21	140.7	44.0684	-87.1472		X
	9576	2021-07-17	164.3	44.1514	-86.6213		X
	9587	2021-07-18	197.8	44.6214	-86.3527		X
	82902	2021-07-21	37.9	43.9182	-87.6240		X
	FR1	2021-07-18	21.0	44.8166	-86.1397		X
	FR3	2021-07-18	46.0	44.8168	-86.1683		X
	FR5	2021-07-18	74.5	44.8164	-86.1967		X
	L245	2021-07-17	44.9	43.5008	-86.5316		X
	L280	2021-07-17	81.6	43.5010	-86.6032		X
	SY5	2021-07-21	77.8	43.9184	-87.3756		X
North	74880	2021-07-19	24.9	45.9085	-85.0249		X
	SB3	2021-07-20	44.2	44.8576	-87.1506		X
	SB5	2021-07-20	80.2	44.8575	-87.0861		X
	SB6	2021-07-20	157.3	44.8575	-86.9232		X
	SC2	2021-07-19	29.6	45.8412	-86.1054		X
	SC3	2021-07-19	43.2	45.8173	-86.1057		X
	SC5	2021-07-19	83.0	45.7563	-86.1057		X

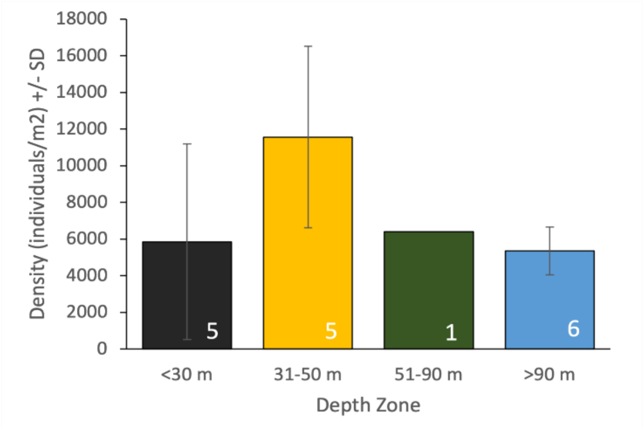

Figure A-1: Mean quagga mussel density (individuals/m^2 ± SD) for a quantitative Ponar survey conducted at a subset of 17 stations in southern Lake Michigan. See Table A1 for station information. The number in the lower right of each bar indicates the number of stations surveyed within that depth zone.

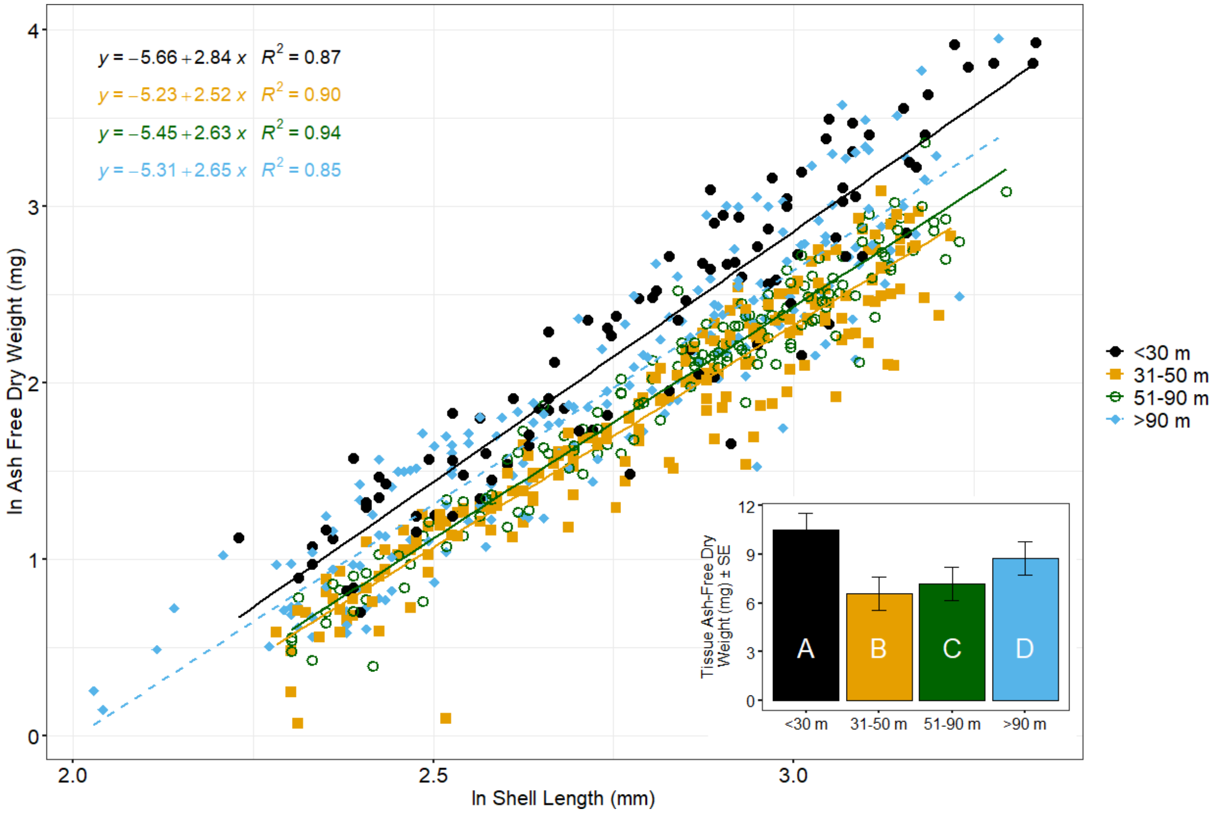

Figure A-2: Lake Michigan 2021 quagga mussel body condition by depth zone. The main figure shows ln tissue ash-free dry weight (AFDW) as a function of ln shell length for quagga mussels collected from four depth zones, <30 m, 31-50 m, 51-90 m, and >90 m. Figure inset displays quagga mussel tissue AFDW by depth zone, expressed as least square means (± SE) from a one-way ANCOVA with depth as the factor and shell length as the covariate. Categories with different letters differ significantly ($p < 0.05$), according to pairwise comparisons.

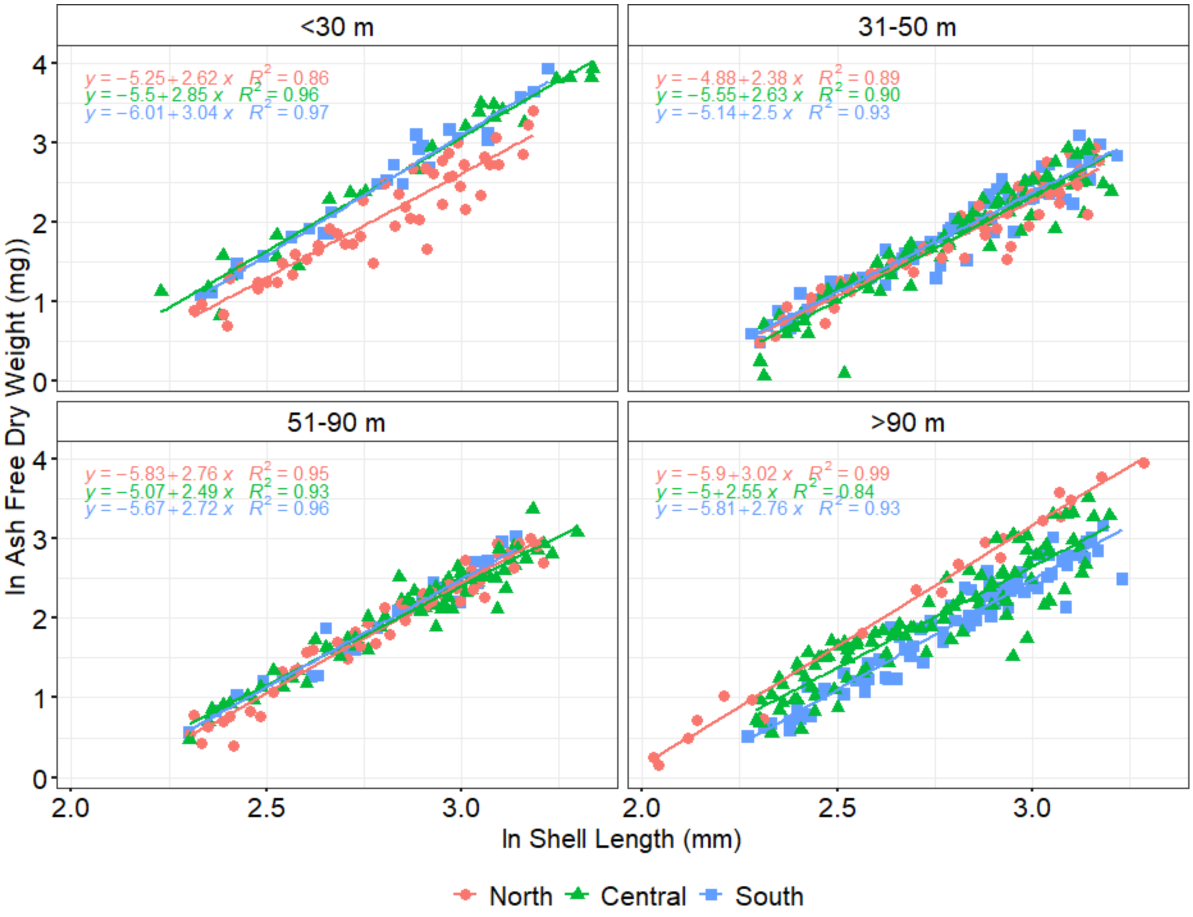

Figure A-3: Lake Michigan 2021 quagga mussel ln tissue ash-free dry weight (AFDW) as a function of ln shell length collected from three regions (North, Central, and South) and four depth zones, (<30 m, 31-50 m, 51-90 m, and >90 m). Regression equations and R^2 are shown for each relationship.

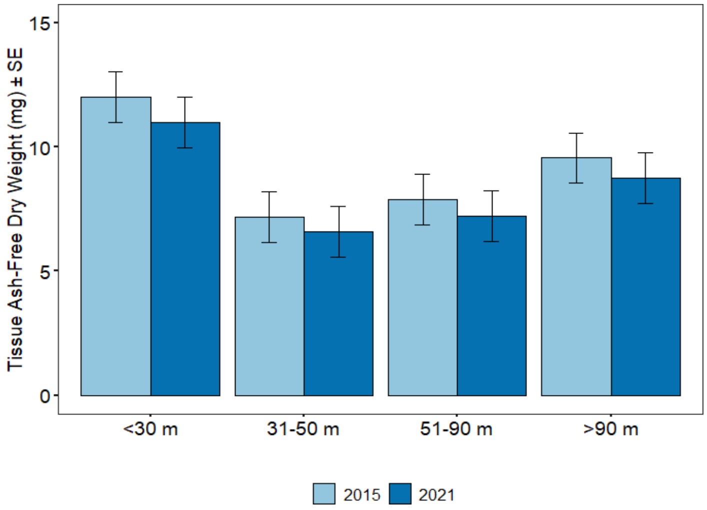

Figure A-4: Quagga mussel ash-free dry weight (mg AFDW), expressed as least square means (± SE) from a two-way ANCOVA with depth zone and year as the factors and shell length as the covariate.

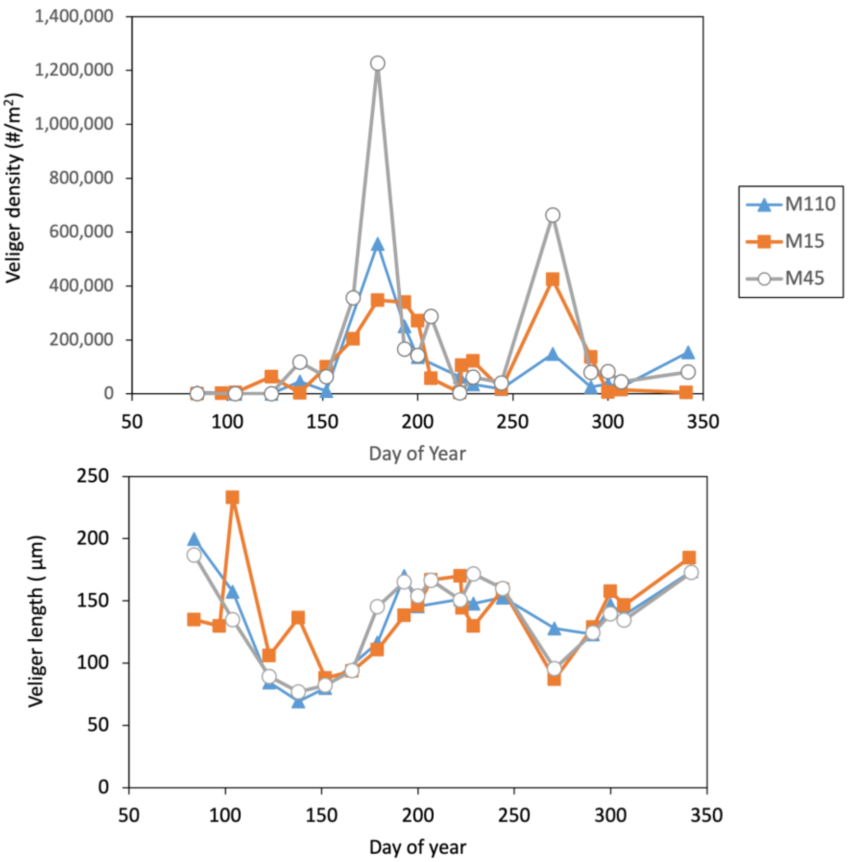

Figure A-5: Mean dreissenid veliger density (top) and mean veliger length (bottom) at three sites in Lake Michigan near Muskegon, MI during 2021. The veligers were collected using a 63-µm mesh plankton net.

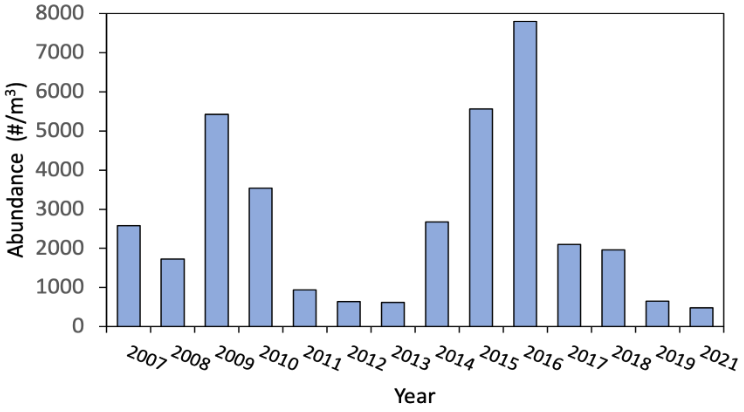

Figure A-6: Mean annual densities of dreissenid veligers sampled at the nearshore site (M15) in a 153-µm mesh net from 2007-2021. Data from Pothoven (unpub).

Subproject B: Food Webs and Nutrients

Overview

To address Lake Michigan CSMI research priorities 1-6, NOAA GLERL and university collaborators (Hunter Carrick - Central Michigan Univ; Casey Godwin - Univ Michigan, CIGLR staff) conducted monthly surveys from May to September at a nearshore (M15), mid-depth (M45), and offshore site (M110, Figure B-1) in southeast Lake Michigan to sample thermal structure, nutrients, optical properties, and make estimates of primary production, species composition, vertical distribution, and biomass or density of the lower food web (phytoplankton, zooplankton, fish larvae, Mysis), and older life stages of fish (Table B-1). Whole water column and fine-scale (5-10m) diel vertical samples revealed effects of UV, CDOM, suspended solids and light on vertical and horizontal distributions of organisms within the lower food web. Advection of fish larvae by currents was modeled using an application of the LMHOFS hydrodynamics model. Bottlenecks to lake whitefish, alewife and bloater larvae recruitment were explored using time series of data on zooplankton densities and species composition, and larval fish densities, vertical distributions, growth rates and diets. Experiments were conducted by scientists at Wayne State University to evaluate effects of mussel veliger consumption on yellow perch larvae growth and survival.

The following sections report methods, results and discussion of sampling efforts separately for NOAA and university partners.

Methods Summary - NOAA

We used CTD, PAR and secchi disk to characterize temperature and light profiles of the water column, and used a range of tools (below) to sample fine-scale distributions of organisms and the factors that affect them. Measures of thermal structure and ultraviolet (UV) wavelengths were used to define sampling strata for characterizing vertical distributions of organisms from May through September.

- Grab samples: nutrients, phosphorus, chlorophyll, and suspended and dissolved solids;
- UV radiometer to measure attenuation of light wavelengths, necessary for understanding vertical distribution of plankton;
- Plankton Survey System (PSS with CTD, a laser optical plankton counter, calibrated fluorometer, CDOM, scattering, and PAR sensors on V-fin) to estimate temperature. light, chlorophyll and zooplankton biomass at depth;
- FluoroProbe (in-situ spectral fluorometer) to measure vertical profiles of algal classes;
- Neuston net to sample surface distributions of fish larvae and Mysis nearshore and offshore, and Bongo nets to sample nearshore subsurface densities of fish larvae;

- MOCNESS (Multiple Opening-Closing Net Environmental Sampling System) to increase sampling efficiency of *Bythotrephes*, *Mysis*, and larval fishes at mid-depth and offshore waters
- Fisheries acoustics to measure biomass and spatial distribution of older fish

Nutrients, suspended solids, optical properties, chlorophyll a (NOAA):

Methods

Water was collected for analysis of nutrients, suspended solids and chlorophyll biomass with a Niskin bottle at various depths in the water column, depending on the thermal structure or specific features (e.g., deep chlorophyll maximum) in the water column.

Total phosphorus was quantified by collecting 50 mL of whole lake water in duplicate and stored at 4ºC in borosilicate tubes until further analysis. In the lab, samples were pre-treated with a potassium persulfate solution and autoclaved at 121 ºC prior to analysis on a SEAL Analytical AutoAnalyzer 3, a continuous segmented flow analyzer, using a modified Murphy and Riley method (Murphy and Riley, 1962; U.S. Environmental Protection Agency, 1984). Modifications to the method include the use of a sodium hydroxide reagent (0.5 N sodium hydroxide with 0.007 M sodium dodecyl sulfate (SDS)) in lieu of the SDS (0.035 M) reagent, the addition of extra SDS (0.035 M) to the ascorbic acid reagent, and an acidified wash pot (0.054 N sulfuric acid solution).

Gravimetric methods were used to determine total suspended solids (TSS) and volatile suspended solids (VSS). Water was filtered through pre-combusted 47 mm GF/F filters. Samples were dried in an oven overnight at 70 °C, weighed, combusted for 4 hours at 450 °C, and weighed again.

Chlorophyll biomass was quantified by concentrating particulate material on a Whatman GF/F filter, extracting in N,N-Dimethylformamide (Speziale et al, 1984), and analyzing on a Turner Designs 10 AU fluorometer. For a subset of samples, we size-fractionated the samples to 53, 20, 10, 5, 2, and 1.2 µm using polycarbonate membrane filters or Nitex mesh.

A Biospherical Instruments Inc. PUV-2500 radiometer was used to make underwater measurements of wavelengths at 305, 313, 320 340, 380, 395 nm and of photosynthetically active radiation (PAR; 400-700 nm). The submerged instrument was paired with a surface instrument (PUV-2510) mounted on top of the research vessel to capture the same wavelengths of incoming solar radiation. The instrument was calibrated for dark offsets as described in the instrument manual on each day the instrument was deployed. The attenuation coefficients (K_d) were calculated as the slope of the linear regression of the natural logarithm of the ratio of ultraviolet readings of the sensor at depth divided by the ambient sensor. The 1% attenuation depth was calculated using the K_d and intercept from the linear regression listed above as: (ln(0.01)-Intercept)/K_d. Only data above 1% of the ambient irradiance were used for both the K_d and 1% attenuation depth calculations.

Results and Discussion

Near surface (2-5 m) total phosphorus concentrations at all sites ranged from 5.6-10.4 µg L^{-1}, with a mean of 8.4 µg L^{-1} throughout the sampling period (Figure B-2). Both total suspended solids (TSS; Figure B-3) and volatile suspended solids (VSS; Figure B-4) remained low (<1 mg L^{-1}) throughout the sampling period at all stations. In general, TSS showed a decreasing trend from nearshore to offshore, while VSS increased from nearshore to offshore. Secchi disk measurements were higher at mid-depth (avg. = 12.4 ± 2.6m) and offshore sites (avg. = 12.5 ± 2.9m), and lowest nearshore (avg. = 6.3 ± 0.8m) (Figure B-5). Peak values of 20-22 m were measured at M45 and M110 in May, before thermal stratification, then declined to a low in July before increasing again in August and September.

Highest attenuation coefficients and lowest 1% attenuation depths were seen for shorter wavelengths as expected (Figure B-6). Attenuation coefficients were highest and 1% attenuation depths were lowest nearshore in all months, except in August when attenuation was slightly higher at M110 compared to M15. The PAR sensor was not working properly in September so no measures were made then.

Near surface (2- 5 m) chlorophyll concentrations at all sites were low, but were highest in late June, early July and September at M15, the nearshore site. Nearshore chlorophyll concentrations were variable across months, but were higher than at mid depth and offshore sites except in August, when chlorophyll biomass was higher at mid-depth and offshore sites (Figure B-7). An intense rainfall event recorded in the Muskegon, Grand and St. Joseph's watershed on June 26 pumped organic material (including duckweed) from tributaries to the nearshore zone, evident during our survey on July 7. This material was advected offshore by an upwelling event in early August (see Biophysical Modeling section, Figures D-4, D-5). Chlorophyll concentrations generally were similar at mid depth and offshore sites and increased from May to August, then declined in September. Size-fractionated chlorophyll showed that the majority of phytoplankton biomass was in the nanoplankton (< 20 µm, Figure B-8), consistent with the changes reported following expansion of Dreissenid mussels (Carrick et al, 2015; Carrick et al, 2017).

Offshore seasonal patterns of temperature, CDOM, and chlorophyll a from the PSS and CTD sensors are shown along with corresponding semi-log plots of UV and PAR penetration for station M110 (Figure B-9). The 1% attenuation depths ranged from 4-7 m for UV-B and from 10-28 m for UV-A. These plots, and their relation to thermal structure and currents, are important for understanding potential impacts of UV radiation on plankton and benthos.

Tables and Figures

Table B-1: GLERL sampling activities during the 2021 Lake Michigan CSMI field season. X=M15, *=M45, += M110. PSS Long Transect sampling ran from sites nearshore (M15) to offshore (M110) while passing through the mid-depth site (M45); Diel PSS sampling was a short (30-45 min) PSS run along the depth isobaths at either M45 or M110 during the day and night.

	May	**June**	**July**	**August**	**Sept.**
Chlorophyll	x+	x+*	x+*	x+*	x+*
CTD	x+*	x+*	x+*	x+*	x+*
Fluoroprobe	x+*	x+		x+*	x+*
Larval Fish	x+*	x+	x+	x+*	x+*
Microbes		x+*	x+*	x+*	x+*
Mysis	x+*	+	+	x+*	x+*
Nutrients	x+	x+*	x+*	x+*	x+*
PSS:	+*	+	+	+	+
Long Transect	x+*				
Diel	+			+	
Secchi	x+*	x*	x+*	x+*	x+*
UV Radiometer	x+*	+*	x+*	x+*	x+*
Zooplankton:					
Full	x+*	x+	x+	x+*	x+*
Depth Stratified	x+*	x+	x+	x+*	x+*
Laboratory Optical Properties Characterization	x	x	x	x	x
Fisheries Acoustics	+*	+	+	+	+

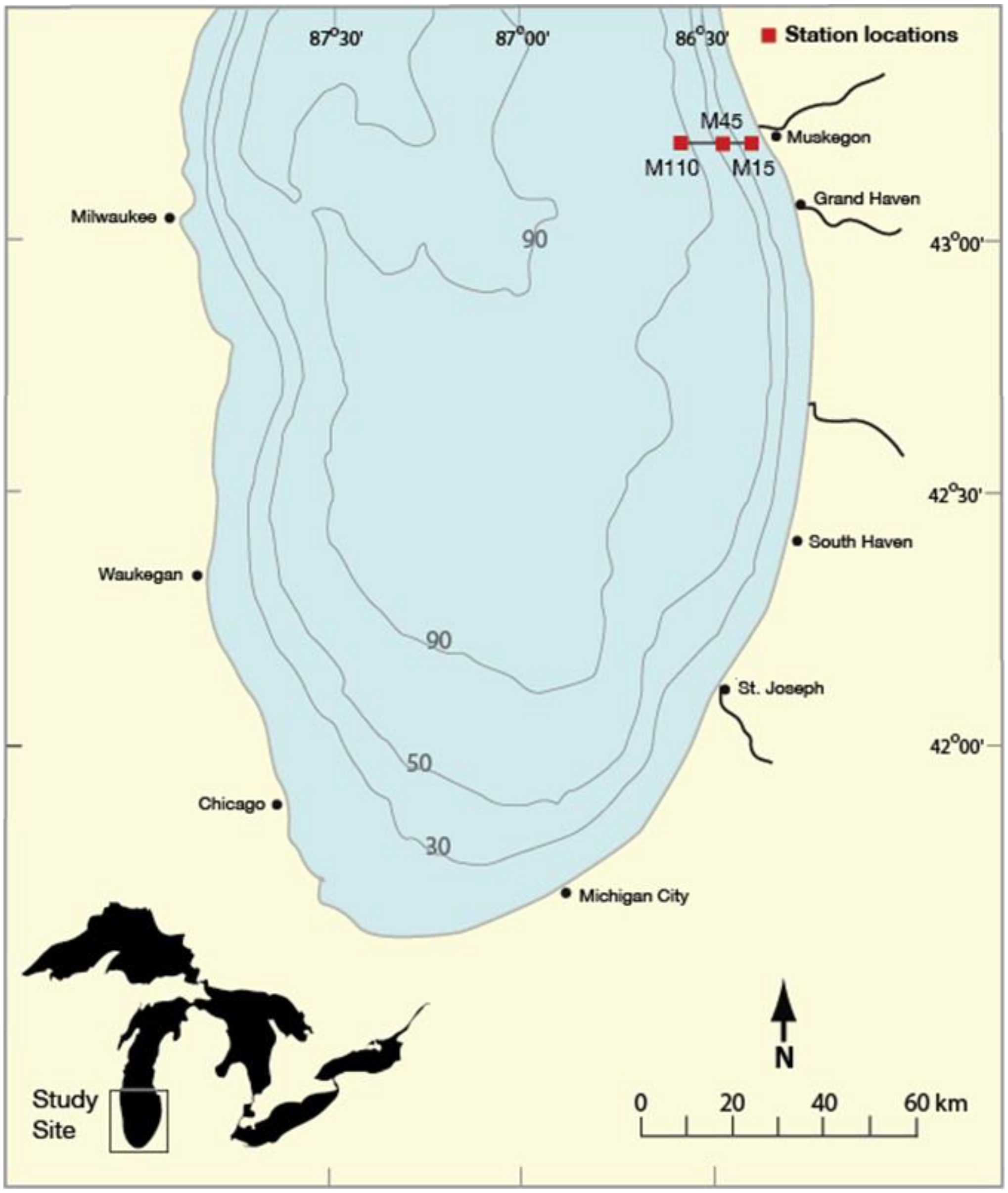

Figure B-1: Sampling sites along the Muskegon transect in Lake Michigan.

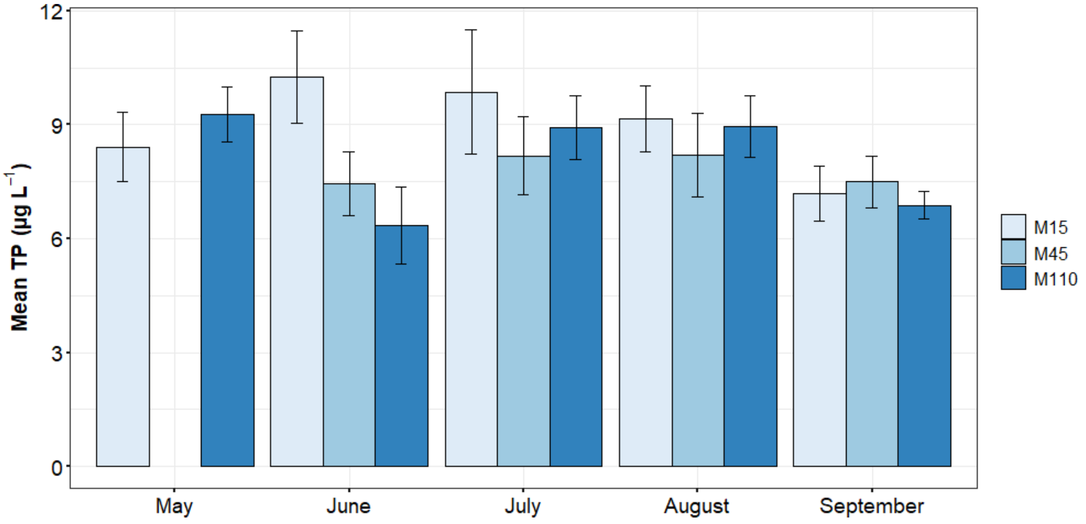

Figure B-2: Near surface (2- 5 m) mean (±SD) TP concentrations at M15, M45, and M110 from May to September in 2021.

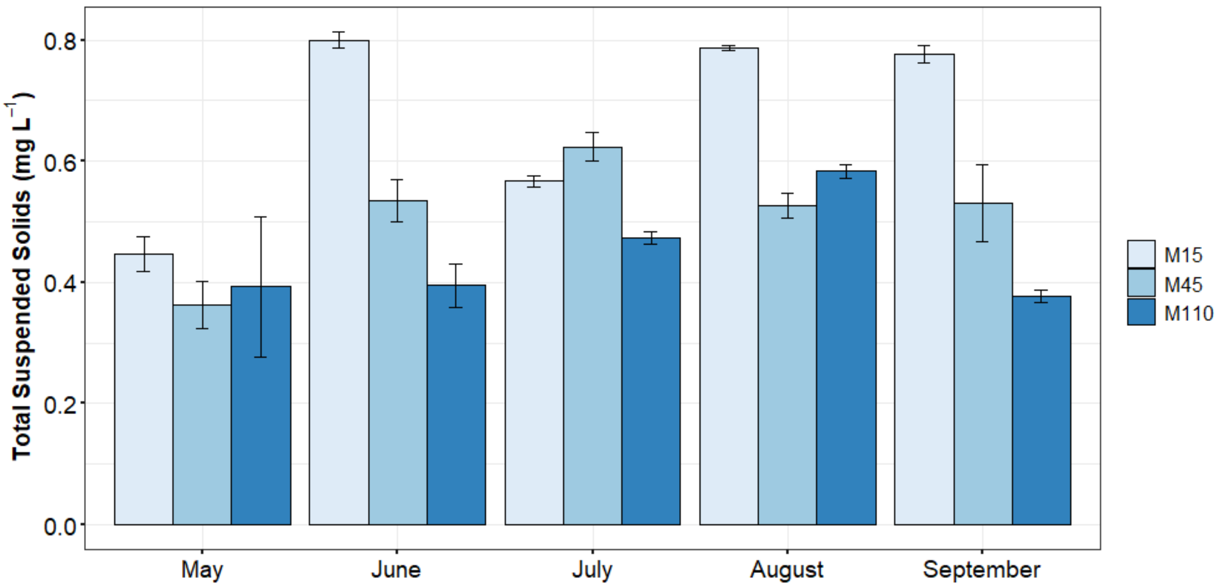

Figure B-3: TSS concentrations measured at 2m at M15, M45, and M110 in May, July and September 2021.

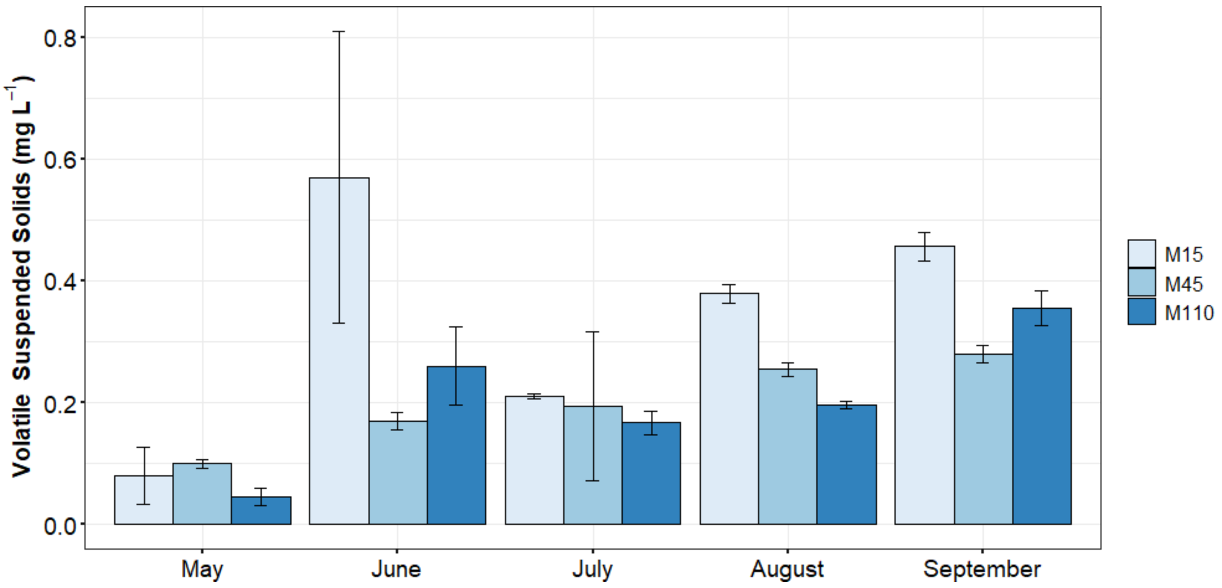

Figure B-4: VSS concentrations measured at 2-m depth at M15, M45, and M110 in May, July and September 2021.

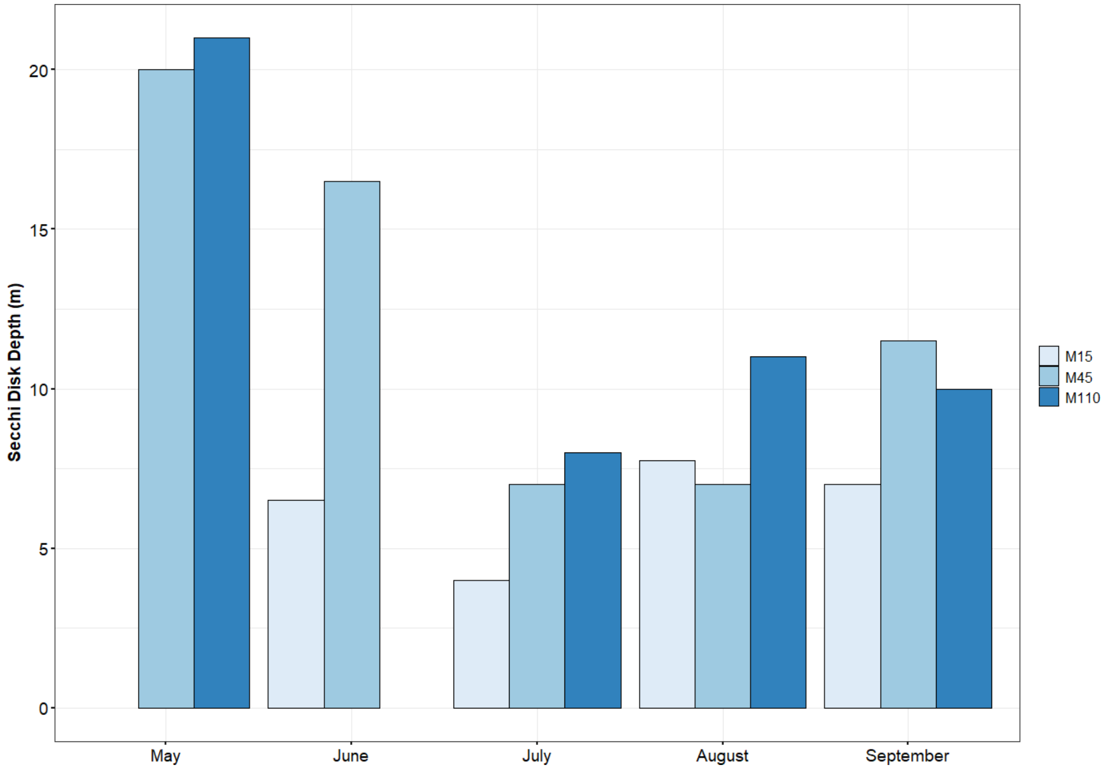

Figure B-5: Secchi disk measurements at nearshore (M15), mid-depth (M45), and offshore (M110) sites off Muskegon in May, July and September 2021.

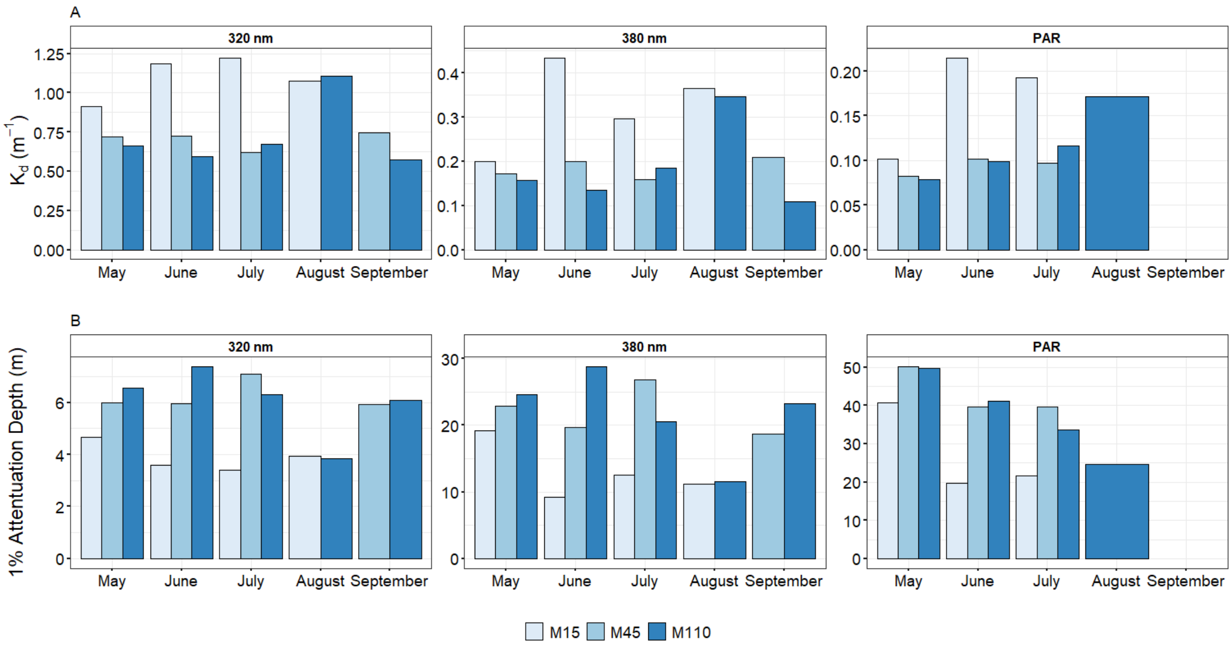

Figure B-6: Attenuation coefficients (A), and 1% attenuation depths (B) at three sites in Lake Michigan in 2021 for wavelengths of UV-B (320 nm), UV-A (380 nm), and PAR (400-700 nm).

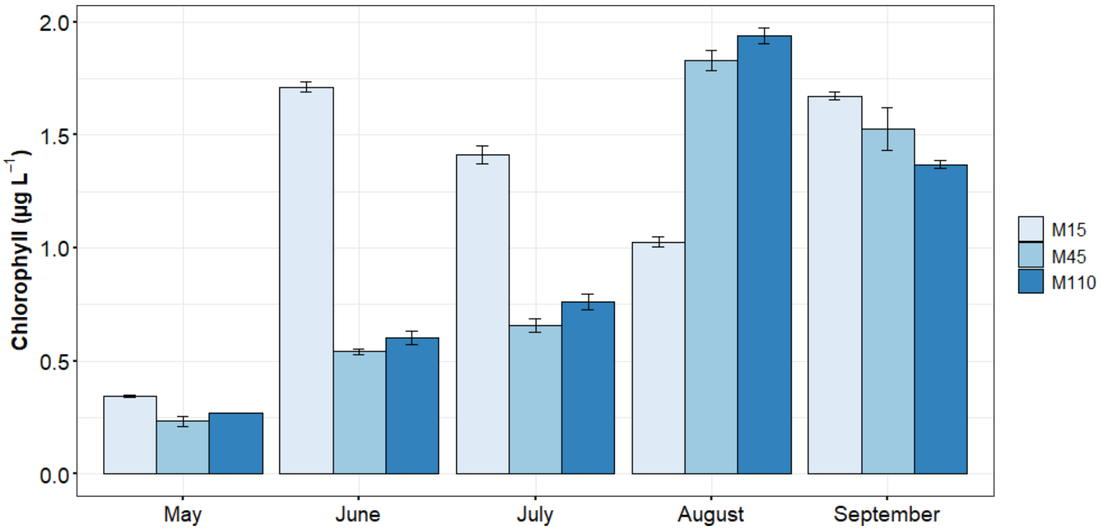

Figure B-7: Near surface (2-5 m) chlorophyll concentrations at the nearshore (M15), mid-depth (M45), and offshore station (M110) from May to September 2021.

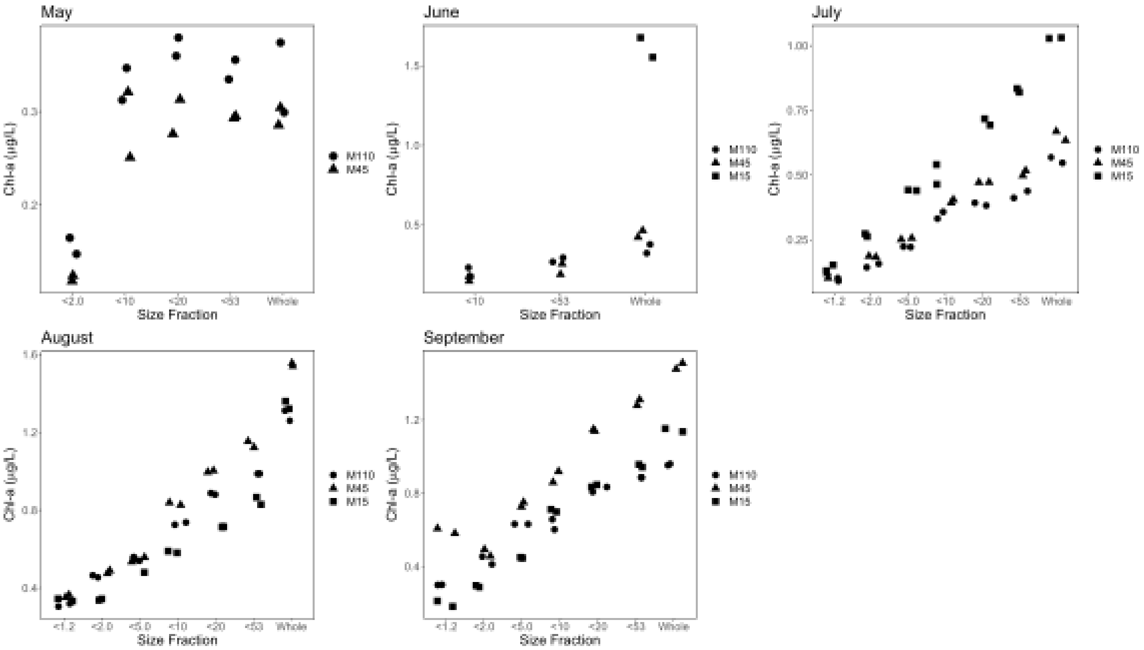

Figure B-8: Concentration of chlorophyll-a greater or equal to each size fraction for five cruises along the Muskegon transect.

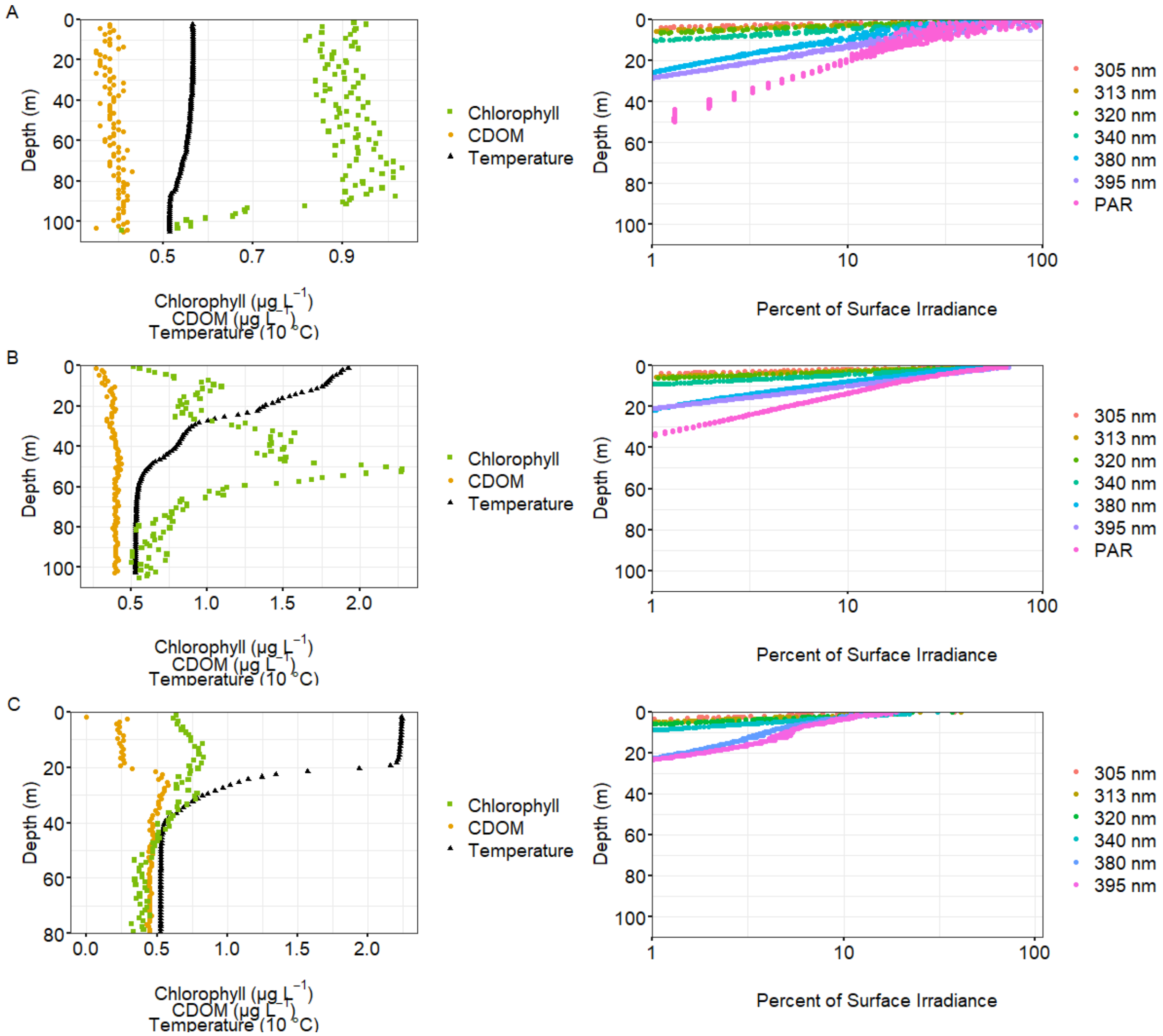

Figure B-9: Chlorophyll, temperature, and CDOM profiles from PSS and CTD profiles, paired with UV profiles for May (A), July (B), and September (C) 2021 at the M110 site in Lake Michigan.

Primary production (^{13}C method), chlorophyll a, optical properties- Casey Godwin, Andrew Camilleri (University of Michigan CIGLR):

Overview

Throughout 2021, we conducted four monthly (June-September) ^{13}C uptake experiments at two sites in Lake Michigan (M45 and M110, Figure B-1) to estimate primary production rates using the ^{13}C method. Photosynthetic rates, normalized to chlorophyll a, were then used to make photosynthesis–irradiance (PI) curves based on the model of Webb et al. 1974. We also measured optical properties of water and effects of chlorophyll on attenuation of light wavelengths.

Methods

Using a peristaltic pump, water was collected from 2 m aboard the R/V Laurentian on June 22nd, July 7th, August 3rd, and September 15th, 2021 at sites M45 and M110. Experiments were performed inside a temperature-controlled water bath with internal recirculation. Each experiment included incubating lake water at seven different levels of light intensity (0-1180 µmoles m^{-2} s^{-1}). We used two or four experimental replicates at each level of light, which consisted of 1 L PET square-sided media bottles. New bottles were used for each experiment. Bottles were filled with 1.0 L of unfiltered lake water and spiked with 20 ml of 10.2 mM $NaH^{13}CO_3$, representing <10% increase in concentration from ambient. Light was supplied by a Waveform Lighting Photon Panel delivering a daylight spectrum from a large array of LEDS. The light intensity gradient was created using a series of mesh filters in a covered 45 gallon polyethylene tank (Bockwoldt 2018). The first 5 light levels contained 4 1-L sample replicates (n=4), while the 6th light level contained 3 replicates (n=3) plus a sample wrapped in foil to achieve complete light exclusion. Light intensity at each level was determined by using an Apogee SQ-500 light meter. To control temperature, the tank was connected to a water circulation bath and heat exchanger while water was circulated through the tank using aquarium pumps. Water was kept within 2 degrees of *in situ* temperature. Samples were incubated in the chamber for 4 hrs and gently inverted every 30 minutes. After incubation, samples were filtered onto a combusted 0.7 µm GF/F filter and frozen until further analysis. In addition to the spiked incubated samples, non-incubated spiked samples and non-incubated raw samples were also filtered onto 0.7 µm GF/F filters at the beginning of each experiment. Prior to isotope analysis, filters were dried at 70 degrees C overnight and acidified by exposing to an atmosphere saturated with HCl from an open beaker of 12 M HCL for ~18 hours. Samples were then sent to the University of Wisconsin-Milwaukee where δ^{13}C was measured on an isotope ratio mass spectrometer (Thermo Scientific Delta V IRMS) with acetanilide as a standard for %C and glutamic acid as a standard for δ^{13}C. Photosynthetic rates were calculated as (Bockwoldt 2018, Hama et al., 1983):

$$P = \frac{C(a_{is}-a_{ns})}{t\,(a_{ic}-a_{ns})} \bullet 1.025$$

Where P=photosynthetic rate (mg m^{-3} hr^{-1}), C = particulate organic carbon (POC) concentration of the incubated sample (mg m^{-3}), a_{is}= ^{13}C atom % of incubated POC, a_{ns} = ^{13}C atom % of ambient background (initial raw samples) POC, a_{ic} = ^{13}C atom % of dissolved organic carbon (DIC) after the ^{13}C spike, and t = time (hr). Isotopic discrimination was corrected for by multiplying the photosynthetic rate by 1.025 (Hama et al., 1983, Bockwoldt 2018). Photosynthetic rates were then normalized to phytoplankton biomass (measured as chl-a).

Because photoinhibition was not apparent in visual inspection of the data (Figure B-10), biomass specific photosynthetic rates were fit to the model of Webb et al. 1974:

$$P^B = PBM \cdot (1-e^{-\alpha I/PBM})$$

Where P^B = photosynthetic rate normalized to biomass (mg C mg chl^{-1} hr^{-1}), PBM = maximum photosynthetic rate normalized to biomass at light saturation, α = initial linear slope (mg C mg chl^{-1} mol $photons^{-1}$ m^2), and I = irradiance (mol photons m^{-2} hr^{-1}). PI parameters were calculated using a Bayesian generalized non-linear model in the “brms” package in R (Bürkner et al. 2017, R Core Team 2022). We used weakly informative priors for the fitted coefficients (i.e. uniform distribution for PBM and alpha). Regressions were fitted using a Markov Chain Monte Carlo algorithm in stan (Stan Development Team 2023) using four chains with 1000 warmup iterations and 1000 sampling iterations each. The parameter estimates are the mean of the posterior samples and the standard error (SE) represents the standard error of posterior samples.

We also measured the attenuation of UV and visible wavelengths using water samples collected from 2 m depth along the Muskegon transect. Those samples were analyzed using an Ocean Insight Flame spectrometer and DH-Mini light source coupled to a World Precision Instruments UltraPath capillary waveguide flow cell with path lengths of 2, 10, 50, and 200 cm. Using a 10 cm path length, this method resolves spectral attenuation from approximately 250 nm to 900 nm. Samples were run both as whole water (containing seston) and only the dissolved fraction (< 0.2 µm).

Results/Discussion

Across all sampling dates and light treatments, photosynthetic rates (mg C mg chl^{-1} hr^{-1}) at M45 averaged 0.66 and ranged from -0.05 to 2.3. At M110 photosynthetic rates (mg C mg chl^{-1} hr^{-1}) averaged 0.30 and ranged from -0.04 to 3.5. No signs of photoinhibition were observed in any experiments (Figure B-10). For both M45 and M110, α was highest in June (Table B-2), possibly suggesting that the phytoplankton community was more efficient at using low levels of light earlier in the season. Throughout all sampling dates, M45 had a lower average α (3.8 mg C mg chl^{-1} mol photons^{-1} m^{2}) compared to M110 (4.5 mg C mg chl^{-1} mol photons^{-1} m^{2}). PBM (max photosynthetic rate at light saturation) showed no discernible seasonal pattern, but was slightly higher at M110 (2.3 mg C mg chl^{-1} mol photons^{-1} m^{2}) compared to M45 (1.8 mg C mg chl^{-1} mol photons^{-1} m^{2}). The range of α values observed at M45 and M110 throughout the season (2.2-8.2 mg C mg chl^{-1} mol photons^{-1} m^{2}) was similar to other studies in Lake Michigan (Bockwoldt 2018). However, the maximum α value observed in this study was lower than that of Bockwoldt 2018. PBM was comparable, but was higher than the PBM values of Bockwoldt 2018.

Laboratory measurements of light attenuation made using the capillary waveguide were in good agreement with the attenuation measured from the UV radiometer (Figure B-11). Figure B-12 shows that particles play a small role in attenuation of UV, but accounted for up to 20% of attenuation at 310 nm. Seston contributed 63% and 37% of total PAR attenuation for seston < 20µm and < 5 µm, respectively, but 20% and 15% of total attenuation at 310 nm. We used the difference between the dissolved and whole water absorbance together with the measurements of chlorophyll, to estimate how the 1% intensity depth would vary as a function of particles (as chlorophyll-a), such as the changes that occurred following expansion of invasive mussels. Figure B-13 shows that the abundance of chl-a containing seston (i.e. phytoplankton) has a large impact on the depth of PAR penetration, less impact on penetration of UV-A, and little discernible impact on penetration of UV-B. These results support the hypothesis that *Dreissena* invasion and expansion affected visible light proportionally more than UV. Though smaller in magnitude, these changes in UV attenuation and penetration can have important effects on zooplankton, larval fish, and photochemical reactions at the surface.

Tables and Figures

Table B-2: Photosynthetic parameters from all experiments. Values in parentheses are the standard error of the estimate.

Date	**Site**	**α (±E)**	**PBM (±E)**
June	M45	4.8 (0.71)	2.2 (0.12)
July	M45	2.5 (0.20)	1.5 (0.05)
August	M45	3.5 (0.30)	2.1 (0.07)
September	M45	2.8 (0.23)	1.4 (0.05)
June	M110	8.2 (1.4)	3.3 (0.21)
July	M110	4.8 (0.27)	2.4 (0.05)
August	M110	2.2 (0.35)	1.4 (0.09)
September	M110	2.9 (0.15)	2.1 (0.04)

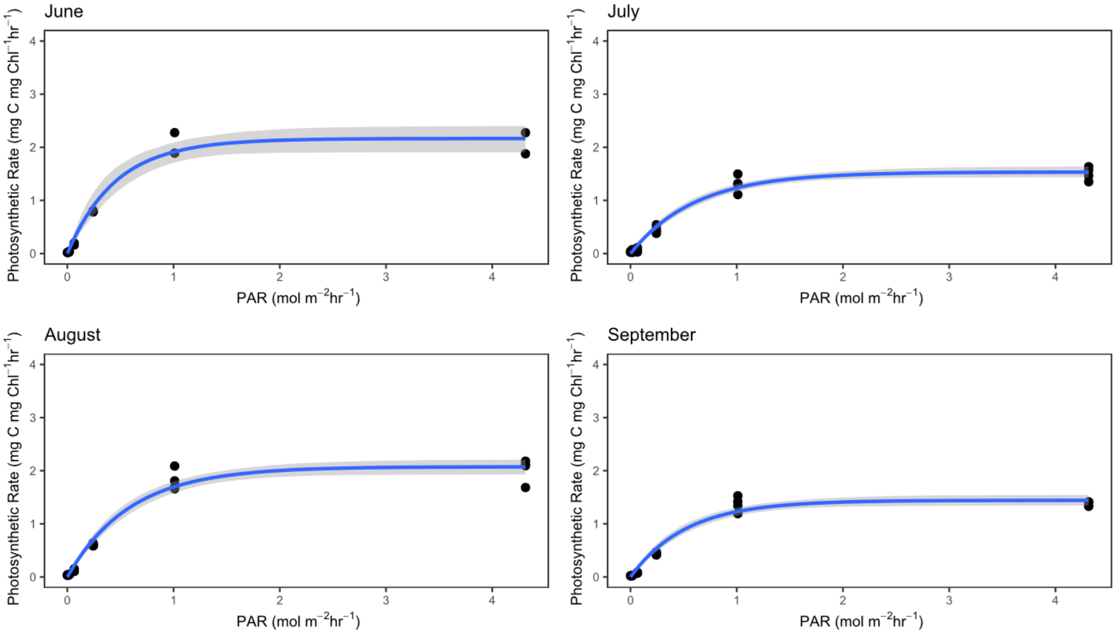

M45

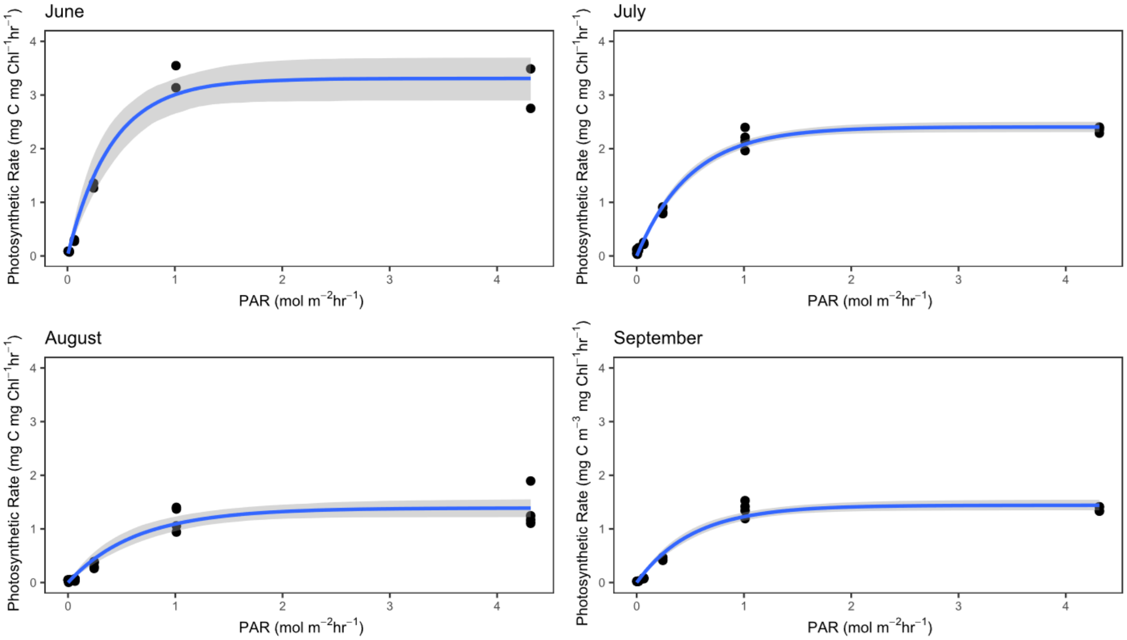

\

M110

Figure B-10: PI curves from all experiments for (TOP) the mid-depth site (M45); and (Bottom) the offshore site (M110). Points represent experimental values. The blue line represents the Bayseian nonlinear model from the equation of Webb et al. 1974. The gray shaded region represents the 95% credible interval for the prediction, which is based on the posterior samples for both parameters.

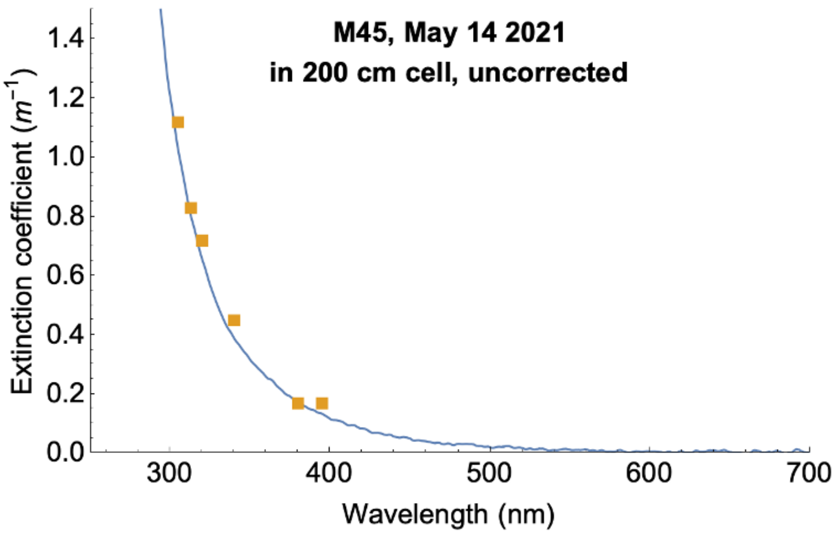

Figure B-11: Extinction coefficients from the laboratory method (blue line) and the UV radiometer profiles (squares).

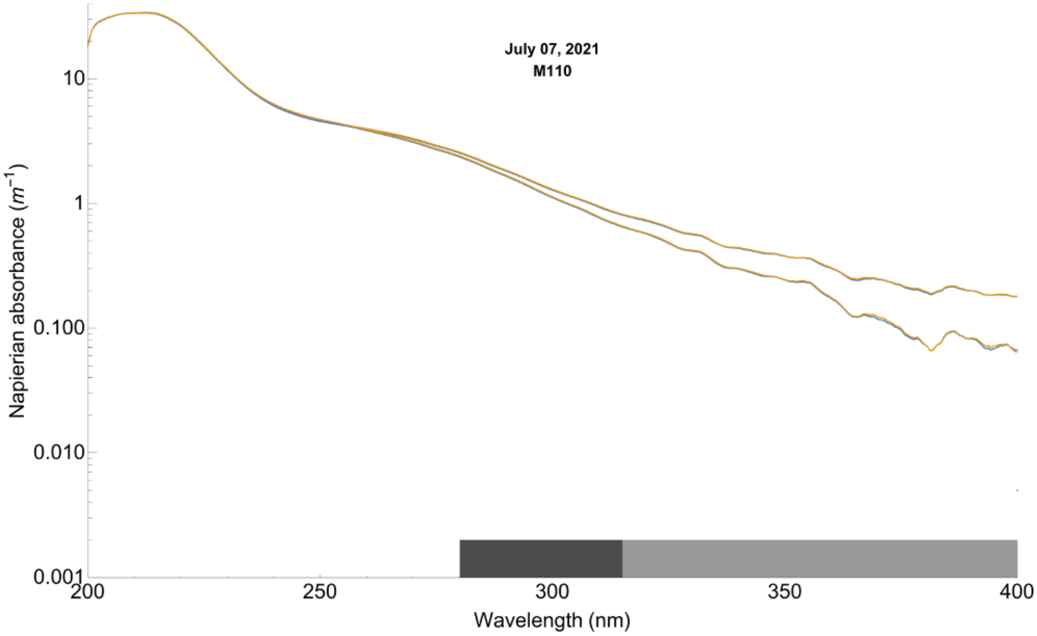

Figure B-12: Napierian absorbance (log scale) in the ultraviolet measured using the laboratory method. The lower lines are replicate spectral scans of the dissolved fraction only and the upper lines are the sample containing seston. The dark gray bar represents UV-B and the light gray bar represents UV-A. Note that due to the 10 cm path length, attenuation measurements below 250 nm are not reliable.

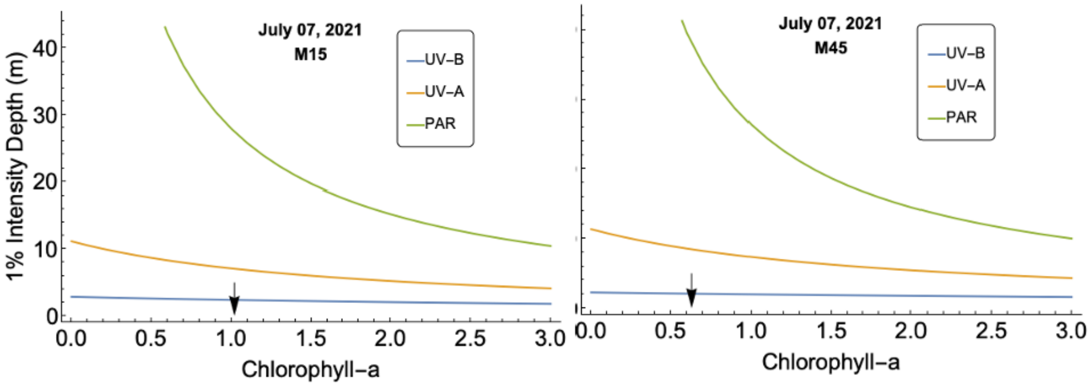

Figure B-13: Predicted change in the 1% intensity depth of UV-A (380 nm), UV-B (310 nm), and PAR (400-700 nm) due to change in abundance of seston as chlorophyll concentration. In each panel the arrow on the horizontal axis denotes the ambient chlorophyll-a concentration at the time of sampling.

Chlorophyll Biomass, Phytoplankton Composition, Primary Production (^{14}C method),* Carrick (CMU)*:

Overview

The hypotheses being tested are that the bulk of seasonal variation in phytoplankton biomass and production can be attributed to spring blooms (diatoms) that occupy a small, nearshore region in the southern basin of Lake Michigan (see Carrick et al. 2015; Denef et al. 2017). Moreover, higher production by small-celled phytoplankton (pico and nanoplankton) contribute the majority of primary production in the lake; their rates of production are large enough to compensate for the overall reduction in phytoplankton biomass (Fahnenstiel and Carrick 1992).

Methods

Taxonomic composition and biomass (as cellular carbon content) of plankton was measured using a stratified enumeration technique that relied on both light and epifluorescence microscopic analysis of preserved water samples (see Carrick and Schelske 1997; Carrick et al. 2015). Two estimates of ^{14}C -based primary production were measured on water samples. At the same time, Pulse-Amplitude Modulated (PAM) fluorometry was used to derive proxies of primary production (see below).

Photosynthesis versus irradiance relationships were determined using a closed incubation system (Fitzwater et al. 1982; Fahnenstiel et al. 1989). Raw lake water (100 ml) was inoculated with NaH^{14}CO3 (final activity 1,000 µCi L^{-1}, Perkin Elmer) and 3-5 ml of labeled water was dispensed into 20 scintillation vials (20 ml) for incubation. Individual vials were incubated at one of 18 different PAR levels, ranging from 2 to 1,600 µmol m^{-2} s^{-1} for relatively short incubation periods (1 hr). One vial was processed immediately as a time zero blank and the other to verify the total activity added. Size-specific carbon uptake was measured from mesocosm type experiments where large volumes of water (replicate 500 ml polycarbonate) were inoculated at low activity (final activity 1 µCi L^{-1}) and incubated for longer time periods (see Fahnenstiel and Carrick 1992). Following incubation, all samples were concentrated onto membranes (0.7 µm, Whatman GFF) and decontaminated in the vials with 1.0 ml of 0.5N HCl for 24 h in a fume hood. Counting fluor (Ecolume) was added to each scintillation vial containing experimental samples; these were assayed using a Beckman 6500 Scintillation counter along with external standards and blanks.

Pulse-Amplitude Modulated (Phyto-PAM) fluorometry was used to estimate wavelength-specific (for red, orange, green, blue, and violet light) phytoplankton photosynthetic capabilities (Waltz, Germany). Electron transport system activity (ETS, a proxy for photosynthesis) versus irradiance curves were constructed by exposing raw lake water (4 mL) to a range of twenty levels of 5 wavelengths of light (red, orange, green, blue, violet) and total light (PAR); these quantities were delivered through pulse modulation (2 to 2,000 µmol m^{-2} s^{-1}). Replicate trials were performed on individual samples (date, site, depth) and averaged together for each sample.

For all experiments, photosynthesis (^{14}Carbon uptake or ETS) estimates were regressed against irradiance using non-linear regression (Phytotools package for R programming). Key parameters were derived from regression analysis that included: Pmax (photosynthesis maximum), Alpha (efficiency of light harvest), and Ik (point of light saturation).

Results and Discussion

Planktonic chlorophyll varied along the near to offshore gradient in 2021; concentrations were higher at M15 nearshore from May-July (Figure B-14) followed by a reversal where concentrations were higher in offshore (M45 and M110) waters, particularly in August. In previous years, phytoplankton biomass was typically higher nearshore during a limited temporal window in spring to early stratification period (Carrick et al. 2015; Pothoven et al. 2020). The unique pattern observed in 2021 was most likely the result of an upwelling event in the southern basin of Lake Michigan that delivered colder, deep water that was recorded at M45 and M110. That said, the phytoplankton size structure based on fractionated chlorophyll showed that the <2 µm (picoplankton) category contributed anywhere from 40-80% of total chlorophyll. Interestingly, the assemblage shifted from <2µm dominance (60-80%) to dominance by phytoplankton >2 µm in August and September after the upwelling. This pattern was reflected in the negative correlation between <2µm chlorophyll and temperature

(Spearman Rank, r= -0.699, n=12, p=0.011). These data also indicate that phytoplankton in Lake Michigan have a carbon to chlorophyll ratio of 70 which is typical for that observed in other parts of the Great Lakes (Carrick et al. 2005).

Phytoplankton cellular carbon estimates were measured in 24 samples in order to evaluate seasonal changes in biomass and taxonomic composition (Figures B-15, B-16). These data showed a slightly different pattern compared with chlorophyll, despite the fact the two measurements were strongly correlated (Figure B-15). On average, phytoplankton carbon was greater at the most offshore station M110, particularly in July and August. The assemblage at all three stations was dominated by Chrysophytes (*Dinobryon* species, *Chrysochromulina parva*) and diatoms (*Cyclotella*, *Discotella*, and *Fragilaria* species), with Cryptophytes being consistently subdominant in nearly all samples (Figure B-16). Several species of dinoflagellates (*Gymnodium helveticum*, *G. varians*, and *Cystodinium*) were abundant nearshore and offshore in July-August. Dinoflagellates commonly occur in the deep chlorophyll layer in Lake Michigan (Carrick and Fahnenstiel 1989; Carrick 1995) and may have been mixed into the surface waters once the thermocline was disrupted. Interestingly, the peak occurrence in phytoplankton biomass we measured was dominated by diatoms and dinoflagellates that generally grow in the spring or in the vicinity of the deep chlorophyll layer in summer. Their occurrence in our samples during early July and August corresponds nicely with lower temperature and increased chlorophyll fluorescence values recorded in early July and August at the 20-m buoy along the Muskegon transect in Lake Michigan (see Figure D-6 below, see Rowe et al. 2022).

To evaluate seasonal variation in size specific primary production, a series of 5 experiments were done at each of the 3 sampling stations along the Muskegon transect (5 x 3= 15, surface water, Figure B-17). Primary production rates (PPr) exhibited seasonal variation among the five sampling dates, although the seasonal pattern was remarkably similar among the three stations. In general, PPr values increased from June to July, and then declined by more than 50% in August and September (Figure B-17). The range in PPr was similar at each station, where average (± standard deviation) rates were 2.89 ± 1.62, 2.89 ± 1.44, 3.48 ± 2.01 at M15, M45, and M110, respectively. Size specific production was dominated by the <2 µm picoplankton fraction and their contribution became more important offshore. The picoplankton contribution ranged from 17-40% at M15, 24-81% at M45, and 21-81 at M110; their contribution decreased throughout the season from June to September. The percent contribution of PPr among plankton size classes also tracked that observed for chlorophyll (see Figure B-14). The percent contribution observed here was higher than those measured previously in Lake Michigan. Fahnenstiel and Carrick (1992) measured 22-52% contribution by picoplankton; these results suggest that production by picoplankton has become more important in recent years (see Carrick et al. 2015).

We performed 17 photosynthesis versus irradiance experiments during 2021 from samples collected along the near to offshore transect (Table B-3). All data were fit using the model of Eilers and Peeters (1988). Our values for P_{max} (maximum rate of light saturated photosynthesis) ranged from 0.63 to 5.77 $\mu gC \bullet \mu gchl^{-1} \bullet h^{-1}$. The values for alpha ranged from 0.01 to 0.16 $\mu gC \bullet \mu gChl^{-1} \bullet \mu Einst^{-1} \bullet m^{-2}$ and value for I_k were 23.8 to 435.6 $\mu Einst.\ m^{-2} \bullet s^{-1}$. We observed photoinhibition in 7 of the 8 experiments done in June and July. These results were interesting because photoinhibition is typically observed on a winter or early spring assemblage, so to observe a pattern in June-July was unique (see Fahnenstiel et al. 1989). Our estimates for P_{max} are comparable with previous results from other locations in the Great Lakes. For instance, Fahnenstiel et al. (1989) measured seasonal values for P_{max} from a similar set of experiments done on surface water assemblages in Lakes Michigan and Huron; their values bracket those measured here (1.07 to 4.06 $\mu gC \bullet \mu gChl^{-1} \bullet h^{-1}$). Similarly, our estimates for both alpha and I_k were comparable with their data (57 to 246 $\mu Einst.\ m^{-2} \bullet s^{-1}$). Hiriart et al. (2002) made lake-wide estimates of PPr parameters in Lake Erie; their values for P_{max} (2.86 to 5.68 $\mu gC \bullet \mu gChl^{-1} \bullet h^{-1}$) and I_k (60.9 to 270.0 $\mu Einst.\ m^{-2} \bullet s^{-1}$) were similar with those we measured here. Depew et al. (2006) worked in the eastern basin of Lake Erie after the establishment of invasive Dreissenid mussels; they derived similar values for both P_{max} (1.67 to 5.04 $\mu gC \bullet \mu gChl^{-1} \bullet h^{-1}$) to ours measured here. Furthermore, Fitzpatrick et al. (2007) presented carbon assimilation estimates of 1.3 to 5.5 $\mu gC \bullet \mu gChl^{-1} \bullet h^{-1}$ made in Lake Erie during the 1970-2002 period, which also spanned a similar range.

Ascertaining the key environmental factors that regulate photosynthetic rates and the associated model parameters can be difficult given the numerous interacting factors at play (e.g., Hecky et al. 2004). Using a stepwise regression analysis, only light transmission was selected out of some 20 physical-chemical variables (r^2=0.50, n=17, p=0.01) as the best predictor of P_{max} estimates. Photosynthetic parameters indicative of light harvesting capabilities varied as a function of phytoplankton composition and size structure. For instance, estimates of alpha were positively correlated with chrysophyte carbon (r=0.485, p=0.048). Chrysophyte taxa in our samples exhibited high growth capacity in previous experiments (Carrick et al. 1992), so that their positive covariance with values of alpha seems to make sense. Moreover, previous experimental work has shown that cyanobacteria species exhibit relatively poor light-harvesting capabilities, particularly when blue light is dominant (e.g., Luimstra et al. 2018). These results dovetail with the findings from our production versus irradiance experiments for Lake Michigan; cyanobacterial carbon was negatively correlated with estimates of alpha (r= -0.615, p=0.048) and positively correlated with estimates of Ik (r= 0.0645, p=0.009).

Forty short-term measurements were performed using pulse amplitude modulated (PAM) fluorometry to evaluate patterns in light utilization by phytoplankton in Lake Michigan (Figure B-18). Electron transport rates (ETR) can be used as a reliable proxy for photosynthesis (e.g., Schmitt-Jansen M and Altenburger R. 2008). In Lake Michigan, phytoplankton performed higher rates of photosynthesis using smaller wavelengths of light (violet and blue) compared with green, orange, red - these rates were 50% greater (Figure B-18). Similarly, phytoplankton had high assimilation rates for violet and blue light (0.15 versus 0.10 ETR • µE •m^{-2}), and hence were more efficient in their use of these wavelengths to fuel metabolism. Conversely, there was very little difference in Ik (average rate of photosynthesis per unit light) values among wavelengths. Size fractions of phytoplankton appear to be utilizing specific wavelengths of light differently, perhaps constituting unique niches (Table B-4). For instance, the abundance of small picoplankton (as < 2µm chlorophyll) was negatively correlated with Kpar, suggesting a need for high light. They also were negatively correlated with assimilation rates (alpha) for orange light, while at the same time, the biomass of median cell sized nanoplankton was correlated with higher rates of photosynthesis (Pmax values) with the addition of orange and red light and assimilation of orange light. The biomass of larger > 20 µm microplankton was correlated with assimilation rates for red light.

Tables and Figures

Table B-3: Parameters derived from photosynthesis versus irradiance experiments using ^{14}C uptake. Samples were collected seasonally along the Muskegon transect in southern Lake Michigan (2021). Alpha and Pmax estimates were derived (average ± one standard error) using the Eilers and Peeters (1988) non-linear regression model.

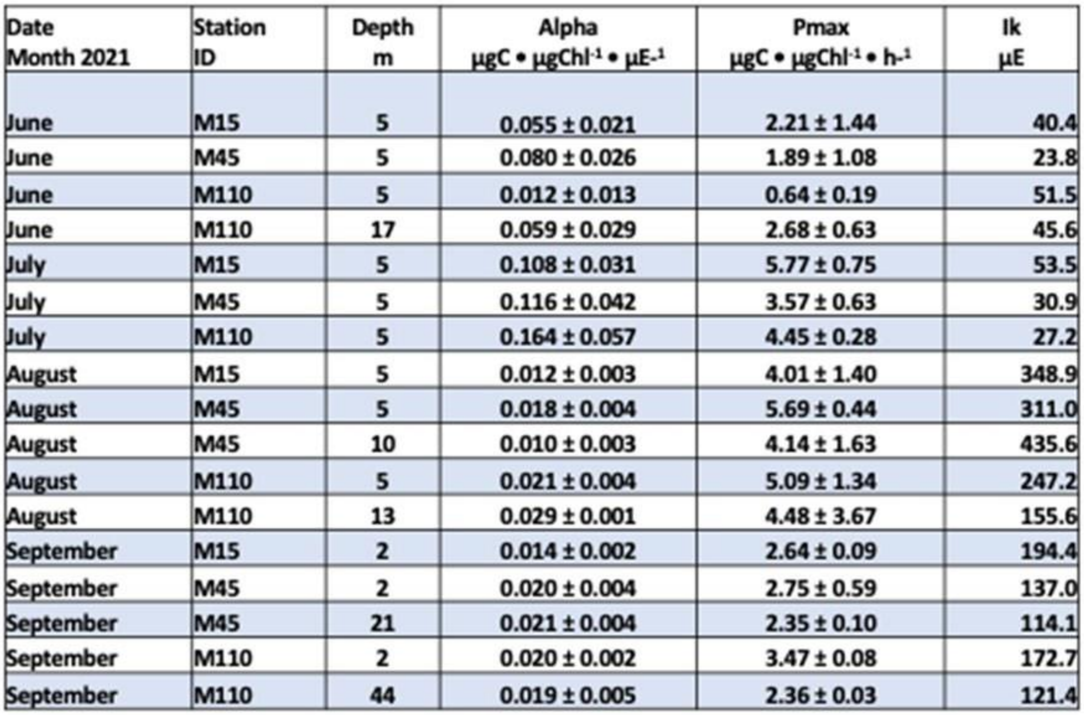

Date Month 2021	Station ID	Depth m	Alpha $\mu gC \bullet \mu gChl^{-1} \bullet \mu E^{-1}$	Pmax $\mu gC \bullet \mu gChl^{-1} \bullet h^{-1}$	Ik μE
June	M15	5	0.055 ± 0.021	2.21 ± 1.44	40.4
June	M45	5	0.080 ± 0.026	1.89 ± 1.08	23.8
June	M110	5	0.012 ± 0.013	0.64 ± 0.19	51.5
June	M110	17	0.059 ± 0.029	2.68 ± 0.63	45.6
July	M15	5	0.108 ± 0.031	5.77 ± 0.75	53.5
July	M45	5	0.116 ± 0.042	3.57 ± 0.63	30.9
July	M110	5	0.164 ± 0.057	4.45 ± 0.28	27.2
August	M15	5	0.012 ± 0.003	4.01 ± 1.40	348.9
August	M45	5	0.018 ± 0.004	5.69 ± 0.44	311.0
August	M45	10	0.010 ± 0.003	4.14 ± 1.63	435.6
August	M110	5	0.021 ± 0.004	5.09 ± 1.34	247.2
August	M110	13	0.029 ± 0.001	4.48 ± 3.67	155.6
September	M15	2	0.014 ± 0.002	2.64 ± 0.09	194.4
September	M45	2	0.020 ± 0.004	2.75 ± 0.59	137.0
September	M45	21	0.021 ± 0.004	2.35 ± 0.10	114.1
September	M110	2	0.020 ± 0.002	3.47 ± 0.08	172.7
September	M110	44	0.019 ± 0.005	2.36 ± 0.03	121.4

Table B-4: Spearman rank correlation coefficients assessing covariation between chlorophyll concentrations in algal size categories and photosynthetic parameters derived for specific wavelengths of light (using PAM fluorometry) or water column kpar. * significant at $p < 0.05$.

Fraction	**Water Kpar**	**Orange light P_{max}**	**Red light P_{max}**	**Orange light Apha**	**Red light Alpha**	**Conclusion**
< 2 µm Pico	-0.671*	-	-	-0.627*	-	Inefficient light, Org
2-20 µm Nano	-	0.691*	0.664*	0.700*	-	Efficient use of Org
>20 µm Micro	-	-	-		0.673*	Efficient use of Red

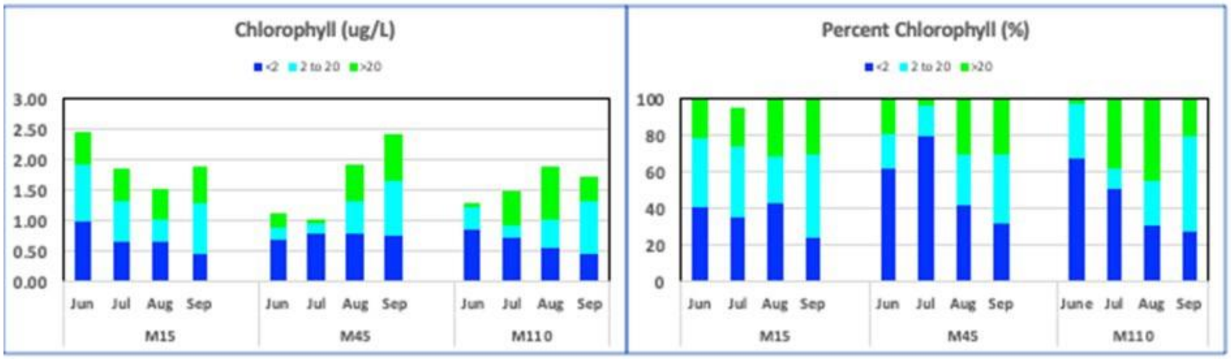

Figure B-14: Size-specific chlorophyll measured in surface water for samples collected along the Muskegon transect in southern Lake Michigan (2021).

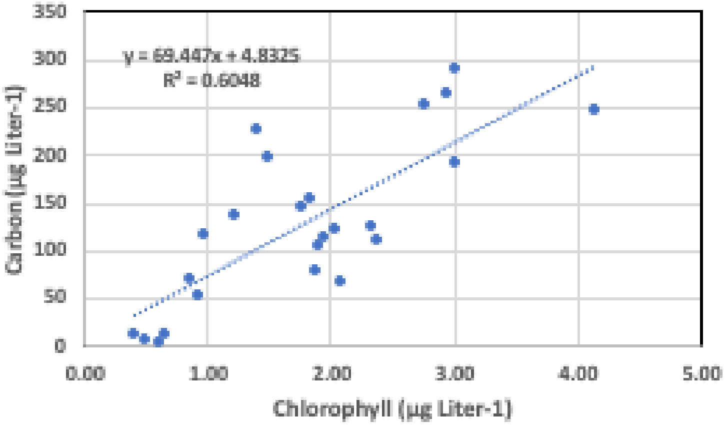

Figure B-15: Relationship between phytoplankton carbon (from cell counts) and chlorophyll concentrations measured from samples collected along the Muskegon transect in southern Lake Michigan (2021).

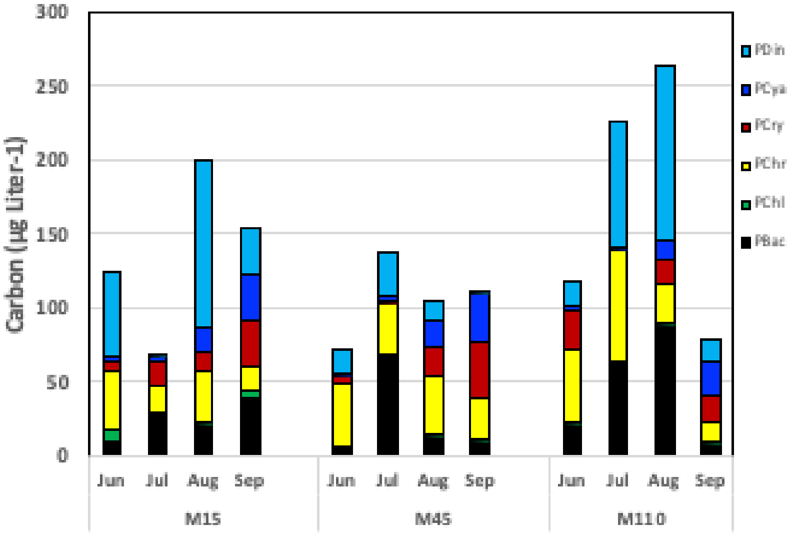

Figure B-16: Taxonomic composition of phytoplankton (as cellular carbon) in the surface waters along the Muskegon transect in southern Lake Michigan (2021). Where PDin= Dinoflagellates, PCya=Cyanobacteria, PCry=Cryptophytes, PChr= Chrysophytes, PChl=Chlorophytes, and PBac=Diatoms.

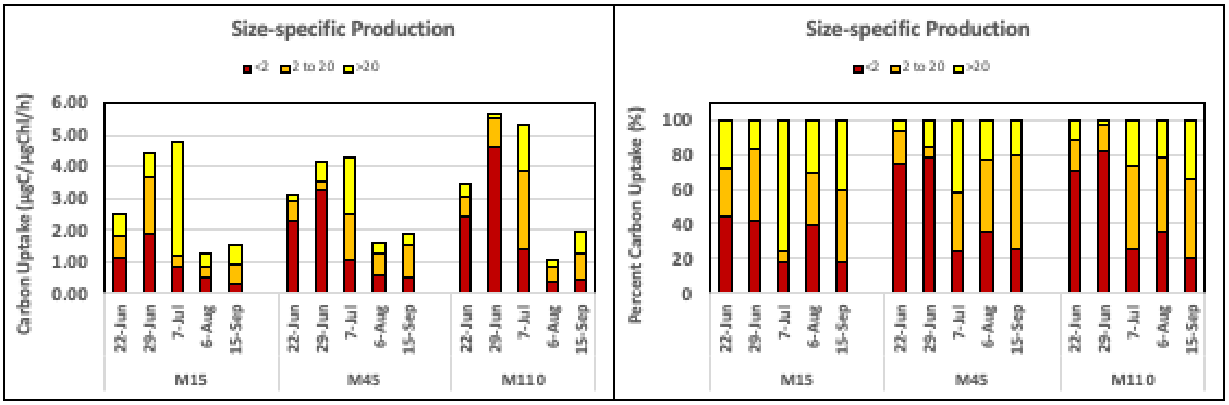

Figure B-17: Size-specific primary production estimates (measured as carbon uptake) for samples collected seasonally along the Muskegon transect in southern Lake Michigan (2021).

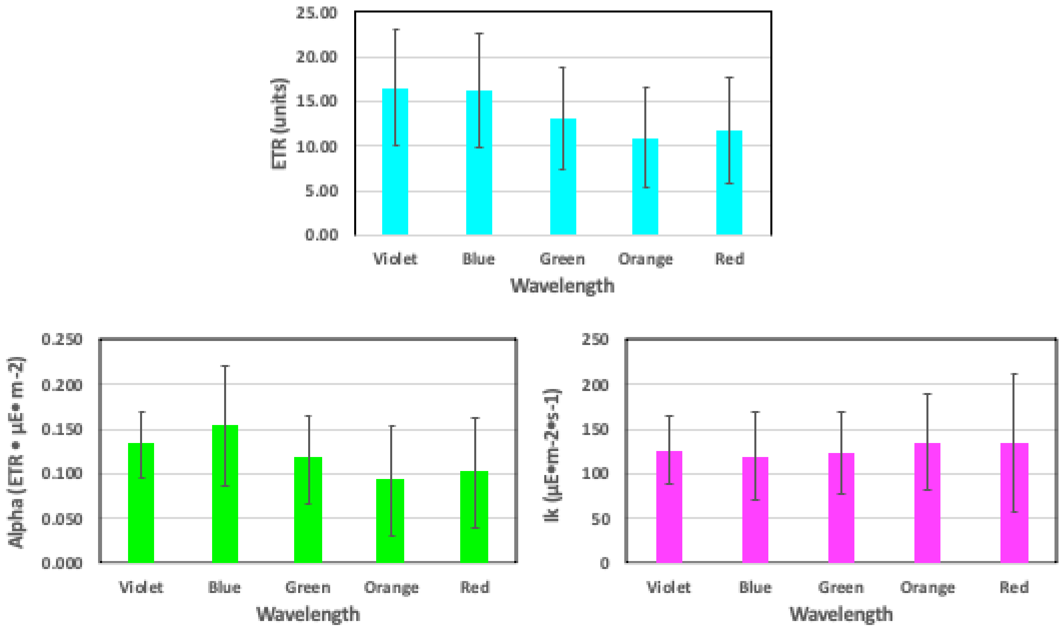

Figure B-18: Wavelength-specific parameters derived from photosynthesis versus irradiance experiments using pulse amplitude modulated (PAM) fluorometry; samples were collected seasonally along the Muskegon transect in southern Lake Michigan (2021).

Zooplankton, Larval Fish, Mysis, and older Fish (NOAA):

Overview

Laboratory experiments and studies in clear mountain lakes have demonstrated UV light is lethal to zooplankton and larval fish, and can affect their vertical distribution (eg., Williamson 2011). We conducted diel sampling in May and August, and daytime sampling in June, July and September at nearshore and offshore sites to determine fine-scale vertical structure of zooplankton, larval fish and Mysis. As *Dreissena* mussel biomass has increased in Lake Michigan, their veligers have become an abundant component of the zooplankton community, and are suspected of having negative effects on larval fish growth. We aged larval fish, estimated their growth rates, and examined their diets to compare larval growth rates with data from past CSMI studies.

Methods

We used LOPC and a suite of metered plankton nets to collect zooplankton, fish larvae, and Mysis, and estimate their density through the water column and at specific depths. At each site, zooplankton were sampled by tow-yoing the Plankton Survey System with LOPC (Table B-1) for 30-40 minutes along an isobath transect at a site, and by replicate tows (n=2) of metered 64 and 153-$\mu\mu$m mesh nets deployed from near bottom to surface and/or tripped at depth. Zooplankton samples were preserved in 5% buffered formalin and identified to species back in the laboratory.

Larval fish were sampled near surface using a 2-m^2 neuston net (505 $\mu\mu$m mesh), or at depth by a paired bongo sampler (60-cm diam., with 333- and 505-$\mu\mu$m mesh), a 2-m^2 Tucker trawl (700 micron mesh), or a multiple opening/closing net and environmental sensing system (MOCNESS, with 1-m^2 opening and 333, 505 or 1000 $\mu\mu$m mesh nets. Mysis biomass and abundance were sampled at depth with MOCNESS and fisheries acoustics. All larval fish and Mysis tows were replicated (n=2) and towed for 5 minutes at a targeted depth. Larval fish samples were preserved in 95% ethanol, brought back to the laboratory and sorted to remove fish and Mysis. Larval fish were identified to species (Auer 1982), measured, and their otoliths were removed to estimate hatch dates and growth rates. Larvae stomachs were removed for further diet analysis. Growth rates (mm/d) of individual larvae were calculated by subtracting larvae length at hatch from length at capture and dividing by estimated age. Larvae growth rates were compared across CSMI years using ANCOVA, (Length~age+year+age*year), and differences were expressed as adjusted mean lengths.

Zooplankton prey items in larval fish diets were identified to species, enumerated, and their dry biomass estimated from plankton lengths. Prey items that could not be identified (UID) were counted as present, but not included in the percent biomass of prey in the larva's stomach. To summarize diet results for Alewife and Bloater, fish were categorized into 5 mm length bins (i.e. 0-5 mm, 5-10 etc.).

Fisheries acoustics (transducer strength = 120khz) was run at the same time as the PSS to get a coupled view of plankton, pelagic planktivore and piscivore biomass. These data are still being processed at this time.

Results and Discussion

Zooplankton

From May 10th to September 16th 2021, we collected a total of 162 zooplankton samples from three sites (M15, M45, and M110) in Lake Michigan, and 4 samples from Muskegon Lake. Of the 168 samples collected, 135 samples have been sorted. Sample processing is still ongoing as of April 2023. Zooplankton species were grouped into major orders or functional groups for reporting purposes.

Total zooplankton biomass nearshore at M15 increased from May through August, then declined in September (Figure B-19). Copepodites, herbivorous cladocerans (Bosmina longirostrus), and predaceous cladocerans comprised the majority of total biomass. Total zooplankton biomass offshore at M110 also increased from May through August and declined in September, and was higher in each month than at M15. Offshore, more herbivorous cladocerans were found in September than in June and July (Figure B-20). Immature diaptomid copepodites (C1-C5) comprised the majority of the total biomass overall (21.7%), followed by Daphnia galeata mendotae (10.1%), female Leptodiaptomus minutus (7.8%), and immature cyclopoids (C1-C5) (7.2%). At M15, omnivorous copepod biomass was very high at night in August compared to other months, especially compared to biomass of other species (Figure B-21). At M110 in July, most groups were found in the metalimnion during the day but smaller zooplankton (nauplii and copepodites) were found near the surface (Figure B-22).

Fish larvae densities

From May 10th to September 16th 2021, we collected a total of 144 samples (28 Bongo replicates, 80 MOCNESS samples, 32 Neuston tows, and 4 Tucker trawls) from Lake Michigan and Muskegon Lake. We collected 250 total fish larvae from 138 samples (24 Bongo replicates, 80 MOCNESS samples, 30 Neuston tows, and 4 Tucker trawls) from Lake Michigan. Alewife made up a majority of the catch (48.4%) followed by Bloater (43.6%), Burbot (3.6%), and Deepwater Sculpin (4%), with 0.4% of the total unidentifiable. No yellow perch larvae were collected from Lake Michigan samples in 2021.

Mean Bloater densities peaked in June (4.1/1000m^3) and Alewife densities peaked in July (14.3/1000m^3) (Figure B-23). Mean density of Alewife and Bloater larvae was higher at night than during the day in August, summarized for all sites, depths, and nets. Alewife mean density at night was 4.6/1000m^3 compared to 3.0/1000m^3 during the day, while Bloater mean density at night was 1.9/1000m^3 compared to 1.3/1000m^3 during the day.

Densities of Alewife and Bloater larvae varied among CSMI years. Alewife larvae mean density was greatest in June 2015, while in 2010 and 2021, densities were highest in July (Figure B-24). In July of all three CSMI years, Alewife larvae were found in the epilimnion at nearshore site M15 (Figure B-25a). In 2010, more Alewife were collected during the day compared to 2015 and 2021 when more were found in the epilimnion compared to the surface (Figure B-25b). In 2021, Bloater density was highest in June 2021 compared to July in both 2015 and 2010 (Figure B-26). More Bloater also were found near surface offshore in 2021 (Figure B-27a), compared to 2010 when most of the Bloater were found near the metalimnion and hypolimnion during the day in July (Figure B-27b).

Fish larvae lengths, ages, growth rates, and hatch dates:

Alewife median lengths varied among CSMI years and were largest in 2021 (Figure B-28a). Although most small and young Alewife were collected nearshore at site M15 in 2021, larger and older Alewife were collected further offshore at M45. Median length of Bloater larvae collected in 2021 also was higher than in 2010 or 2015 (Figure B-28b).

Lengths at age of Alewife were significantly higher ($p<0.0001$) in 2021 than in 2010 or 2015 (Table B-5, Figure B-29), and were higher than Alewife lengths at age elsewhere in Lake Michigan in 2015 (Eppehimer et al. 2019). Fewer Alewife were collected in 2021 and 2010 than in 2015, but the average individual growth rates of larvae also were higher in those two years than in 2015 (Table B-6). In 2021, the majority of Bloater were collected offshore (site M110) and were seven to fifteen days old. The mean lengths of Bloater adjusted for age did not vary significantly among years (Table B-7). The average individual growth rate for Bloater in 2021 (0.42 mm/day) was comparable to growth in 2010 (0.46 mm/day), and higher than the 2015 average growth rate (0.16 mm/day, Table B-8; Figure B-30).

Most Alewife larvae (80%) were collected during our August 2-5 cruise, and of these, most larvae were hatched during the latter half of July, with relatively few surviving from early hatch dates in May, June or early July (Figure B-31a). The disparity between hatch and capture date distributions of larvae, and the offshore spatial distribution of captured larvae suggests that frequent upwelling events off Muskegon during late spring and summer 2021 (Figure C-2) may have caused some mortality, as it did for Alewife captured off Muskegon during CSMI 2015 sampling. In contrast, hatch and capture date distributions of Alewife were closer in time in 2010, a year of high recruitment, and lack of upwelling in that year suggests that most larvae that were hatched were not subject to displacement and episodic mortality.

In contrast to Alewife, capture date distributions of most Bloater larvae overlapped their estimated hatch date distributions (Figure B-31b). This pattern differed from prior CSMI surveys in 2010 and 2015, when most Bloater were captured well after their estimated hatch dates. Nearly all Bloater larvae were captured offshore, suggesting that nearshore upwelling events had little effect on their survival to capture.

Fish larvae diets:

Out of 120 total Alewife examined from Lake Michigan, 106 (88.3%) had empty stomachs, and only 14 (11.7%) Alewife had prey items. Out of 109 Bloater analyzed, 82 had prey items present (75.2%). Any prey items that could not be identified were marked as UID (unable to identify), but were still included as “prey present”. UID prey items were not included in the prey type analysis.

Of prey that could be identified and counted in Alewife diets, Calanoid copepods were most abundant (71.7% of total) followed by Copepod nauplii (15.3% of total). The prey composition of Alewife diets collected in August was more varied and numerous compared to Alewife collected in July (Figure B-32). When grouped by length, small Alewife (5-10 mm) consumed more Copepod nauplii compared to larger fish that had eaten Calanoid copepods and Daphnia. For Alewife (5-15 mm), Calanoid copepods comprised 100% of the biomass prey (dry weight) in July, but in August larvae primarily ate nauplii, rotifers and cyclopoid copepods. Alewife sampled closer to shore also ate more nauplii, rotifers and cyclopoid copepods compared to larvae sampled offshore that ate calanoid copepods.

Bloater consumed more types of prey items compared to Alewife and had a lower percentage of empty stomachs. Of the total diet items counted, Calanoid copepods comprised the majority of prey items (63.2% of total number), followed by dreissenid veligers (13.89%). Bloater diets varied most in July compared to other months (Figure B-33). Larger Bloater larvae had less variety in diet compared to smaller Bloater, as the majority of fish over 20 mm had only calanoid copepods in their diet. When grouped by length and month of collection, diets of Bloater collected in July were most varied, followed by larvae collected in August. Since most Bloater were collected at station M110, the pattern of decreased variety of diet as Bloater size increased was evident as calanoid copepods comprised most of the diet of larger fish.

Mysis Densities

Mysis densities sampled by MOCNESS were highest at the offshore site in both May and August. Depth stratified tows in August indicated Mysis densities were highest in the metalimnion (Figure B-34).

Tables and Figures

Table B-5: Results of linear model testing whether slopes of Alewife length vs age relationships were significantly different among CSMI years (2010, 2015, 2021). The model was length ~ age + year + age*year.

Variable	Estimate	Std. Error	t value	Pr(>/t/)
Intercept	1.97	0.30	6.59	<0.0001*
Age	0.61	0.02	33.64	<0.0001*
Year 2015	-1.75	0.83	-2.10	0.04*
Year 2021	0.15	0.63	0.24	0.81
Age : Year 2015	0.01	0.05	0.21	0.83
Age: Year 2021	0.17	0.04	3.88	0.0001*

Table B-6: Average individual growth rate of Alewife larvae sampled off Muskegon in Lake Michigan CSMI years.

Year	Mean Growth Rate (mm/day)	SE	n
2010	0.44	0.02	127
2015	0.37	0.02	59
2021	0.65	0.01	119

Table B-7: Results of linear model testing whether slopes of Bloater length vs age relationships were significantly different among CSMI years (2010, 2015, 2021). The model was length ~ age + year + age*year.

Variable	Estimate	Std. Error	t value	Pr(>/t/)
Intercept	7.35	0.84	8.78	<0.0001*
Age	0.57	0.04	14.96	<0.0001*
Year 2015	-1.56	1.39	-1.12	0.26
Year 2021	-0.35	0.98	-0.36	0.72
Age: Year 2015	-0.15	0.08	-1.79	0.07
Age: Year 2021	0.10	0.06	1.77	0.08

Table B-8: Average individual growth rate of Bloater larvae sampled off Muskegon in Lake Michigan CSMI years.

Year	Mean Growth Rate (mm/day)	SE	n
2010	0.46	0.01	57
2015	0.16	0.02	37
2021	0.42	0.02	98

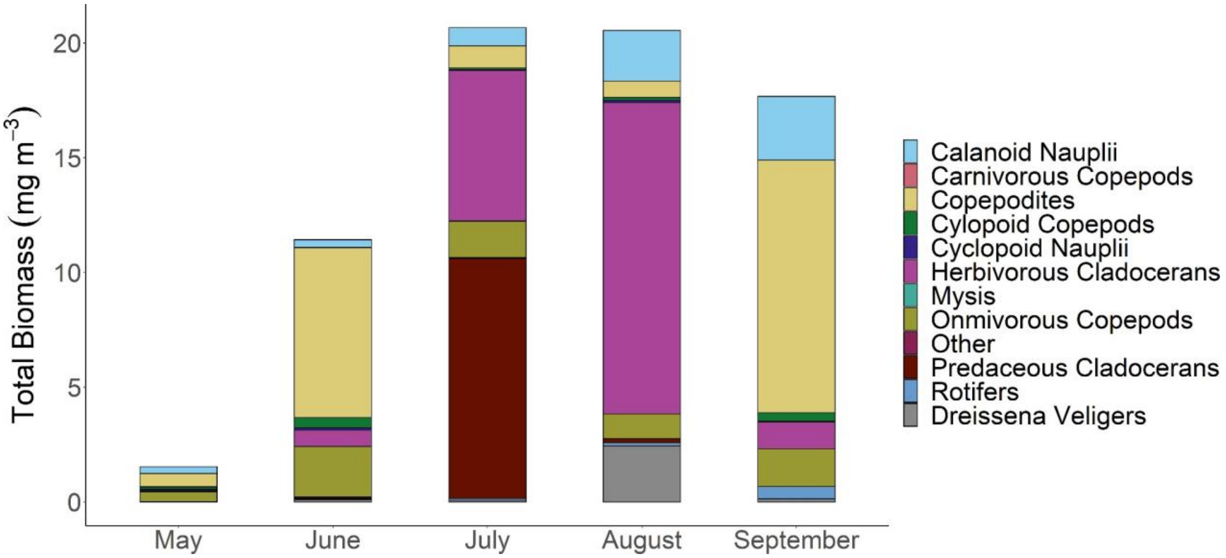

Figure B-19: Estimated zooplankton biomass by month in 2021 sampled during the day at station M15 using the 64$\mu\mu$m mesh net. Zooplankton taxa are grouped and color coded in the legend.

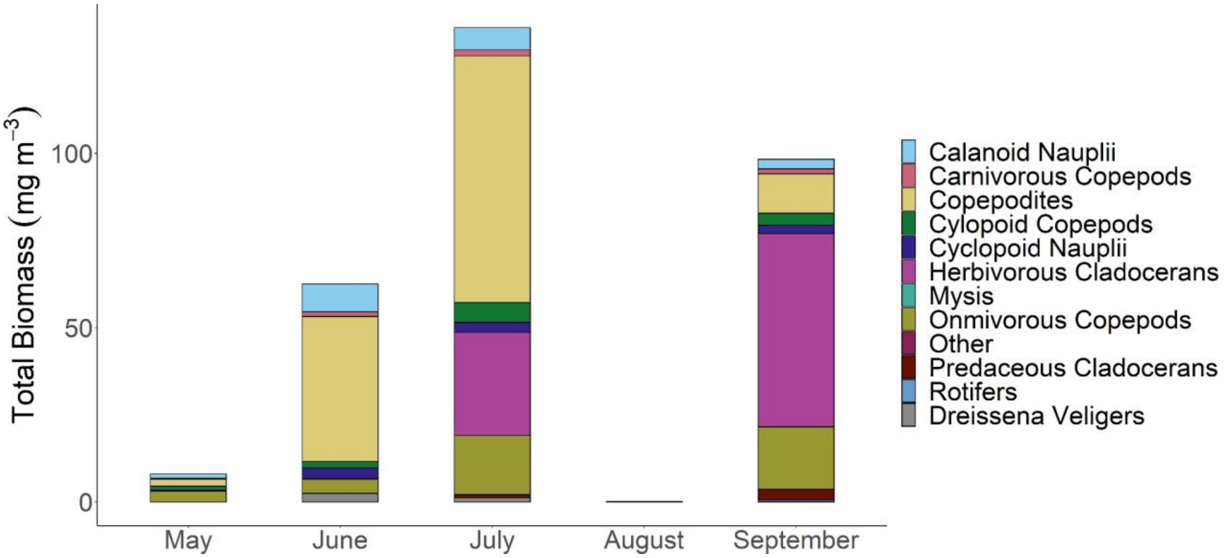

Figure B-20: Estimated zooplankton biomass (dry wt.) by month in 2021 sampled at the offshore site (M110) during the day using the 64$\mu\mu$m mesh net. Zooplankton taxa are grouped and color coded in the legend. No zooplankton were collected during the day in August 2021.

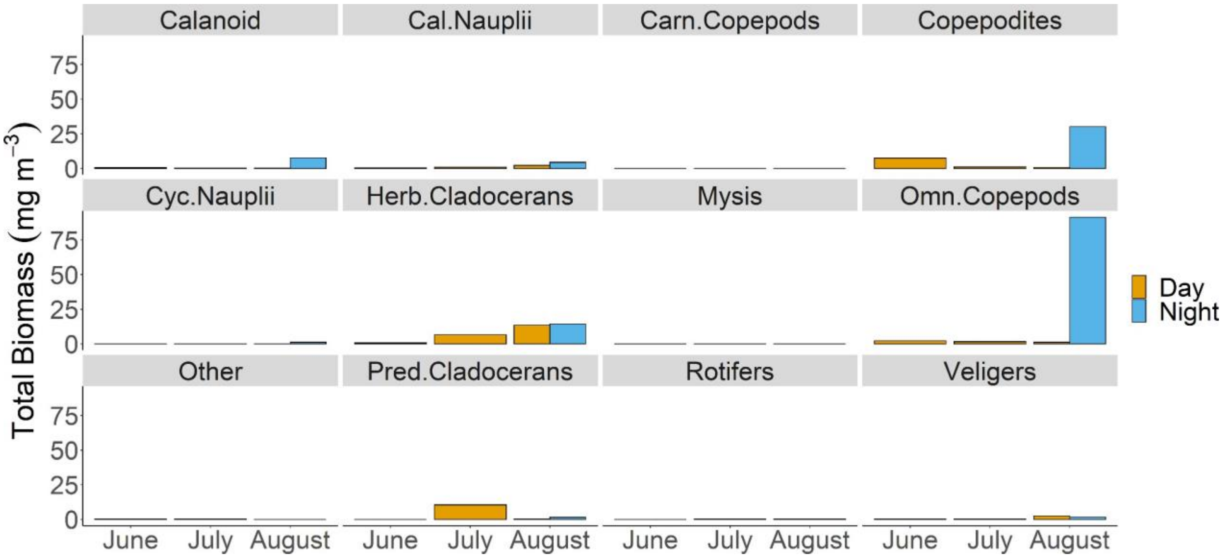

Figure B-21: Estimated zooplankton biomass (dry wt.) by month at station M15 sampled using the 64$\mu\mu$m mesh net. Zooplankton were sampled during the day in June and July, and during the day and night only in August.

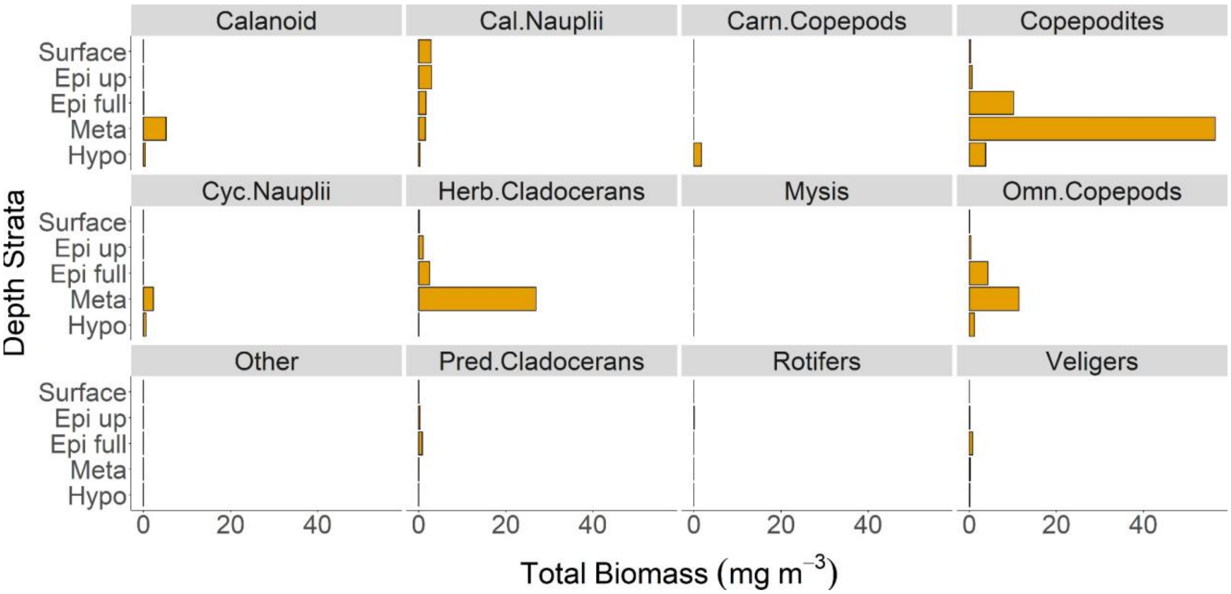

Figure B-22: Daytime vertical distribution of taxon-specific zooplankton biomass (dry wt.) at the offshore site (M110) sampled using the 64 $\mu\mu$m mesh net in July 2021. Zooplankton taxa are grouped (panel).

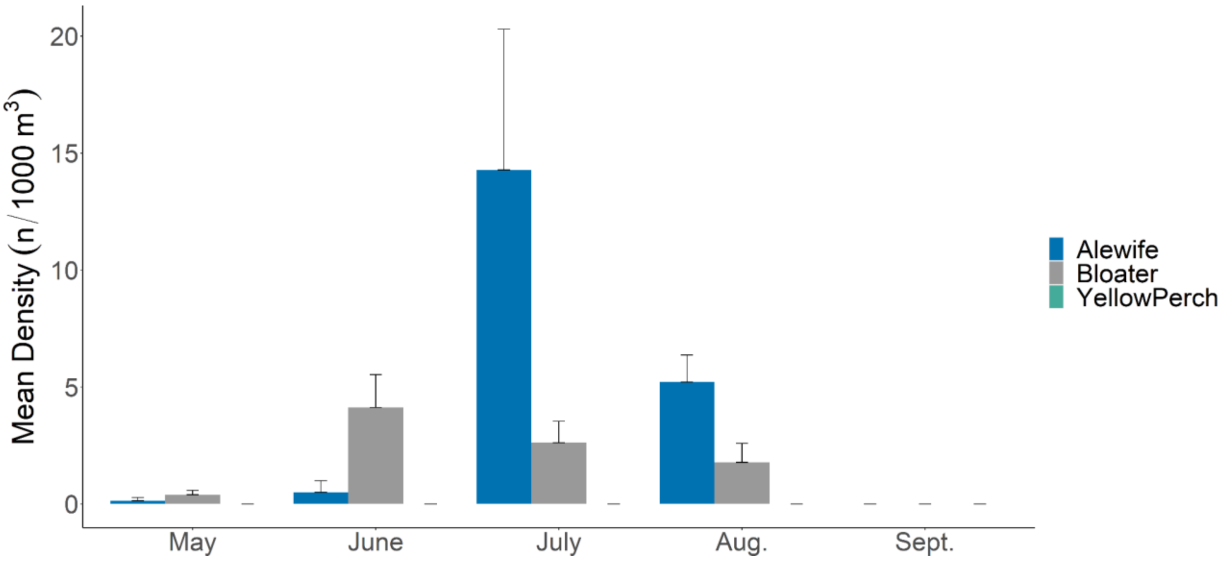

Figure B-23: Mean density (+ 1 s.e.) of Alewife, Bloater and Yellow Perch larvae by month in 2021.

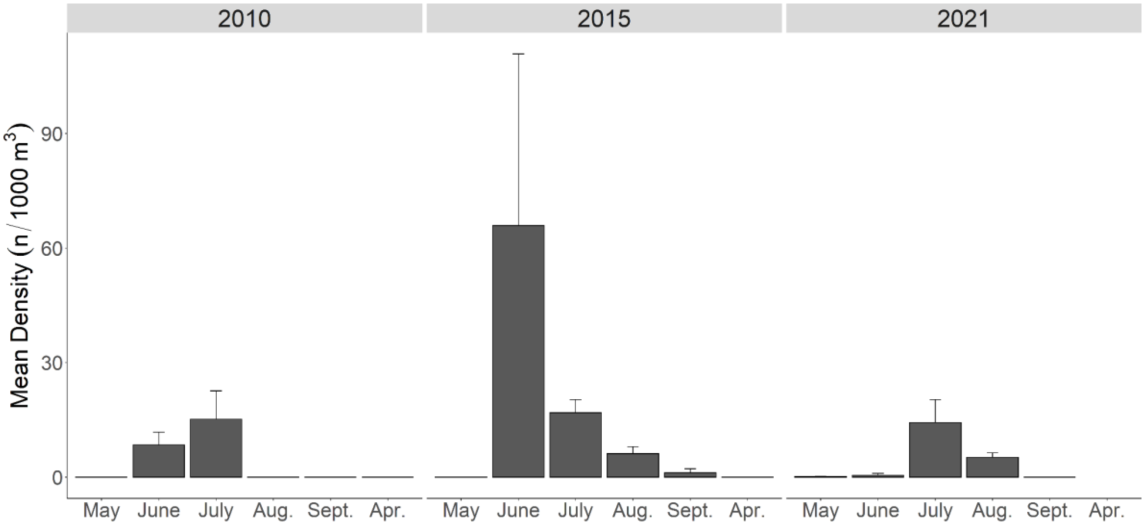

Figure B-24: Alewife (*Alosa pseudoharengus*) larvae mean density (+1 s.e.) by month in CSMI years 2010, 2015 and 2021.

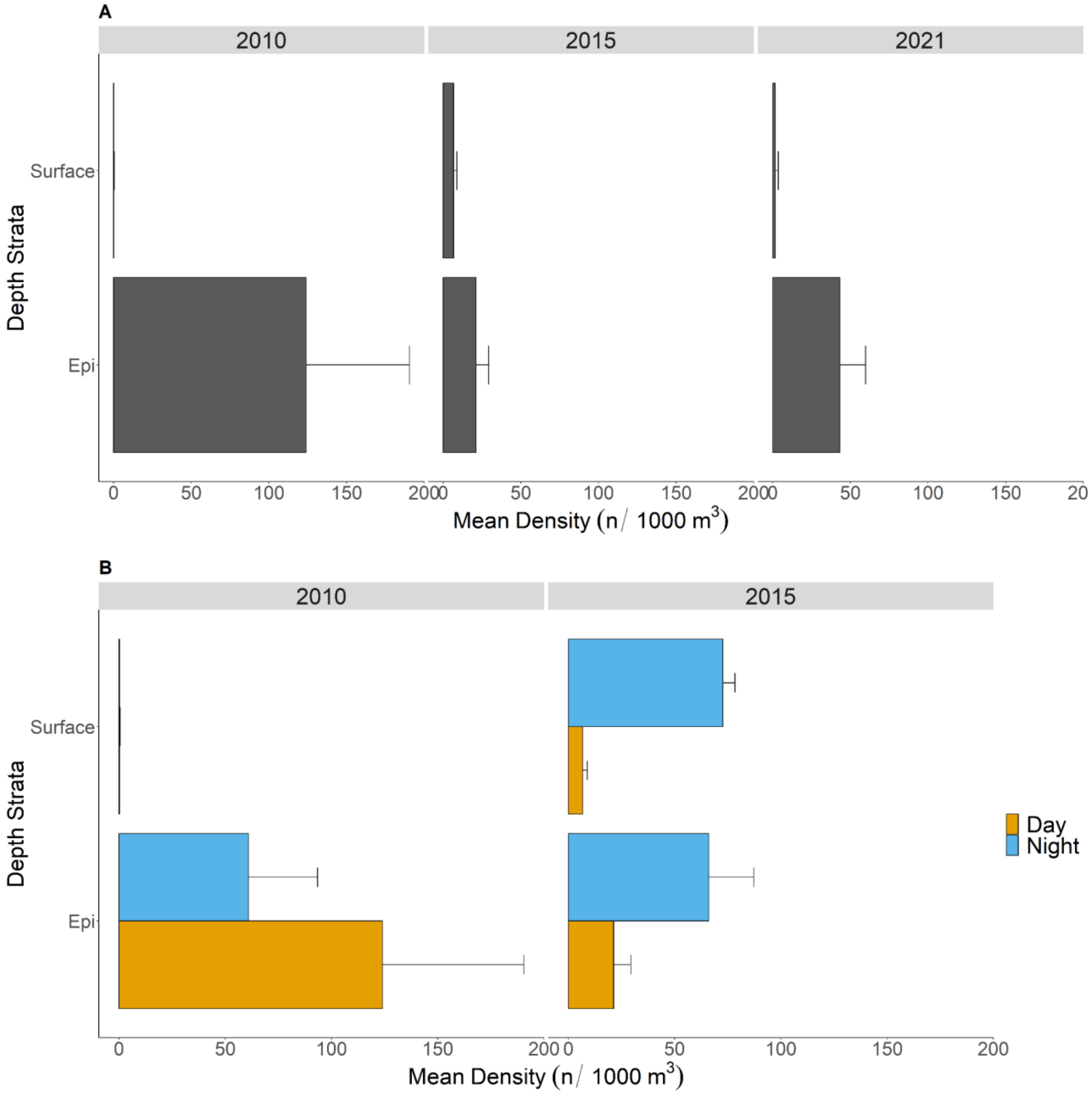

Figure B-25: (A) July mean densities (± 1 s.e.) and vertical distributions of Alewife (*Alosa pseudoharengus*) larvae ***during the day*** at the 15m nearshore site (M15) of each CSMI year: 2010, 2015 and 2021; (B) ***Diel*** mean densities (± 1 s.e.) and vertical distributions of Alewife larvae at the 15 m nearshore site in July 2010 and 2015.

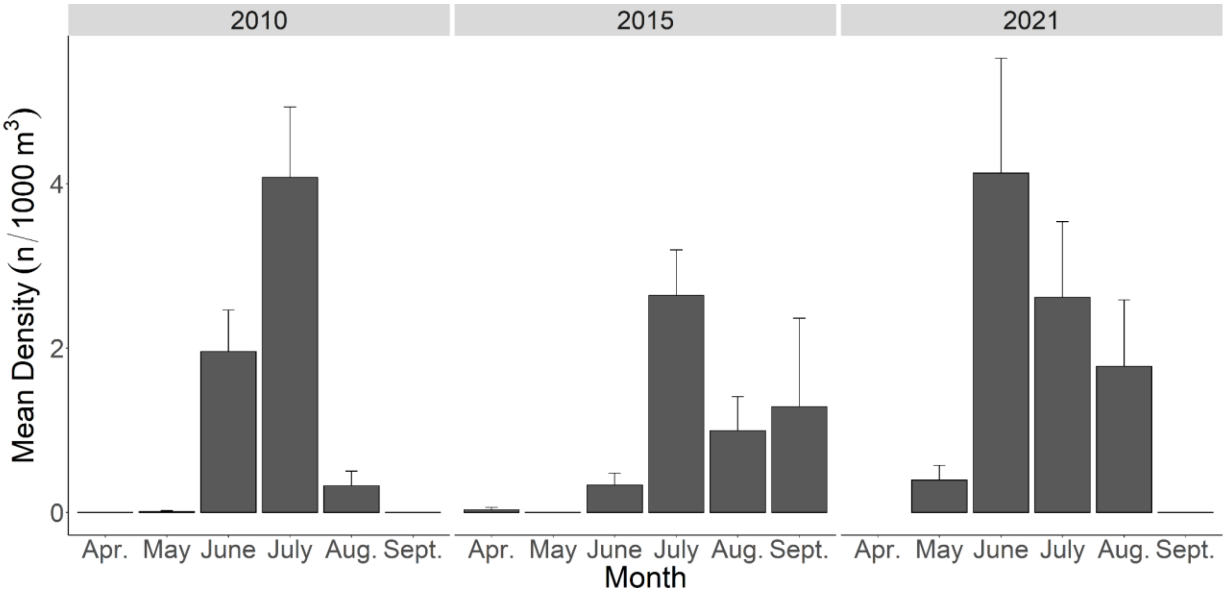

Figure B-26: Bloater (*Coregonus hoyi*) larvae mean density (+ 1 s.e.) by month for CSMI years 2010, 2015 and 2021.

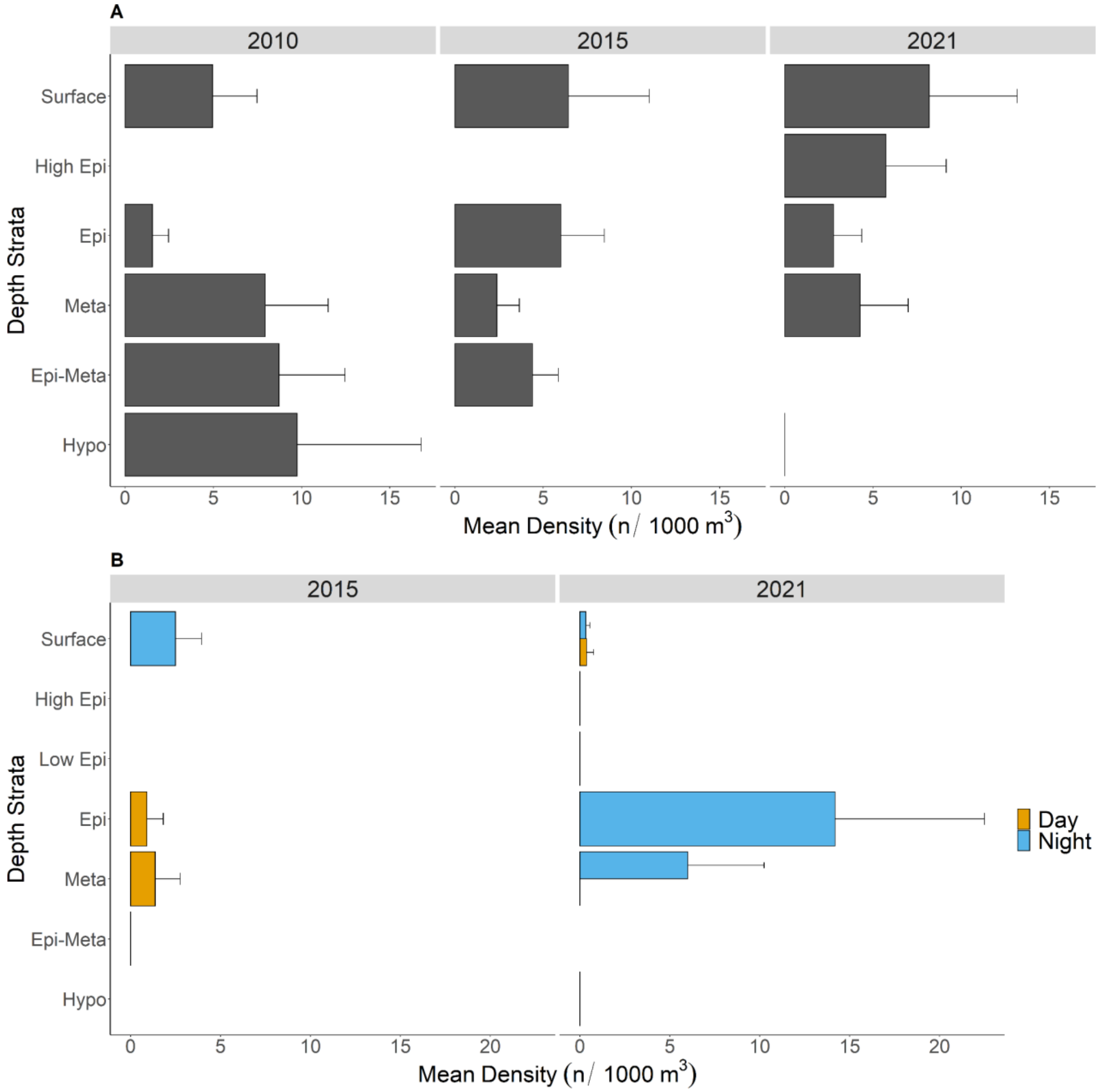

Figure B-27: (A) July mean densities (± 1 s.e.) of Bloater (*Coregonus hoyi*) larvae by depth strata at offshore site M110 ***during the day*** for each CSMI year (2010, 2015, 2021). (B) ***Diel*** mean densities (± 1 s.e.) and vertical distributions of Bloater (*Coregonus hoyi*) larvae by depth strata at offshore site M110 in August of 2015 and 2021.

Fig. 28a.

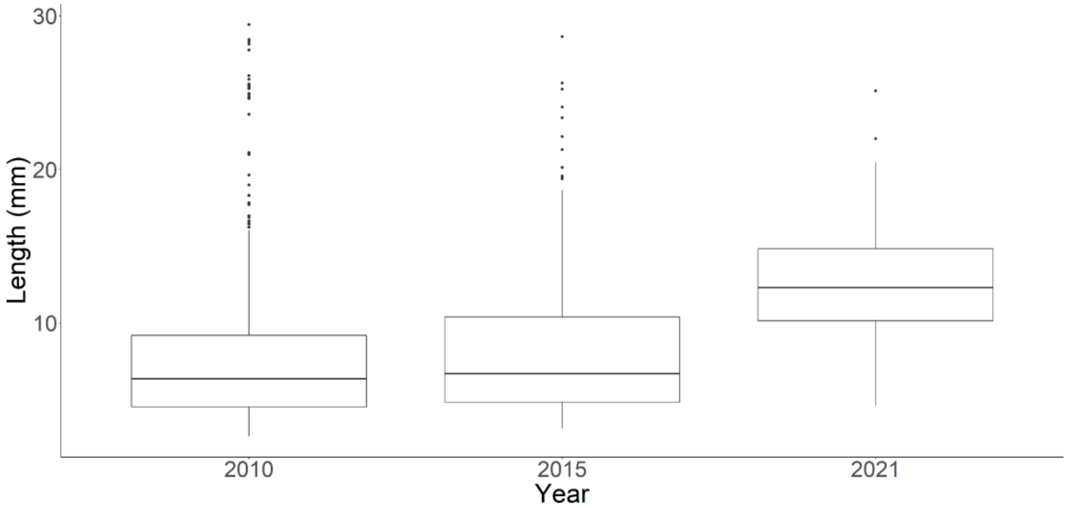

Fig. 28b.

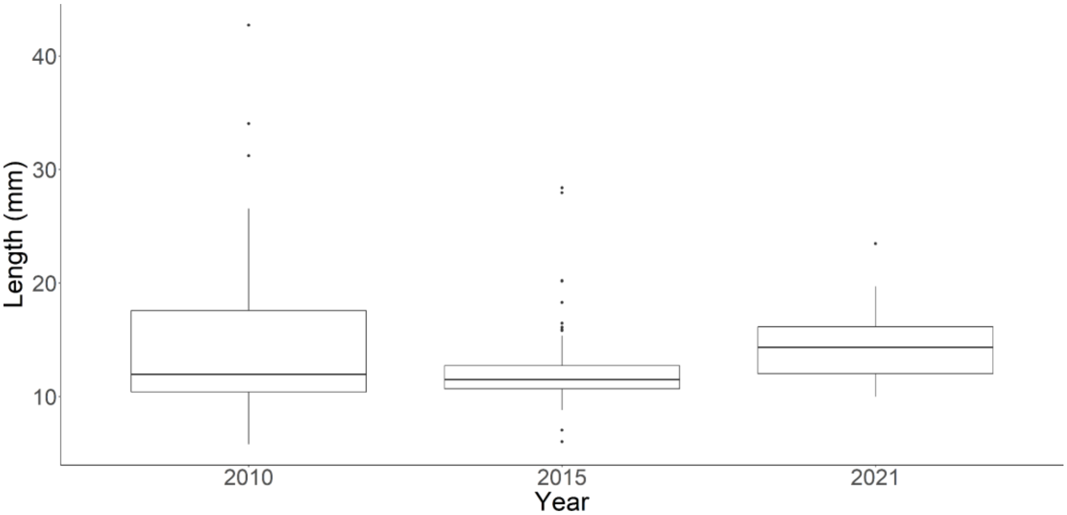

Figure B-28: Median lengths of (a) larval Alewife and (b) larval Bloater sampled off Muskegon in Lake Michigan CSMI years 2010, 2015 and 2021.

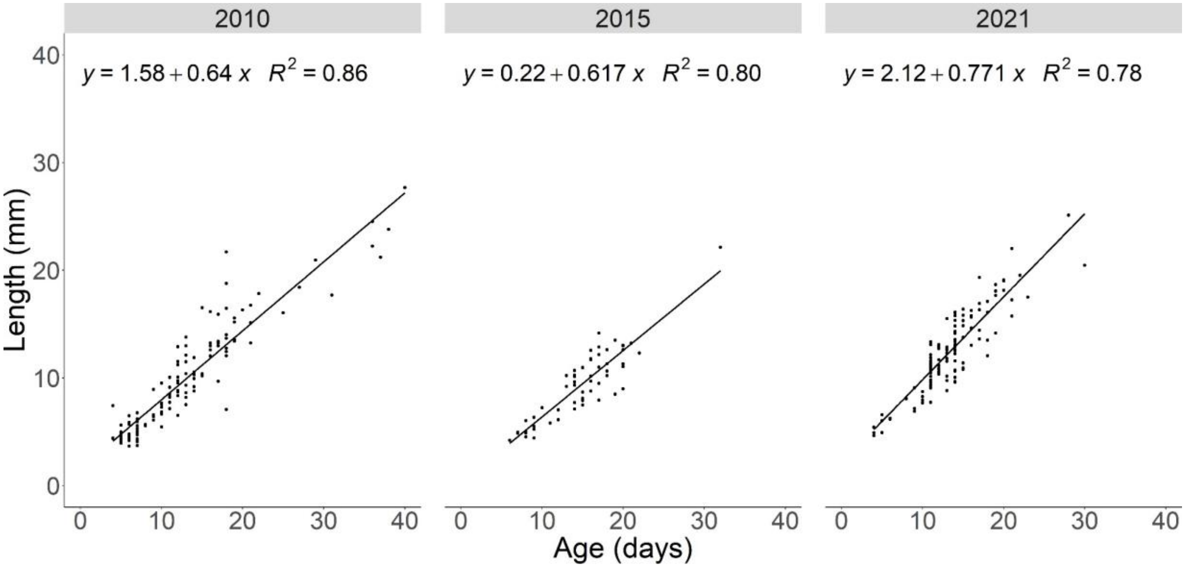

Figure B-29: Alewife (*Alosa pseudoharengus*) larvae length at age (mm/day) in CSMI years 2010, 2015, and 2021.

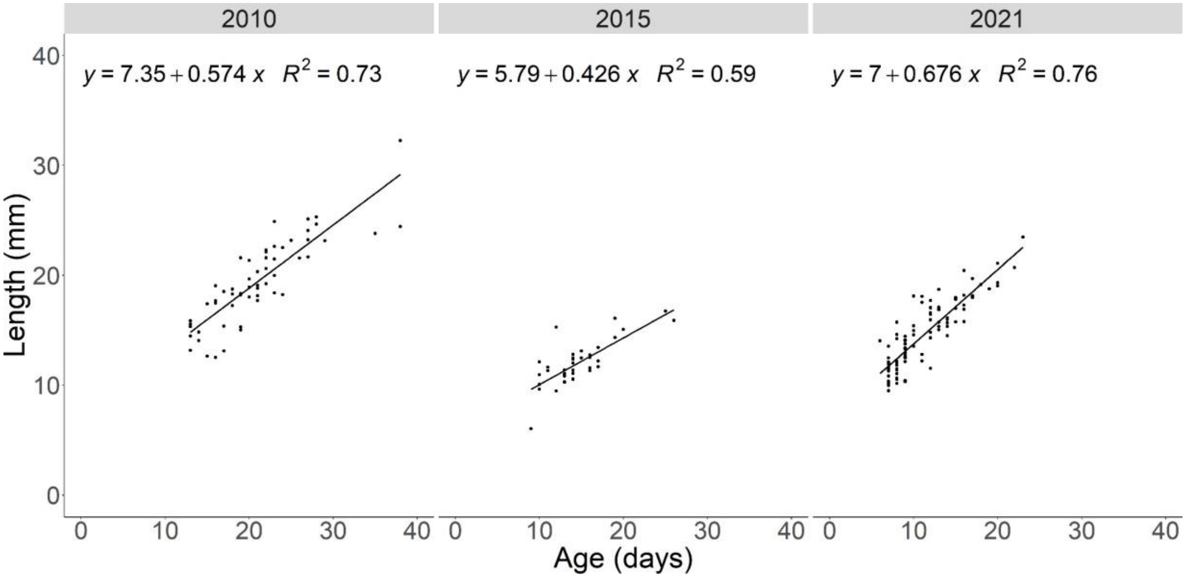

Figure B-30: Bloater (*Coregonus hoyi*) larvae length at age in CSMI years 2010, 2015 and 2021.

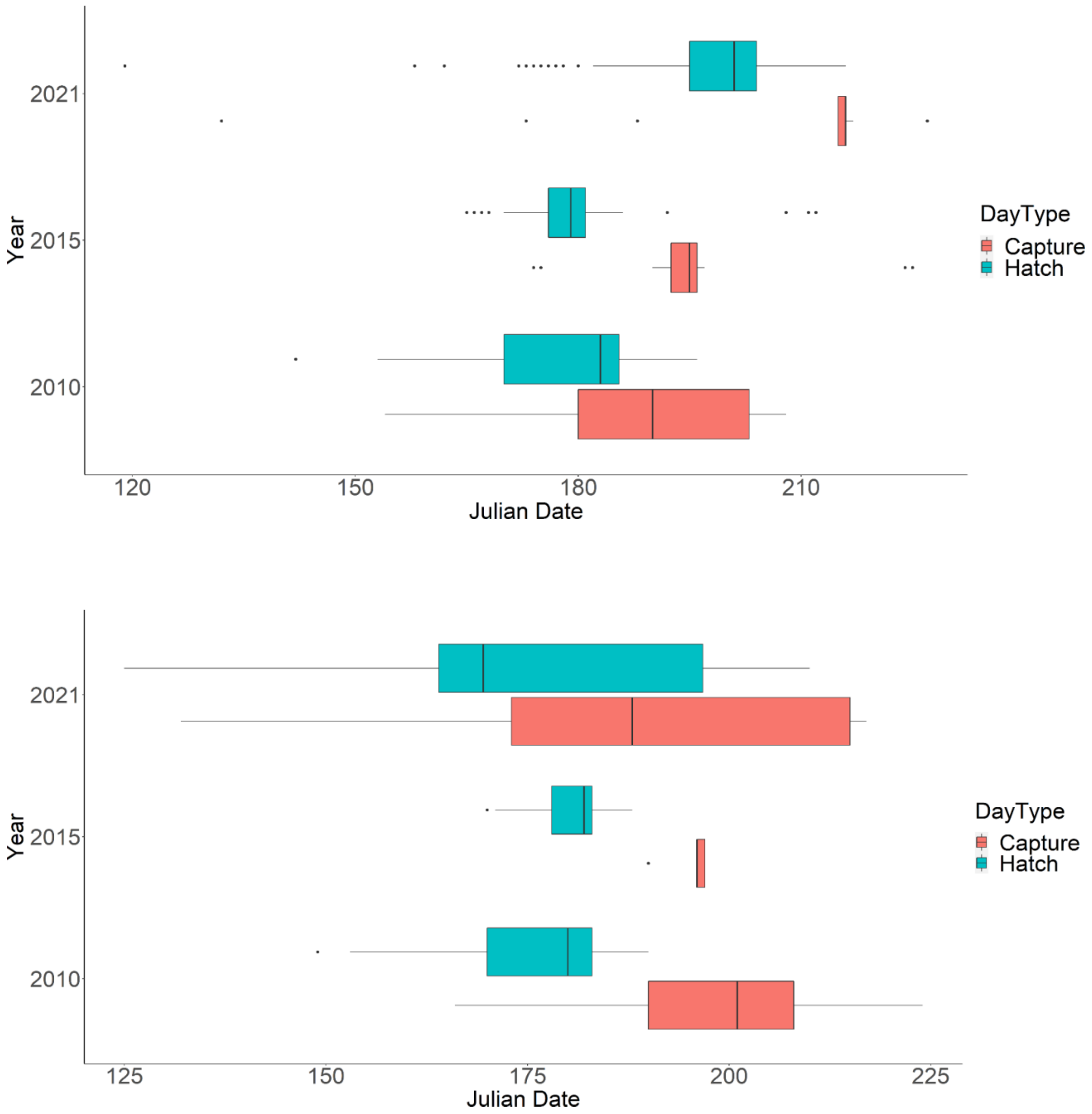

Figure B-31: Distributions of (TOP) Alewife and (BOTTOM) Bloater larvae hatch dates and capture dates off Muskegon in 2021.

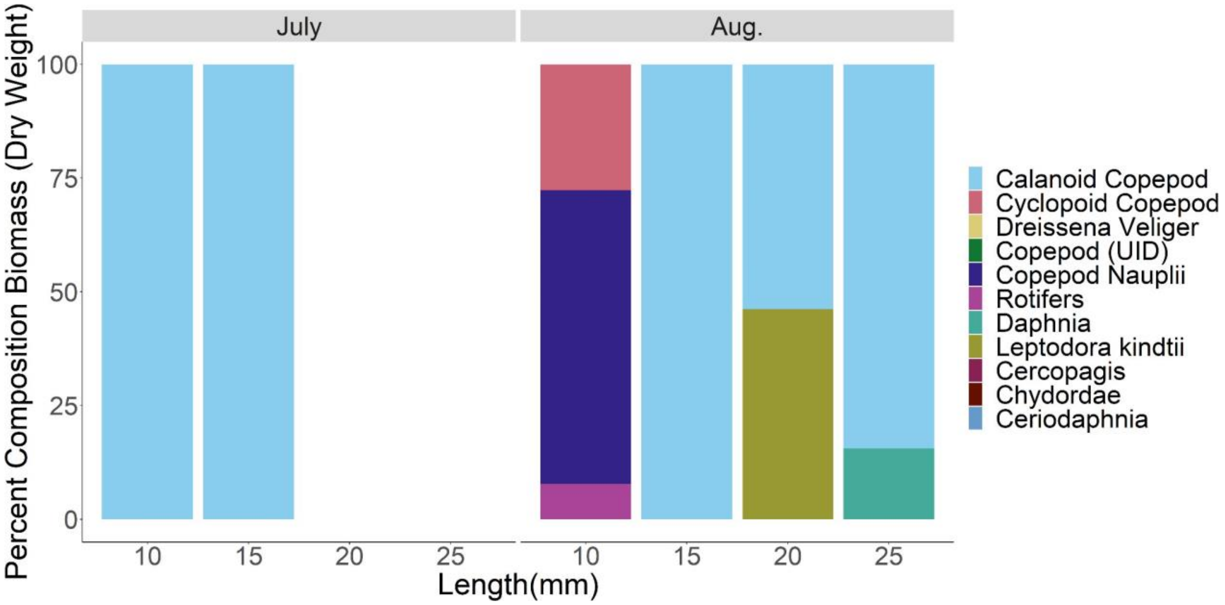

Figure B-32: Percent biomass (dry weight) composition of Alewife (*Alosa pseudoharengus*) larvae diet items grouped by fish length during month of collection date. Diets were binned by fish lengths as follows: 5-10mm, 11-15mm, and so on. Prey taxa in diet are color coded in the legend.

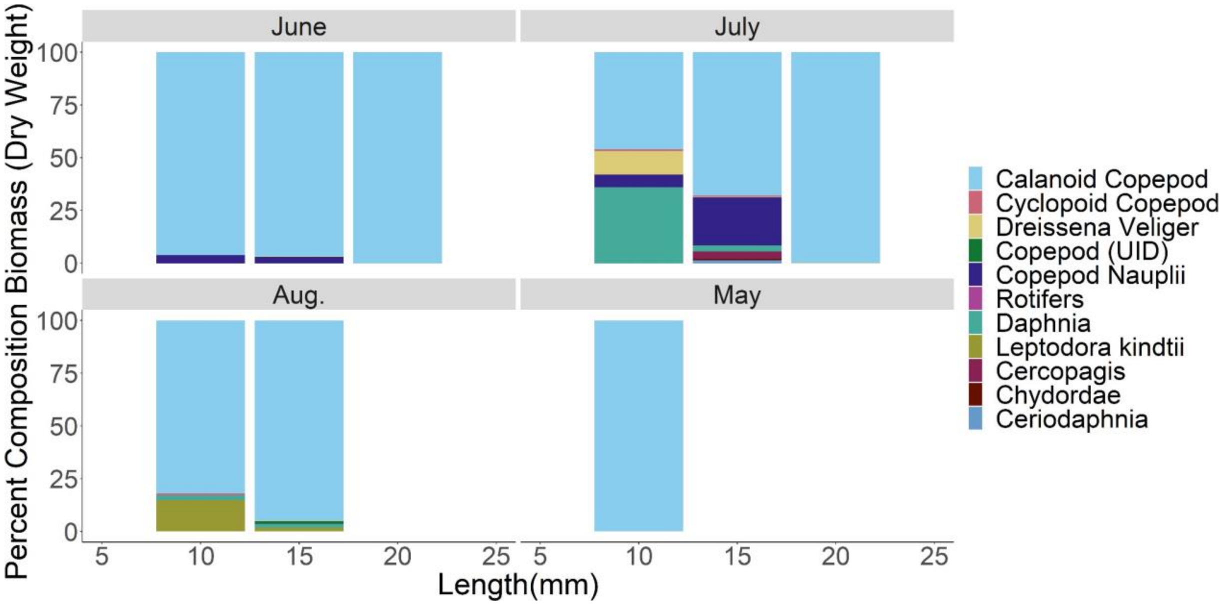

Figure B-33: Percent biomass (dry weight) composition of Bloater (*Coregonus hoyi*) larvae diet items grouped by fish length during month of fish collection. Diets of larvae were classified into larval length bins as follows: 5-10 mm, 11-15 mm, and so on. Prey taxa in diet are color coded in the legend.

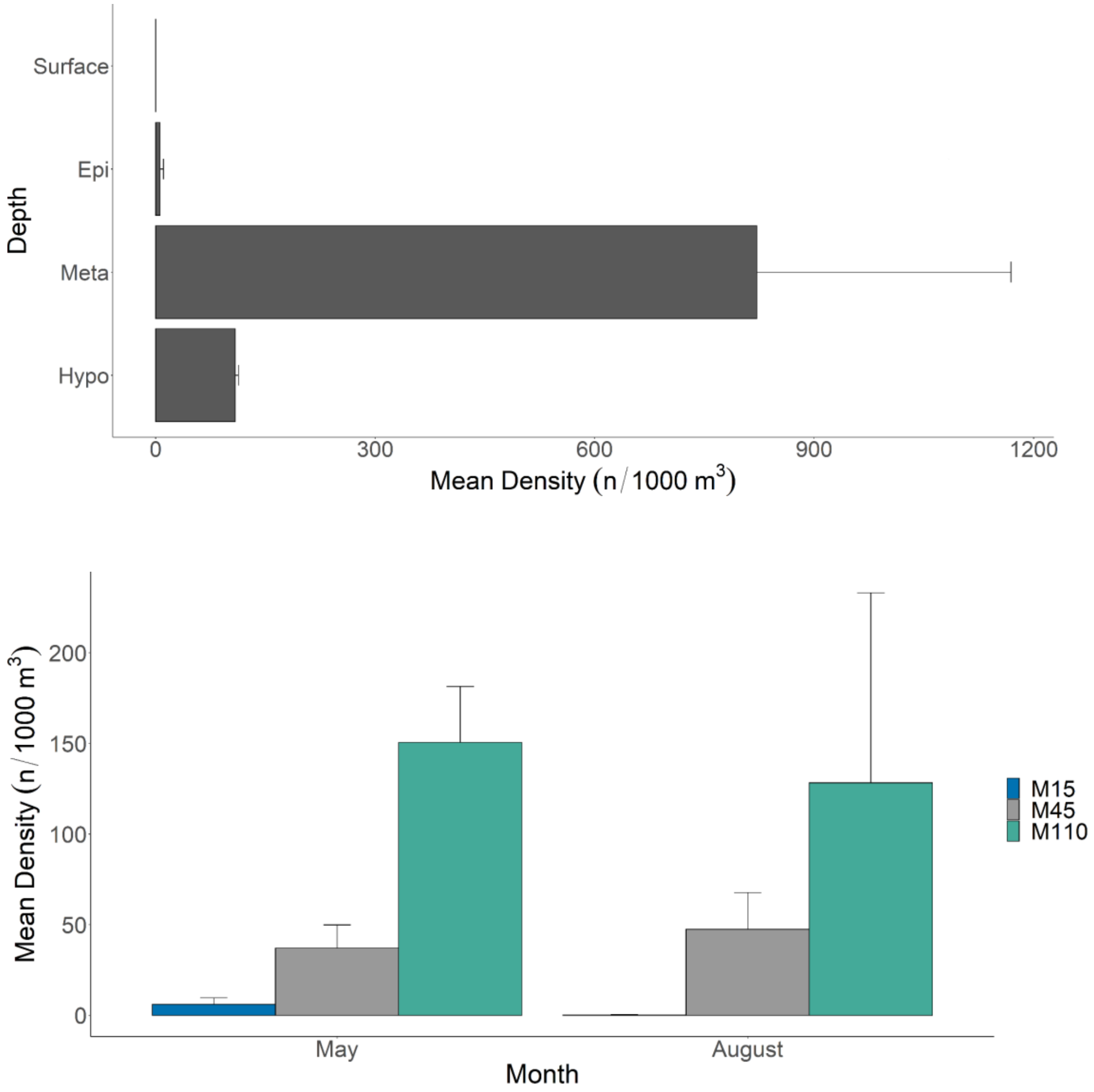

Figure B-34: (A) Mysis mean density (+1 s.e.) in vertical thermal strata offshore (site M110) at night in August 2021. (B) Mysis density (+1 s.e.) averaged over all thermal strata at nearshore, mid-depth and offshore sites at night in May and August, 2021.

Effects of Dreissena veliger consumption by Yellow Perch larvae on larval growth and survival in laboratory experiments: K. Lewandowski, D. Kashian: (Wayne State University):

Overview

Laboratory experiments were conducted at Wayne State University to evaluate the effects of veliger consumption on growth and survival of fish larvae. It was hypothesized that consumption of veligers is at least partially associated with poor growth of fish larvae after quagga mussels irrupted in Lake Michigan after 2004, and present a bottleneck to early life survival and potential recruitment.

Methods

In Spring of 2022, laboratory experiments were performed to test the effects of veliger abundance on diet, survival, and growth of Yellow Perch (YP) larvae. YP eggs were obtained from Lake St. Clair, MI, and hatched in the laboratory at Wayne State University. Percent composition of veligers in diets offered to YP larvae was varied in inverse proportion to alternate prey (brine shrimp (*Artemia salina*)) to test the relative effects of veligers on YP larvae survival and growth. *Dreissena* mussel veligers were collected by zooplankton drift nets from the Detroit River. Once daily from 5-20 days post-hatch, YP larvae were offered prey concentrations of 200 prey/L to one of four replicated (n=5 reps,100 larvae/replicate) treatments: 1) 100% brine shrimp nauplii, 0% veligers (control treatment); 2) 80% brine shrimp, 20% veligers; 3) 20% brine shrimp, 80% veligers; and 4) 100% veligers. Tank concentrations of prey were monitored daily and following the experiment, fish were measured and gut content was recorded to identify the proportion of veligers consumed.

Results and Discussion

Results indicated that a diet high in veligers leads to poor larvae growth and survival. In 2022, YP larvae survival differed ($p<0.05$) among all treatments except between the control (0% veligers) and the 20% veliger treatment (Figure B-35). Survival was greatly reduced for treatments high in veligers and low in Artemia nauplii (80 and 100% veligers). The experiment was repeated in spring 2022 and results were similar. Survival (S=61%) of YP larvae in the control (100% *Artemia* nauplii) treatment was high compared to survival (S=1%) in the 100% veliger treatment. Growth rate of YP, estimated from change in length of YP larvae before and after the 21-d experiment, was reduced in the 100 % veliger treatment compared to all other treatments (Figure B-36). Yellow perch in treatments high in veligers had reduced growth and smaller body condition (Figure B-37).

Figures

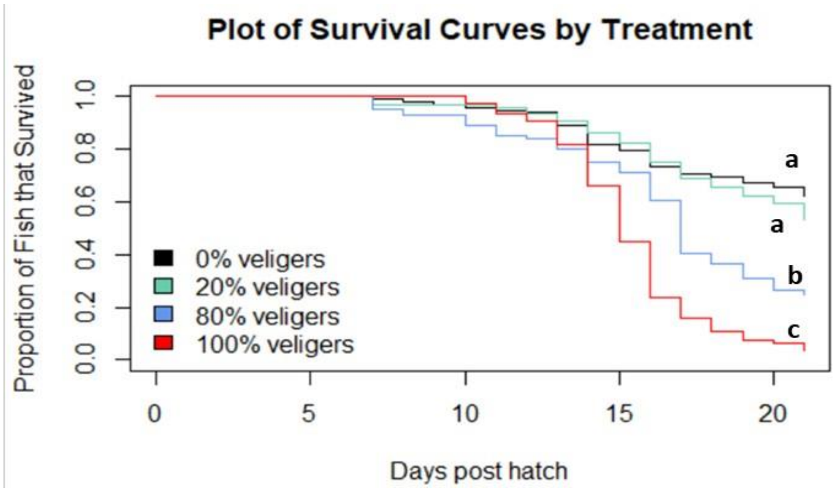

Figure B-35: Yellow perch survival by treatment for the duration of the 21-day experiment. Larvae in the control or 0% veliger treatment were fed a diet of Artemia nauplii. Treatments increased in relative proportion of veliger prey. Pairwise comparisons were performed with Log-rank test and p-values adjusted with Bonferroni. Letters denote significance, p<0.05.

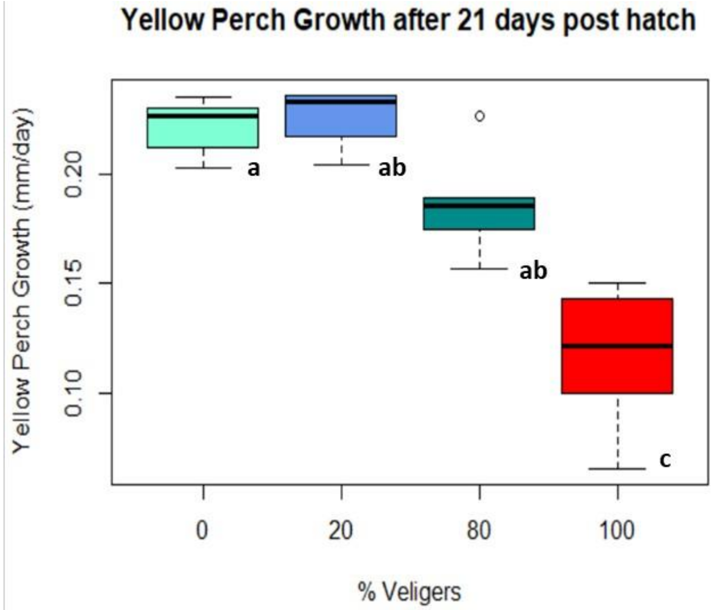

Figure B-36: Yellow perch growth rates (mm/d) fed different treatments of veligers and alternate prey after 21 days. Growth was calculated as the difference between final size and initial size, divided by 21 days. Treatments are represented on the x-axis as increasing percentage concentrations of veliger prey. A single-factor ANOVA was performed with Tukey's HSD for pairwise comparisons between each treatment. Letters denote significance, p<0.05.

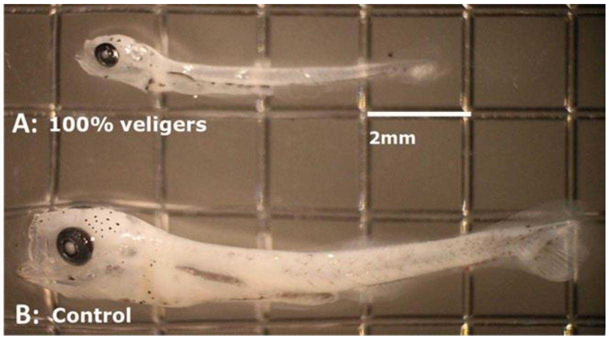

Figure B-37: Individual fish from treatment A (100% veligers) and the control treatment (0% veligers). Both individuals were 21 dph, and were euthanized at the end of the experiment.

Subproject C: Observing Systems

Lake Michigan Long-term Water Temperature Observations (NOAA)

Long-term, year-around vertical water temperature observations have been collected since 1990 in the southern basin of Lake Michigan from a fixed mooring. Observations were collected from the deepest location in the southern basin of Lake Michigan, which is approximately 150 m. The mooring deployments are retrieved and replaced with a new set of thermistors annually, which causes the depth of temperature observation to vary somewhat between deployments. The temperature observations are collected as continuously as possible over the period of record, though there are some breaks in the temporal collection for maintaining equipment annually or due to loss of equipment. These observations are collected to understand the vertical thermal structure in the deep waters of Lake Michigan. This unique data set reveals that deep water temperatures are rising in the winter and provides precise measurements of the timing of fall overturn, the point of minimum temperature, and the duration of the winter cooling period. Relationships from the data show that a shortened winter season results in higher subsurface temperatures and earlier onset of summer stratification. Shifts in the thermal regime of Lake Michigan could have profound impacts on ecosystems (Anderson, et al 2021)

Surface waters cool in the fall (Figure C-1c), the overturn causes a sharp rise in subsurface water temperatures (“O”, Figure C-1d), establishing a mixed water column. From this point, the bottom waters cool over the winter, as the water column becomes inversely stratified, until a point of minimum temperature is reached (“M”, Figure C-1d). As spring conditions bring increased surface heat into the lake, the now isothermal water column becomes fully mixed again and bottom waters warm until summer stratification is reached (“S”, Figure C-1d). The time between the date of fall overturn and minimum temperature is the only cooling period experienced by deep waters.

Figure C-2 indicates a delayed fall overturn, lengthening summer stratification, and a shorter cooling period at the 110m depth beginning in 1997. Physical changes in Lake Michigan, driven by global climate change, are currently affecting the timing of lake mixing with longer term concern regarding the ecosystem impact should the lake remain in a stratified condition throughout the winter. These changes will also have an impact on lake evaporation and ice cover.

<u>Note</u>: Data from this observing site for the years 2020-2022 were recently retrieved at the end of the 2022 field season. We are currently updating these figures with these recent observations.

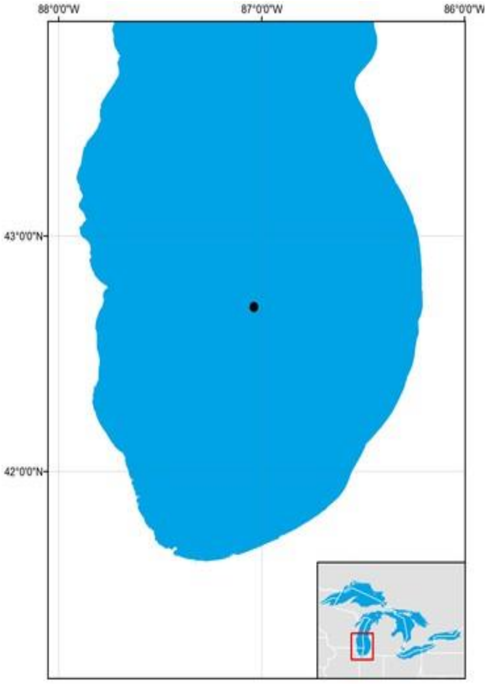

Figure C-1: Location of the thermistor mooring in southern Lake Michigan.

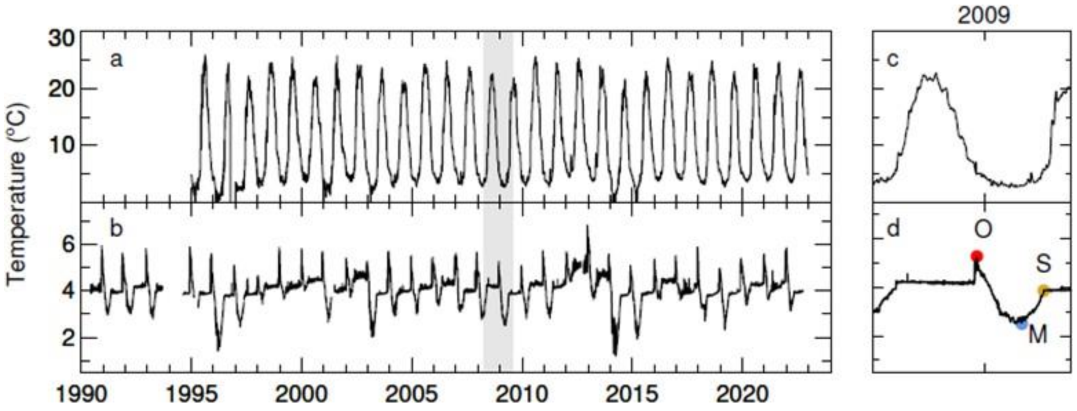

Figure C-2: Updated plot from Anderson, et al 2021 to include data through 2022. a Daily lake surface temperature from the GLSEA at the thermistor location. b Water temperature time-series at the 110 m depth. c, d A zoomed surface and subsurface temperature record for 2008–2009, equivalent to the period highlighted in gray in a and b, indicating the 110 m overturn date, "O", minimum temperature/date, "M", and stratification temperature/date, "S".

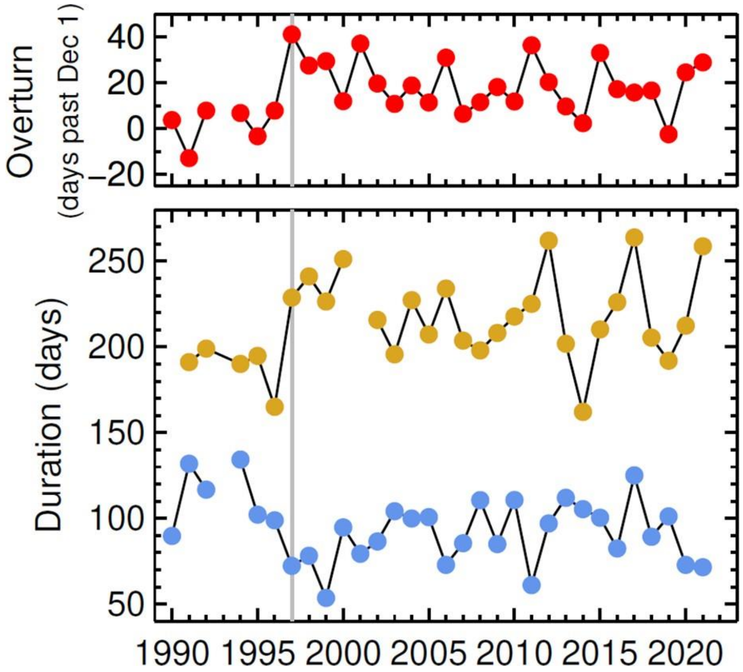

Figure C-3: Updated plot from rom Anderson, et al 2021 to include data through 2022. a Overturn date at the 110 m depth (red), b cooling period duration (blue), and duration of summer stratification (gold) reveal shifts after 1997 (vertical gray line).

Muskegon Lake Observatory (Biddanda- GVSU)

Overview

The Muskegon Lake Observatory (MLO) collaborative project operated a robust multi-sensor observing array in Muskegon Lake estuary – an EPA-AOC and NOAA-HFA site undergoing restoration. The acquisition of time-series data from multiple depths and multiple locations provided many new insights into the annually recurring phenomena of lake-wide eutrophication, HABs and hypoxia in this Great Lakes estuary with impacts on water quality and fish habitat. By enabling tracking of eutrophication, hypoxia and CyanoHABs, our collaborative advanced ecosystem science, restoration and management. Our project was a low-cost GVSU-AWRI and NOAA-GLERL collaborative that utilized GLERL-LMFS resources and resulted in 12 years of operation of a key regional Great Lakes observing infrastructure that openly shares time-series weather and water quality data with students, scientists and resource managers to benefit both science and society.

A second objective from our CSMI effort was to deploy CIGLR's deep-water buoyancy glider to characterize distributions of primary producer biomass, chromophoric dissolved organic matter (CDOM), and physical parameters throughout the southern basin. That deployment would complement shipboard sampling along the Muskegon transect.

Methods

The MLO broadly consists of a 5' diameter buoy topped with 2-solar panels and a meteorological sensor, with batteries inside to store power for overnight measurements. Cables from the main buoy provide power to a subsurface water quality buoy measuring water temperature, dissolved oxygen, chlorophyll a, phycocyanin, turbidity, pH, specific conductivity, ORP, nitrate, PAR, and CDOM, at one or more depths throughout the ~12m water column. Key sensor clusters are located at 2, 5, 8 and 11 m to yield insights into water-column dynamics. A separate cable provides power to an Acoustic Doppler Current Profiler (ADCP) which monitors water current speed and direction throughout the water column. The main buoy is held in place by 2-500 lb cement weights.

CIGLR deployed a buoyancy glider along the Muskegon transect during the August and September sampling cruises, targeting the 45m and 110 stations. The glider was deployed before the transect cruises and performed repeated profiles between those two stations (Figure C-5). The glider collected fine-scale (1 second) measurements of temperature, conductivity, depth, chromophoric dissolved organic matter (CDOM), backscatter, chlorophyll-a fluorescence, dissolved oxygen, and photosynthetically active radiation (PAR).

Results and Discussion

The MLO was successfully operated during 2020 and 2021, and open access sharing of time-series data was achieved (www.gvsu.edu/buoy/), The deployment in 2020 began later in the year than planned due to access restrictions due to COVID-19. With the successful deployment of the MLO from 2020-2021, we have completed 12 years of operations in Muskegon Lake. MLO gathered about ~1 million weather and water quality data from Muskegon Lake – data that is openly shared with all users through the project website: https://www.gvsu.edu/wri/buoy/. MLO data are part of the visual in the AWRI long-term Muskegon Lake project dashboard. MLO data are also hosted on the Great Lakes node of the Global Ocean Observing System, the Great Lakes Observing System at www.glos.us. Several major problems were fixed from the prior year including re-establishing buoy data uploads to GLOS as well as temperature data upload to the buoy website, a valuable asset to local fishermen. MLO data and findings were shared with teachers and students in the AWRI classroom and onboard the R/V W.G. Jackson during 2021 and 2022.

Science products supported by this deployment have been published or submitted (Dugener et al in review; Mancuso et al 2021; Mancuso et al 2021b; and Biddanda et al 2021). The project made important findings on how variable weather affects water quality and algal blooms, trained and mentored 8 personnel (2 techs, 4 graduate and 2 undergraduate students) and resulted in 5 conference presentations, 9 publications (3 peer-reviewed and 6 non-peer-reviewed) and coverage in an environmental science magazine (1). The project supported the successful completion of a master's thesis by one student and supported the beginning of another master's student's project. Data gathered supported a joint effort with GVSU Computing and Information Systems Department faculty and students, and the Biddanda lab to further develop a new, more user-friendly, data dashboard which would improve the connection between the buoy data and the local community. The scientific findings, and educational and outreach outcomes of the project, helped prepare a proposal to the National Science Foundation's Major Research Instrumentation program in 2022.

Autonomous Vehicle High Spatial Resolution Observations (Miller, Godwin- CIGLR)

The Slocum buoyancy glider was deployed from August 2-17 and September 9-30, 2023. Glider deployment data were deposited in the National Glider Data Assembly Center

(https://gliders.ioos.us/erddap/tabledap/glos_870-20210802T1913-delayed.html, https://gliders.ioos.us/erddap/tabledap/glos_870-20210909T1754-delayed.html).

Figure C-4: The Slocum buoyancy glider.

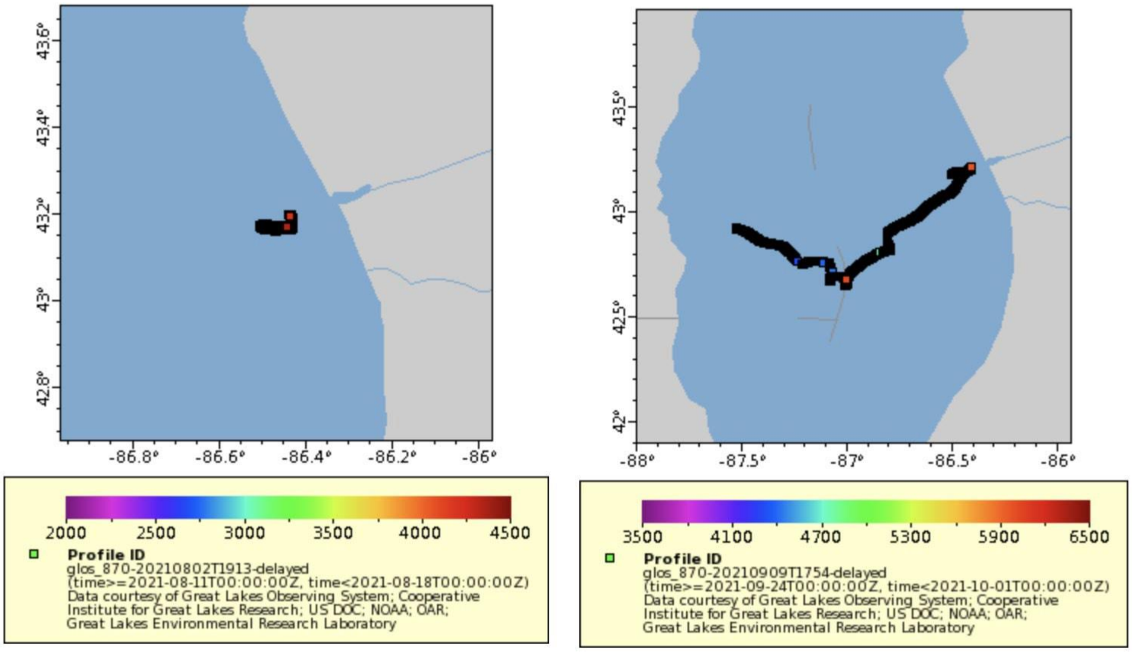

Figure C-5: Tracks of glider deployments in August (left) and September (right).

Lake Michigan 20 meter ReCON Buoy (NOAA)

The Lake Michigan Real-time Coastal Observation Network buoy was deployed in Lake Michigan at 43 10.956'N/86 21.600'W at a depth of 20 meters. The ReCON buoy provides real-time, high-resolution time-series observations of meteorological, physical, biological and chemical parameters. The M20 buoy was deployed from May 3 through November 10, 2021. Observations are used for model development and monitoring of seasonal change. Temperature and chlorophyll observations from the YSI EXO2 are shown in Figure C-6.

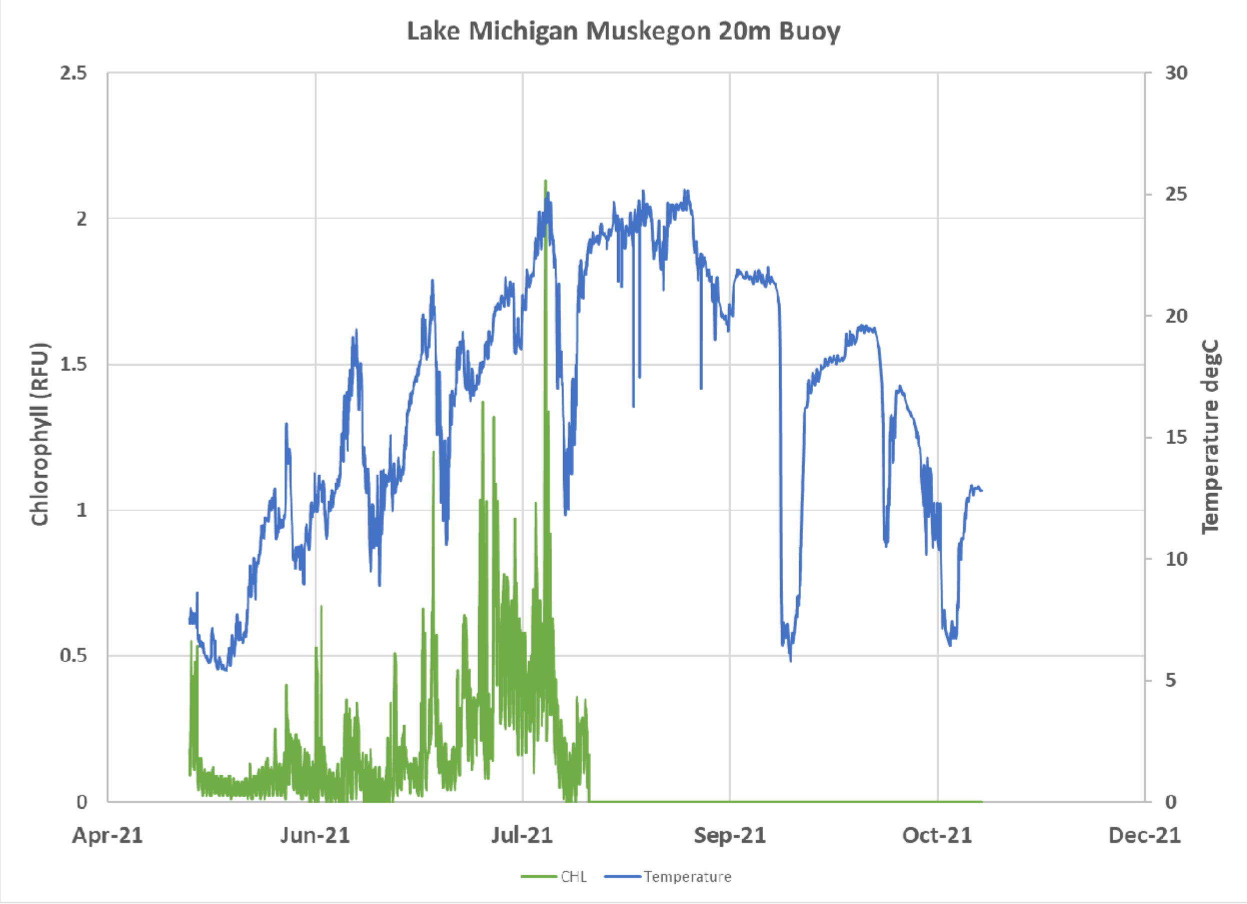

Figure C-6: Surface chlorophyll (green) and temperature (blue) for the period from May 3 through November 10, 2021. Observations of temperature indicate upwellings in each month except October with subsequent decreases in the chlorophyll signal during these events. Upwellings on the east side of Lake Michigan are often caused by north winds resulting in Ekman transport of warmer water offshore and colder hypolimnetic waters coming to the surface. The chlorophyll sensor failed in early August after a significant upwelling event.

Satellite Remote sensing (Sayers- MTRI)

Satellite observations of Lake Michigan primary productivity were intended to be a part of our work under CSMI 2021. However, algorithm development has been delayed due to concerns about the NOAA polar orbiting satellite Visible Infrared Imaging Radiometer Suite (VIIRS) sensor. The satellite algorithm uses the VIIRS sensor to estimate chlorophyll and light extinction to estimate primary productivity. Concerns about the need to recalibrate the potential drift of the 410nm band have delayed this effort. We are hoping to have this issue resolved to provide a satellite time-series of primary productivity in time for the Lake Superior CSMI report. Once the algorithm is working properly, it will be applied to the Lake Michigan 2021 CSMI data.

Subproject D: Biophysical Modeling

Overview

In 2020 and 2021, we provided daily nowcasts and forecasts of nearshore to offshore transport of water that is likely to contain elevated nutrients and larval fish numbers in support of CSMI field operations. We used biophysical models linked to the Lake Michigan Huron Operational Forecast System (LMHOFS) model to: (1) visualize transport of water likely to contain larval fish from presumed nearshore spawning areas, using a Lagrangian particle model linked to LMHOFS; and (2) visualize transport of river inputs of phosphorus. CSMI collaborators were notified of the availability of the forecasts by group email on September 11, 2020, April 27, 2021, July 2, 2021, and May 17, 2022. The Michigan and Huron biophysical forecasts were also highlighted in the Summer 2022 IAGLR Lakes Letter, and September 2022 CIGLR e-newsletter, GLERL's Twitter on June 14, 2022. In addition to the real time forecasts, we applied the Lagrangian particle model and biophysical model linked to LMHOFS retrospectively to estimate likely hatch locations of aged larval fish collected in 2021.

Methods

The Experimental Biophysical Nowcast/Forecast for Lake Michigan CSMI 2020-21 (Figure D-1; Table D1) was an application of the Finite Volume Community Ocean Model – General Ecosystem Module (FVCOM-GEM), with state variables representing a phosphorus-limited lower food web with dissolved organic carbon (DOC) included as a tracer for river inputs. Calibration and assessment of the lower food web model was reported previously (Rowe et al. 2017). FVCOM was implemented as in the Great Lakes Coastal Forecast System, with meteorological forcing from the High Resolution Rapid Refresh meteorological model. River discharge was obtained from the USGS National Water Information System for 37 tributaries, with estimated phosphorus (Dolan and Chapra, 2012; Robertson and Saad 2019) and DOC concentrations. Graphics of modeled surface chlorophyll-a and DOC were matched with satellite-derived estimates (Table D1) from the NOAA Coastwatch Great Lakes node, on dates when clear images were available. Satellite derived Chlorophyll-a and DOC were produced operationally by NOAA using data from the Visible Infrared Imaging Radiometer Suite (VIIRS) and the Color Producing Agent Algorithm (CPA-A).

The Experimental Larval Fish Dispersion Forecast for Lake Michigan CSMI 2020-21 used currents, temperature, and turbulent diffusivity from the FVCOM simulations described above, with a Lagrangian particle dispersion (LPD) model applied to simulate dispersion of larval fish from nearshore spawning regions (Rowe et al., 2022). In the real time simulations (Table 1), particles were initiated at a uniform concentration from locations with bathymetric depth < 10 m, with a new simulation initiated each week. Since the initial concentration of hatching larval fish is not known, the modeled concentrations were expressed as a relative concentration (simulated concentration divided by the assumed initial concentration). In addition, backward trajectory simulations were conducted to estimate the likely origin locations of aged larval fish collected in Lake Michigan (Rowe et al., 2022).

Results and Discussion

Archived graphics from the Experimental Biophysical Nowcast/Forecast for Lake Michigan CSMI 2020-21 and the Experimental Larval Fish Dispersion Forecast for Lake Michigan CSMI 2020-21 can be accessed through the NOAA GLERL website (Table D-1) for retrospective analysis of conditions associated with field sampling events. Model output or custom graphics can be made available upon request.

The biophysical model simulations depict a number of dynamic events in nearshore water quality, some of which could be confirmed using the paired satellite images. For example, the model depicted an upwelling event along the western shore that caused an area of elevated nearshore chlorophyll-a to expand on May 27, in comparison to May 21, 2020 (Figure D-2). The expansion of nearshore chlorophyll-a was visible in the satellite images on the same dates. Coastal upwelling is a common wind-driven phenomenon in Lake Michigan during the stratified season, and can bring sub-surface chlorophyll-a to the surface (Rowe et al., 2017; Rowe et al., 2022). Also in May, 2020, an historic precipitation and flooding event affected Michigan, causing flooding and a dam failure in Midland county. In western Michigan, the Muskegon and Grand Rivers also experienced high discharge. In the biophysical model simulation on May 27, a plume of DOC is visible near Muskegon and Grand Haven in the model graphics, and a similar feature was observed in the satellite imagery on the same date (Figure D-3).

While field operations were limited in 2020 due to pandemic restrictions, in 2021, model guidance was provided during field research cruises. Research cruises were conducted offshore of Muskegon on June 28 and July 7, coincident with a period of elevated river discharge along the southeast Lake Michigan shore, which produced elevated nearshore surface chlorophyll concentrations (Figure D-4). The elevated nearshore chlorophyll concentrations moved offshore and inshore in response to coastal upwelling and downwelling, and were gradually transported northward during the first week of July. Another phenomenon of interest that occurred during a research cruise, was a strong upwelling event on August 2, which largely relaxed by August 6 (Figure D-5-6). The upwelling event was observed at the Muskegon 20-m buoy (Figure D-6). Upwelling events were characterized as a minimum in surface temperature, and downwelling events as a maximum in bottom temperature. The model captured upwelling and downwelling events reasonably well in comparison to observations at the Muskegon 20-m buoy (Figure D-6). Modeled surface chlorophyll tended to peak during upwelling events, and to be low during downwelling events at the Muskegon 20-m buoy, which may be associated with a subsurface chlorophyll maximum surfacing during upwelling. Modeled chlorophyll agreed reasonably well with grab samples during June-August, with less agreement in May and September. The model illustrates the potentially dynamic nature of nearshore chlorophyll concentrations, which is difficult to capture in periodic grab samples. For example, the August 4 cruise took place at a transition between upwelling and downwelling, which may have contributed to the reversed trend of surface chlorophyll concentration in August along the Muskegon transect, compared to other months (Figure B-7). The fluorescence chlorophyll recorded at the Muskegon 20-m may need calibration, and/or correction for photochemical quenching, to be comparable to observations.

The Experimental Larval Fish Dispersion Forecast for Lake Michigan CSMI 2020-21 (Figure D-7) provided guidance to field researchers regarding the expected spatial distribution of larval fish that were assumed to hatch from nearshore (< 20 m) spawning areas, and be passively transported by currents. In coastal Lake Michigan during the stratified season, coastal upwelling and downwelling are a dominant feature, responding to changing winds on a typical time scale of 3-4 days. Upwelling conditions cause gradual offshore transport of nearshore drifters, while downwelling can produce rapid alongshore transport (Rowe et al., 2022). As a result, larval fish in the passive drifting phase (<~30 days) are likely to occur in higher concentrations nearshore, with decreasing concentrations offshore. To assess the simulated relative concentration of larval fish, we compared simulated relative concentrations to observed larval alewife density from sampling offshore of Muskegon at the 15, 45, and 110 m-depth stations. A quantile regression line for the 75th percentile value of observed density had an increasing slope, as a function of simulated relative concentration (Figure D-8), indicating that higher observed densities are more likely to occur as simulated relative concentration increases. Given that little is known regarding the specific locations of spawning and initial densities of fish in Lake Michigan, aside from assuming it occurs in shallow nearshore areas, a high level of model skill was not expected, but the results indicate that the simulated relative concentrations may have some value in guiding field researchers to locations that are more likely to contain larval fish. Backward trajectory simulations of aged larval fish collected offshore of Muskegon indicated that the fish most likely originated from nearshore areas to the south, and on the same side of the lake as the collection location (Figure D-9); this finding was similar to the backward trajectory simulations from CSMI Lake Michigan 2015 (Rowe et al., 2022).

The biophysical modeling effort associated with CSMI 2020-21 produced novel realtime nowcast/forecast simulations to provide guidance for field researchers to locate and study transient phenomena of nearshore water quality and larval fish transport. There will be additional opportunities for comparison of models to observations as additional observations become available. However, the preliminary analyses presented here indicate that the models showed some skill in simulating chlorophyll-a distributions associated with coastal upwelling, river plumes associated with high discharge events, and spatial patterns of larval fish distribution. Given the logistical constraints associated with field research on large lakes, adapting cruise plans to real time forecasts is a challenge, but having realtime information on transient phenomena may present opportunities to sample and study these events. In addition, the model simulations will likely be of value in retrospective analysis to provide context for in-situ observations, in terms of physical and ecological phenomena that were occurring around the sampling events.

Tables and Figures

Table D-1: Archived Nowcast/Forecast biophysical models developed and run for CSMI 2020-21 Lake Michigan. Model graphics can be viewed on the web page for each day.

Title	Date range	URL
Experimental Biophysical Nowcast/Forecast for Lake Michigan CSMI 2020	2020-01-01 to 2020-12-31 2021-01-01 to 2021-12-31	https://www.glerl.noaa.gov/res/lmhofs-bio/LM-CSMI-Model.html
Experimental Larval Fish Dispersion Forecast for Lake Michigan CSMI 2020	2020-03-30 to 2020-07-31 2021-03-18 to 2021-09-10	https://www.glerl.noaa.gov/res/glcfs-fvcom/larval-tracker-csmi2020/ https://www.glerl.noaa.gov/res/glcfs-fvcom/larval-tracker-csmi2021/
Lake Mich-Huron FVCOM Muskegon Transect Temperature and Currents	Provided daily updated forecast graphics during field seasons 2020-2022	https://www.glerl.noaa.gov/res/glcfs/muskegon.html

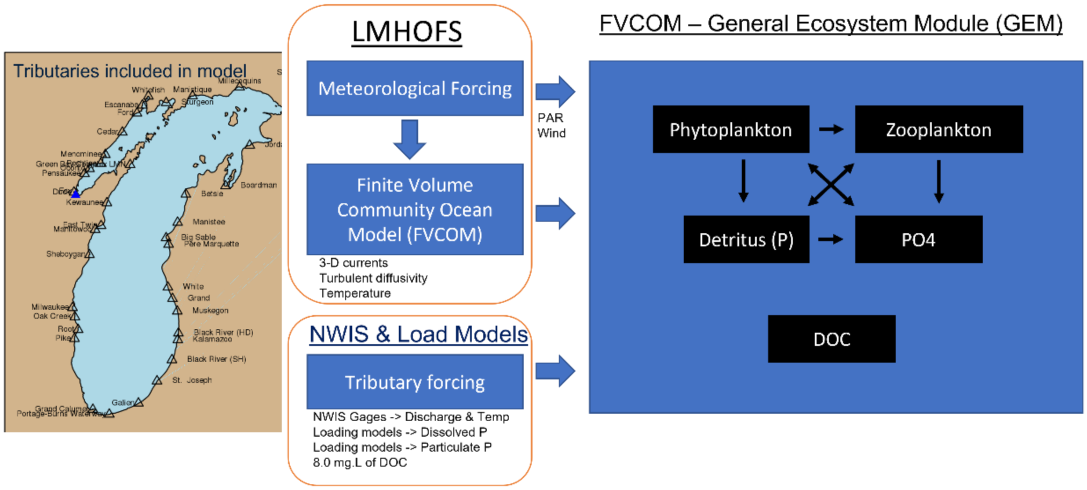

Figure D-1: Components of the Experimental Biophysical Nowcast/Forecast for Lake Michigan CSMI 2020. The biophysical model was an application of the Finite Volume Community Ocean Model – General Ecosystem Module, with state variables representing a phosphorus-limited lower food web (Rowe et al. 2017) with dissolved organic carbon (DOC) included as a tracer for river inputs. River discharge was obtained from the USGS National Water Information System for 37 tributaries, with estimated dissolved phosphorus and DOC concentrations.

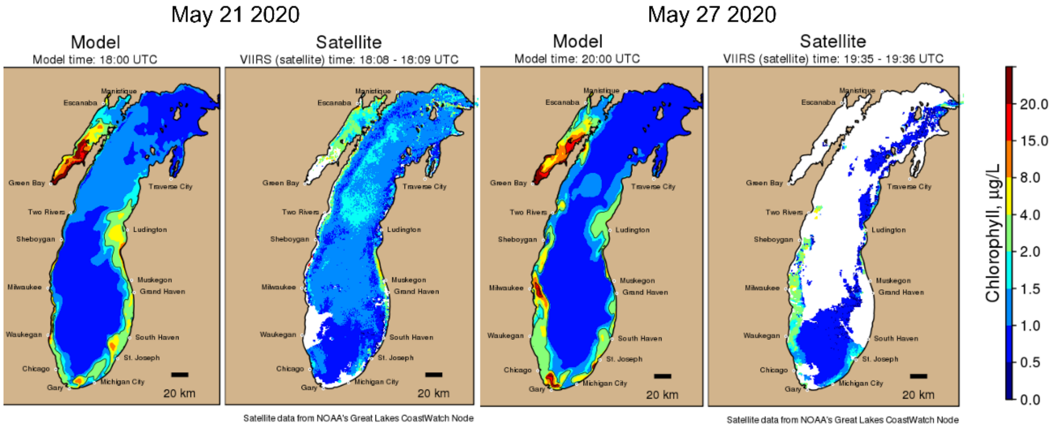
May 21 2020

Model

Model time: 18:00 UTC

Satellite

VIIRS (satellite) time: 18:08 - 18:09 UTC

May 27 2020

Model

Model time: 20:00 UTC

Satellite

VIIRS (satellite) time: 19:35 - 19:36 UTC

Satellite data from NOAA's Great Lakes CoastWatch Node

Figure D-2: Graphics from the Experimental Biophysical Nowcast/Forecast for Lake Michigan CSMI 2020, paired with satellite-derived chlorophyll-a on the same dates. A coastal upwelling event caused an expansion of the area of elevated surface chlorophyll-a along the western shore near Milwaukee, on May 27 compared to May 21.

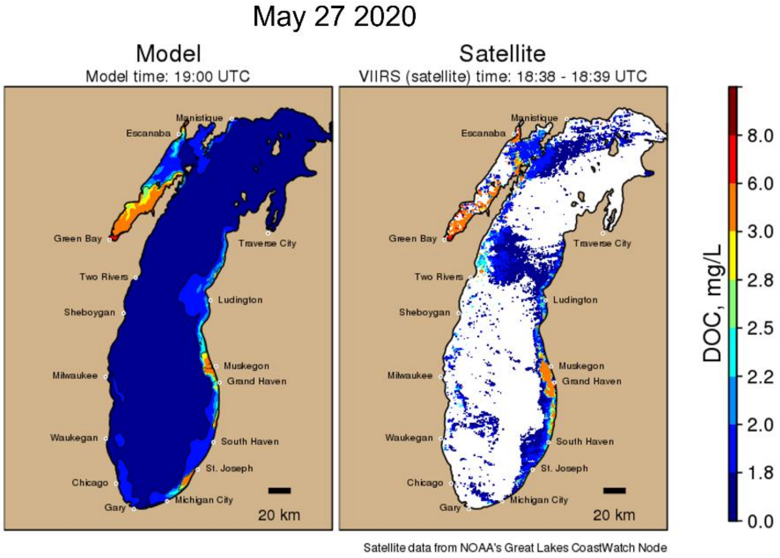
May 27 2020

Model

Model time: 19:00 UTC

Satellite

VIIRS (satellite) time: 18:38 - 18:39 UTC

Satellite data from NOAA's Great Lakes CoastWatch Node

Figure D-3: Graphics from the Experimental Biophysical Nowcast/Forecast for Lake Michigan CSMI 2020, paired with satellite-derived dissolved organic carbon (DOC) on the same date. A major precipitation and river discharge event caused a plume of DOC on the eastern shore near Muskegon and Grand Haven, visible in the model simulation and in the satellite imagery.

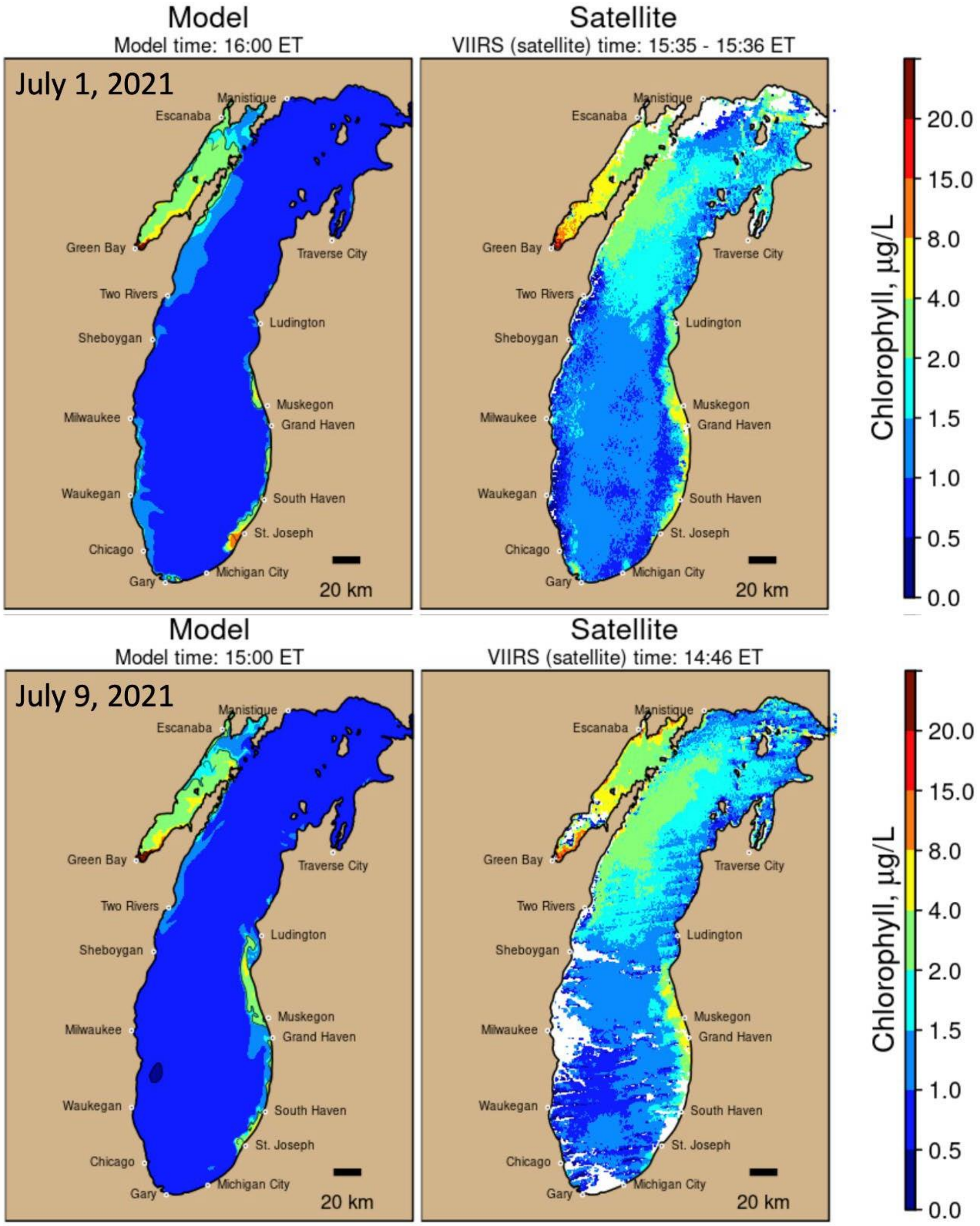

Figure D-4: Biophysical model graphics and paired satellite imagery showing elevated surface chlorophyll concentrations along the southeast Lake Michigan shore, associated with a period of elevated river discharge from approximately June 28 through July 9.

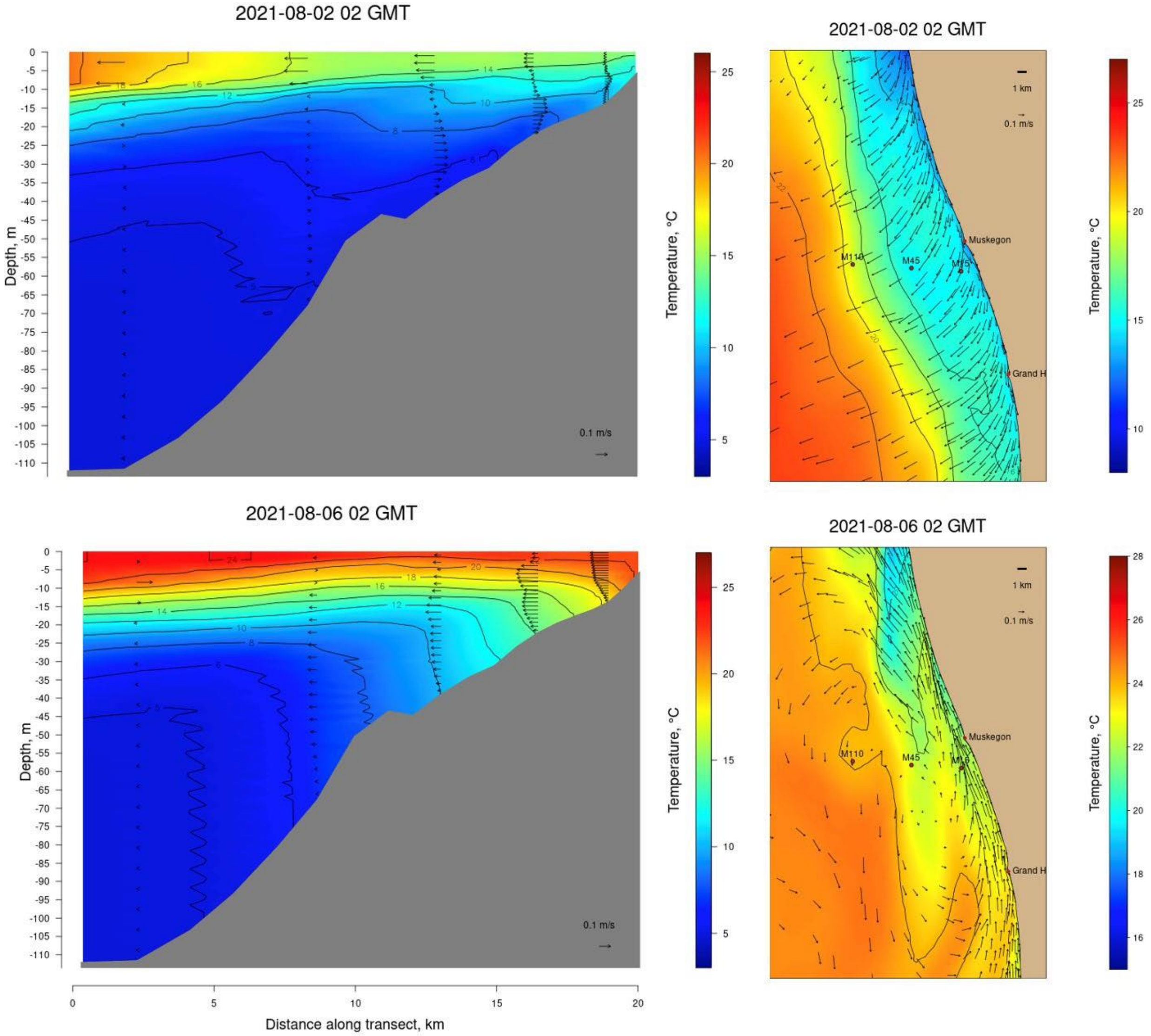

Figure D-5: Surface and cross-sectional view of the Muskegon transect region, showing modeled temperature and currents. A strong upwelling event was simulated offshore of Muskegon on August 2, 2021, and had relaxed by August 6, coincident with a field research cruise along the Muskegon transect.

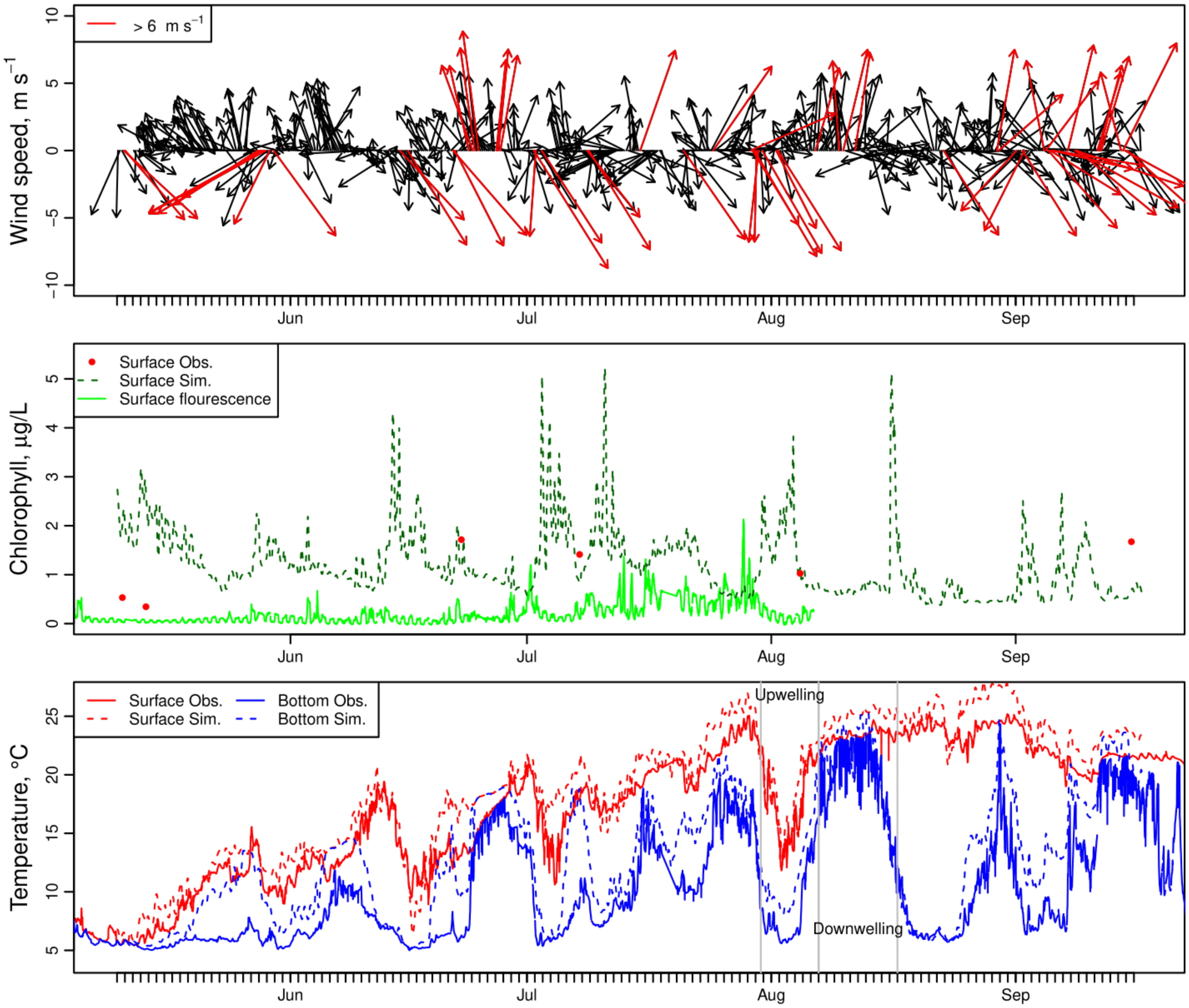

Figure D-6: Time series of wind speed, fluorescence chlorophyll, surface and bottom temperature from the Muskegon 20-m buoy, with modeled chlorophyll and temperature, and sampled chlorophyll.

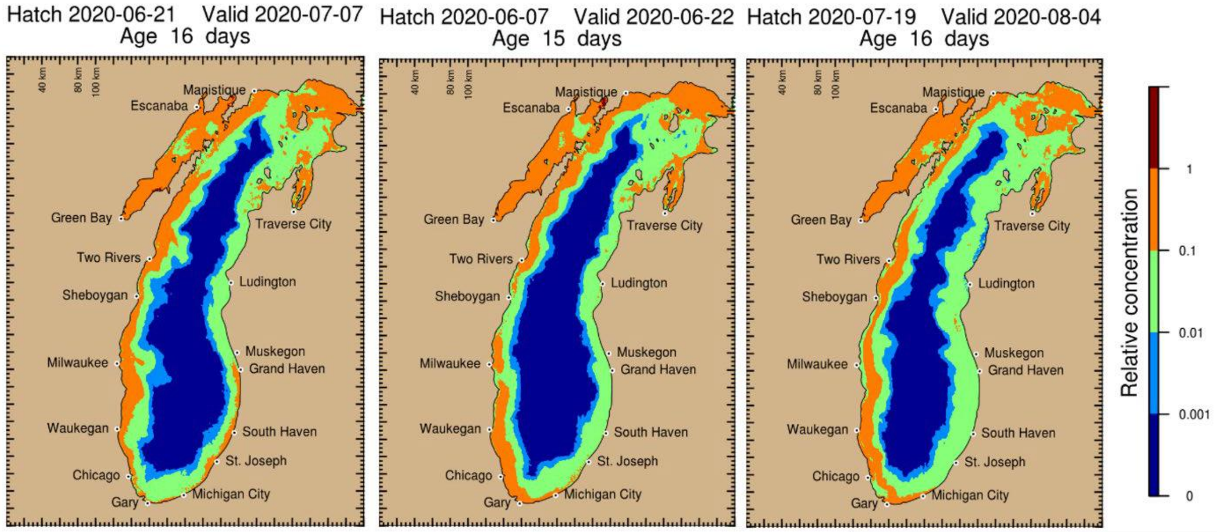

Figure D-7: Graphics from the Experimental Larval Fish Dispersion Forecast for Lake Michigan CSMI 2020 on dates of larval fish sampling offshore of Muskegon, showing the expected spatial distribution of 15-16 day old larval fish hatched in nearshore areas (< 10 m) where spawning is assumed to occur.

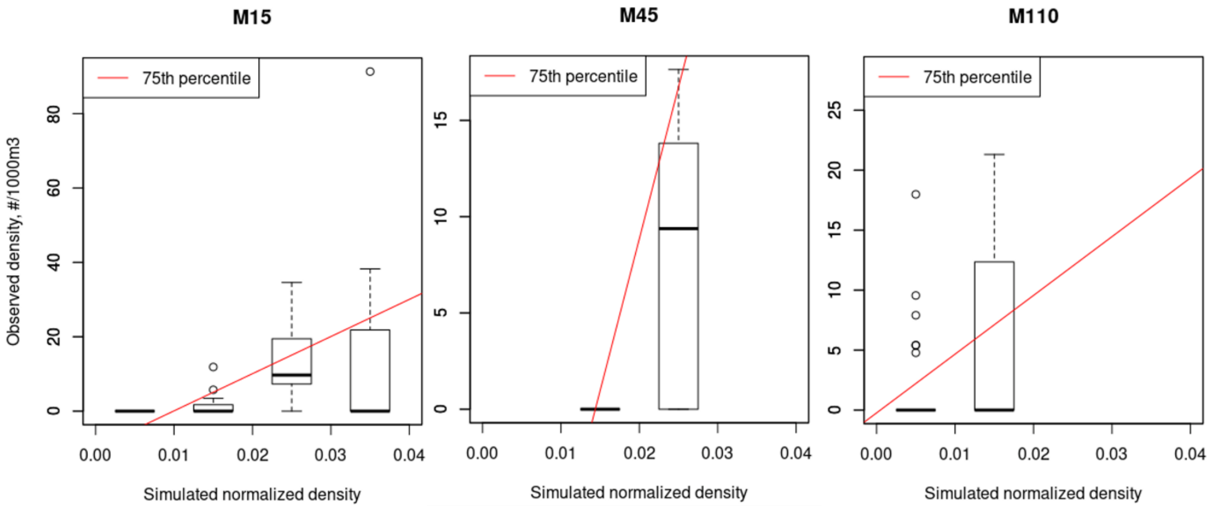

Figure D-8: Comparison of simulated normalized density of larval fish from the Experimental Larval Fish Dispersion Forecast for Lake Michigan CSMI 2021 to observed larval alewife density from sampling offshore of Muskegon at the 15, 45, and 110 m-depth stations. A quantile regression line for the 75th percentile is shown with a red line.

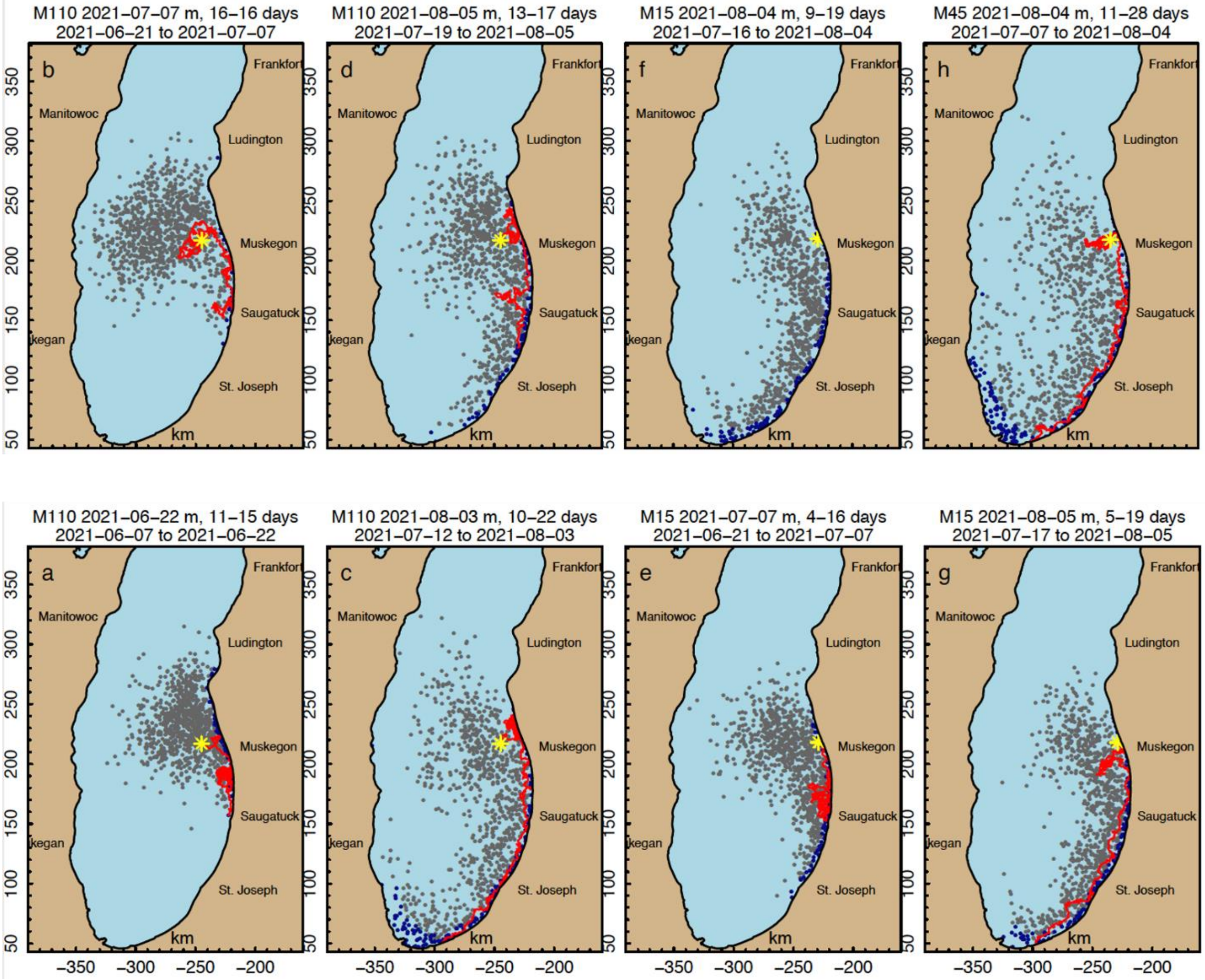

Figure D-9: Backward trajectory simulations of aged larval fish collected offshore of Muskegon (yellow asterisk), showing the likely region of origin (blue dots), and a randomly selected example from the ensemble of 1000 simulated trajectories (red line). Gray dots indicate simulated possible origin locations that were considered unlikely because they were not in shallow nearshore locations (< 20 m).

Acknowledgements

We thank the captains and crews of the EPA R/V Lake Guardian and NOAA vessels. We also thank Rachel Orzechoswki and Aaron Dunnuck (CIGLR/GVSU) who assisted with lab and field work, as well as Ashley Burtner, Glenn Carter, Christine Kitchens, and Kelly McCabe (CIGLR) who assisted with lab work. We appreciate our collaboration with colleagues from EPA (Beth Hinchey Malloy, Annie Scofield, Joel Hoffman), SUNY Buffalo State (Alexander Karatayev, Lyuba Burlakova), and Wayne State University (Donna Kashian).

Literature Cited

Anderson, E.J., Stow, C.A., Gronewold, A.D., Mason, L.A., McCormick, M.J., Song, S.Q., Ruberg, S.A., Beadle, K., Constant, S.A., Hawley, N.. Seasonal overturn and stratification changes drive deep-water warming in one of Earth's largest lakes. *Nature Communications* 12, 1688 (2021). https://doi.org/10.1038/s41467-021-21971-1

Auer, N. A. (Ed.). (1982). *Identification of larval fishes of the Great Lakes basin with emphasis on the Lake Michigan drainage* (Vol. 82, No. 3). Great Lakes Fishery Commission.

Biddanda, B., Dila, D., Weinke, A., Mancuso, J., Villar-Argaiz, M., Medina-Sánchez, JM., González-Olalla, JM., and P. Carrillo (2021). Housekeeping in the Hydrosphere: Microbial Cooking, Cleaning and Control Under Stress. Life doi:10.3390/life11020152; https://www.mdpi.com/2075-1729/11/2/152

Bockwoldt, Katelyn Alexis, "Spatial and Temporal Variation of Phytoplankton Production in Lake Michigan" (2018). Theses and Dissertations. 1755

Bürkner, P. C. (2017). brms: An R package for Bayesian multilevel models using Stan. Journal of statistical software, 80, 1-28.

Carrick, H.J., and C.L. Schelske. 1997. Have we underestimated the importance of small phytoplankton in productive waters***?*** Limnol. Oceanogr. 42: 1613-1621.

Carrick, H.J. 2005. Under-appreciated aspects of biodiversity in planktonic communities: The role of protozoa in Lake Michigan (A case study). Revue of Hydrobiologia. 551: 17-32.

Carrick, H.J, J.B. Moon, and G.F. Gaylord. 2005. Phytoplankton dynamics and hypoxia in Lake Erie: Evidence for benthic-pelagic coupling in the central basin. J. Great Lakes Res. 31: 111-124.

Carrick HJ, Butts E, Daniels D, Fehringer M, Frazier C, Fahnenstiel GL, Pothoven S, Vanderploeg HA. 2015. Variation in the abundance of pico, nano, and microplankton in Lake Michigan: Historic and basin-wide comparisons. J. Great Lakes Res. 41: 66-74.

Carrick, H.J., E. Cafferty, A. Ilacqua, S. Pothoven, and G.L. Fahnenstiel. 2017. Seasonal abundance, biomass, and morphological diversity of picoplankton in Lake Superior: Importance of water column mixing. Internat. J. Hydrology, 1(6): 00034.

Denef, V., H. Carrick, A. Burtner, J. Cavaletto, E. Chiang, T.H. Johengen, D. Palladino, R. Props, M. Schmidt, and Vanderploeg. 2017. Lake bacterial assemblage composition is sensitive to biological disturbance caused by an invasive filter feeder. mSphere 2e00189-17.

Dolan, D. M., & Chapra, S. C. (2012). Great Lakes Total Phosphorus Revisited: 1. Loading Analysis and update (1994–2008). Journal of Great Lakes Research, 38(4), 730–740. https://doi.org/10.1016/j.jglr.2012.10.001

Dugener, N., I. Stone, A. Weinke and B. Biddanda. Out of oxygen: Stratification and loading drove hypoxia during a warm and productive year in a Great Lakes estuary. J. Great lakes Research (Submitted November 2022, In Review).

Eilers, P.H.C. and Peeters, J.C.H. 1988 A model for the relationship between light intensity and the rate of photosynthesis in phytoplankton. Ecological Modeling. 42, 199–215.

Elgin, Ashley K.; Glyshaw, Paul W.; NOAA Great Lakes Environmental Research Laboratory (2021). Quagga mussel (*Dreissena rostriformis bugensis*) shell and tissue measurements collected from the R/V LAKE GUARDIAN, R/V LAURENTIAN, and other small boats in the Laurentian Great Lakes from 2015-07-20 to 2021-07-21 (NCEI Accession 0242500). NOAA National Centers for Environmental Information. Dataset. https://www.ncei.noaa.gov/archive/accession/0242500.

Eppehimer, D.E., Bunnell, D.B., Armenio, P.M., Warner, D.M., Eaton, L.A., Wells, D.J., Rutherford, E.S. Densities, diets, and growth rates of larval Alewife and Bloater in a changing Lake Michigan ecosystem. 2019. Trans. Am. Fish. Soc. 148:755-770.

Fahnenstiel, G.L., J.F. Chandler, H.J. Carrick, and D. Scavia. 1989. Photosynthetic characteristics of Lakes Huron and Michigan Phytoplankton communities: P-I parameters and end-products. J. Great Lakes Res. 15: 394-407.

Fahnenstiel, G.L., and H.J. Carrick. 1992. Phototrophic picoplankton in Lakes Huron and Michigan: Abundance, distribution, composition, and contribution to biomass and production. Can. J. Fish Aquat. Sci. 49: 379-388.

Fitzpatrick, M.A.J., M. Munawar, Leach, J.H., Haffner, G.D. 2007. Factors regulating primary production and phytoplankton dynamics in western Lake Erie. archive fur Hydrobiol. 169/2: 137-152.

Fitzwater, S. E., G. A. Knauer, and others. 1982. Metal contamination and its effects on primary production measurements. Limnol.Oceanogr. 27: 544-551.

Glyshaw, P. W., Riseng, C. M., Nalepa, T. F., & Pothoven, S. A. (2015). Temporal trends in condition and reproduction of quagga mussels (*Dreissena rostriformis bugensis*) in southern Lake Michigan. *Journal of Great Lakes Research*, *41*, 16-26.

Hama, T., Miyazaki, T., Ogawa, Y., Iwakuma, T., Takahashi, M., Otsuki, A., & Ichimura, S. (1983). Measurement of photosynthetic production of a marine phytoplankton population using a stable ^{13}C isotope. *Marine Biology*, *73*, 31-36.

Hecky RE, Smith REH, Barton DR, Guildford SJ, Taylor WD, Charlton MN, Howell T. 2004. The nearshore phosphorus shunt: a consequence of ecosystem engineering by dreissenids in the Laurentian Great Lakes. Can. J. Fish. Aquat. Sci. 61: 1285-1293.

Lenth, R.V., 2016. Least-Squares Means: The R Package lsmeans. J. Stat. Softw. 69. https://doi.org/10.18637/jss.v069.i01

Luimstra VM, Schuurmans JM, Verschoor AM, Hellingwerf KJ, Huisman J, Matthijs HCP. 2018. Blue light reduces photosynthetic efficiency of cyanobacteria through an imbalance between photosystems I and II. Photosynth Res 138:177–189.

Mancuso, J.L., A.D. Weinke, I.P. Stone, S.E. Hamsher, M. Villar-Argaiz and B.A. Biddanda (2021). Cold and Wet: Diatoms dominate the phytoplankton community in a year of anomalous weather in a Great Lakes estuary. J. Great Lakes Res. 47: 1305-1315. https://doi.org/10.1016/j.jglr.2021.07.003

Mancuso, J.L., A.D. Weinke, I.P. Stone, S.E. Hamsher, M.M. Woller-Skar, E.B. Snyder, and B.A. Biddanda (2021): Bloom and bust: Historical trends of harmful algal blooms in Muskegon Lake, Michigan, a Great Lakes estuary. Freshwater Science. 40: 463-477. https://www.journals.uchicago.edu/doi/full/10.1086/716236

Murphy J, Riley JP. A modified single solution method for the determination of phosphate in natural waters. Anal Chim Acta. 1962: 27:31–36.

Nalepa, T. F., Fanslow, D. L., & Pothoven, S. A. (2010). Recent changes in density, biomass, recruitment, size structure, and nutritional state of *Dreissena* populations in southern Lake Michigan. *Journal of Great Lakes Research*, *36*, 5-19.

Nalepa, T.F., L.E. Burlakova, A.K. Elgin, A.Y. Karatayev, G.A. Lang, and K. Mehler. 2020. NOAA Tech memo GLERL-175. Abundance and biomass of benthic macroinvertebrates in Lake Michigan in 2015, with a summary of temporal trends. Technical Memo, NOAA Great Lakes Environmental Research Laboratory, NOAA Great Lakes Environmental Research Laboratory, Ann Arbor MI.

Pothoven, S.A., and Elgin, A.K., 2019. Dreissenid veliger dynamics along a nearshore to offshore transect in Lake Michigan. Journal of Great Lakes Research 45:300-306 doi: 10.1016/j.jglr.2019.01.001

Pothoven, S.A., and Vanderploeg, H.A. 2020. Seasonal patterns for Secchi depth, chlorophyll a, total phosphorus, and nutrient limitation differ between nearshore and offshore in Lake Michigan. Journal of Great Lakes Research 46: 519-527 doi:10.1016/j.jglr.2020.03.013.

R Core Team (2022). R: A language and environment for statistical computing. R Foundation for Statistical Computing, Vienna, Austria.

Rowe, M. D., Anderson, E. J., Vanderploeg, H. A., Pothoven, S. A., Elgin, A. K., Wang, J., Yousef, F. (2017). Influence of invasive quagga mussels, phosphorus loads, and climate on spatial and temporal patterns of productivity in Lake Michigan: A biophysical modeling study. *Limnology and Oceanography*, 62(6), 2629-2649.

Rowe, M. D., Prendergast, S. E., Alofs, K. M., Bunnell, D. B., Rutherford, E. S., & Anderson, E. J. (2022). Predicting larval alewife transport in Lake Michigan using hydrodynamic and Lagrangian particle dispersion models. *Limnology and Oceanography*, *67*(9), 2042-2058.

Robertson, D.M., and Saad, D.A., 2019, Spatially referenced models of streamflow and nitrogen, phosphorus, and suspended-sediment loads in streams of the Midwestern United States: U.S. Geological Survey Scientific Investigations Report 2019–5114, 74 p. including 5 appendixes https://doi.org/10.3133/sir20195114

Schmitt-Jansen, M, and Altenburger, R. 2008. Community-level microalgal toxicity assessment by multiwavelength-excitation PAM fluorometry. Aquatic Toxicology 86: 49-58.

Speziale BJ, Schreiner SP, Giammatteo PA, Schindler JE. Comparison of N, N-Dimethylformamide, Dimethyl Sulfoxide, and Acetone for Extraction of Phytoplankton Chlorophyll. Can J Fish Aquat Sci. 1984; 41(10): 1519-1522.

U.S. Environmental Protection Agency. MDQARL Method Study 4, Automated Methods. Cincinnati (OH): National Environmental Research Center.
Webb, W. L., Newton, M., & Starr, D. (1974). Carbon dioxide exchange of *Alnus rubra*. Oecologia, 17(4), 281-291.

Williamson, C. E., Fischer, J. M., Bollens, S. M., Overholt, E. P., & Breckenridge, J. K. (2011). Toward a more comprehensive theory of zooplankton diel vertical migration: Integrating ultraviolet radiation and water transparency into the biotic paradigm. *Limnology and Oceanography*, *56*(5), 1603-1623.

Report: Lake Michigan CSMI Lower Food Web Survey Data Summary

Lake and Year: Lake Michigan CSMI 2021
Lead Organization: EPA Office of Research and Development Great Lakes Toxicology and Ecology Division

Authors of This Report:
Kansas Keeton, EPA ORISE
Tom Hollenhorst, EPA ORD
Sam Miller, EPA ORD
Paul McKinney, EPA ORISE
James Gerads, EPA ORD
Annie Opseth, EPA ORD
Ryan Lepak, EPA ORD
Aabir Banerji, EPA ORD
Joel Hoffman, EPA ORD

Contact(s) for Questions About this Report:
Joel Hoffman, hoffman.joel@epa.gov,
Kansas Keeton, keeton.kansas@epa.gov

Project Overview

Lake Michigan has undergone substantial biological change in the lower food web, as evidenced by lake-wide changes in primary productivity (Stadig et al., 2020), zooplankton abundance and composition (Barbiero et al., 2019), fish recruitment (Eppehimer et al., 2020), and trophic transfer of contaminants (Lepak et al., 2019). Changes in the lower food web have been attributed to invasive species, particularly Dreissenid mussels, as well as to changes in nutrient inputs to the lake (Bunnell et al. 2018). Specifically, diversion of nutrient and energy flow following Dreissenid establishment has resulted in nutrient rich nearshore areas and nutrient poor offshore pelagic areas (Hecky et al., 2004; USEPA, 2019). Thus, these changes have not been uniform throughout the lake or through time, which presents multiple challenges for lake managers to determine a course of action and increases the amount of spatial and temporal information required to support management decisions. This project addresses numerous priorities identified by the Lake Michigan Partnership Management Committee (LMPMC) regarding *Nutrient-Food Web Dynamics in a Changing Ecosystem*. The priorities identified by the LMPMC specifically address needs to improve our understanding of how nutrient inputs, phytoplankton and zooplankton abundance, as well as invasive species are changing, and how this change influences prey fish and game fish growth and recruitment.

Specifically, this project was organized around the following science priorities and research questions:

- Priority #1: Advance the understanding of nutrient dynamics that directly influence lower trophic level productivity and offshore fish production.
- Priority #3: Investigate understudied but important components of the food web, including: fall/winter/early spring nearshore (including shallow shoreline areas) community structure, Dreissenid mussel veligers (including their nutrition as prey for larval fish), *Limnocalanus* copepods, *Mysis* crustaceans, the microbial loop (bacteria and microzooplankton), and round gobies (which are under-sampled by traditional gears).
- Priority #6: Continue nearshore and offshore monitoring of key food web species (e.g., phytoplankton, zooplankton, *Diporeia* amphipods, and Dreissenid mussels.

For this project, researchers from the US Environmental Protection Agency (USEPA) Office of Research and Development Great Lakes Toxicology and Ecology Division (GLTED) collaborated with researchers from the US Geological Survey (USGS) and USEPA Great Lakes National Program Office (GLNPO) to sample a set of lake-wide stations at 16 nearshore-offshore transects during July 2021 (Fig. 1). Water chemistry was collected at 64 stations, and zooplankton was collected at 105 stations. Larval fish were sampled using surface nets and pelagic trawls at the same transect sites (Bunnell et al., 2023). To sample inshore-offshore changes in water quality and zooplankton, seven stations were positioned at specific distances from shore: 5 km, 8 km, 12 km, 17 km, 23 km, 30 km, and 38 km. Zooplankton were sampled at all stations, whereas every alternate station was targeted for water quality analysis (typically, 5 km, 17 km, and 38 km from shore). Moreover, a few additional water quality stations were sampled during the 2015 Cooperative Science and Monitoring Initiative benthos study (Fig. 1, EPA GLNPO stations). The stations' depths along each transect typically ranged from 10 m to 20 m at the most inshore station to 50 m to 130 m at the most offshore station.

Water quality was sampled from two discrete layers at each station: the epilimnion (5 m below surface) and the deep maximum chlorophyll layer (depth varied from 10 m to 43 m). Zooplankton were also sampled by depth-integrated vertical net tows from two layers based on the ultra-violet (UV) characteristics of the water column. The upper layer sampled extended from the surface to the estimated extinction depth to 1% of ambient UV radiation (generally, from surface to 5 m to 10 m). The lower layer extended from the 1% of ambient UV radiation extinction depth down to either the upper hypolimnion (generally, 35 m to 40 m) or 2 m above bottom at shallow locations.

To better characterize patterns in primary production, a Teledyne Webb Research G2 glider (hereafter 'glider') was deployed from July 12-23 near the Rowley Bay transect (Fig. 1) to compare chlorophyll data collected by virtual mooring to those collected via ship-based sampling methods.

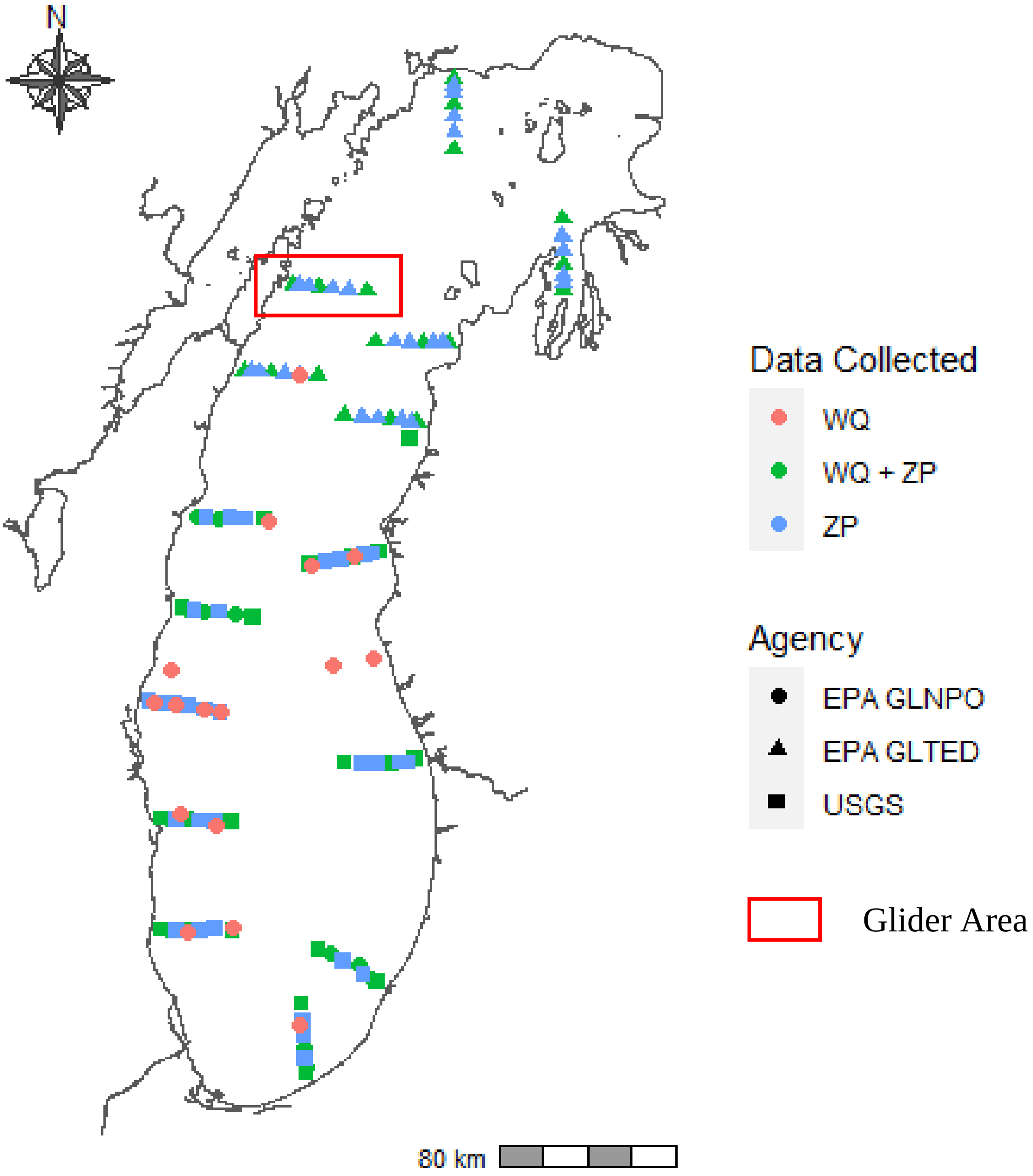

Figure 1. Lake Michigan CSMI 2021 sampling locations. Data collected: WQ = Only water quality data (at former transect stations sampled in 2015), WQ + ZP = water quality and zooplankton data, ZP = only zooplankton data. Agency: EPA = Environmental Protection Agency, GLNPO = Great Lakes National Program Office, GLTED = Great Lakes Toxicology and Ecology Division, USGS = United States Geological Survey.

Study Highlights

Water Chemistry

- Total Phosphorus (TP) concentrations were higher in Lake Michigan north of Manitowoc, possibly influenced by the upwelling of cold, phosphorus-rich waters.
- Cations and anions that are sometimes used as tracers of urban influence (e.g., Cl^-, Na^+) did not show distinct inshore-offshore gradients, indicating the design had poor resolution for urban influence; however, several, including nitrates and nitrites, total Nitrogen, Chlorophyll a, and Silica exhibited a slight positive correlation with depth.

Primary Production

- Chlorophyll concentration within the deep maximum chlorophyll layer was lower at the stations closer to shore and higher at offshore stations, increasing linearly with station depth. This spatial pattern differs markedly from previous analyses of surface chlorophyll a concentration.
- Multiple methods to measure chlorophyll a produced similar results but different insights as to the pattern of chlorophyll a both within the water column and the differences between nearshore and offshore locations.

Zooplankton Density + Taxonomy

- Generally, zooplankton densities were higher in the "No UV" zone (lower layer sampled) compared to the "1% UV" zone (upper layer sampled), likely at least in part owing to diel vertical migration during the day when the tows were conducted.
- *Limnocalanus* copepod concentrations were low, and *Limnocalanus* were primarily captured at offshore stations.
- Dreissenid veliger concentrations were high compared to other taxa; they were generally highest at nearshore stations, and some moderate densities were observed at mid-offshore stations.
- Rotifers had the highest density of all taxonomic groups.

Subproject A: Water Chemistry

Overview

Surface and metalimnetic waters were sampled to measure concentrations of nutrients, chlorophyll a (Chl a), and common cations and anions. The data were analyzed to investigate inshore-offshore differences in water chemistry, which may influence both primary production and secondary production.

Methods

At each station sampled by USEPA ORD, a Sea-bird Electronics 911 conductivity–temperature–depth (CTD) rosette system was deployed (0.25 m/sec after a 2-minute acclimation period at 3 m depth). The CTD was fitted with additional sensors for fluorescence (470nm excitation and 685nm emission wavelengths; Seapoint Sensors), light transmittance (C-Star; Wet Labs), oxygen (Sea-bird SBE 43), pH (Sea-bird SBE 18), and photosynthetically active radiation (PAR; Biospherical Instruments). At each station sampled by USGS, a Sea-bird Electronics 19plusV2 conductivity–temperature–depth (CTD) bathythermograph was deployed (0.5 m/sec after a 1-minute acclimation period just below surface). The CTD was fitted with additional sensors for turbidity and fluorescence (Wet Labs), colored dissolved organic matter (CDOM; Wet Labs), dissolved oxygen (Sea-bird SBE 43), pH (Sea-bird SBE 18), and photosynthetically active radiation (PAR; Biospherical Instruments).

Water samples were collected at two discrete depths: the epilimnion and the deep maximum chlorophyll layer. The epilimnion sample was collected at 5 m below the surface. The deep chlorophyll maximum layer was defined as a doubling in fluorescence from surface values coincident with the metalimnion–hypolimnion boundary. Where a deep chlorophyll maximum layer was present, water was sampled at the depth of maximum fluorescence. Not all sites were thermally stratified, and those that were stratified did not always support a deep maximum chlorophyll layer.

Water samples were analyzed for total and dissolved nitrogen (N) and phosphorus (P), dissolved cations and anions, and Chl a concentration. In the field, approximately 100 mL of unfiltered water was added to acid-washed (10% HCl) and deionized (DI) water–rinsed 125 mL polyethylene bottles for total nutrient analyses. Water was filtered through 0.45 mm hydrophilic nylon filters and split into acid-washed polyethylene bottles for dissolved inorganic nutrients; DI water–washed 125 mL polyethylene bottles for anions and cations. For Chl a analysis, water samples (100 ml) were filtered through a GF/C filter. Nutrient samples and filters were stored frozen. Cation and anion samples were refrigerated until analysis.

Nutrient analyses were performed on a Lachat 8500 QuikChem Series 2 automated flow injection system (QuickChem 2011). Total Nitrogen (TN) and Total Phosphorus (TP) determinations were made on unfiltered samples by digestion via an autoclave (50 min at 121^{o}C) after addition of 3.3 mL of 0.148 mol potassium persulfate and 3.75 mol NaOH reagents. Nitrogen was measured after cadmium reduction (method 4500-N F; APHA 1998). Phosphorus in the digested sample was measured after forming an antimony–phosphomolybdate complex, with ascorbic acid reduction (method 4500-P F; APHA 1998). From undigested filtered samples, inorganic dissolved nitrate (NO_3) plus nitrite (NO_2) (represented by NO_x) was measured using the phenolate method with cadmium reduction; the cadmium reduces all nitrate to nitrite (method 4500-N E; APHA 1998) and soluble reactive phosphorus (SRP) with the molybdate–ascorbic acid method (method 4500-P F; APHA 1998). Silica (Si) was measured using a molybdate reactive method with a stannous chloride reductant (EPA method 366.0;

QuikChem method 31-114-27-1-D). Aliquots for silica analysis are taken from unpreserved, refrigerated anion samples.

Magnesium (Mg^{2+}), calcium (Ca^{2+}), potassium (K^{+}), and sodium (Na^{+}) samples were preserved (50 µL nitric acid) and concentration was measured by atomic absorption spectroscopy (PerkinElmer PinAAcle 900T Atomic Absorption Spectrometer). Methods for each cation were developed on this specific instrument and then run consecutively on each sample. Chloride (Cl^{-}) and sulfate (SO_4^{2-}) sample concentrations were measured via ion chromatography on a Thermo Fisher IC5000+ Dual System Ion Chromatograph (Thermo Fisher Scientific; method 4110-C; APHA 1998).

Chlorophyll a was extracted from filters using an acetone solvent saturated with magnesium carbonate and measured using a Turner Designs Fluorometer (Turner Designs).

Results and Discussion

Most cations and anions did not display substantial inshore-offshore differences in epilimnetic concentrations (ranges as follows: Potassium (K): 1.22 – 1.48 $mg \cdot L^{-1}$; Sodium (Na): 6.85 – 8.11 $mg \cdot L^{-1}$; Calcium (Ca): 25.86 – 36.72 $mg \cdot L^{-1}$, Magnesium (Mg): 11.78 – 12.66; Chloride (Cl): 11.91 – 14.58 $mg \cdot L^{-1}$; and Sulfate (SO4): 21.02 – 24.89 $mg \cdot L^{-1}$).

Measured concentrations of total and dissolved nutrients ranged widely; concentrations were less variable for Chl a and Si; ranges as follows: SRP: 1.81 – 123 $\mu g \cdot L^{-1}$; TP: 2.65 – 14.1 $\mu g \cdot L^{-1}$; NOx: 134 – 443 $\mu g \cdot L^{-1}$; TN: 396 – 517 $\mu g \cdot L^{-1}$; Chl a: 0.22 – 3.23 $\mu g \cdot L^{-1}$; Si: 3.64 – 5.93 $mg \cdot L^{-1}$). Within the epilimnion, neither SRP nor TP concentrations demonstrated discernible inshore-offshore differences; however, we measured higher TP concentrations in the north than the south (Figs. 2a and 2b). TP concentrations were associated with low temperatures (Pearson's correlation = 0.13, *p*-value = 0.01), suggesting that high TP concentrations in the epilimnion were possibly caused by upwelling of deep, cold, phosphorus-rich waters in northern Lake Michigan. Alternatively, cold waters may have been associated with low primary productivity and thus high TP availability. Epilimnetic Si, NOx, and TN concentrations did not exhibit any discernable south-to-north or inshore-offshore differences (Figs. 2c, 2d, and 2f). In contrast, chlorophyll a concentrations were generally increasing from south to north, and in some cases from inshore to offshore (Fig 2e).

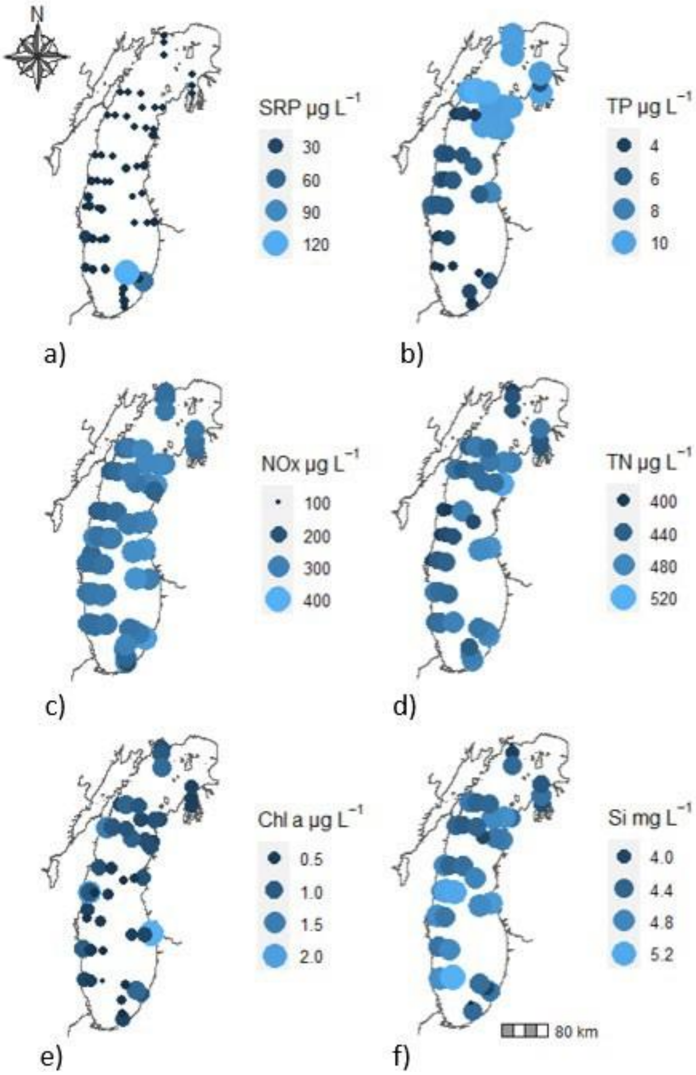

Figure 2: Spatial variability of analyte concentrations measured from epilimnion water samples: a) Soluble Reactive Phosphorus (SRP, µg L^{-1}), b) Total Phosphorus (TP, µg L^{-1}), c) Nitrate (NOx, µg L^{-1}), d) Total Nitrogen (TN, µg L^{-1}), e) Chlorophyll a (µg L^{-1}), f) Silica (Si, mg L^{-1}).

In contrast to the epilimnion concentrations, we found depth-specific relationships in nitrogen, Chl a, and Si concentrations measured from the deep chlorophyll maximum within the metalimnion (Fig. 3). For TN, NO_x, and Si, this highlights the role of deep, offshore waters as an important nutrient reservoir during stratification. The Chl a pattern could be the result of local adaptation to the light environment or represent a change in total algal biomass (or a combination of both). Both forms of phosphorous had variable concentrations that did not demonstrate a depth-specific pattern from inshore to offshore.

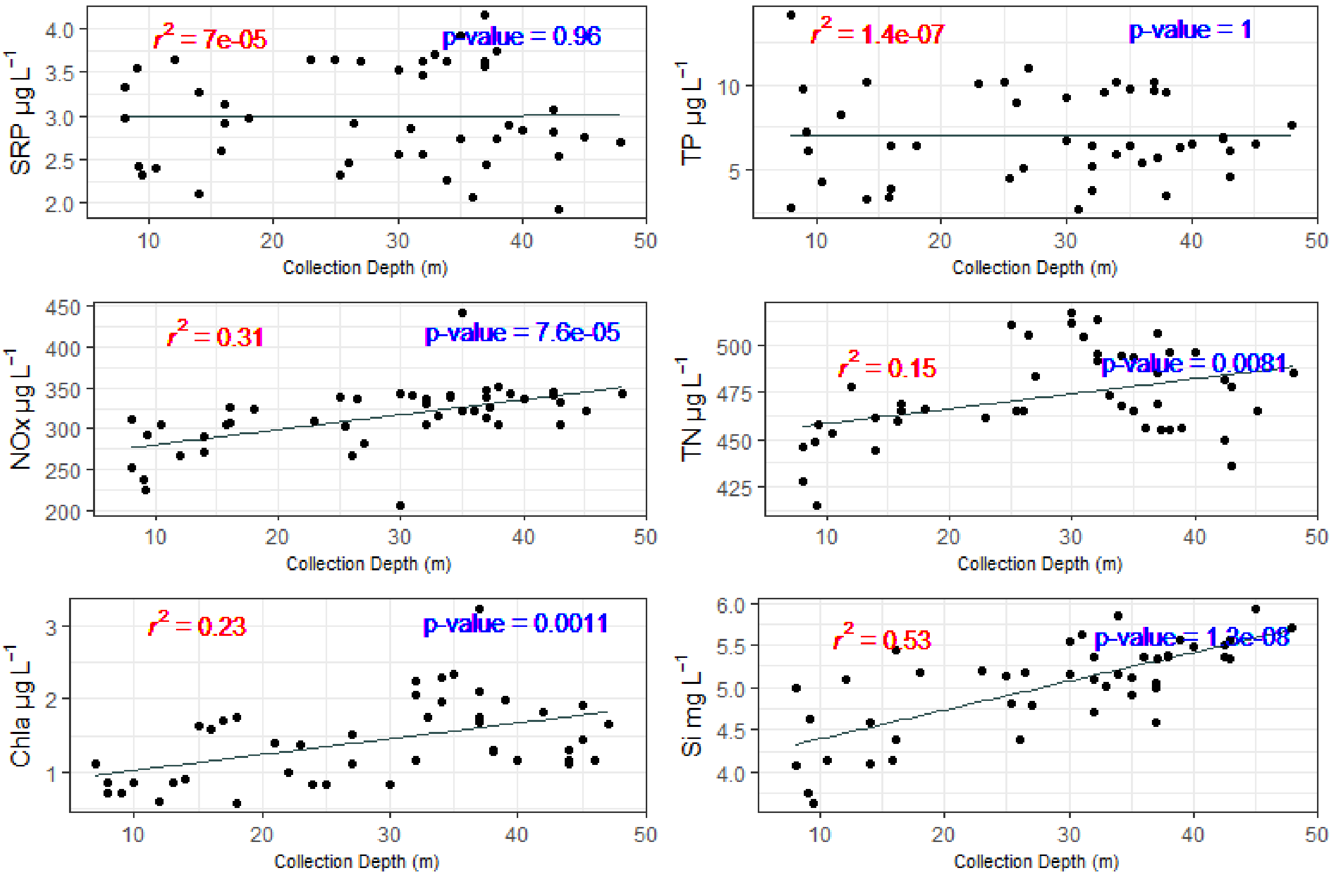

Figure 3. Metalimnion analyte concentration by depth at which the water was sampled (Collection Depth). SRP = Soluble Reaction Phosphorus (µg L^{-1}), TP = Total Phosphorus (µg L^{-1}), NOx = Nitrate + Nitrite (µg L^{-1}), TN = Total Nitrogen (µg L^{-1}), Chl a = Chlorophyll a (µg L^{-1}), Si = Silica (mg L^{-1}). Lines are best-fit (sum of squares) linear regressions, including r^2 and p-values.

Based on the CTD, the average deep chlorophyll maximum layer was found at a depth of 32.3m with a temperature of 8.2^{o} C and an associated florescence equivalent of 1.35 mg m^{-3} (Fig. 4a), which corresponds well to the measured chlorophyll a concentrations (Fig. 3). Based on the CTD, the deeper stations had an increased maximum florescence at greater depths (Fig. 4a). This is consistent with the extracted chlorophyll a data (Fig. 3). Notably, the depth at which the deep chlorophyll maximum layer was observed changed as a function of station depth, with a maximum depth of about 40 m at stations 100 m to 150 m deep.

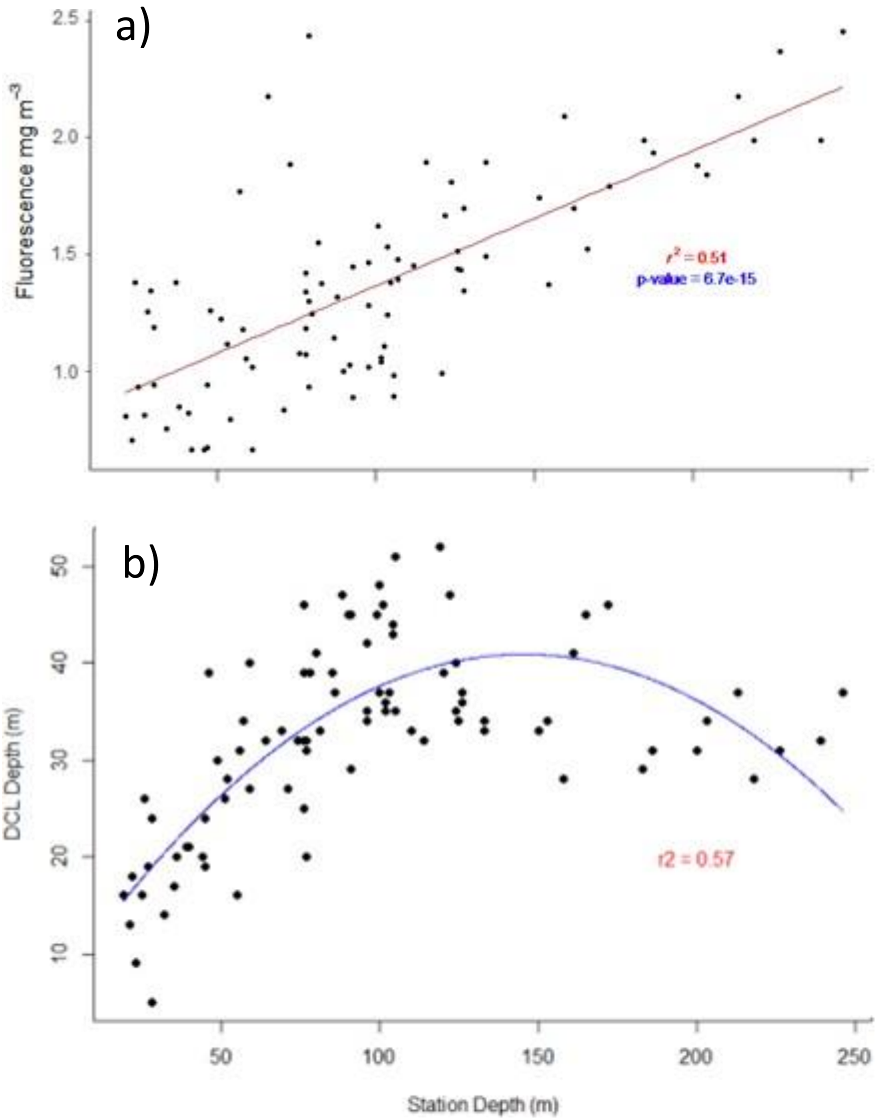

Figure 4: Fluorescence concentration by station depth (m) (top) and depth at which the deep chlorophyll maximum layer was observed by station depth (bottom) from the CTD at the stations sampled by USEPA ORD and USGS. Lines represent the best fit (least squares) linear regression (top) and quadratic function (below), including r^2 and p-value.

Subproject B: Zooplankton

Overview

Zooplankton were sampled at transect stations to investigate inshore-to-offshore differences in taxonomic composition and abundance. In addition, samples were obtained from shallow surface waters with high UV radiation exposure (down to 1% exposure depth, generally 5 m to 10 m depth) and waters beneath with low exposure (1% UV radiation depth to the upper hypolimnion) to contrast feeding environments for young-of-year fish, especially alewife (*Alosa psuedoharengus*) and bloater (*Coregonus hoyi*). In accordance with the LMPMC priorities, we focus the reporting on taxa identified as important, Dreissenid veligers and *Limnocalanus macrurus* (hereafter, *Limnocalanus*) copepods, as well as report on taxa that are important for YOY fish consumption, particularly *Bosmina* spp (hereafter, *Bosmina*), and copepod nauplii. Summed count data are also provided for general taxonomic groups, including rotifers, adult cladocerans, and adult cyclopoid and calanoid copepods.

Methods

At each transect station, two depth layers by vertical, depth-integrated net tow were sampled (closing plankton net: 0.5 m diameter, 64 μm mesh, 3 m length). The first depth layer extended from the surface to the depth at which 1% incident UV radiation was estimated to be, typically between 5m and 10 m. The second layer extended from the depth of 1% incident U radiation to the upper hypolimnion, generally 35 m to 40 m. At some stations, the second layer was sampled by splitting it into two tows to avoid net clogging. Samples were immediately preserved in 5% buffered formalin. A flow meter was installed in the net opening to measure the tow distance (EPA GLNPO and EPA ORD: TSK flow meter; USGS: General Oceanics 2030R). Sampling occurred during daytime. In the laboratory, zooplankton were enumerated using the EPA Great Lakes National Program Office aliquot method (Great Lakes National Program Office [GLNPO], 2016). Sample count estimates were converted into density estimates using volumes based on measured tow distances.

Ultraviolet radiation was measured by Biospherical Instruments' UV radiometer (BIC). This was performed first by taking two surface measurements for each the reference cell that would then be submerged and the deck cell that continuously captures surface radiation. Next the reference cell was lowered to just below the water surface to get a measurement of the surface refraction prior to performing a vertical profile to a depth of 50 m (the cable length) or 2 m above the sediment-water interface at stations less than 50 m depth.

Results and Discussion

Bosmina (cladocerans) and *Limnocalanus* (copepods) had relatively low densities throughout the lake and were not captured at every location sampled (Fig. 4). *Bosmina* was captured at higher densities than *Limnocalanus* and the highest densities of *Bosmina* were found close to shore (Fig. 5a). Densities were generally higher in the "No UV" than the "UV" layer. In contrast, *Limnocalanus* had very low densities (<50 indiv·m^{-3}) and was captured at mid-shore and offshore stations only (Fig. 5b). Further, *Limnocalanus* was captured more frequently within the shallow ("UV") layers than the deep ("No UV") layers; however, densities in the deep "No UV" layer (maximum 400 indiv·m^{-3}) were higher than in the "UV" layer.

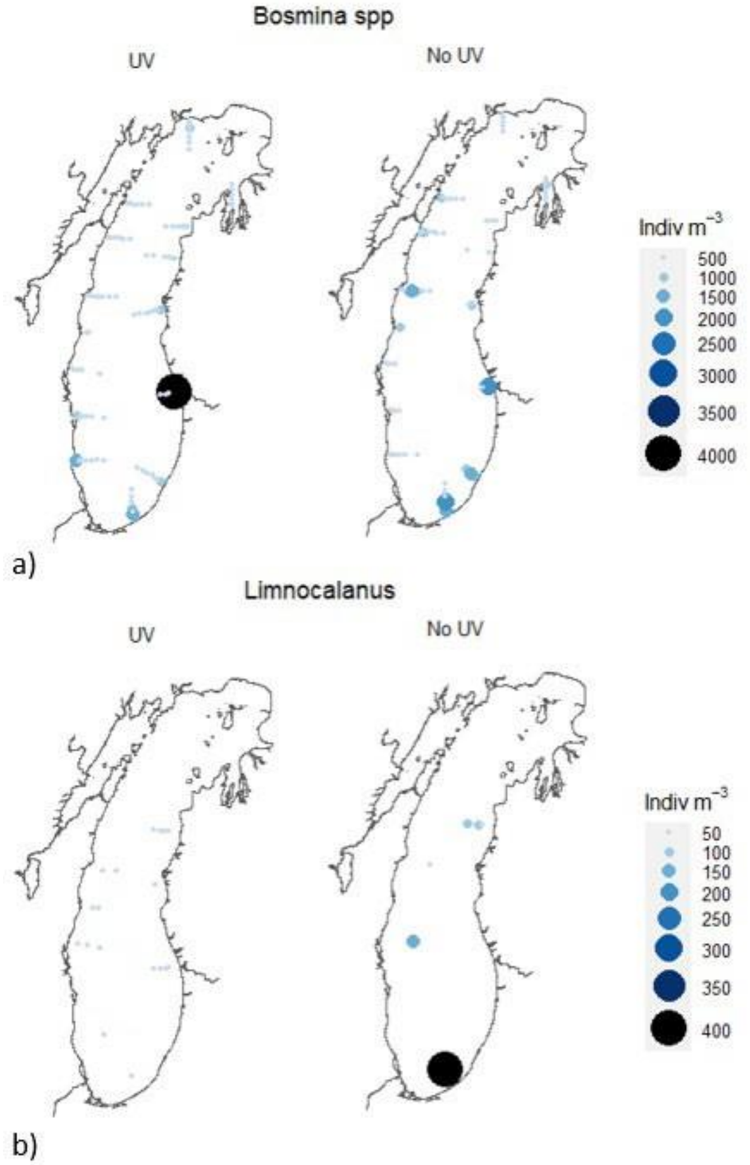

Figure 5. Densities of a) Bosmina spp. (cladoceran) and b) Limnocalanus copepods in 1% UV exposure (left) and No UV exposure (right).

Dreissenid veligers and copepod nauplii were captured at nearly every location sampled and occurred at higher densities than *Bosmina* and *Limnocalanus*. Dreissenid veligers had very high densities at two nearshore sites along the western shoreline; moderate densities were found in the offshore (Fig 6a). Within the shallow "UV" layer, copepod nauplii had the highest densities in the southern part of the lake; observed densities may have been influenced by cold upwelling waters in northwest Lake Michigan (Fig 6b). Within the deep "No UV" layer, we found high densities at locations throughout Lake Michigan. As with *Bosmina* and *Limnocalanus*, and likely owing at least in part to daytime sampling, we found lower densities in the "UV" layer than in the "No UV" layer.

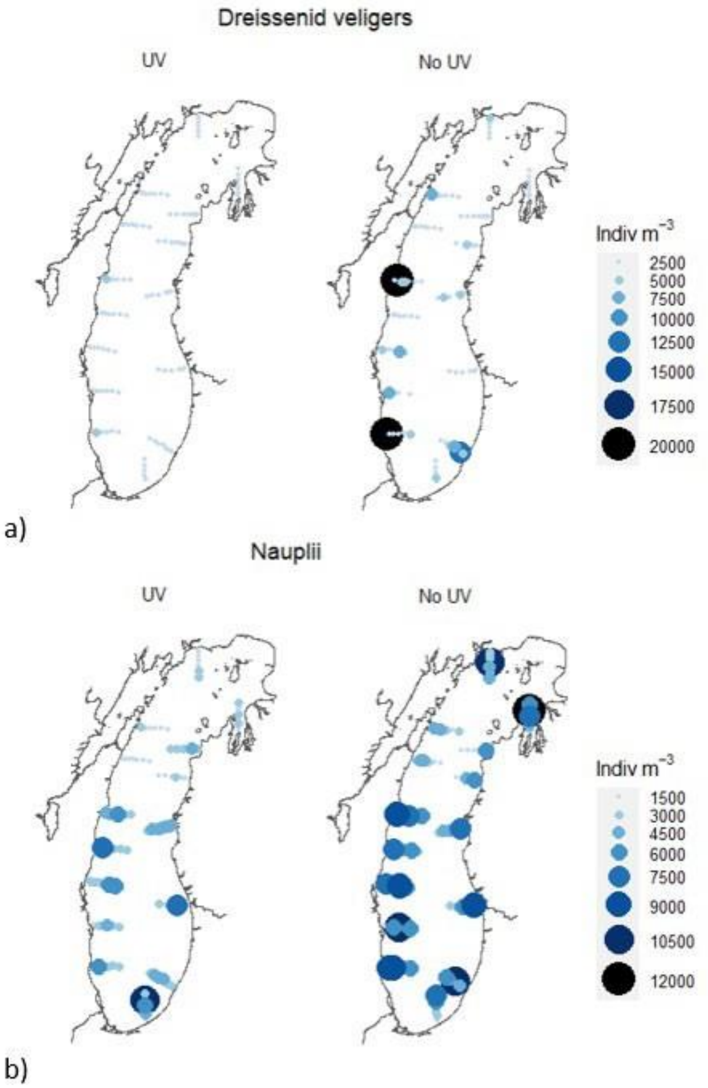

Figure 6: Densities of a) Dreissenid veligers and b) copepod nauplii in 1 % UV exposure (left) and No UV exposure (right).

Among the key taxonomic groups, including rotifers, adult calanoids, adult cyclopoids, and cladocerans, rotifers were most abundant (Fig. 7). Cyclopoid copepods and especially rotifers generally exhibited the highest densities at mid- or offshore sampling locations (Figs. 7a and 7d). In contrast, calanoid copepods and cladocerans generally exhibited a shift from high densities at inshore sampling locations to low densities at offshore sampling locations (Figs. 7b and 7c). Overall, zooplankton density was highest in the deep “No UV” layer, indicative of diel vertical migration. However, rotifers had the lowest densities within the deep “No UV” layer in northern Lake Michigan and the highest densities within the shallow “UV” layer southern Lake Michigan (although mean densities in the northern part were higher than mean densities in the southern part) within the “UV” layer.

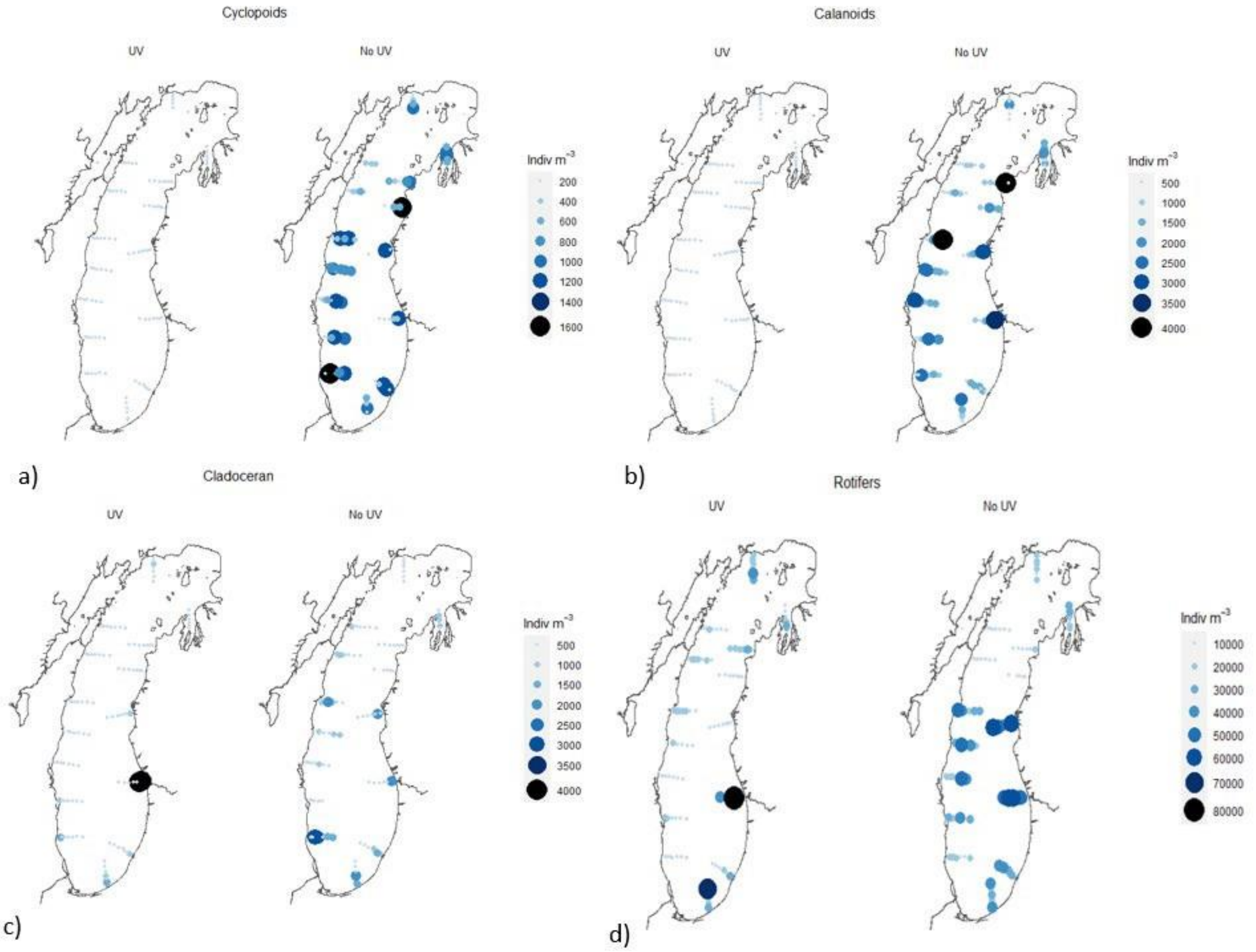

Figure 7. Densities in 1% UV exposure and No UV exposure of zooplankton taxonomic groups a) adult cyclopoid copepods, b) adult calanoid copepods, c) adult cladocerans, d) rotifers.

Subproject C: Glider Deployment

Overview

The objective was to deploy the glider as a 'virtual mooring' along a sampling transect (Rowley Bay), collecting data over longer time periods than typical ship-based sampling, to provide broader temporal context for data obtained by ship-based sampling.

Methods

A Teledyne Webb Research G2 Slocum Glider was deployed to compare data from a 24-hr mooring to comparable ship measurements at the same location. The glider was outfitted with a Seabird pumped CTD, Aanderaa dissolved oxygen optode, and WetLabs FLBBCDSLC Environmental Characterization Optics (ECO) optical sensor (McKinney et al., 2022). Fluorescence at excitation/emission wavelengths of 470/695 nm, and 370/460 nm is converted to chlorophyll a and colored dissolved organic matter (CDOM) concentration using factory calibration standards. Water depth is calculated while underway as the sum of altimeter and pressure readings.

The glider was deployed from July 12-23 in the northwestern part of the main lake basin at the Rowley Bay transect, which included sampling sites at 5, 8, 12, 17, 23, 30, and 38 km from shore (Fig. 8). The glider sampling plan was intended to remain at each of the transect sites for a 24-hour period, during which the glider would continuously maintain position as close as possible to the station. Science and engineering data were stored onboard the glider and downloaded after the mission was completed. Files in native binary format were converted to ascii using software supplied by the manufacturer for additional processing. Chlorophyll a concentration is calculated internally by the optical sensor based on detection of fluorescence; however, fluorescence is downregulated in cells exposed to daylight and thus we report chlorophyll concentration in the surface 0 m to 20 m depth from night-time sampling only. For the Rowley Bay transect the glider completed just over a thousand vertical profiles.

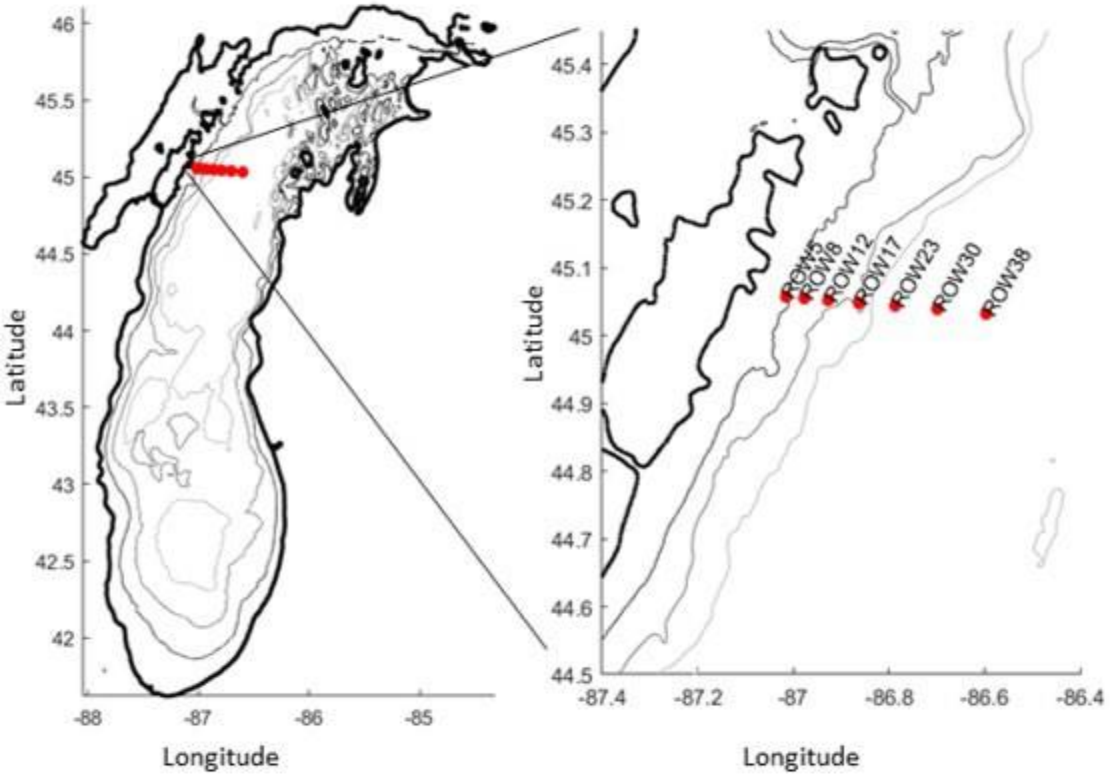

Figure 8. Location of the Rowley Bay transect (left) and location of transect stations (right). Station numbers indicate distance from shore. Contour lines are at 40m intervals (40, 80, and 120 m water depth).

Results and Discussion

Chlorophyll a concentration varied by depth in the water column, with the highest median values observed in the metalimnion (20 m to 50 m depth), ranging from 0.48 to 0.70 μg L^{-1} (Fig. 9). The lowest median concentrations were observed in the hypolimnion, <0.30 μg L^{-1}. The pattern of depth-specific variation changed with distance from shore, along the Rowley transect. The biggest difference between mid-depth median concentrations relative to either epilimnion or hypolimnion median concentrations occurred farther offshore, consistent with the increase in the deep maximum chlorophyll values observed from the shipboard CTD (Fig. 4a). Further, chlorophyll a concentration measured in the hypolimnion also increased with distance from shore.

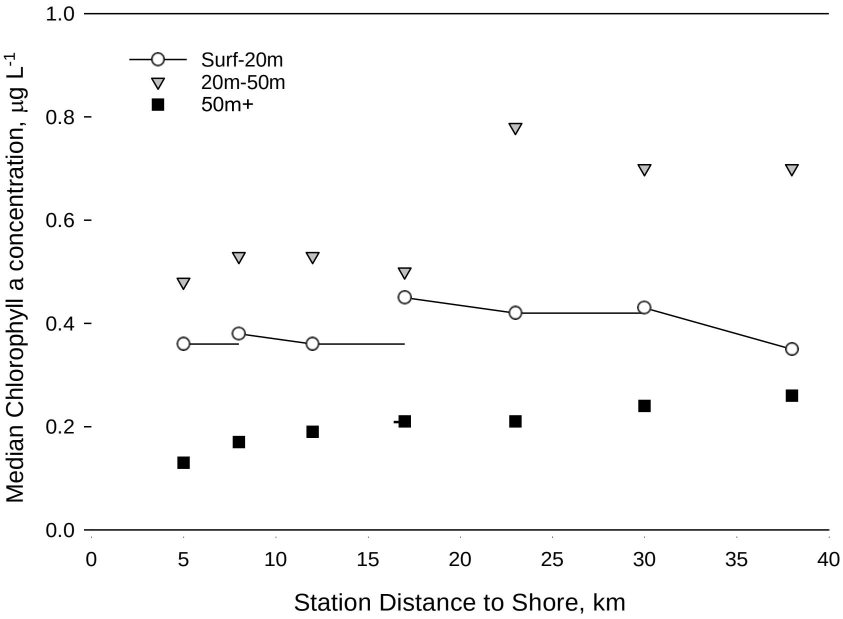

Figure 9. Chlorophyll concentration at depth range 0-20m (top), 20-50m (middle), and greater than 50m, by station distance to shore.

Overall, the maximum chlorophyll concentration observed, generally 1-2 μg L^{-1}, was similar to values measured both the CTD and based on extracted chlorophyll from water samples (Fig. 10). The width of the deep maximum chlorophyll layer was less at shallow, nearshore stations (ROW12, ROW8, ROW 4) compared to those offshore. The data visually suggest physical mixing in shallow (<80m) nearshore waters, disrupting the deep chlorophyll layer.

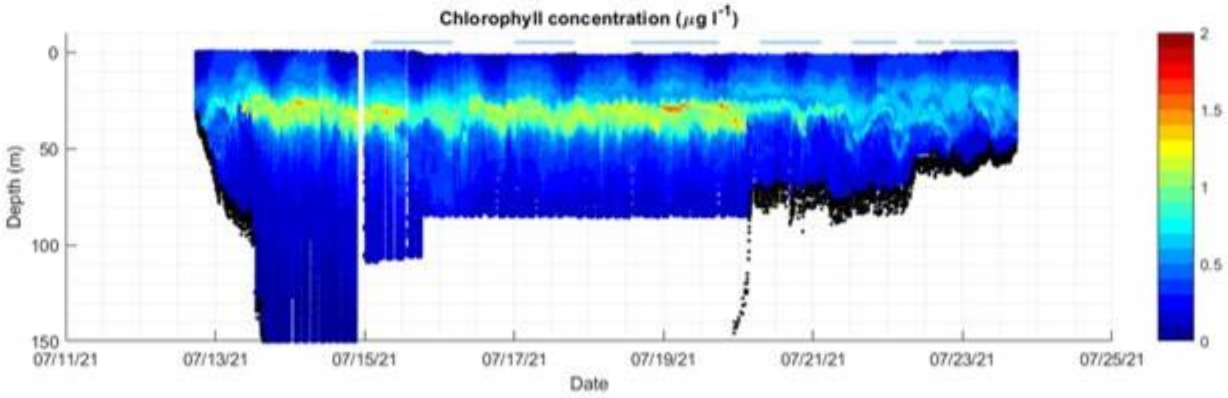

Figure 10. Chlorophyll concentration observed by the EPA glider during the Lake Michigan deployment July 2021. Light blue lines indicate time when glider was at Rowley Bay stations (from left, ROW38, ROW30, ROW23, ROW17, ROW12, ROW8, ROW5). The ROW5 line also includes time when glider was transitioning from ROW5 station north within 5km of shore to where it was recovered.

Summary

Our combined results highlight the need to integrate lower food web data with fishery data to evaluate how changing spatial patterns in primary production, long-term change in zooplankton community composition, and invasive species are altering trophic relationships and fish recruitment.

- *Priority #1*: Advance the understanding of nutrient dynamics that directly influence lower trophic level productivity and offshore fish production.
- *Summary:* In combination, measures of chlorophyll a suggest that primary production within the deep chlorophylla layer was greatest in the offshore regions of the lake. This observation differs markedly from reported spatial patterns in surface waters, in which there is a decline in chlorophyll a concentration from the nearshore to the offshore (Stadig et al., 2020). There was not strong evidence for a bottom-up control on algal biomass based on the nutrient data because we did not find a nearshore-offshore gradient in SRP or TP. It is possible that the observed chlorophyll gradient relates to nearshore physical mixing, which is consistent with the glider data, or possibly also higher grazing pressure in the nearshore.

- *Priority #3*: Investigate understudied but important components of the food web, including: fall/winter/early spring nearshore (including shallow shoreline areas) community structure, Dreissenid mussel veligers (including their nutrition as prey for larval fish), *Limnocalanus* copepods, *Mysis* crustaceans, the microbial loop (bacteria and microzooplankton), and round gobies (which are under-sampled by traditional gears).

- *Priority #6*: Continue nearshore and offshore monitoring of key food web species (e.g., phytoplankton, zooplankton, *Diporeia* amphipods, and Dreissenid mussels.
- *Summary*: We observed calanoid and rotifer densities as high or higher in offshore sampling locations, very high copepod nauplii densities throughout the lake, and cladoceran densities generally low and only in the nearshore, corroborating other data sets demonstrating a long-term conversion to a calanoid-dominated zooplankton community (Barbiero et al. 2019). Further, the zooplankton data reinforced the perspective that Lake Michigan has been greatly impacted by invasive species as Dreissenid veligers were found at the highest density of any planktonic animal except rotifers.

Acknowledgements

We thank the captains and crews of the EPA R/V *Lake Explorer II*, the EPA R/V *Lake Guardian*, and the USGS R/V *Sturgeon* for assistance in field sampling. The views expressed in this article are those of the author(s) and do not necessarily represent the views or the policies of the U.S. Environmental Protection Agency.

References

APHA (1998) Standard Methods for the Examination of Water and Wastewater. 20th Edition, American Public Health Association, American Water Works Association and Water Environmental Federation, Washington DC.

Barbiero, R.P., Rudstam, L. G., Watkins, J.M., Lesht, B.M. 2019. A cross-lake comparison of crustacean zooplankton communities in the Laurentian Great Lakes, 1997−2016. J. Great Lakes Res. 45:672−690.

Bunnell, D.B., Carrick, H.J., Madenjian, C.P., Rutherford, E.S., Vanderploeg, H.A., Barbiero, R.P., Hinchey-Malloy, E., Pothoven, S.A., Riseng, C.M., Claramunt, R.M., and eight others. 2018. Are changes in lower trophic levels limiting prey-fish biomass and production in Lake Michigan? Great Lakes Fishery Commission Miscellaneous Publication 2018-01, Ann Arbor, Michigan. 52pp.

Bunnell, D.B., R. Kraus, D. Hondorp, and Y. Kao. 2023. USGS activities in support of 2020-2021 Lake Michigan CSMI In P. Collingsworth and C. Foley (eds.), Cooperative Science and Monitoring Initiative (CSMI) Lake Michigan 2020-2021 Report, Illinois-Indiana Sea Grant.

Eppehimer, D.E., Bunnell, D.B., Armenio, P.M., Warner, D.M., Eaton, L.A., Wells, D.J., Rutherford, E.S. 2019. Densities, diets, and growth rates of larval Alewife and Bloater in a changing Lake Michigan ecosystem. Trans. Am. Fish. Soc. 148:755–770.

GLNPO (Great Lakes National Program Office) 2016. Standard operating procedure for zooplankton analysis. U. S. EPA Great Lakes National Program Office, Method LG403. Revision 07.

Hecky, R.E., Smith, R.E., Barton, D.R., Guildford, S.J., Taylor, W.D., Charlton, M.N., Howell, T. 2004. The nearshore phosphorus shunt: a consequence of ecosystem engineering by dreissenids in the Laurentian Great Lakes. Can. J. Fish. Aquat. Sci. 61:1285–1293.

Lepak, R.F., Hoffman, J.C., Janssen, S.E., Krabbenhoft, D.P., Ogorek, J.M., DeWild, J.F., Tate, M.T., Babiarz, C.L., Yin, R.; Murphy, E.W. 2019. Mercury source changes and food web shifts alter contamination signatures of predatory fish from Lake Michigan. Proc. Nat. Acad. Sci. 116:23600−23608.

Stadig, M.H., Collingsworth, P.D., Lesht, B.M., Höök, T.O. 2020. Spatially heterogeneous trends in nearshore and offshore chlorophyll a concentrations in lakes Michigan and Huron (1998–2013). Freshw. Biol. 65:366–378.

USEPA (United States Environmental Protection Agency). 2019. Science and Monitoring Priorities for the 2020 CSMI Field Year on Lake Michigan. U. S. EPA Great Lakes National Program Office, Memorandum.

Lake Michigan CSMI results for phytoplankton and primary production, 2021

Euan D. Reavie, Natural Resources Research Institute, University of Minnesota Duluth, Duluth, MN 55811; Office 218.788.2692 | Email ereavie@d.umn.edu

Most of this work was funded as part of the USEPA-GLNPO Great Lakes Biological Monitoring Program; Contact: **Annie Scofield**, USEPA Great Lakes National Program Office, Chicago, Illinois

CSMI phytoplankton sampling in Lake Michigan comprised integrated sampling of the homogeneous water column in shallow, nearshore and deepwater, offshore locations in spring (April) and summer (August) (Fig. 1). Discrete samples from the summer deep chlorophyll layer (DCL) were also collected. Greater details of sampling protocols are provided by Reavie et al. (2014). Nearshore samples collected as part of CSMI efforts represent collections at stations with water column depth shallower than 30 m.

2021 Results. Phytoplankton abundance was higher in summer when compared to spring (Fig. 2), a phenomenon that is typical of the Great Lakes with the exception of Lake Erie (Reavie et al. 2014). Nearshore and offshore waters differed negligibly in abundance and composition, an observation that varies from distinct nearshore-offshore differences that have been noted in the other lakes. In terms of cell density cyanophytes strongly dominate the community overall, though these phytoplankton comprise a very small portion of the total biovolume due to their small cell size.

Spring phytoplankton biovolume was dominated by flagellated chrysophytes and cryptophytes, as well as some centric diatoms. Lake Michigan's algal load was composed of several species with no single algal division comprising an overwhelming dominance. The most abundant taxa in spring were dinoflagellates (e.g. *Gymnodinium*), chrysophytes (largely undefined ovoids), haptophytes, cryptophytes (e.g., *Cryptomonas erosa*, *Rhodomonas minuta*, *Cryptomonas reflexa*, and *Rhodomonas lens*) and centric diatoms (largely cyclotelloids). Summer was dominated by dinoflagellates (e.g., *Gymnodinium*), cyanobacteria (e.g., *Oscillatoria limnetica* and *Aphanocapsa*), chrysophytes (largely undefined ovoids), haptophytes, cryptophytes (e.g., *Cryptomonas erosa*, *Rhodomonas minuta*, *Cryptomonas reflexa*, and *Rhodomonas lens*) and centric diatoms (largely cyclotelloids).

Though not specifically focused on CSMI efforts, long-term monitoring from 2001 through 2021 in the pelagic waters (Reavie et al. 2014, plus more recent data presented in Fig. 3) indicate that spring phytoplankton abundance has stabilized at a relatively low level after dropping rapidly in the early 2000s following the quagga mussel invasion. Though a significant increase in abundance has been detected in summer, this change is subtle and subject to year-to-year variability. We note what appears to be an increase in spring relative abundance of flagellates such as cryptophytes in spring, which may also be related to the mussel population expansion, but this phenomenon is under investigation.

Paleolimnological records from deepwater cores (Reavie et al. 2021) further enhance the phytoplankton and primary productivity record for Lake Michigan. The paleolimnology of the northern and southern regions of Lake Michigan had many similarities in their historical geochemistry, but the timing of events varied for north and south regions (Fig. 4). Sediment accumulation rate increased from baseline levels from ~1850 through to ~1890. After ~1890 the relative proportion of sediment organics and TOC began to increase, as did %TON, $\delta^{15}N$, $\delta^{13}C_{org}$ and C:N, all indicating increasing productivity and organic inputs from catchment sources. However, accumulation rates of inorganic materials decreased during this time while the organic proportion increased, so a decline in inorganic dilution cannot be ruled out as a driver of these changes. Trends in chlorophyll *a* declined from a baseline concentration of ~4 to ~1.5 µg g^{-1}. The change in C:N suggests rising terrestrial sources, though the ratio remained below 10, indicating phytoplankton as the main source of sedimentary carbon. This most recent decades in the northern region demonstrates a revived increase in sediment accumulation. Inorganic materials continued to decline in favor of organic materials. %TOC, %TON, $\delta^{15}N$ and $\delta^{13}C_{org}$ continued to increase from the previous period. C:N decreased during this period from 8.6 to 7.2, and chlorophyll a was higher for most of the period. This period more consistently indicates an increase in lake productivity with the exception of the most recent ~20 years, when chlorophyll *a* was suddenly much lower, with the trend indicating oligotrophication well below anything previously observed in the record and corresponding to the period of the quagga mussel invasion (Vanderploeg et al. 2010).

In the south over the course of the 19th century, carbonate accumulation declined in favor of a relative increase in inorganic materials. $\delta^{13}C_{org}$ increased while %TOC and C:N decreased. Very high sediment accumulation began around 1910, especially around 1930, when the proportion of inorganic materials peaked in opposition to carbonate and organic materials. The more northerly and shallower of these two cores (mid-south) had approximately fivefold higher accumulations. %TON, $\delta^{15}N$, $\delta^{13}C_{org}$ and C:N had unremarkable changes, though %TON and C:N exhibited a brief drop during the short period of high sediment accumulation around the 1930s. This period started with undetectable concentrations of chlorophyll *a*, but it exhibited a distinct rise during the 1930s, after which it declined again to undetectable levels. In the most recent decades proportions indicate a 10–20 % drop in inorganics in favor of organic materials and carbonates. %TOC, %TON, $\delta^{15}N$, $\delta^{13}C_{org}$ and trends in chlorophyll *a* all increased during this period, indicating a gradual increase in productivity and probably more carbon from catchments since the mid-20th century. C:N declined to its lowest levels at the top of each core, indicating a consistent dominance and relative increase of autochthonous carbon sources.

Overall, Lake Michigan's paleorecords had consistently increasing values of $\delta^{13}C_{org}$ and $\delta^{15}N$, suggesting increasing productivity through most of the 20th century that corresponded with higher %TOC and %TON. Based on sediment accumulation rates and proportion of inorganic matter, Lake Michigan underwent substantial inputs of allochthonous sediment around the turn of the 20th century following periods of catchment development that varied temporally depending on location. In the southern basin this accumulation was especially high, possibly a short-term slug of erosional sediment related to a massive storm event, such as the "Great Lakes Storm of 1913" (Murty and Polavarapu 1975). Differences in paleorecords between the northern and southern basins are likely driven by gyral separation (Kerfoot et al. 2008) that makes for a strong north-south gradient in physical, chemical and biological conditions (Cai and Reavie 2018).

How do these findings respond to CSMI Research Priorities? The following priority questions (numbered according to Foley et al. 2021) are supported by the data presented herein.

1. Advance the understanding of nutrient dynamics (i.e. loading, transport, and cycling, spatial and temporal variability, and gradients) that directly influence lower trophic level productivity and offshore fish production.

Nutrients determine phytoplankton abundance, and the long-term phytoplankton record in Lake Michigan is strongly determined by nutrient dynamics driven by the effects of pollution and mussel-induced oligotrophication. Multiple stoichiometric considerations are important, such as nitrogen and silica limitation.

2. Identify and quantify the role of biological 'hot spots' (e.g., Green Bay, major tributaries/nearshore areas, reefs, and upwelling events) and substrate heterogeneity in supporting Lake Michigan productivity. Seek opportunities to leverage existing work in these areas, including the large array of acoustic receivers in Green Bay.

While current phytoplankton data do not address hotspots, future work is scoped to reconstruct the long-term primary producer record of these nearshore areas, including Green Bay.

3. Investigate understudied but potentially important components of the food web, including: fall/winter/early spring and nearshore (including shallow shoreline areas) community structure, dreissenid veligers (including their nutrition as a prey for larval fish), Limnocalanus copepods, Mysis, the microbial loop (bacteria and microzooplankton), and round gobies (which are undersampled by traditional gears).

New, understudied components have been added to the primary producer biological monitoring program, including assessments of picoplankton abundance and sampling outside the usual spring and summer cruise windows, including new winter sampling efforts in eastern Lake Michigan.

5. Further understanding of the current and future impacts of terrestrial and aquatic invasive species upon the health of the Lake Michigan ecosystem.

Strong responses by the phytoplankton to the quagga mussel invasion are evident.

6. Continue nearshore to offshore monitoring of key food web components (e.g., phytoplankton, zooplankton, Diporeia and dreissenid mussels).

Nearshore-offshore monitoring of the phytoplankton is expected to be a permanent component of the Great Lakes Biological Monitoring Program. Combined with paleolimnological efforts we will continue to track the strong effect of the mussel invasion on primary producers.

13. Quantify the effects of land cover/land use changes on terrestrial and aquatic cycling of nutrients, carbon, and mercury.

The paleorecord of primary producers clearly describes the upland anthropogenic impacts on lake nutrients and sediments, especially during historical periods of urban development.

References

Cai M, Reavie ED (2018) Pelagic zonation of water quality and phytoplankton in the Great Lakes. Limnology 19: 127-140

Foley C, TePas K, Collingsworth P (2021) Cooperative Science and Monitoring Initiative Lake Michigan Sampling Prospectus.

Kerfoot WC, Budd JW, Green SA, Cotner JB, Biddanda BA, Schwab DJ, Vanderploeg HA (2008) Doughnut in the desert: Late-winter production pulse in southern Lake Michigan. Limnol Oceanogr 53: 589-604

Meyers PA (1994) Preservation of elemental and isotopic source identification of sedimentary organic matter. Chem Geol 114: 289–302

Murty TS, Polavarapu RJ (1975) Reconstruction of some of the early storm surges on the Great Lakes. J Gt Lakes Res 1: 116-129

Reavie ED, Barbiero RP, Allinger LE, Warren GJ (2014) Phytoplankton trends in the Great Lakes: 2001-2011. J Gt Lakes Res 40: 618-639

Reavie ED, Cai M, Werne JP, Meyer-Jacob C, Smol JP (2021) Long-term productivity trends in the Laurentian Great Lakes: a comparison of geochemical methods. J Paleolimnol 65: 299-314

Sgro GV, Reavie ED (2018a) Lake Erie's ecological history reconstructed from the sedimentary record. J Gt Lakes Res 44: 54-69

Sgro GV, Reavie ED (2018b) Fossil diatoms, geochemistry, and the Anthropocene paleolimnology of Lake Huron. J Gt Lakes Res 44: 765-778

Stoermer EF, Emmert G, Julius ML, Schelske CL (1996) Paleolimnologic evidence of rapid recent change in Lake Erie's trophic status. Can J Fish Aquat Sci 53: 1451-1458

Vanderploeg HA, Liebig JR, Nalepa TF, Fahnenstiel GL, Pothoven SA (2010) *Dreissena* and the disappearance of the spring phytoplankton bloom in Lake Michigan. J Gt Lakes Res 36: 50-59

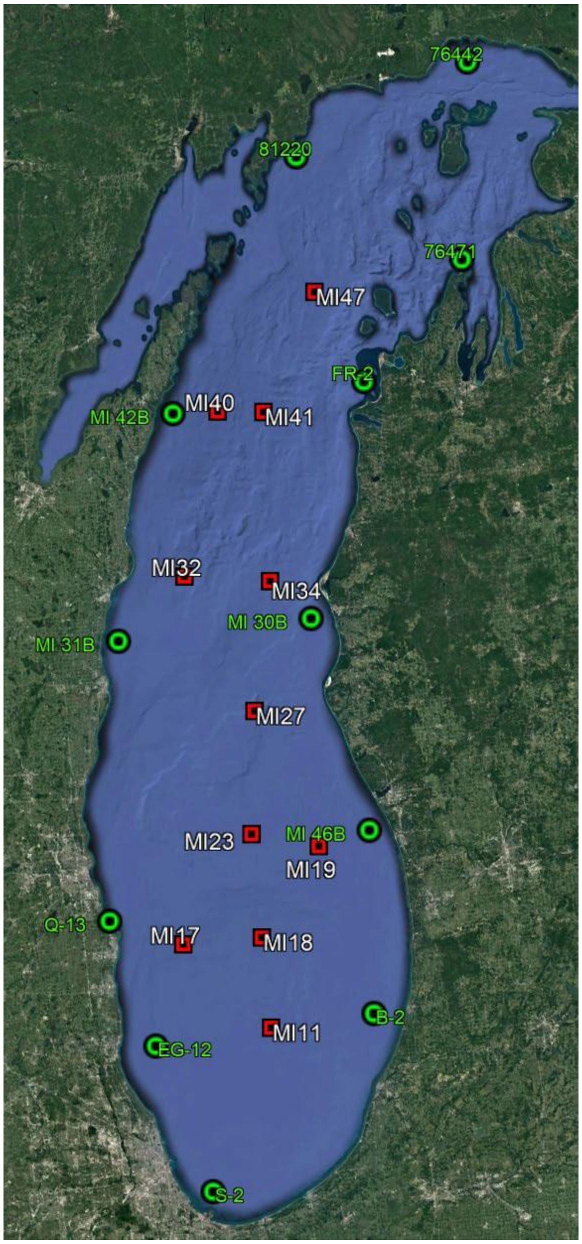

Figure 1. Map of Lake Michigan showing the standard set of pelagic (offshore) sampling locations (red squares, sampled twice a year) and nearshore CSMI stations (green circles, sampled twice a year during CSMI years).

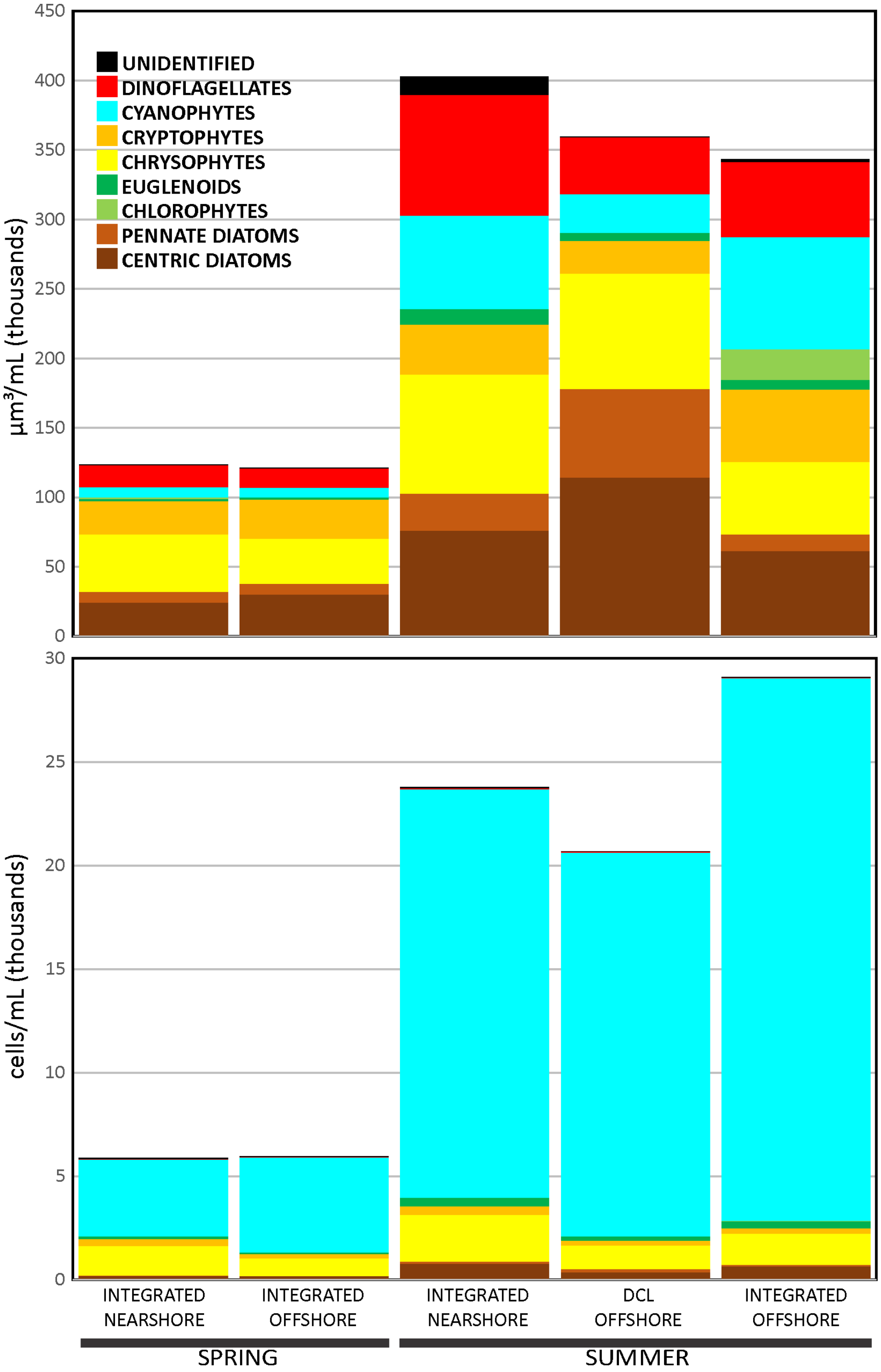

Figure 2. Basin-wide sample averages of phytoplankton abundance in Lake Michigan in 2021. Abundance data are summarized for spring and summer for algal biovolume (top) and density (bottom). Nearshore and offshore data are presented separately as stacked histograms of broad algal groups. Integrated samples represent combined samples from throughout the homogeneous upper water column (spring = whole water column; summer = epilimnion) and deep chlorophyll level (DCL) samples represent discrete samples collected from the summer chlorophyll maxima.

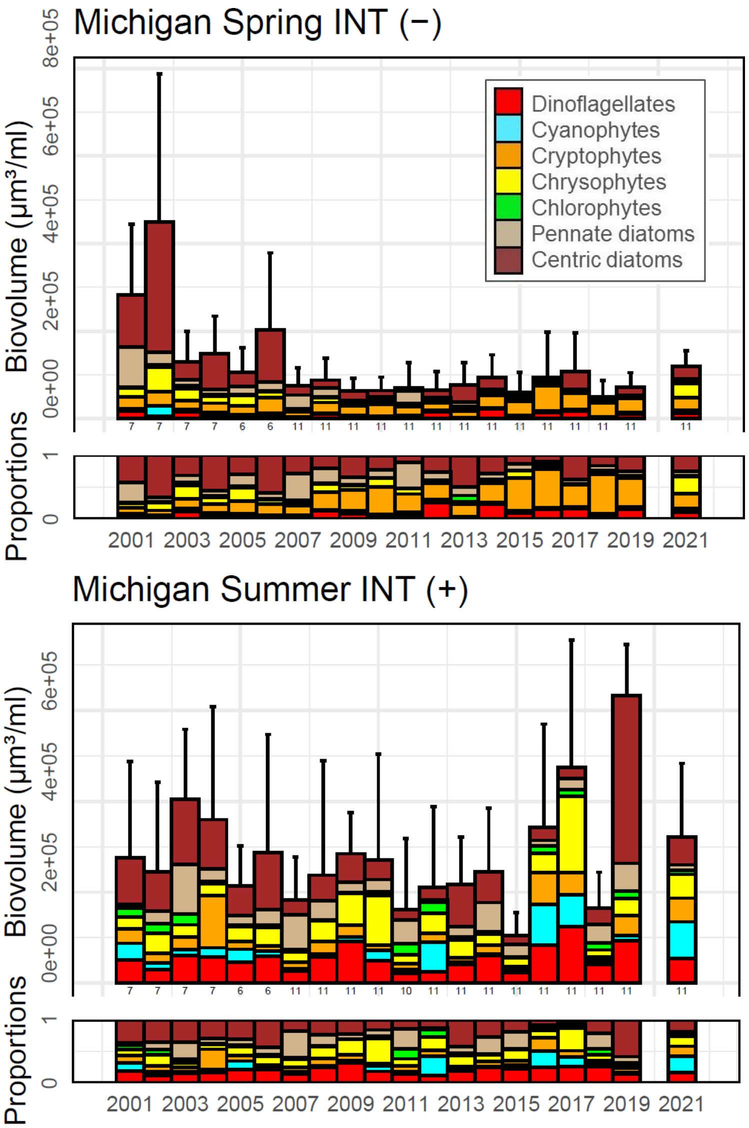

Figure 3. Basin-wide averages of offshore phytoplankton abundance in integrated (INT) isothermal layer samples from Lake Michigan. Abundance data are summarized for spring and summer, from 2001 to 2021 (as of writing 2021 data are not yet verified). Numbers at the bottom of each biovolume bar indicate the number of samples averaged, and below that the relative abundances are shown as proportions. Error bars represent a standard error of the sample totals. A significant overall trend for the period based on a Kendall's rank correlation test ($P < 0.05$) is presented as a (+) or (-) at the top of each figure panel in the respective heading.

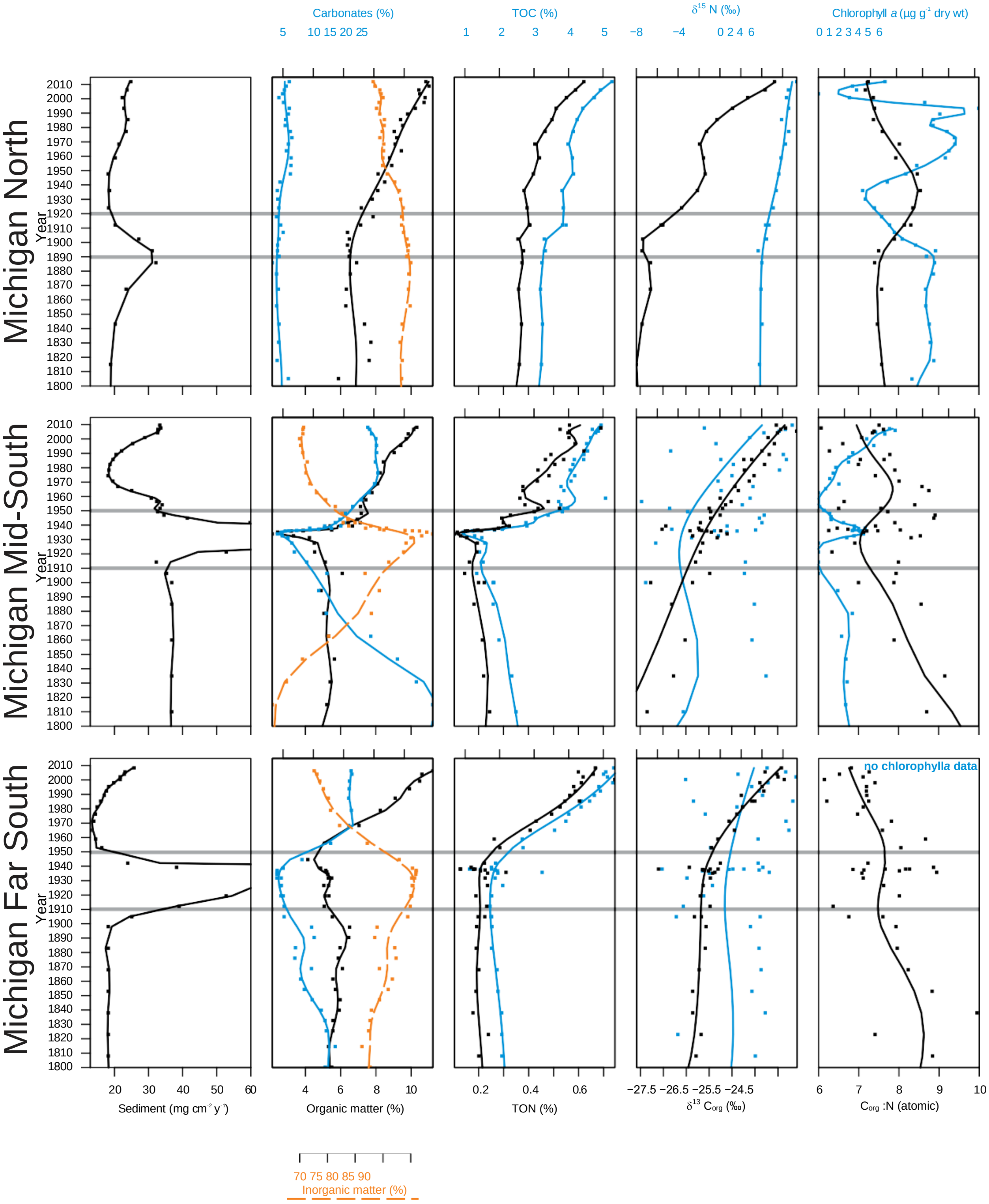

Figure 4. Temporal variation in geochemical proxies within sediment cores from Lake Erie. All profiles are presented as generalized additive models (lines) and original data (dots). Line colors in each plot are identified by the corresponding color of the x-axis label. Horizontal lines denote transitions between temporal zones as described in Reavie et al. (2021).

http://greatlakescenter.buffalostate.edu/

LAKE MICHIGAN BENTHOS SURVEY COOPERATIVE SCIENCE AND MONITORING INITIATIVE 2021

Technical Report

Principal Investigators: Lyubov E. Burlakova
Alexander Y. Karatayev

Great Lakes Center
SUNY Buffalo State University
1300 Elmwood Ave, Buffalo, New York USA 14222

January 2023

Suggested citation for the report:

Burlakova, L. E. and Karatayev, A.Y. 2023. Lake Michigan Benthos Survey Cooperative Science and Monitoring Initiative 2021. Technical Report. USEPA-GLRI GL00E02254. Great Lakes Center, SUNY Buffalo State University, Buffalo, NY. Available at: http://greatlakescenter.buffalostate.edu/sites/greatlakescenter.buffalostate.edu/files/uploads/Documents/Publications/LakeMichiganBenthosSurveyCSMI2021FinalReport.pdf

TECHNICAL REPORT: LAKE MICHIGAN BENTHOS SURVEY
COOPERATIVE SCIENCE AND MONITORING INITIATIVE 2021

Lake and Year: Lake Michigan, 2021
Lead Organization: SUNY Buffalo State University

Authors of This Report:
Lyubov E. Burlakova, Great Lakes Center, SUNY Buffalo State University
Alexander Y. Karatayev, Great Lakes Center, SUNY Buffalo State University

Contacts for Questions About This Report:
Lyubov E. Burlakova, burlakle@buffalostate.edu, 716-878-4504
Alexander Y. Karatayev, karataay@buffalostate.edu, 716-878-5423

Project Overview

In this report, we present results of a benthic survey of Lake Michigan conducted as part of the United States Environmental Protection Agency (U.S. EPA) Great Lakes National Program Office (GLNPO) Great Lakes Biology Monitoring Program (GLBMP). Consistent with the sampling scheme of previous CSMI benthic surveys, a lake-wide survey was conducted in 2021 at 95 stations in Lake Michigan to assess the status of the benthic macroinvertebrate community and at an additional 19 stations sampled exclusively for *Dreissena* and Amphipoda. The project was organized around the Lake Michigan 2021 science priorities to continue nearshore to offshore monitoring of key food web components (e.g., phytoplankton, zooplankton, *Diporeia* and dreissenid mussels) that will further our understanding of the current and future impacts of aquatic invasive species upon the health of the Lake Michigan ecosystem. The primary focus of this survey was the status of benthic community, including the invasive quagga mussels (*D. rostriformis bugensis*) in comparison with historic data. In addition, we compared the results of rapid video assessment of dreissenid populations with data obtained from traditional Ponar grabs to assess the advantages and disadvantages of both methods.

Study Highlights

- 106 species and higher taxa of benthic macroinvertebrates were found in Lake Michigan in 2021. The most diverse and most widely occurred taxa throughout the lake were Oligochaeta, representing 20% of lake-wide density and 0.2% of biomass.
- *Diporeia* was found at only 10 stations (9% of total) at low densities and continues to decline even in the deepest parts of the lake. Similar continuous decline was found in densities of sphaeriids. In contrast, Oligochaeta abundance progressively increased in shallow and intermediate-depth intervals in the last decade.
- Exotic mollusc New Zealand mud snail *Potamopyrgus antipodarum,* first recorded in the lake in 2006, increased in abundance and distribution in the last 5 years. In 2021 species lake-wide density

increased 25-fold compared to 2015, comprising 93% of total lake-wide gastropod density and 79% of biomass, and its occurrence increased 3-fold.

- Exotic bivalve *Dreissena r. bugensis* was found at 98% of all stations and comprised 75% of lake-wide benthos density and 99.7% of biomass. Lake-wide quagga mussel population in 2021 exceeded 2015 density by 30% largely due to a 3-fold increase in density in the shallowest depth zone caused by recently settled mussels. A significant increase in both quagga mussel density and biomass was found only in the deepest zone (>90 m). Overall, the last 10 years lake-wide population density of quagga mussels somewhat stabilized, although there is an ongoing change in the spatial distribution with the bulk of mussel populations expanding to deep depths.
- Lake-wide *Dreissena* occurrence obtained using Benthic Imaging System (BIS) was only slightly lower than occurrence obtained using Ponar grab (94% vs. 98%). The difference between lake-wide average densities estimated using videography and Ponar for mussels >5 mm was within 10% supports our assessment that underwater videography could be a very useful tool in *Dreissena* rapid population assessment.

CONTENTS

Project Overview……178

Study Highlights……178

CHAPTER 1. MAJOR FINDINGS FROM THE CSMI BENTHIC MACROINVERTEBRATE SURVEY IN LAKE MICHIGAN IN 2021 WITH AN EMPHASIS ON LONG-TERM TRENDS IN BENTHIC COMMUNITY……181

Overview……181

Methods……181

Sampling protocol……181
Laboratory Procedures……183
Historic data……183
Data analysis……183

Results and Discussion……184

Status of Lake Michigan benthic community in 2021……184
Long-term trends in benthos……187
Dreissena spatial and temporal trends .... **Error! Bookmark not defined.**
Literature Cited……193

CHAPTER 2. RAPID ASSESSMENT OF *DREISSENA* POPULATIONS IN LAKE MICHIGAN USING UNDERWATER VIDEOGRAPHY……196

Overview……196

Methods……196

Results and discussion……197

Acknowledgements……200

Literature Cited……200

Appendix. List of sampling stations……202

CHAPTER 1. MAJOR FINDINGS FROM THE CSMI BENTHIC MACROINVERTEBRATE SURVEY IN LAKE MICHIGAN IN 2021 WITH AN EMPHASIS ON LONG-TERM TRENDS IN BENTHIC COMMUNITY

Overview

A lake-wide benthic survey of Lake Michigan was conducted in 2021 as part of the U.S. EPA Great Lakes National Program Office (GLNPO) Great Lakes Biology Monitoring Program (GLBMP). Consistent with the sampling scheme of previous CSMI benthic surveys, benthic samples were collected at 95 stations to assess the status of the benthic macroinvertebrate community, and at an additional 19 stations sampled exclusively for invasive mussel *Dreissena* and deep-water amphipod *Diporeia* to follow long-term trends in their distribution.

Lake Michigan has one of the longest time series (spanning almost a century) of benthic surveys in the Laurentian Great Lakes (Mehler et al., 2020). One of the first larger scale benthic studies conducted in 1893 in the Traverse Bay region found that the benthic community was dominated by *Pontoporeia hoyi* (currently *Diporeia*) (Ward, 1896). *Diporeia* remained the dominant species in 1931 and 1932 (Eggleton, 1937) and together with Oligochaeta and Sphaeriidae they comprised about 94% of benthic species abundance in Lake Michigan. In 1964-67, Alley and Mozley (1975) found a similar pattern in the benthic community, but densities of *Diporeia*, Oligochaeta, and Sphaeriidae in the 1960s were 1.5, 2.6, and 4.3 times higher compared to those of 1931, likely due the significant increase in plankton standing crop between the late 1920s and late 1950s (Damann, 1960). Continued increases in the abundances of *Diporeia*, Oligochaeta, and Sphaeriidae in nearshore waters in the 1970s and early 1980s were attributed to increasing nutrient loads and greater lake productivity (Madenjian et al., 2002; Nalepa, 1987). During the 1980s and early 1990s, since the implementation of the Great Lakes Water Quality Agreement, primary production in the nearshore waters declined (Johengen et al., 1994, Madenjian et al., 2002), likely causing a decline in abundances of *Diporeia*, Oligochaeta, and Sphaeriidae (Madenjian et al., 2002; Nalepa et al., 1998). The introduction of *D. polymorpha* (in 1989, Griffiths et al., 1991) and *D. r. bugensis* (1997, Nalepa et al., 2001) and expansion of *D. r. bugensis* to deeper depths in the 2000s were associated with a further decline in primary production (Madenjian et al., 2015) and a general shift in production from the pelagic to the benthic zone (Cuhel & Aguilar 2013), followed by the drastic lake-wide decline of *Diporeia* (Nalepa et al., 2009).

The objective of this study was to describe the status of Lake Michigan benthic community, including the invasive zebra mussels (*Dreissena polymorpha*) and quagga mussels (*D. rostriformis bugensis*) in comparison with historic data. This report contains detailed descriptions of benthic communities in Lake Michigan in 2021, including information on sampling design (station locations, sampling and laboratory procedures), the taxonomy and abundance of benthic invertebrates, and long-term changes in major taxonomic groups since the 1930s. Detailed analysis of results obtained within this study are being prepared for peer-reviewed publications.

Methods

Sampling protocol

Samples for benthic macroinvertebrates were collected in triplicate from 99 CSMI stations located throughout Lake Michigan in July 13-22, 2021 (Fig. 1.1, Appendix), including historically sampled sites. Of these 297 samples, 240 (from 80 stations) were processed for all benthos, and only *Dreissena* and Amphipoda were identified from the remaining 57 samples collected at 19 stations. This report also includes benthos data from 15 long-term monitoring stations collected in September 2021 (not shown on the map). All stations were sampled aboard the U.S. EPA R/V *Lake Guardian* using a regular Ponar grab (sampling area 0.0523 m^2, coefficient used to calculate density per m^2 = 19.12). Together with the long-term monitoring stations, a total of 285 samples from 95 stations were analyzed for benthos, and 342 samples collected at 114 stations were used for *Dreissena* and *Diporeia* population assessment.

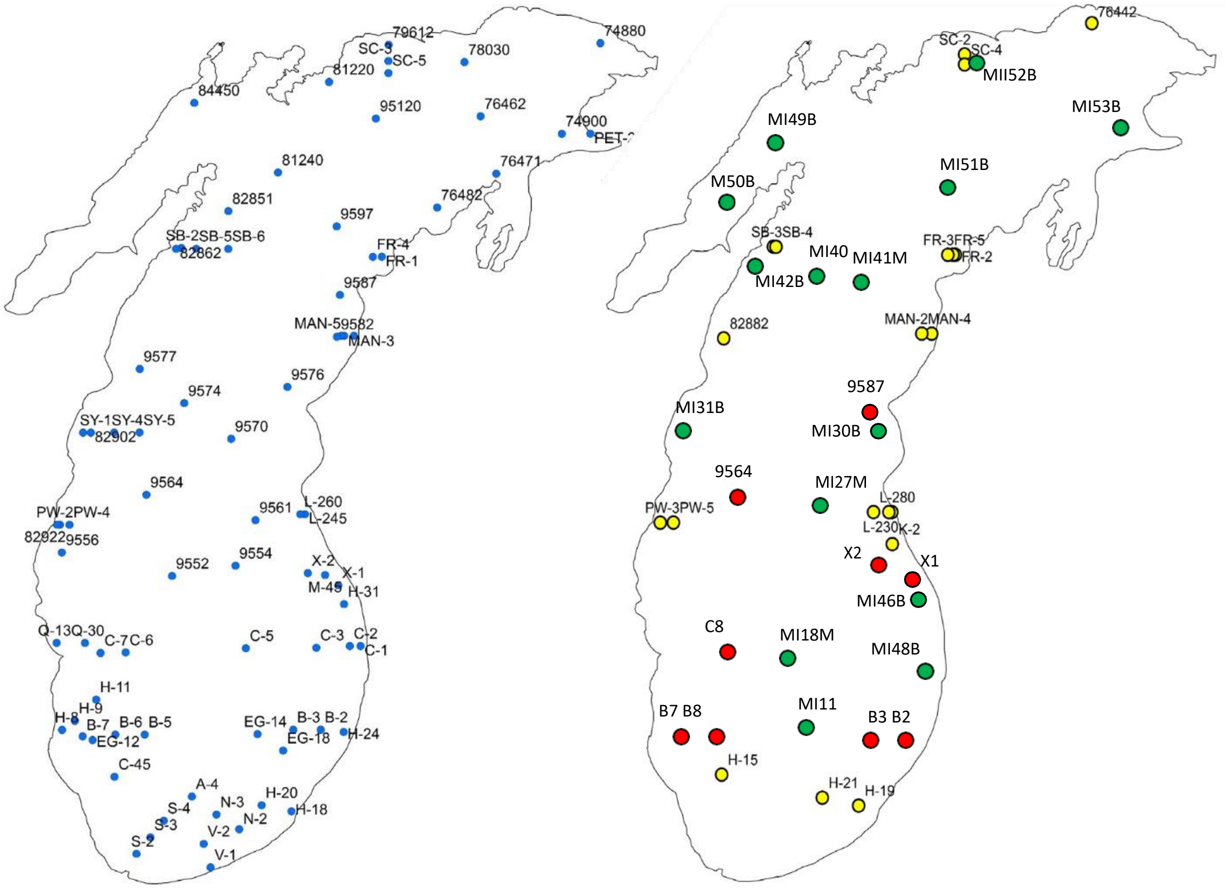

Figure 1.1. Location of benthic stations surveyed in Lake Michigan in 2021. The left map indicates the locations of 80 CSMI benthic stations (blue). The right map indicates the 19 CSMI stations (in yellow) that are *Dreissena* and Amphipoda-only stations, 15 long-term monitoring benthic stations (in green), and 8 historic stations (in red) sampled in 1931/32 (Eggleton, 1937), 1964-1967 (Alley & Mozley, 1975), 1980, 2000, 2005, 2010 (Nalepa et al., 2014), and 2015 (Cooperative Science and Monitoring Initiative 2015, Karatayev & Burlakova, 2017; Nalepa et al., 2017; Mehler et al., 2020).

Upon collection, each sample was placed separately into an elutriation device and then washed through a 500-µm mesh screen. All retained organisms and sediments were placed into a collection jar and preserved with neutral buffered formalin with Rose Bengal stain to a final concentration of 5 – 10%. Detailed methods are described in the EPA GLNPO Standard Operating Procedure for Benthic Invertebrate Field Sampling (US EPA, 2021: SOP LG406, Revision 14, January 2021).

Laboratory Procedures

All organisms found in each replicate sample collected at the 95 benthos stations were sorted, identified, counted, and weighed (total wet weight). Organisms were separated under low magnification using a dissecting microscope. Oligochaetes and chironomids were mounted on slides and identified using a compound microscope; other organisms were identified using a dissecting microscope. Adult oligochaetes and Naididae were identified to species; immature Tubificidae, Lumbriculidae, and Enchytraeidae were identified to the lowest taxonomic level possible, usually family, and included in density and biomass estimates. Counts of oligochaete fragments were excluded from density analyses but fragment weight was considered in the determination of biomass. Immature Oligochaeta (in cocoons) were recorded but excluded both from density and biomass calculations for comparison with historic data. Chironomids were identified to the lowest practical taxonomic level, usually genus. Other invertebrates were identified to species, when possible.

Dreissena from all samples were identified to species, measured to the nearest millimeter with a caliper, counted, and the whole sample was weighed to the nearest 0.0001 g after being blotted dry on absorbent paper (total wet weight of tissue and shell, TWW); details are described in the EPA GLNPO Standard Operating Procedure for Benthic Invertebrate Laboratory Analysis (US EPA, 2015: SOP LG407, Revision 09, April 2015). All *Dreissena* collected during this survey were quagga mussels (*D. rostriformis bugensis*).

Historic data

Historic data sets, spanning between 1931/32 and 2015 (Eggleton, 1937; Alley & Mozley, 1975; Nalepa et al., 2014; Karatayev & Burlakova, 2017; Nalepa et al., 2017; Mehler et al., 2020) were used to examine long-term changes in major benthic taxonomic groups in Lake Michigan (details in Mehler et al., 2020). The long-term data included only stations from the main basin (e.g., excluding Green Bay, Thunder Bay, and Muskegon Bay), and used ash free dry tissue weight (AFDTW) of *Dreissena*.

Data analysis

To test for differences in benthic community composition between time periods and between depth zones, Analysis of Similarity (ANOSIM) was used in Primer 7 (Plymouth Routines in Multivariate Ecological Research, Version 7.0.13, Primer E- Ltd. 2006) performed on Bray-Curtis similarity matrix calculated on fourth-root transformed benthic densities. Differences in benthic community composition between lake regions and depth zones were considered significant when $P < 0.05$, and the test statistic R was used as an index of the degree of separation between groups. Similarity Percentage (SIMPER) analysis was used to determine the contribution of species to similarity among depth zones. We used shade ("heat map") plots presenting the species clustered against sampled stations to provide a visual representation of the data matrix. The species Y axis is re-ordered in line with a cluster analysis of the species, using Whittaker's Index of Association to give among-species similarities, and the second X-axis re-orders samples in line with a cluster analysis of the samples. Only the 30 most abundant species were used in the analysis, as inclusion of rare species cannot produce sensible assessments of similarity with other species due to their random nature of occurrences.

Results and Discussion

Status of Lake Michigan benthic community in 2021

We found 106 species and higher taxa of benthic macroinvertebrates in Lake Michigan in 2021, in addition to unidentified immature tubificids and Chironomidae. The most diverse were Oligochaeta (44 species and higher taxa), Insecta (Chironomidae, 33), Mollusca (13 species, 10 Gastropoda and 3 Bivalvia); and Malacostraca (5 species: 4 Amphipoda and 1 Mysida). Other classes were represented by less than 3 taxa, or were not identified to species level (e.g., Trichoptera, Hydrozoa, Nemertea). Among Oligochaeta, the most diverse were Tubificidae (23 species and higher taxa), and Naididae (19).

The most widely occurred taxa throughout the lake were Oligochaeta found at all 95 stations (Lumbriculidae: 88%, Tubificidae: 70%, Enchytraeidae: 50%, and tubificid *Limnodrilus hoffmeisteri*: 46%), followed by chironomids (78%, *Heterotrissocladius subpilosus* group and *Micropsectra* sp.: 43% each, *Paracladopelma winnelli*: 27%). Exotic bivalve *Dreissena r. bugensis* was found at 98% of all 114 stations sampled for benthos and *Dreissena*.

Another exotic mollusc, gastropod *Potamopyrgus antipodarum,* was first recorded in the lake in 2006 (Benson et al., 2022) and during 2015 CSMI survey was found at 9 stations (7% of total) at average lake-wide densities 3.1m^{-2} and biomass 0.03 gm^{-2}. In 2021 *P. antipodarum* was found at average densities of 78 m^{-2} and biomass 0.31 gm^{-2} at 21% of stations, comprising 93% of total lake-wide gastropod density and 79% of biomass. *Diporeia* was found at low abundance (average density 12.4 m^{-2}, average biomass 0.013 gm^{-2}) only at 10 of all 114 benthic and "*Dreissena* and Amphipoda" stations combined. *Mysis* was recorded at low density at 36% (34) of all stations (Table 1.1).

Dreissena r. bugensis comprised a large percentage of lake-wide benthos density (75%), followed by Oligochaeta (20%), Chironomidae (3%) and non-dreissenid Mollusca (1.2%). Contribution of other groups (Amphipoda, Hirudinea, Trichoptera, Platyhelminthes, etc.) to total benthos density was less than 1% each. Among Oligochaeta, the most numerous were Tubificidae (65%) and Lumbriculidae (28%).

Dreissena r. bugensis dominated lake-wide benthos by biomass (99.7% of total wet biomass, Table 1.1). The remaining benthic biomass was represented by Oligochaeta (0.21%, dominated by Lumbriculidae (50%) and Tubificidae (23%)), Mollusca (other than *Dreissena*, 0.04%; mainly *P. antipodarum,* 0.03%), and Chironomidae (0.01%) (Table 1.1).

Benthic communities were not different between central and northern (R = 0.03, P = 0.10), central and southern (R = 0.01, P = 0.24), and northern and southern regions (R = 0.10, P = 0.015) (Fig. 1.2A). Only communities in Green Bay were significantly different from all other regions (P < 0.02, pairwise tests after 1-way ANOSIM), likely due to their location in shallow depths: benthic communities were significantly different among depth zones (R = 0.57, P = 0.01, 1-way ANOSIM, Fig. 1.2B), and the largest differences were found between 0-30 and >50 m (R > 0.60, P < 0.01).

Dreissena r. bugensis, Lumbriculidae (both immature and mature *Stylodrilus heringianus*) and Chironomidae *Heterotrissocladius subpilosus* group were the most contributing species (>87% combined) to similarity of communities at depths >50 m (SIMPER, Fig, 1.3, note the cluster of species in Fig. 1.4).

Shallow benthic communities (<30 m) were more diverse but still characterized mainly by *D. r. bugensis* and tubificids.

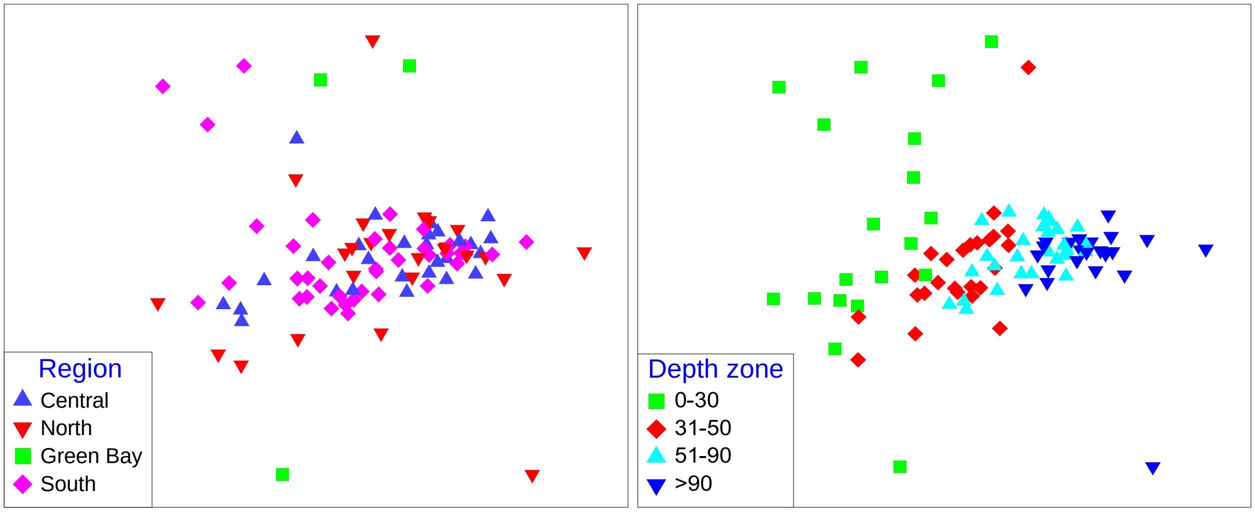

Figure 1.2**.** Non-parametric multidimentional (NMDS) ordination plots of Lake Michigan benthic community structure in 2021 (Stress = 0.16). Density (ind./m^2) of benthic taxa collected at all permanent sites were fourth-root transformed and converted to similarity matrix using Bray-Curtis similarity index. Stations are indicated by: A) lake regions (blue triangles – central, red inverse triangles – northern, green squares – Green Bay, magenta diamonds – southern Lake Michigan) and B) by depth zones (green squares – 0-30 m, red diamonds – >30-50 m, blue triangles – >50-90 m, dark blue inverse triangles – >90 m). The largest differences were found among the shallow (0-30 m) and deeper lake zones, while communities were not well separated by lake region.

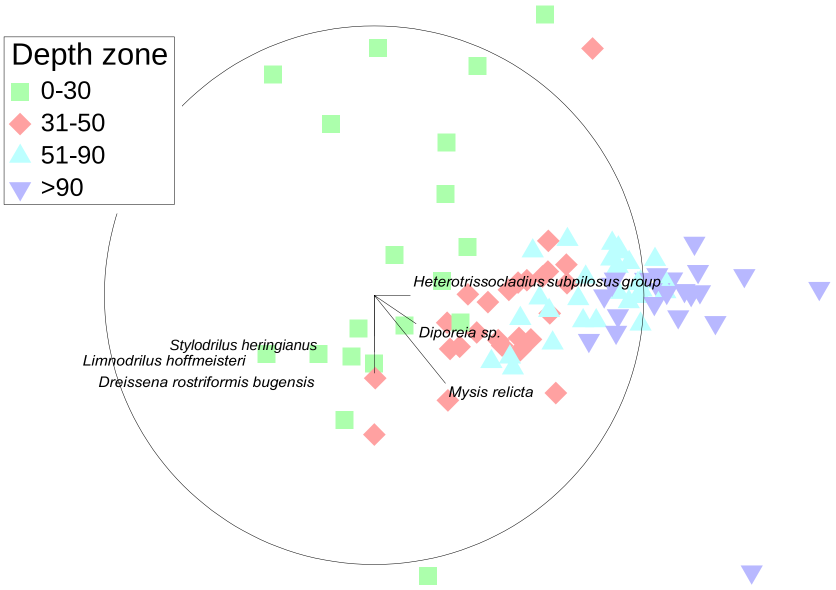

Figure 1.3. Non-parametric multidimentional (NMDS) ordination plots of Lake Michigan benthic community structure in 2021 (Stress = 0.16). Stations are indicated by depth zones (green squares – 0-30 m, red diamonds – >30-50 m, blue triangles – >50-90 m, dark blue inverse triangles – >90 m). Species that have the largest correlations with NMDS 1 and 2 and responsible for the differences among the depth zones are indicated.

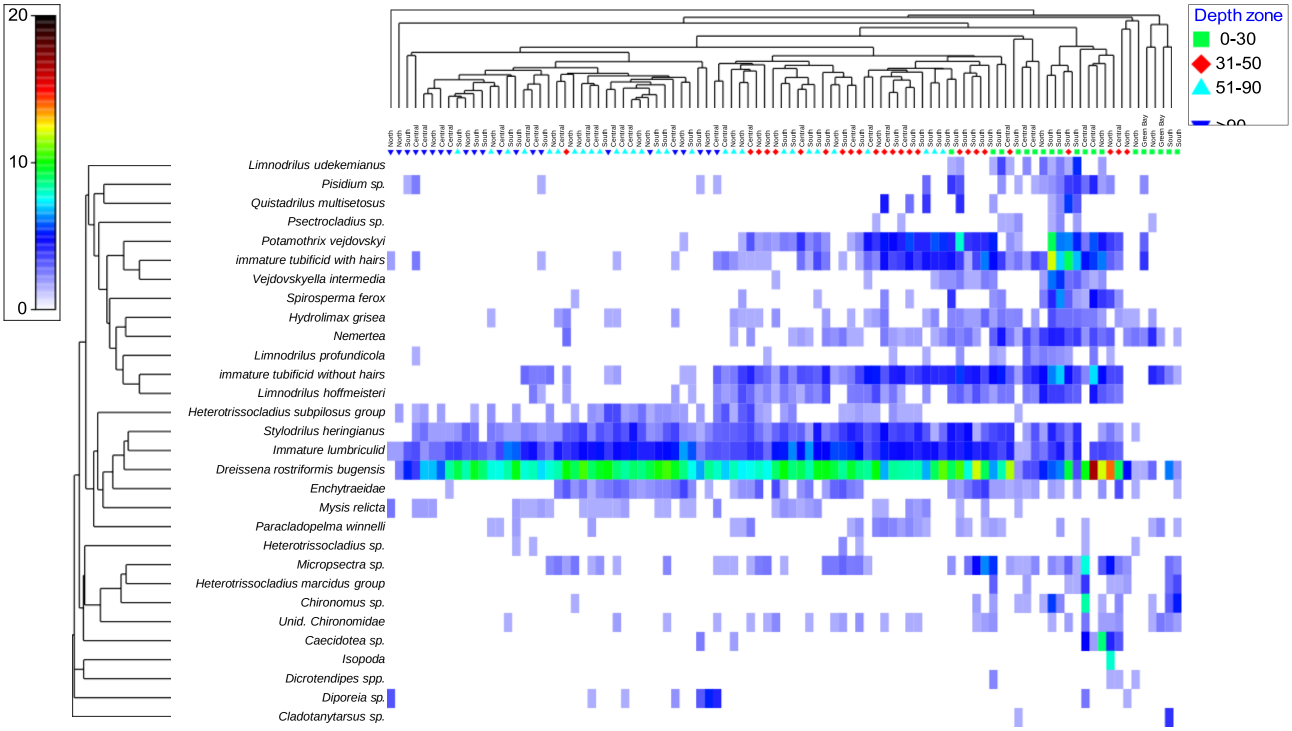

Figure 1.4. Shade plot grouping of benthic species and Lake Michigan stations where they were collected in 2021. Color intensity increases with species density; station and species clustering categories are indicated in the legends. The Y axis is ordered in line with a cluster analysis of the species (using Whittaker's Index of Association). Only 30 most abundant species were used in the analysis. Note the *Dreissena*-associated cluster of species at deep stations.

Table 1.1. Average (± standard error) density (ind. m^{-2}) and wet biomass (g m^{-2}) of major taxonomic groups of benthic invertebrates collected from 95 benthic stations in Lake Michigan in 2021 and averaged by depth zones, and lake-wide average (not stratified by depth). n.r. – not recorded. Number of stations given in parentheses. Average densities and biomass of *Diporeia* and *Dreissena* are provided separately for the benthic survey (95 stations), and for all sampled stations (e.g., combined 95 benthic stations and additional 19 "*Dreissena* and *Diporeia* only" stations, total 114 stations*).

Taxa	0 – 30 m (19)	>30 – 50 m (25)	>50 – 90 m (29)	>90 m (22)	Lake-wide (95)
Amphipoda** (ind. m^{-2})	1.3±0.8	0.26±0.26	0.22±0.22	n.r.	0.40±0.19
(g m^{-2})	<0.001	<0.001	<0.01	n.r.	<0.001
Chironomidae (ind. m^{-2})	750±523	221±71	40±9	17±7	224±108
(g m^{-2})	0.34±0.26	0.12±0.03	0.04±0.01	0.02±0.01	0.11±0.05
Diporeia (95 stations)					
(ind. m^{-2})	2.7±2.7	0.3±0.3	0.4±0.3	59.1±35.9	14.4±8.5
(g m^{-2})	0.004±0.004	0.001±0.001	0.003±0.003	0.054±0.027	0.014±0.007
Diporeia (114 stations)					
(ind. m^{-2})	2.3±2.3	0.2±0.2	1.5±1.2	59.1±35.9	12.4±7.2
(g m^{-2})	0.003±0.003	0.001±0.001	0.008±0.006	0.054±0.027	0.014±0.006

Taxa		0 – 30 m (19)	>30 – 50 m (25)	>50 – 90 m (29)	>90 m (22)	Lake-wide (95)
Dreissena (95 stations)						
	(ind. m^{-2})	6581±4075	8199±1510	6329±559	4181±648	6374±927
	(g m^{-2})	447±282	1432±199	1257±78	538±108	975±94
Dreissena (114 stations)						
	(ind. m^{-2})	6587±3544	7650±1212	6676±471	4181±648	6451±785
	(g m^{-2})	430±243	1380±162	1256±69	538±108	993±81
Sphaeriidae	(ind. m^{-2})	54±23	14±9	2±2	3±2	16±6
	(g m^{-2})	0.1±0.4	0.01±0.04	0.03+0.03	0.004±0.003	0.03±0.01
Gastropoda	(ind. m^{-2})	377±298	31±13	2±1	n.r.	84±60
	(g m^{-2})	1.5±1.2	0.4±0.2	<0.01	n.r.	0.4±0.2
Mysis	(ind. m^{-2})	0.3±0.3	3.1±1.0	5.5±1.3	7.5±2.7	4.3±0.8
	(g m^{-2})	0.001±0.001	0.05+0.02	0.05±0.01	0.10±0.05	0.05±0.01
All Oligochaeta	(ind. m^{-2})	3903±1828	1964±450	955±117	351±100	1670±400
	(g m^{-2})	2.44±0.70	2.93±0.43	1.91±0.26	0.79±0.22	2.03±0.22
-Lumbriculidae	(ind. m^{-2})	212±62	577±73	653±81	318±92	467±43
	(g m^{-2})	0.52±0.17	1.46±0.25	1.26±0.18	0.57±0.16	1.01±0.11
-Naididae	(ind. m^{-2})	392±148	78±24	11±4	n.r.	102±33
	(g m^{-2})	0.04±0.02	0.008±0.002	0.002±0.001	n.r.	0.011±0.004
-Tubificidae	(ind. m^{-2})	3292±1676	1265±448	273±99	19±9	1079±371
	(g m^{-2})	1.24±0.37	0.59±0.19	0.15±0.05	0.03±0.02	0.46±0.10
All benthos	(ind. m^{-2})	12186±4998	10654±1759	7340±587	4621±705	8552±1142
	(g m^{-2})	452±283	1436±199	1259±78	539±108	978±94
All benthos w/o *Dreissena*	(ind. m^{-2})	5604±2027	2455±506	1011±117	440±103	2177±462
	(g m^{-2})	4.73±1.60	3.53±0.48	2.04±0.27	0.97±0.22	2.75±0.38

*The distribution of all 114 stations by depth zones (together with the 19 *Dreissena* and *Diporeia*-only stations) was: 0 – 30 m (22 stations); >30 – 50 m (32); >50 – 90 m (38); and >90 m (22), total 114 stations.

**other than *Diporeia.*

Long-term trends in benthos

Since 2021 was only the second (after 2015) survey when the entire benthic community was examined, lake-wide long-term trends in taxa other than *Diporeia,* Oligochaeta and Sphaeriidae could not be assessed. 2021 survey data show that the amphipod *Diporeia* continued to decline (Table 1.2, Fig. 1.5). In 2015, *Diporeia* was collected at only one station that was < 90 m, and at 9 stations that were >90 m. In comparison, in 2021 *Diporeia* was collected at 5 stations <90 m (including one shallow station in northern region at 24 m depth, and another one in Green Bay at 44 m depth), and at 5 stations >90 m. While at depths <90 m *Diporeia* densities were extremely low and did not change, in the deepest zone (>90) we found an almost 9-fold decline compared to 2015 (Table 1.2) along with the total bottom area occupied by *Diporeia* (Fig. 1.5).

Diporeia was historically the most abundant benthic macroinvertebrate in the lake contributing >65% to the total benthic density in the 1930s at depths <50 m (Eggleton, 1937). *Diporeia*, Oligochaeta, and Sphaeriidae experienced an increase in abundance in nearshore waters (<50 m) during 1964–1980 (Table

1.2), when P loading was presumably increasing, and declined in the nearshore in the next decade when P loading was decreasing (Mehler et al., 2020). The drastic decrease in *Diporeia* abundance in the late 1980s and in the 2010s has been attributed to the decline in primary production and indirect impacts of the dreissenid mussel invasions (Madenjian et al., 2015; Nalepa et al., 1998; Mehler et al., 2020). Our study indicated that this decline in *Diporeia* is ongoing even in the deepest part of the lake.

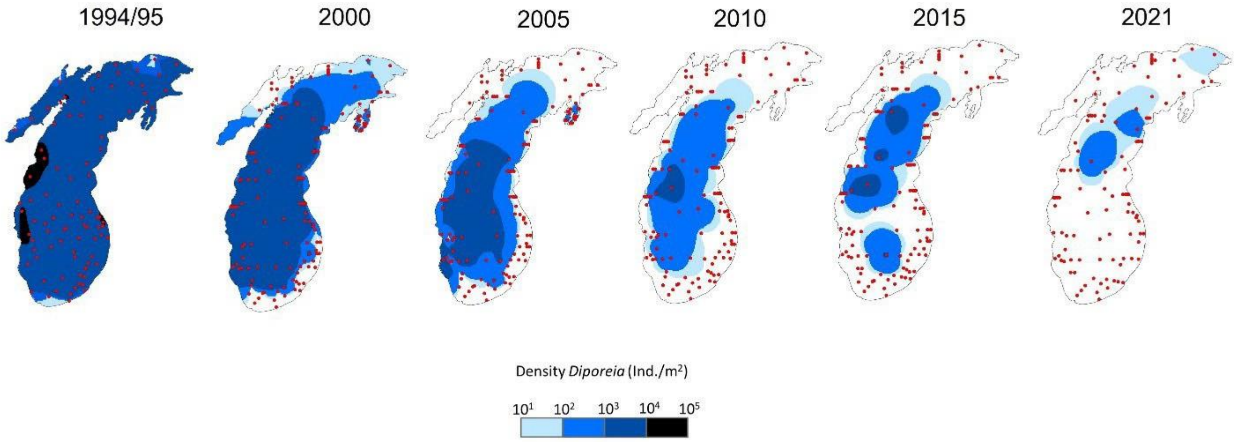

Figure 1.5. Spatial distribution of *Diporeia* sp. in Lake Michigan from 1994 to 2021, expressed as density (ind.m^{-2}). Red dots indicate sampling stations.

Similar continuous decline was found in densities of sphaeriids that were lower at all depth intervals in 2015 and 2021 compared to the 1960s (Table 1.2). A decline in sphaeriids at all depths was first observed soon after *Dreissena* became established in the southern basin (Nalepa et al., 1998), likely due to competition with *Dreissena* for available food.

Oligochaeta abundance somewhat increased in the last decade indicating that dreissenids may have positive effects on Oligochaeta abundance (Mehler et al., 2020; Bayba et al., 2022; Table 1.2). *Dreissena* filters particulate material (mainly phytoplankton) from the water column and subsequently deposits this organic material in the benthic zone in the form of feces and pseudofeces. This fresh organic material is quickly utilized by bacteria (Lohner et al., 2007), and both serve as an added food source for benthic detritivores (MacLellan-Hurd, 2020; Eifert et al., in review). Oligochaetes are detritivores and thus likely benefit from these added food inputs.

Table 1.2. Dynamics of mean (+ standard error) densities of major benthic macroinvertebrate taxa in Lake Michigan from 1930 to 2021 by depth zones. Density data for 1931/32 are from Eggleton (1937) and Mehler et al. (2020); for 1964–67 are from Alley & Mozley (1975); for 1994/95, 2000, 2005, and 2010 are from Nalepa et al. (2014); and 2015 and 2021 from Karatayev & Burlakova (2017), Nalepa et al. (2017), this report. n/d – taxa not documented.

Depth zone	Taxa/Year	1931/32	1964-67	1994/95	2000	2005	2010	2015	2021
<30m	*Diporeia*	716±218	4945±1160	3907±1005	853±315	104±88	1±1	0	2.7±2.7
	Oligochaeta	174±48	2152±927	n/d	n/d	n/d	n/d	2985±726	3903±1828
	Sphaeriidae	73±19	1357±505	n/d	n/d	n/d	n/d	76±36	54±23
>30-50 m	*Diporeia*	1387±293	7559±829	6111±1377	2116±563	24±16	<1	0	0.3±0.3
	Oligochaeta	352±139	2469±718	n/d	n/d	n/d	n/d	3568±603	1964±450
	Sphaeriidae	211±70	3022±552	n/d	n/d	n/d	n/d	5±6	14±9
>50-90 m	*Diporeia*	875±114	3976±454	6521±562	3469±464	548±131	98±49	0.2+0.2	1.9±1.5
	Oligochaeta	312±60	1181±440	n/d	n/d	n/d	n/d	1625±253	955±117
	Sphaeriidae	108±24	1015±370	n/d	n/d	n/d	n/d	2±1	2±2
>90 m	*Diporeia*	557±77	2065±331	4547±385	2804±453	1244±217	429±122	528±186	59±36
	Oligochaeta	192±46	387±81	n/d	n/d	n/d	n/d	558±96	351±100
	Sphaeriidae	16±5	124±39	n/d	n/d	n/d	n/d	18±4	3±2

Dreissena spatial and temporal trends

Long-term dynamics in zebra and especially quagga mussels in Lake Michigan are well documented (Karatayev et al., 2021a; Mehler et al., 2020; Nalepa et al., 2017, 2020). Below is a brief analysis of changes in *Dreissena* spp. population in 2021 compared to the previous years. For consistency with long-term data, for this analysis we excluded Green Bay data and used ash free dry tissue weight (AFDTW, calculated from total wet weight (TWW) using Nalepa et al. (2018) relationship gAFDTW = 0.01996*gTWW).

Previous studies in Lake Michigan have shown that dreissenids reached their population maximum in the shallow (0-30 m) to mid (>30-50 m and >50-90 m) depth zones by 2010, 13 years after the first detection in the lake in 1997, and then declined (Fig. 1.6, 1.7; Karatayev et al., 2021a; Mehler et al., 2020; Nalepa et al., 2017, 2020). Such a decline may be expected if quagga mussels in shallow to mid-depth zones had increased to densities greater than their carrying capacity. Similar declines in dreissenid densities in the nearshore zone, along with a shift of the maximum density to deeper areas, were also observed in lakes Huron and Ontario (Karatayev et al., 2020, 2021a, 2021b, 2022). In the deepest zone (>90 m) mussel population was always growing. The increases in mussel density at depths >90 m have a strong influence on lake-wide values because by area, 43.5% of the lake bottom is >90 m deep.

Data from our previous survey conducted in 2015 demonstrated that the lake-wide population of dreissenids declined for the first time since their invasion (Fig. 1.7, Table 1.3). This decline potentially indicated that the lake-wide population of quagga mussels in Lake Michigan might have reached its carrying capacity, and further decline could be expected in 2021. In contrast to our predictions, lake-wide quagga mussel population in 2021 exceeded 2015 density by 30%. This increase, however, was not significant lake-wide due to a large variation in mussel densities across depth zones (P = 0.372, Kruskal-Wallis test).

Even more unexpected was an over 3-fold increase in mussel density in the shallowest depth zone, caused mostly by large densities of small (<5 mm) recently settled mussels comprising 87% of all dreissenids in this zone. This increase, however, was again not significant due to large variability in densities at these shallow depths (P = 0.66, Fig. 1.7). As survival of small mussels over winter is low, further observations are needed to evaluate whether this increase will transform into an increase in densities in this shallowest zone long-term. As expected, there was a further increase (by 60%) in quagga mussel density in the deepest zone (>90 m), and this increase was significant (P = 0.031, multiple comparisons after Kruskal-Wallis test). Changes in quagga mussel biomass in 2021 compared to 2015 were smaller than in density and a significant increase was found at the >90 m zone only (P = 0.041). The lake-wide (excluding Green Bay) AFDTW biomass did not changed significantly (P = 0.61). Overall, recent data suggest that during the last 10 years (since 2010) lake-wide population density of quagga mussel in Lake Michigan has stabilized, although there is an ongoing change in the spatial distribution with the bulk of mussel populations expanding to deep depths (Fig. 1.6, 1.7). Similar patterns were recorded in other deep Great Lakes (Karatayev et al., 2020, 2021a, 2021b, 2022; Karatayev & Burlakova, 2022).

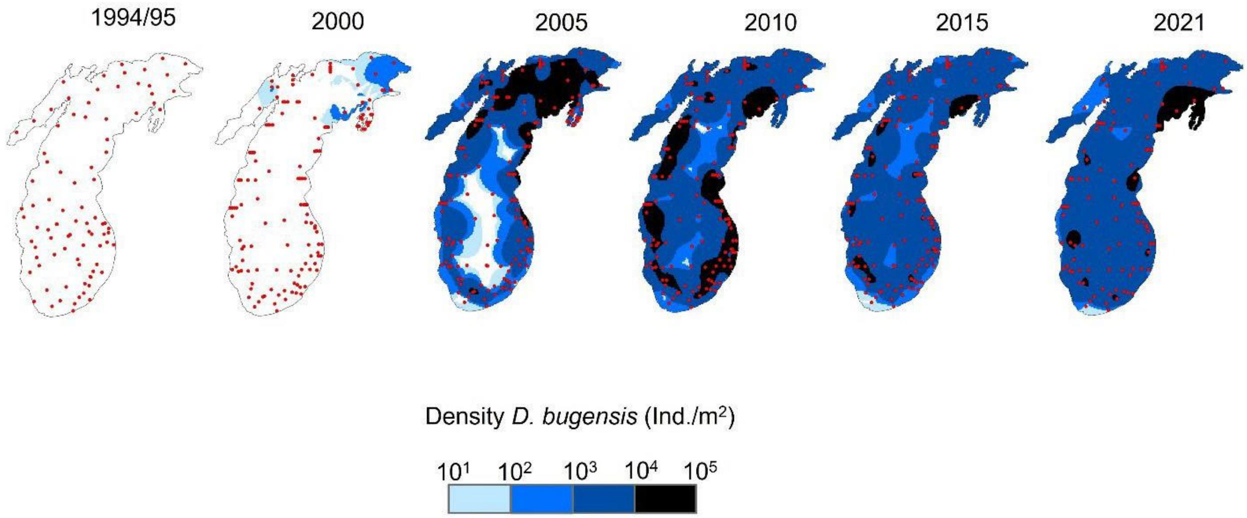

Figure 1.6. Spatial distribution of *Dreissena rostriformis bugensis* in Lake Michigan from 1994 to 2021, expressed as density (ind.m^{-2}). Red dots indicate sampling stations.

Table 1.3. Long-term dynamics of *Dreissena polymorpha* and *D. rostriformis bugensis* density (m^{-2}) in Lake Michigan (excluding Green Bay). Average ± standard errors. Here lake-wide densities were calculated as weighted averages from four depth zones. Sample size given in parenthesis.

Depth / Species	1994 (84)	2000 (129)	2005 (145)	2010 (150)	2015 (149)	2021 (111)
0-30 m						
D. polymorpha	730±510	1827±467	261±90	0	0	0
D. r. bugensis	0	37±23	6412±1418	9443±1594	2405±710	7175±3382
Both species	730±510	1864±470	6673±1456	9443±1594	2405±710	7175±3382
>30-50 m						
D. polymorpha	231±219	1316±570	385±98	0.5±0.5	0	0
D. r. bugensis	0	25±17	16213±2583	13572±1424	6105±633	7876±1230
Both species	231±219	1340±585	16598±2601	13573±1423	6105±633	7876±1230
>50-90 m						
D. polymorpha	0.2±0.2	16±8	34±27	0	0	0
D. r. bugensis	0	0	6382±1559	14555±1220	8977±745	6676±471
Both species	0.2±0.2	16±8	6416±1573	14555±1220	8977±745	6676±471
>90 m						
D. polymorpha	0	0	0	0	0	0
D. r. bugensis	0	0	749±740	2346±890	2598±718	4181±648
Both species	0	0	749±740	2346±890	2598±718	4181±648
Lake-wide						
D. polymorpha	188±116	550±120	107±24	0	0	0
D. r. bugensis	0	11±6	4958±643	7991±619	4428±398	5826±933
Both species	188±116	561±122	5065±649	7991±619	4428±398	5826±933

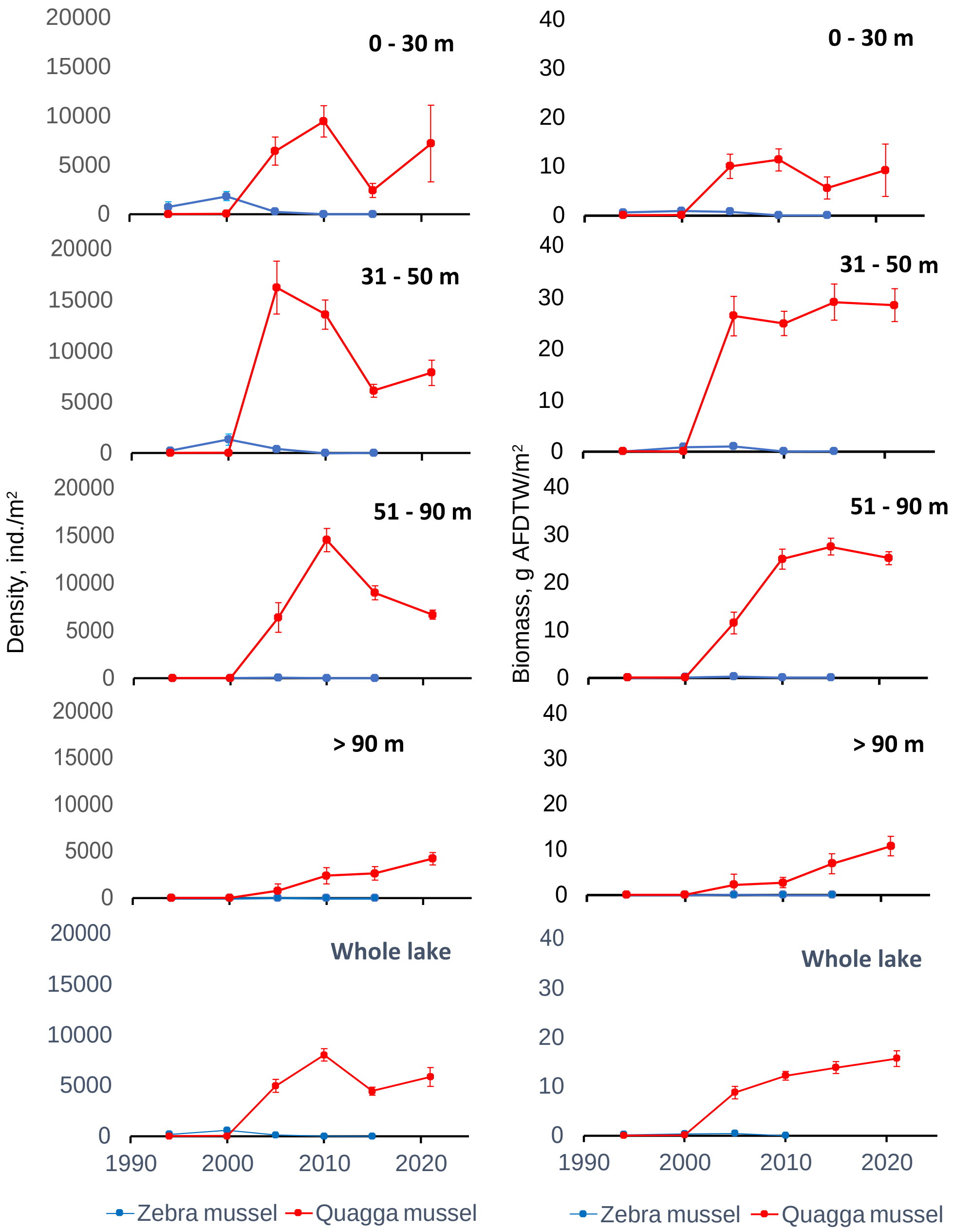

Figure 1.7. Population dynamics of quagga mussels (densities, m^{-2} and biomass, re-calculated as g of ash free dry tissue weight per m^{-2}) at different depth zones in the main basin of Lake Michigan (excluding Green Bay, Thunder Bay, and Muskegon Bay). Vertical lines denote standard error of mean. Whole lake densities and biomass are represented by means stratified by depth zones.

Literature Cited

Alley, W. P., & Mozley, S. C. (1975). Seasonal abundance and spatial distribution of Lake Michigan macrobenthos, 1964-67. Great Lakes Research Division Special Report. No 54, University of Michigan, Ann Arbor, Michigan.

Bayba, S., Burlakova, L. E., Karatayev, A. Y., & Warren II, R. J. (2022). Non-native *Dreissena* associated with increased native benthic community abundance with greater lake depth. *Journal of Great Lakes Research*, 48 (3): 734-745.

Benson, A. J., Kipp, R. M. Larson, J., & Fusaro, A. (2022) *Potamopyrgus antipodarum* (J.E. Gray, 1853): U.S. Geological Survey, Nonindigenous Aquatic Species Database, Gainesville, FL, and NOAA Great Lakes Aquatic Nonindigenous Species Information System, Ann Arbor, MI, https://nas.er.usgs.gov/queries/greatlakes/FactSheet.aspx?Species_ID=1008&Potential=N&Type=0 Revision Date: 11/1/2022, Access Date: 12/8/2022

Cuhel, R. L., & Aguilar, C. (2013). Ecosystem transformations of the Laurentian Great Lake Michigan by nonindigenous biological invaders. *Annual Review of Marine Science,* 5, 289-320.

Damann, K. E. (1960). Plankton studies of Lake Michigan. II. Thirty-three years of continuous plankton and coliform bacteria data collected from Lake Michigan at Chicago Illinois. *Trans. Am. Micros. Soc.*, 79, 397-404.

Eggleton, F. E. (1937). Productivity of the profundal benthic zone in Lake Michigan. *Papers Mich. Acad. Sci.,* 22, 593–611.

Eifert, R.-A., Burlakova, L. E., Karatayev, A. Y., Daniel, S. E., Scofield, A. E., & Hinchey, E. K. (In review). Could quagga mussels impact offshore benthic community and surface sediment-bound nutrients in the Laurentian Great Lakes? *Hydrobiologia*.

Griffiths, R. W., Schloesser, D. W., Leach, J. H., & Kovalak W. P. (1991). Distribution and dispersal of the zebra mussel (Dreissena polymorpha) in the Great Lakes region. *Can. J. Fish. Aquat. Sci.,* 48, 1381-1388.

Johengen, T. H., Johannsson, O. F., Laird Pernie, G., & Millard, E. S. (1994). Temporal and Seasonal Trends in Nutrient Dynamics and Biomass Measures in Lakes Michigan and Ontario in Response to Phosphorus Control. *Can. J. Fish. Aquat. Sci.*, 51, 2570-2578.

Karatayev, A. Y., & Burlakova, L. E. (2017). Lake Erie and Lake Michigan Benthos: Cooperative Science and Monitoring Initiative. Final Report. USGS-GLRI G14AC00263. Great Lakes Center, SUNY Buffalo State, Buffalo, NY. Available at: http://greatlakescenter.buffalostate.edu/sites/greatlakescenter.buffalostate.edu/files/uploads/Documents/Publications/LakeErieandMichiganBenthos_CSMI2014-2015_FinalReport.pdf

Karatayev, A. Y., & Burlakova, L. E. (2022). *Dreissena* in the Great Lakes: What have we learned in 30 years of invasion. *Hydrobiologia,* first on-line https://doi.org/10.1007/s10750-022-04990-x

Karatayev, A. Y., Burlakova, L. E., Mehler, K., Daniel, S. E., Elgin, A. K., & Nalepa, T. F. (2020). Lake Huron Benthos Survey Cooperative Science and Monitoring Initiative 2017. Technical Report. USEPA-GLRI GL00E02254. Great Lakes Center, SUNY Buffalo State, Buffalo, New York, USA: 59 pp. Available at: http://greatlakescenter.bufalostate.edu/sites/greatlakescenter.bufalostate.edu/files/uploads/Documents/Publications/LakeHuronBentho SurveyCSMI2017FinalReport.pdf

Karatayev, A. Y., Karatayev, V. A., Burlakova, L. E., Mehler, K. Rowe, M. D. Elgin A. K.& Nalepa, T. F. (2021a). Lake morphometry determines *Dreissena* invasion dynamics. Biological Invasions 23: 2489–2514.

Karatayev, A. Y., Burlakova, L. E., Mehler, K., Daniel, S. E., & Hrycik, A. R. (2021b). Lake Ontario Benthos Survey Cooperative Science and Monitoring Initiative 2018. Technical Report. USEPA-GLRI GL00E02254. Great Lakes Center, SUNY Buffalo State, Buffalo, NY. Available at:

https://greatlakescenter.buffalostate.edu/sites/greatlakescenter.buffalostate.edu/files/uploads/Documents/Publications/LakeOntarioBenthosSurveyCSMI2018FinalReport.pdf

Karatayev, A. Y., Burlakova, L. E., Mehler, K., Rudstam, L. G., Watkins, J. M., & Wick, M. (2022). *Dreissena* in Lake Ontario 30 years post-invasion. *Journal of Great Lakes Research*, 48, 264–273.

Lohner, R. N., Sigler, V., Mayer C. M., & Balogh, C. (2007). A comparison of the benthic bacterial communities within and surrounding *Dreissena* clusters in lakes. *Microb. Ecol.* 54(3), 469–477.

MacLellan-Hurd, R. (2020). Quagga mussel induced phosphorus cycling changes in Lake Michigan (MS). University of Wisconsin Milwaukee School of Freshwater Sciences, Milwaukee, Wisconsin, United States of America.

Madenjian, C. P., Fahnenstiel, G. L., Johengen, T. H., Nalepa, T. F., Vanderploeg, H. A., Fleischer, G. W., Schneeberger, P. J., Benjamin, D. M., Smith, E. B., Bence, J. R., Rutherford, E. S., Lavis, D. S., Robertson, D. M., Jude, D. J., & Ebener, M. P. (2002). Dynamics of the Lake Michigan food web, 1970-2000. *Can. J. Fish. Aquat. Sci.*, 59, 736-753.

Madenjian, C. P., Bunnell, D. B., Warner, D. M., Pothoven, S. A., Fahnenstiel, G. L., Nalepa, T. F., Vanderploeg, H. A., Tsehaye, I., Claramunt, R. M., & Clark, R. D., Jr. (2015). Changes in the Lake Michigan food web following dreissenid mussel invasions: A synthesis. *J Great Lakes Res.,* 41, Supplement 3, 217-231.

Mehler, K., Burlakova, L. E., Karatayev, A. Y., Elgin, A. K., Nalepa, T. F., Madenjian, C. P., & Hinchey, E. (2020). Long-term trends of Lake Michigan benthos with emphasis on the southern basin. *J. Great Lakes Res.,* 46, 528-537.

Nalepa, T. F. (1987). Long term changes in the macrobenthos of southern Lake Michigan. *Can. J. Fish. Aquat. Sci.,* 44, 515-524.

Nalepa, T. F., Hartson, D. J., Fanslow, D. L., Lang, G. A., & Lozano, S. J. (1998). Declines in benthic macroinvertebrate populations in southern Lake Michigan, 1980-1993. *Can. J. Fish. Aquat. Sci.,* 55, 2402-2413.

Nalepa T. F., Schloesser D. W., Pothoven S. A., Hondorp, D. W., Fanslow D. L., Tuchman, M. L., & Fleischer, G. W. (2001). First finding of the amphipod *Echinogammarus ischnus* and the mussel *Dreissena bugensis* in Lake Michigan*. J. Great. Lakes Res.,* 27, 384-391.

Nalepa, T. F., Fanslow, D. L., & Lang, G. A. (2009). Transformation of the offshore benthic community in Lake Michigan: recent shift from the native amphipod *Diporeia* spp. to the invasive mussel *Dreissena rostriformis bugensis*. *Freshw. Biol.,* 54, 466-479.

Nalepa, T. F., Fanslow, D. L., Lang, G. A., Mabrey, K., & Rowe, M. (2014). Lake-wide benthic surveys in Lake Michigan in 1994-95, 2000, 2005, and 2010: abundances of the amphipod *Diporeia* spp. and abundances and biomass of the mussels *Dreissena polymorpha* and *Dreissena rostriformis bugensis*. NOAA Technical Memorandum GLERL-164. NOAA, Great Lakes Environmental Research Laboratory, Ann Arbor, MI.

Nalepa, T. F., Burlakova, L. E., Elgin, A. K., Karatayev, A. Y., Lang, G. A., & Mehler, K. (2017). Major Findings from the CSMI Benthic Macroinvertebrate Survey in Lake Michigan in 2015 with an Emphasis on Temporal Trends. Chapter 3. In: Lake Erie and Lake Michigan Benthos: Cooperative Science and Monitoring Initiative. Final Report. USGS-GLRI G14AC00263. Great Lakes Center, SUNY Buffalo State, Buffalo, NY. Available at: https://greatlakescenter.buffalostate.edu/sites/greatlakescenter.buffalostate.edu/files/uploads/Documents/Publications/LakeErieandMichiganBenthosCSMI2014-2015FinalReport.pdf

Nalepa, T. F., Burlakova, L. E., Elgin, A. K., Karatayev, A. Y., Lang, G. A., Mehler, K. (2020). NOAA Tech Memo GLERL-175. Abundance and biomass of benthic macroinvertebrates in Lake Michigan in 2015, with a summary of temporal trends. Tech. Memo, NOAA Great Lakes Environmental Research Laboratory, NOAA Great Lakes environmental Research Laboratory, Ann Arbor MI. doi:10.25923/g0d3-3v41.

US EPA (2015). SOP LG407, Standard Operating Procedure for Benthic Invertebrate Laboratory Analysis, Revision 09, April 2015. Great Lakes National Program Office, U.S. Environmental Protection Agency, Chicago, IL.

US EPA (2021). SOP LG406, Standard Operating Procedure for Benthic Invertebrate Field Sampling, Revision 14, January 2021. Great Lakes National Program Office, U.S. Environmental Protection Agency, Chicago, IL.

Ward, H. B. (1896). A biological examination of Lake Michigan in the Traverse Bay region. *Bulletin of the Michigan Fish Commission,* No. 6, 100pp.

CHAPTER 2. RAPID ASSESSMENT OF *DREISSENA* POPULATIONS IN LAKE MICHIGAN USING UNDERWATER VIDEOGRAPHY

Overview

To quantify their ecological role, timely and reliable estimates of *Dreissena* densities are extremely important, however samples obtained using conventional methods (bottom grabs or diver assessments) require a long time for processing (reviewed in Karatayev et al., 2018a). Typically, results of lake-wide *Dreissena* population assessments became available for stakeholders after the sampling event in 2 years (Nalepa et al., 2010), 3 years (Hunter & Simons, 2004; Patterson et al., 2005; Karatayev et al., 2014), or even 4 years later (Watkins et al., 2007; Karatayev et al., 2018b). Underwater videography could be a useful tool providing quicker *Dreissena* population assessment (reviewed in Karatayev et al., 2018a; 2021a). Since 2015, in support of the CSMI, the Great Lakes Center at SUNY Buffalo State began conducting lake-wide *Dreissena* population assessments in the Great Lakes, based on the estimation of mussel coverage from 100 still images randomly distributed along the 500 m video footage from a GoPro camera mounted on a benthic sled towed by the U.S. Environmental Protection Agency (US EPA) R/V *Lake Guardian* (Karatayev et al., 2018a; 2020), and ground-truthed with Ponar samples. This method greatly increases the number of replicates analyzed per station and reduces the cost and time for information processing and data reporting. However, the video method does not allow for direct counting of *Dreissena* mussels and therefore a substantial amount of time is still required for Ponar sample processing (on the order of months after the sampling event) and mussel enumeration. To overcome these shortcomings, Karatayev et al. (2021a) applied a novel sampling method in 2019 by using Benthic Imaging System (BIS, a drop frame equipped with a GoPro camera) across all three Lake Erie basins to estimate *Dreissena* populations. In this study, we used the BIS across Lake Michigan to estimate *Dreissena* populations (presence/absence, and density) in near real-time (aboard R/V *Lake Guardian* during CSMI and summer cruises). These preliminary data were later compared with dreissenid data obtained from traditional Ponar grabs to assess the advantages and disadvantages of both methods.

Methods

Video images were collected during the 2021 CSMI Lake Michigan benthos survey from July 13-22 from 98 stations and during long-term monitoring sampling from September 4-9 from 16 stations using a BIS equipped with two GoPro cameras (one down-looking and one oblique (i.e., side-looking) camera), and two underwater lights per camera attached to a custom-built stainless-steel carriage. On the base of this frame is a marked scale. The down-looking camera was fixed 56 cm above substrate, and the side-looking camera was fixed 30 cm above substrate at an angle of about 45 degrees, resulting in a horizontal distance from the lens to the substrate of 1 m. At each station, the BIS was lowered from the starboard side of R/V *Lake Guardian* down to the lake bottom (US EPA, 2015, SOP LG407). The BIS remained on the lake bottom for one minute (the first replicate, or RFS). This time duration was enough to increase the probability that a clear view of the area within the marked scale would be obtained, as any resuspended sediment was allowed to settle or clear from view. After one minute, the BIS was lifted 1 to 2 m from the bottom for 30 seconds, then lowered again to remain on the lake bottom for another minute (second replicate - FD1), lifted again for 30 seconds and then lowered to remain on the lake bottom for another minute (third replicate - FD2). All replicate BIS and Ponar grab samples were collected within the boundaries of an EPA station, with only one GPS record for each station. An EPA station is defined as a bottom area of approximately 300 m in diameter (US EPA, 2014, SOP LG100). After the frame was retrieved from the water, videos from both cameras were immediately downloaded to an external hard drive for onboard analysis. A total of 342 images from 115 stations were initially collected from the down-looking camera. At three stations, the lake bottom in all three replicates were completely covered with algae, preventing mussel counts. At four additional stations, all images were not usable due to technical problems. Of the remaining 108 stations a total of 299 usable videos were collected with at least one usable image per station. In addition, on several stations at least one replicate was excluded due to missing image (4 images, accidentally deleted), algae cover (2 images), or technical problems (15 images). Of all usable images collected, 172 were evaluated as high quality where mussels were counted with "high confidence", 43 images as medium quality ("medium confidence"), and 56 images as low quality ("low confidence"). Twenty-eight images did not have mussels.

For each replicate, we used the clearest still image (screen shot) to estimate *Dreissena* coverage and density. Occasionally, the frame sunk into the sediment; to avoid erroneous estimation of *Dreissena* size and counts we used the screen shot taken the moment the frame hit the lakebed. For density estimations all visible mussels were counted in the entire original clipped still image and the counts were converted to density (individuals/m^2) using BIS sampling area that was determined for each sample separately. For each station we averaged *Dreissena* density using all useable replicates collected at the station.

According to US EPA Standard Operation Procedure (US EPA, 2021, SOP LG410) at least 10% of randomly selected still images should be recounted by a different analyst. For this study, a *Dreissena* count error of <10% difference in density between analysis was deemed acceptable. However, a higher percentage of error was found in images with few (<30) mussels (samples 9570 RFS, 29%, and H18 FD2, 23%), or where mussels were covered with algae or mud (sample 84450 FD1, 15%). On average across all images, the difference in *Dreissena* density calculated by different analysts was 5.4%.

Results and discussion

In 2021 *Dreissena* on BIS images was found at 94% of all 107 stations sampled, with the lowest occurrences (77%) recorded in the shallowest (≤30 m) depth zone. Lake-wide occurrence obtained using BIS was only slightly lower than the percentage determined based on Ponar data (98%).

According to our rapid assessment, the average *Dreissena* densities in 2021 compared to 2015 may have declined in all depth zones except at >90 m (Table 2.1). The largest decline observed occurred in the shallowest zone, where densities decreased by a factor of 9.2, and the densities lake-wide declined by a factor of 1.4. We suggested that this decline could be due to the underestimation of small (<5 mm) mussels on video images. However, it was also possible that the *Dreissena* population in Lake Michigan continued to decline, as the average density in 2015 was 1.8-fold lower than in 2010 (Nalepa et al., 2017).

Table 2.1. *Dreissena* population density (mussels per m^{-2}, average ± standard error) in four depth zones and lake-wide averages (weighted by depth zone) estimated using Ponar grab in 2010 and 2015, and BIS in 2021.

Depth zone	Ponar density 2010	Ponar density 2015	BIS density 2021	Ratio between Ponar 2015 and BIS 2021
0-30	9443±1593	2404±710	259±103	9.2
>30-50	13573±1423	6105±633	3700±622	1.7
>50-90	14555±1220	8977±745	4969±330	1.8
>90	2346±890	2598±718	2581±596	1.0
Lake-wide	7991±751	4428±398	3310±283	1.4

However, when 2021 Ponar data became available, we found that, in contrast to our prediction, *Dreissena* lake-wide density have increased by 32% compared to Ponar estimates in 2015, and the largest increase (by a factor of 3) was found in the shallowest zone (Tables 2.1 and 2.2).

Comparison of BIS and Ponar data for 2021 revealed that mussel counting on video images underestimated lake-wide density by a factor of 2 (Table 2.2). The largest difference was found in the shallowest zone which was dominated by small (<5 mm) mussels comprising 87% of dreissenids. An additional confounding factor was the relatively poor quality of images collected in the shallowest zone, where only 4 of the total of 30 images analyzed were of a high quality, limiting the usage of BIS. The difference between BIS and Ponar estimates in lake-wide *Dreissena* densities became smaller when we excluded stations with images that resulted in counts of "low confidence" and even smaller when we used only stations with video images of a "high confidence" (99% all 107 stations used; 77% only high and medium confidence stations; 43% only high confidence stations used). This trend in estimations of *Dreissena* density along with the increase in the image quality suggests that underwater videography could be improved with the improvement of video systems.

We found that if mussels <5 mm are excluded from Ponar estimates, the densities obtained with BIS and Ponar became almost identical (Table 2.2). The only significant difference was found in the shallowest, most turbid zone. The difference in the lake-wide estimates was within 10%. The mussels of very small size (<5 mm) contribute only a small proportion of total *Dreissena* population biomass, and their ecosystem impact is also limited. The large agreement in population estimates of mussels >5 mm between BIS and Ponar confirm that underwater videography is a very useful tool in *Dreissena* rapid population assessment. The next Lake Michigan CSMI survey will provide us with an opportunity to directly compare the 2021 and 2025 BIS datasets for changes in *Dreissena* population density estimated by rapid assessment.

Table 2.2. *Dreissena r. bugensis* density (mussels per m^{-2}, average ± standard error) and sample size (in parenthesis) in four depth zones and lake-wide averages estimated using Ponar grab and BIS in Lake Michigan in 2021. Only 107 stations for which both Ponar and BIS data were available were used in the table. Bold font indicates significant differences ($P < 0.05$) in paired *t*-tests.

Depth zone	BIS density	Ponar density, all mussels	Ratio between Ponar (all mussels) and BIS	Ponar density, mussels >5mm	Ratio between Ponar (mussels >5 mm) and BIS	Proportion of mussels > 5 mm, %
0-30 (19)	259±103	7365±4086	28.4	961±376	**3.7**	13
>30-50 (28)	3700±622	7864±1353	**2.1**	4514±518	1.2	57
>50-90 (38)	4969±330	6676±471	**1.3**	4989±418	1.0	75
>90 (22)	2581±596	4181±648	**1.6**	2318±499	0.9	55
Lake-wide (107)	3310±283	6596±828	**2.0**	3600±278	1.1	55

We also found an overall strong correlation between density estimation at the station level using BIS and Ponar (Fig. 2.1). The correlation coefficient ($R^2 = 0.81$) was high considering that *Dreissena* generally has a patchy distribution, as indicated by the fact that differences among replicates within a station can reach an order of magnitude or more. This high correlation between Ponar and BIS estimates is another confirmation that underwater videography is a reliable tool for surveying mussel populations.

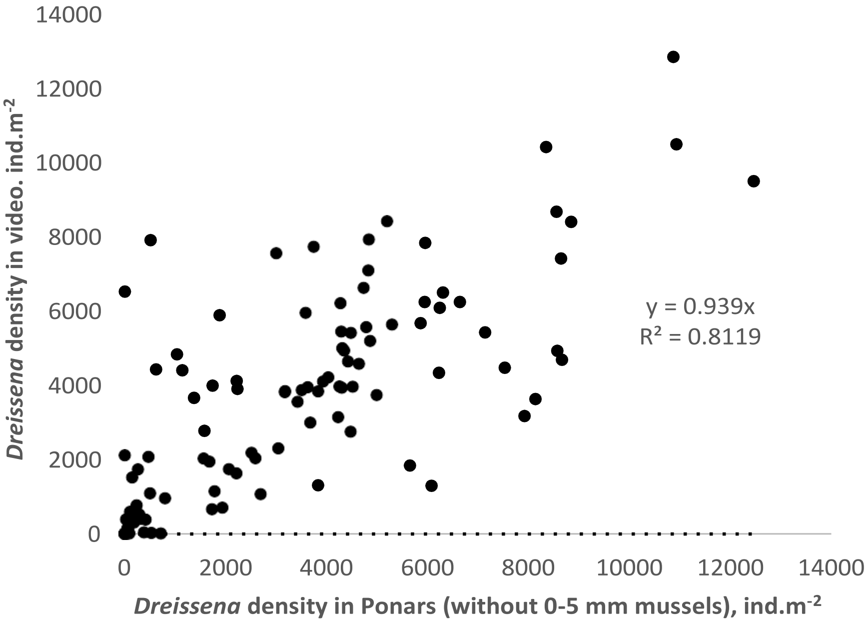

Figure 2.1. Relationship between *Dreissena* estimation using the BIS and Ponar (without mussels <5 mm) in Lake Michigan in 2021. The regression through the origin was significant ($P < 0.001$).

Acknowledgements

This study was funded by US EPA through the Great Lakes Restoration Initiative under Prime Agreement with Cornell University, Department of Natural Resources Award GL00E02254 "Great Lakes Long-Term Biological Monitoring 2017-2022" (PI Lars Rudstam) and Subaward # 82839-10916 to SUNY Buffalo State and supports the 2019 Lake Erie Cooperative Science and Monitoring Initiative. We appreciate the assistance of the captain and crew of the US EPA R/V *Lake Guardian* in sample collection**.** We thank Great Lakes Center research scientists Susan E. Daniel and Allison Hrycik, technicians Kit Hastings, Erik M. Hartnett, Brianne Tulumello and Angela Tulumello, and student technicians for help with sample processing. We are very grateful to Knut Mehler for preparing maps of *Dreissena* and *Diporeia* distribution, and to Annie Scofield, Elizabeth K. Hinchey (U.S. EPA GLNPO), and Susan Daniel for reviewing this report. We also would like to thank SUNY Buffalo State, Great Lakes Center Administrative Assistant Susan Dickinson for proofreading the report. Any views expressed in this report are those of the authors and do not necessarily represent the views or policies of the US EPA. Any use of trade, product or firm names is for descriptive purposes only and does not imply endorsement by the US EPA.

Literature Cited

Hunter, R. D., & Simons, K. A. (2004). Dreissenids in Lake St. Clair in 2001: evidence for population regulation. *Journal of Great Lakes Research*, 30, 528–537.

Karatayev, A. Y., Burlakova, L. E., Pennuto, C., Ciborowski, J., Karatayev, V. A., Juette, P., & Clapsadl, M. (2014). Twenty five years of changes in *Dreissena* spp. populations in Lake Erie. *J. Great Lakes Res.,* 40, 550–559.

Karatayev, A. Y., & Burlakova, L. E. (2017). Lake Erie and Lake Michigan Benthos: Cooperative Science and Monitoring Initiative. Final Report. USGS-GLRI G14AC00263. Great Lakes Center, SUNY Buffalo State, Buffalo, NY. Available at: http://greatlakescenter.buffalostate.edu/sites/greatlakescenter.buffalostate.edu/files/uploads/Documents/Publications/LakeErieandMichiganBenthos_CSMI2014-2015_FinalReport.pdf

Karatayev, A. Y., Burlakova, L. E., Mehler, K., Hinchey, E. K. & Warren, G. (2018a). Benthic video image analysis facilitates monitoring of Dreissena populations across spatial scales. *Journal of Great Lakes Research* 44: 629–638.

Karatayev, A. Y., Burlakova, L. E., Mehler, K., Barbiero, R. P., Hinchey, E. K., Collingsworth, P. D., Kovalenko K. E., & Warren, G. (2018b). Life after *Dreissena*: the decline of exotic suspension feeder may have significant impacts on lake ecosystems. *Journal of Great Lakes Research*, 44, 650–659.

Karatayev, A. Y., Burlakova, L. E., Mehler, K., Daniel, S. E., Elgin, A. K. & Nalepa, T. F. (2020). Lake Huron Benthos Survey Cooperative Science and Monitoring Initiative 2017. Technical Report. USEPA-GLRI GL00E02254. Great Lakes Center, SUNY Buffalo State, Buffalo, NY. Available at: https://greatlakescenter.buffalostate.edu/sites/great lakescenter.buffalostate.edu/files/uploads/Documents/ Publications/LakeHuronBenthosSurveyCSMI2017Final Report.pdf.

Karatayev, A. Y., Burlakova, L. E., Mehler, K., Hinchey, E. K., Wick, M., Bakowska, M., & Mrozinska, M. (2021a). Rapid assessment of *Dreissena* population in Lake Erie using underwater videography. *Hydrobiologia*, 848, 2421-2436.

Nalepa, T. F., Fanslow, D. L., & Pothoven, S. A. (2010). Recent changes in density, biomass, recruitment, size structure, and nutritional state of *Dreissena* populations in southern Lake Michigan. *Journal of Great Lakes Research*, 36, 5–19

Nalepa, T .F., Burlakova, L. E., Elgin, A. K., Karatayev, A. Y., Lang, G. A., & Mehler, K. (2017). Major Findings from the CSMI Benthic Macroinvertebrate Survey in Lake Michigan in 2015 with an Emphasis on Temporal Trends. Chapter 3. In: Lake Erie and Lake Michigan Benthos: Cooperative Science and Monitoring Initiative. Final Report. USGS-GLRI G14AC00263. Great Lakes Center, SUNY Buffalo State, Buffalo, NY. Available at: http://greatlakescenter.buffalostate.edu/sites/greatlakescenter.buffalostate.edu/files/uploads/Documents/Publications/LakeErieandMichiganBenthos_CSMI2014-2015_FinalReport.pdf

Patterson, M. W. R., Ciborowski, J. J. H., & Barton, D.R. (2005). The distribution and abundance of *Dreissena* species (Dreissenidae) in Lake Erie, 2002. *Journal of Great Lakes Research,* 31, 223–237. US EPA, 2015.

US EPA (2014). SOP LG100, Standard Operating Procedure for General Shipboard Scientific Operation, Revision 05, March 2014. Great Lakes National Program Office, U.S. Environmental Protection Agency, Chicago, IL.

US EPA (2015). SOP LG407, Standard Operating Procedure for Benthic Invertebrate Laboratory Analysis, Revision 09, April 2015. Great Lakes National Program Office, U.S. Environmental Protection Agency, Chicago, IL.

US EPA (2021). SOP LG410, Standard Operating Procedure for Collection and Processing of Drop-Down Camera Images for Dreissena spp. and round goby (*Neogobius melanostomus*) monitoring. Version 1, February 2021. Great Lakes National Program Office, U.S. Environmental Protection Agency, Chicago, IL.

Watkins, J. M., Dermott, R., Lozano, S. J., Mills, E. L., Rudstam, L. G., & Scharold, J. V. (2007). Evidence for remote effects of dreissenids mussels on the amphipod *Diporea*: analysis of Lake Ontario benthic surveys, 1997-2003. *Journal of Great Lakes Research,* 33: 642–657

Appendix. List of sampling stations.

Table A1. The 99 CSMI stations sampled on Lake Michigan in July 2021 and 15 long-term monitoring stations with information on lake basins, location (decimal coordinates), water depth, taxa reported, and main substrates. We used a coefficient of 19.12 to calculate density per m^2 for Ponar with a sampling area 0.0523 m^2. Taxa reported: All – all benthic taxa; D – *Dreissena* and *Diporeia* only. Samples from stations 9577 and MAN-2 (highlighted in grey) were not collected in July due to bad weather. Station 9577 was re-sampled during summer survey on September 6, 2021. Fifteen long-term monitoring stations sampled in September 2021 are listed below. In total, 342 samples from 114 stations were successfully collected from Lake Michigan in 2021.

Station	Basin	Latitude	Longitude	Depth, m	Sample type	Substrate
9552	Central	43.185	-87.2097	84.5	All	silty sand
9554	Central	43.2377	-86.8862	110	All	silt
9556	Central	43.3056	-87.7718	72	All	silty sand
9561	Central	43.4709	-86.7841	138	All	silt
9564	Central	43.6006	-87.3405	134.4	All	clay
9570	Central	43.8862	-86.9082	166	All	silt
9574	Central	44.0684	-87.1472	140	All	clay
9576	Central	44.1514	-86.6213	164.3	All	silt
9577	Central	44.2434	-87.3743	76	All	N/A
9582	Central	44.4084	-86.3684	121	All	silt and organic matter
9587	Central	44.6214	-86.3527	196	All	silt
9597	North	44.972	-86.3699	161.1	All	silt
74880	North	45.9085	-85.0249	24.9	All	sand and *Cladophora*
74900	North	45.4455	-85.2217	56	All	clay
76442	North	46.0009	-85.4095	19.6	D	silt and sand
76462	North	45.5348	-85.6359	57	All	silty sand
76471	North	45.2417	-85.5557	26.2	All	sand and shells
76482	North	45.0688	-85.8571	28.3	All	sand, silt, and shells
78030	North	45.8118	-85.7177	35	All	silt and sand
79612	North	45.9001	-86.105	20.1	All	sand
81220	North	45.7102	-86.4088	57.2	All	sand
81240	North	45.2474	-86.6692	56	All	sand
82851	North	45.05	-86.9227	81.2	All	silt, sand, and clay
82862	North	44.8576	-87.1896	12.7	All	sand
82882	Central	44.3893	-87.4226	60	D	sand
82902	Central	43.9182	-87.624	37.2	All	sand and clay
82922	Central	43.4469	-87.7961	18	All	sand and *Cladophora*

84450	Green Bay	45.603	-87.0961	9.9	All	sand
95120	North	45.5235	-86.1695	135	All	silt
A-4	South	42.0582	-87.1085	73	All	silty clay
B-2	South	42.3999	-86.4507	50	All	silt
B-3	South	42.3996	-86.5914	62.5	All	silt
B-5	South	42.375	-87.3493	105	All	silt
B-6	South	42.3755	-87.4991	82.9	All	silt
B-7	South	42.3662	-87.666	47.5	All	clay and sand
C-1	South	42.8277	-86.2481	18	All	sand
C-2	South	42.8276	-86.3027	44	All	silt
C-3	South	42.8192	-86.4735	76	All	silt
C-45	South	42.1594	-87.5033	45.8	All	sand
C-5	South	42.8165	-86.8332	135	All	clay
C-6	South	42.7946	-87.4466	97.6	All	clay, sand, gravel
C-7	South	42.7921	-87.5747	50.8	All	sand
EG-12	South	42.3477	-87.6153	54.7	All	clay and sand
EG-14	South	42.3776	-86.7737	94.1	All	silt
EG-18	South	42.2936	-86.6431	58.6	All	silt
FR-1	Central	44.8166	-86.1397	21	All	sand and shells
FR-2	Central	44.8167	-86.1558	32	D	sand
FR-3	Central	44.8168	-86.1683	45	D	sand and silt
FR-4	Central	44.8165	-86.1852	56	All	sand and silt
FR-5	Central	44.8164	-86.1967	74.5	D	clay and sand
H-11	South	42.5542	-87.597	73.3	All	sand
H-15	South	42.1587	-87.4337	58.5	D	sand
H-18	South	41.983	-86.6006	18.6	All	sand
H-19	South	42.0001	-86.6848	35	D	silt
H-20	South	42.014	-86.7527	55	All	silt
H-21	South	42.0403	-86.8834	71	D	silt
H-24	South	42.3881	-86.3344	18	All	sand
H-31	South	43.0416	-86.3326	44	All	silt and sand
H-8	South	42.3993	-87.7711	13	All	clay, silt, and sand
H-9	South	42.4457	-87.7057	39.9	All	sand, shells, clay
K-2	Central	43.3371	-86.5004	48	D	sand and silt
L-220	Central	43.5008	-86.5032	21.2	D	sand
L-230	Central	43.5007	-86.5193	34.7	D	sand
L-245	Central	43.5008	-86.5316	43	All	sand, clay, and silt
L-260	Central	43.501	-86.5552	62	All	silt and woody debris
L-280	Central	43.501	-86.6032	81.6	D	silt

M-45	South	43.1903	-86.4287	50	All	silt and sand
MAN-1	Central	44.4133	-86.2816	19.1	All	sand and shells
MAN-2	Central	44.413	-86.2853	36	D	N/A (not collected)
MAN-3	Central	44.4129	-86.3316	46.5	All	sand and clay
MAN-4	Central	44.4135	-86.3393	60.3	D	sand and clay
MAN-5	Central	44.4129	-86.3471	75.1	All	sand and clay
N-2	South	41.8917	-86.8668	37.4	All	silty clay
N-3	South	41.9665	-86.9833	60.8	All	silt
PET-2	North	45.4457	-85.0759	39.7	All	sand and clay
PW-2	Central	43.4471	-87.7819	30	All	silt
PW-3	Central	43.447	-87.7694	43	D	silt
PW-4	Central	43.4472	-87.7333	60.1	All	sand
PW-5	Central	43.4472	-87.6977	78.6	D	sand, clay, and silt
Q-13	South	42.8436	-87.7986	14.3	All	sand
Q-30	South	42.8431	-87.654	30.8	All	sand
S-2	South	41.7654	-87.3914	11.1	All	sand
S-3	South	41.8497	-87.3202	26	All	sand
S-4	South	41.9347	-87.2521	41.9	All	gravel
SB-2	North	44.8617	-87.1618	34.7	All	clay, silt, and sand
SB-3	North	44.8576	-87.1506	45	D	sand
SB-4	North	44.8571	-87.1366	60.7	D	sand
SB-5	North	44.8575	-87.0861	80.2	All	silty sand
SB-6	North	44.8575	-86.9232	157	All	clay and silt
SC-2	North	45.8412	-86.1054	31.2	D	sand
SC-3	North	45.8173	-86.1057	46	All	sand
SC-4	North	45.7899	-86.1053	65.9	D	silt
SC-5	North	45.7563	-86.1057	83	All	silt
SY-1	Central	43.9179	-87.6638	22	All	sand and shells
SY-4	Central	43.918	-87.5048	59.9	All	clay and sand
SY-5	Central	43.9184	-87.3756	79.1	All	silt
V-1	South	41.6966	-87.0133	17.8	All	sand
V-2	South	41.8165	-87.0484	29	All	sand
X-1	South	43.1376	-86.3615	36	All	silt and sand
X-2	South	43.2	-86.5171	105	All	silt and sand

Long-term monitoring stations:

Station	Basin	Latitude	Longitude	Depth, m	Sample type	Substrate
MI 11	South	42.38333	-87	128	All	silt
MI 18M	South	42.73333	-87	161	All	silt
MI 27M	Central	43.6	-86.9167	112	All	silt, sand
MI 30b	Central	43.93333	-86.5667	39	All	silt
MI 31b	Central	43.91667	-87.6167	42	All	fine silt
MI 40	North	44.76	-86.9667	160	All	silt
MI 41M	North	44.73667	-86.7217	250	All	silt
MI 42b	North	44.77056	-87.2128	49	All	sand, clay
MI 46b	South	43.10306	-86.3722	51	All	silt
MI 48b	South	42.68333	-86.3333	53	All	silt
MI 49b	Green Bay	45.49361	-87.0328	44	All	sand, silt
MI 50b	Green Bay	45.11667	-87.4167	20	All	silt
MI 51b	North	45.18333	-86.1	106	All	sand, silt, clay
MI 52b	North	45.80833	-86.0456	54	All	fine silt
MI 53b	North	45.43333	-85.2167	60	All	very fine silt

Report: Contaminants, Stable Isotopes, and Fatty Acids in the Lake Michigan Food Web

Bernard Crimmins	AEACS
Junda Ren	Clarkson University
Sujan Fernando	Clarkson University
Philip Hopke	Clarkson University
Thomas Holsen	Clarkson University

Contact:
Bernard Crimmins
Email: bernard.crimmins@aeacsllc.com
Phone: 202-368-6926

Address:
AEACS, LLC
New Kensington, PA 15068

Brief Description

The U.S. Environmental Protection Agency (EPA) Great Lakes Fish Monitoring and Surveillance Program (GLFMSP) has measured contaminants in Great Lakes top predator fish for five decades (U.S. EPA 2021a, 2021b). Lake trout (in all Great Lakes) and walleye (in western Lake Erie only) collections occur annually in each lake and top predator fish are analyzed for several different classes of contaminants including polychlorinated biphenyls (PCBs), polyfluoroalkyl substances (PFAS), polychlorinated dibenzodioxins and furans (PCDD/PCDF) and dechlorinated analogues DDD and DDE (dichlorodiphenyldichloroethane and dichlorodiphenyldichloroethylene, respectively). Figure 1 displays GLFMSP sampling sites located in each lake. Lake trout and walleye are top predator fish species in the lakes that have enriched chemical concentrations due to bioaccumulative processes in the food web. Therefore, these species serve as bioindicators of anthropogenic chemical impacts on ecosystem health.

In addition to the base monitoring component, an intensive sampling is performed on one lake each year. This intensive sampling aligns with the Cooperative Science and Monitoring Initiative (CSMI) field year schedule and provides an in-depth analysis of the contaminant flow within each lake ecosystem. The sampling sites are the same as used in the base monitoring program (2 locations per lake). The analysis includes a series of markers such as fatty acids and stable isotopes of nitrogen and carbon to develop predator-prey relationships, trophic level hierarchy, and energy source similarities, respectively. These metrics are then paired with contaminant concentration measurements to trace the relationship between contaminant concentrations and trophodynamics (Ren et al. 2021; Ren et al. 2022, 2023).

The spatial collection coverage during the 2020 CSMI field year was reduced due to the disruptions caused by the Covid-19 pandemic, which decreased the quantity of analyses that could be performed. The following report provides a summary of the limited sampling and analysis that was performed in support of the GLFMSP as part of the 2020 Lake Michigan CSMI. Results presented include stable isotopes, fatty acids, PFAS, and mercury concentrations in the forage and top predator fish from the GLFMSP Saugatuck site in Lake Michigan. Stable isotopes and fatty acids have been used as effective tools used to understand the trophic structure of aquatic systems (Kidd et al. 1995b; Hebert et al. 2006; Sierszen et al. 1996; Kidd et al. 1995a). Nitrogen ratios (^{14}N to ^{15}N) provide insight into the relative trophic position of an organism. The ^{15}N is enriched with increasing trophic levels and the relative $\delta\ ^{15}N$ (‰) value can be used to determine the feeding level within the aquatic food web. Stable isotopes of carbon ratios (^{12}C to ^{13}C) are indicative carbon sources (benthic vs. pelagic) and the $\delta\ ^{13}C$ values are a metric to catalog species utilizing similar carbon (or energy) sources; pelagic sources tend to be more negative than benthic sources (Zanden and Rasmussen 2001). These metrics provide insight into the potential sources and movement of bioaccumulative chemical contaminants in the Lake Michigan food web.

Methods

Collection. Sample collections during the 2020 CSMI year were limited due to the Covid-19 pandemic. Biological samples were only collected at one GLFMSP Base Monitoring Program (BMP) site in Lake Michigan, near Saugatuck, MI (Figure 1). The approximate depth at the sample collection site was 30m and is about 16km offshore. Samples were collected in September, 2020. Samples could not be collected at the Sturgeon Bay, WI site due to Covid-19 restrictions in place by sampling partners. Lake trout (*Salvelinus namaycush*), bloater (*Coregonus hoyi*), round goby **(***Neogobius melanostomus*), rainbow smelt (*Osmerus mordax*), alewife (*Alosa pseudoharengus*) and gizzard shad (*Dorosoma cepedianum*) were the only biological samples collected (Table 1). The US EPA's *R/V Lake Guardian* did not deploy in the summer of 2020 due to Covid-19 restrictions. No water, invertebrates, or sediments were collected at either site.

Analysis. Stable isotopes of carbon (^{12}C and ^{13}C) and nitrogen (^{14}N and ^{15}N) were determined by Environmental Isotope Laboratory, University of Waterloo (https://uwaterloo.ca/environmental-isotope-laboratory/). Specifics on the determination of PFAS and Hg concentrations in the biological media can be found in previous publications from the Clarkson University laboratory (Point et al. 2019; Zananski et al. 2011).

Results

Stable Isotopes. A summary plot of the stable isotope measurements at the Saugatuck site is provided in Figure 2. The bloater and alewife exhibited the lowest δ ^{15}N values (mean ± standard deviation) in 2020 (6.9± 0.3 ‰ and 7.0 ± 0.3 ‰, respectively). The species values increased in the following order: spottail shiner (8.4 ± 0.1 ‰), rainbow smelt (9.0 ± 0.3 ‰), round goby (9.4 ± 0.2 ‰), gizzard shad (11.0 ± 0.3 ‰), and lake trout (11.9 ± 0.3 ‰). The δ ^{13}C values increased in the following order: alewife (-28.0 ± 0.4 ‰), lake trout (-27.6 ± 0.7 ‰), rainbow smelt (-27.0 ± 0.2 ‰), gizzard shad (-26.9 ± 0.8), round goby (-25.4 ± 0.5 ‰), bloater (-24.0 ± 0.2 ‰), and spottail shiner (-23.0 ± 0.8 ‰). As mentioned above no samples were collected from the Sturgeon Bay site for comparison.

Fatty acids (FA) were also determined for prey fish and lake trout. Two feeding strategy fatty acid markers have been used to develop predator-prey relationships. At the time of this report minimal statistical analysis has been performed to develop these relationships. Figure 3 provides a summary of the concentrations of a benthic marker, cis-7-hexadecenoic acid (16:1n-7), and pelagic marker oleic acid (18:1n-9). The majority of the prey fish (gizzard shad, round goby, spottail shiner) have similar concentrations of these two FAs. However, alewife has a significantly greater abundance of oleic acid consistent with their pelagic feeding strategy. Lake trout also exhibits a significantly higher proportion of oleic acid.

Food Web PFAS. Figure 4 shows the total PFAS (t-PFAS) concentrations in the various compartments of the Lake Michigan food web. The highest concentrations were observed in the spottail shiner (60 ± 30 ng/g), followed by lake trout (51 ± 13 ng/g), bloater (50 ± 12 ng/g), alewife (44 ± 4 ng/g), and rainbow smelt (38 ± 5 ng/g). Round goby and gizzard shad concentrations were less than those of the other fish collected except for rainbow smelt, by approximately a factor of 2 (22 ± 6 ng/g and 23 ± 4 ng/g, respectively). Unfortunately, no pelagic or benthic invertebrates were collected in 2020 to assess PFAS concentrations in these lower food web organisms. Previous studies have shown an increased t-PFAS concentrations in benthic feeding fish, surpassing top predator PFAS concentrations in Lake Ontario (Ren et al. 2021; Ren et al. 2022, 2023). The prey fish and lake trout collected at the Saugatuck site in Lake Michigan exhibited similar concentrations as Lake Ontario fish, with the exception of round goby and gizzard shad which had significantly lower ($p<0.05$) PFAS concentrations than lake trout and spottail shiner.

Food Web Mercury. The mercury concentrations in the Lake Michigan food web followed a more traditional legacy contaminant bioaccumulation trend with concentrations increasing with increasing trophic levels. Lake trout had Hg concentrations ~ 10-fold higher (230 ± 52 ng/g) than each of the prey fish species collected (Figure 5). Similar to t-PFAS, spottail shiner Hg concentrations were the highest of each of the prey fish species (33 ± 0.7 ng/g) followed closely by alewife (30 ± 3 ng/g). The gizzard shad, round goby and rainbow smelt had similar Hg concentrations (18 ± 2 ng/g, 17 ± 2 ng/g and 15 ± 2 ng/g, respectively). The lowest Hg concentrations were observed in bloater (10 ± 4 ng/g).

Summary

As part of the CSMI the Great Lakes Fish Monitoring and Surveillance Program performed an intensive contaminant monitoring of the Lake Michigan food web and trophodynamic markers. Due to the Covid-19 pandemic only a limited number of fish species were collected from the Saugatuck GLFMSP site. No water, sediments, or invertebrates were obtained for the 2020 CSMI year for Lake Michigan. The forage and top predator fish have been analyzed for stable isotopes of nitrogen, carbon, fatty acids, PFAS, and Hg.

The fatty acid profiles showed that rainbow smelt, alewife and lake trout have elevated concentrations of the pelagic fatty acid marker (oleic acid) relative to cis-7-hexadecenoic acid, a benthic feeder fatty acid marker consistent with their pelagic feeding strategies. Spottail shiner had the highest PFAS concentrations followed by lake trout even though spottail shiner had significantly lower $\delta\ ^{15}$N values. The carbon source for the spottail shiner was also significantly different than for lake trout. The more positive $\delta\ ^{13}$C values for spottail shiner are consistent with a benthic energy source which exposes this species to a potential sediment repository of PFAS. The Hg bioaccumulation observed provides an example of traditional hydrophobic chemical bioaccumulation increasing with trophic level in Lake Michigan. Future analysis will include development of predator prey relationships to assess the bioaccumulation of PFAS in Lake Michigan.

References

Hebert, Craig E., Michael T. Arts, and D. V. Chip Weseloh. 2006. Ecological Tracers Can Quantify Food Web Structure and Change, *Environmental Science & Technology*, 40: 5618-23.

Kidd, K. A., D. W. Schindler, R. H. Hesslein, and D. C. Muir. 1995a. Correlation between stable nitrogen isotope ratios and concentrations of organochlorines in biota from a freshwater food web, *Sci Total Environ*, 160-161: 381-90.

Kidd, K., D. Schindler, R. Hesslein, and D. Muir. 1995b. Correlation between stable nitrogen isotope ratios and concentrations of organochlorines in biota from a freshwater food web, *The Science of the total environment*, 160-161: 381-90.

Point, Adam D., Thomas M. Holsen, Sujan Fernando, Philip K. Hopke, and Bernard S. Crimmins. 2019. Towards the development of a standardized method for extraction and analysis of PFAS in biological tissues, *Environmental Science: Water Research & Technology*, 5: 1876-86.

Ren, Junda, Adam D. Point, Sadjad Fakouri Baygi, Sujan Fernando, Philip K. Hopke, Thomas M. Holsen, and Bernard S. Crimmins. 2022. Bioaccumulation of polyfluoroalkyl substances in the Lake Huron aquatic food web, *Science of The Total Environment*, 819: 152974.

Ren, Junda, Adam D. Point, Sadjad Fakouri Baygi, Sujan Fernando, Philip K. Hopke, Thomas M. Holsen, and Bernard S. Crimmins. 2023. Bioaccumulation of perfluoroalkyl substances in the Lake Erie food web, *Environmental Pollution*, 317: 120677.

Ren, Junda, Adam Point, Sadjad Fakouri Baygi, Sujan Fernando, Philip K. Hopke, Thomas M. Holsen, Brian Lantry, Brian Weidel, and Bernard S. Crimmins. 2021. Bioaccumulation of perfluoroalkyl substances in a Lake Ontario food web, *Journal of Great Lakes Research*.

Sierszen, Michael E., Janet R. Keough, and Cynthia A. Hagley. 1996. Trophic Analysis of Ruffe (Gymnocephalus cernuus) and White Perch (Morone americana) in a Lake Superior Coastal Food Web, Using Stable Isotope Techniques, *Journal of Great Lakes Research*, 22: 436-43.

U.S. Environmental Protection Agency. 2021a. Great Lakes Fish Monitoring and Surveillance Program Technical Report: Status and Trend of Contaminants in Whole Fish through 2016. EPA 905-R-20-002.

U.S. Environmental Protection Agency. 2021b. Great Lakes Fish Monitoring and Surveillance Program Technical Report: Status and Trend of Contaminants in Whole Fish through 2017. EPA 905-R-20-002.

Zananski, Tiffany J., Thomas M. Holsen, Philip K. Hopke, and Bernard S. Crimmins. 2011. Mercury temporal trends in top predator fish of the Laurentian Great Lakes, *Ecotoxicology*, 20: 1568-76.

Zanden, M. Jake Vander, and Joseph B. Rasmussen. 2001. Variation in δ15N and δ13C trophic fractionation: Implications for aquatic food web studies, *Limnology and Oceanography*, 46: 2061-66

Figure 1. Locations of GLFMSP sampling sites in each Great Lake (U.S. EPA 2021a, 2021b)

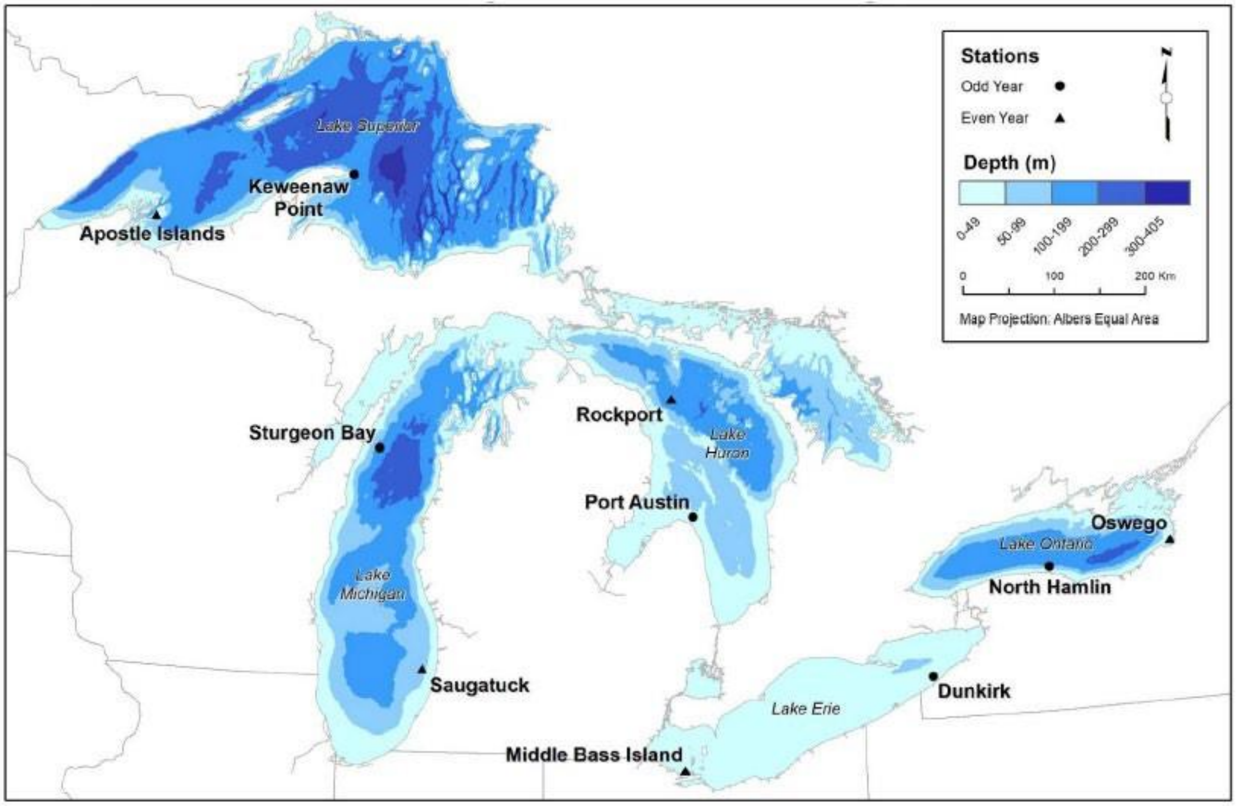

Table 1. Fish collected in September of 2020 by the GLFMSP at the Lake Michigan Saugatuck sampling site.

Species	Collection Month	Collection Method
Spottail shiner	October	Bottom Trawl
Round goby	October	Bottom Trawl
Rainbow smelt	October	Bottom Trawl
Gizzard shad	October	Bottom Trawl
Bloater	October	Bottom Trawl
Rainbow smelt	October	Bottom Trawl
Alewife	October	Bottom Trawl
Lake trout	October	Gill net

Figure 2. Stable isotope summary of nitrogen and carbon in the Lake Michigan food web measured as part of the 2020 CSMI sampling effort. This is based on one sampling site and should not be inferred to be representative of all of Lake Michigan.

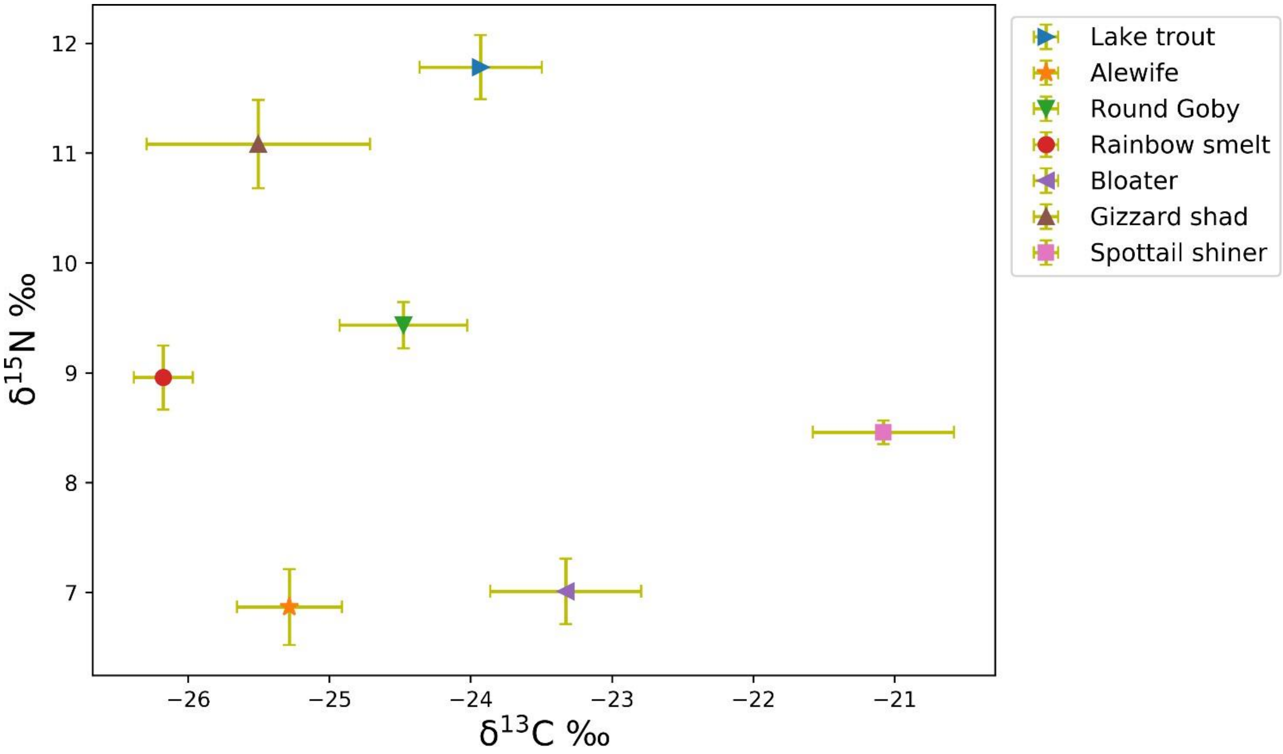

Figure 3. Summary of marker fatty acid concentrations in Lake Michigan sample types collected as part of the 2020 CSMI sampling effort. Error bars represent standard deviation among replicates. This is based on one sampling site and should not be inferred to be representative of all of Lake Michigan.

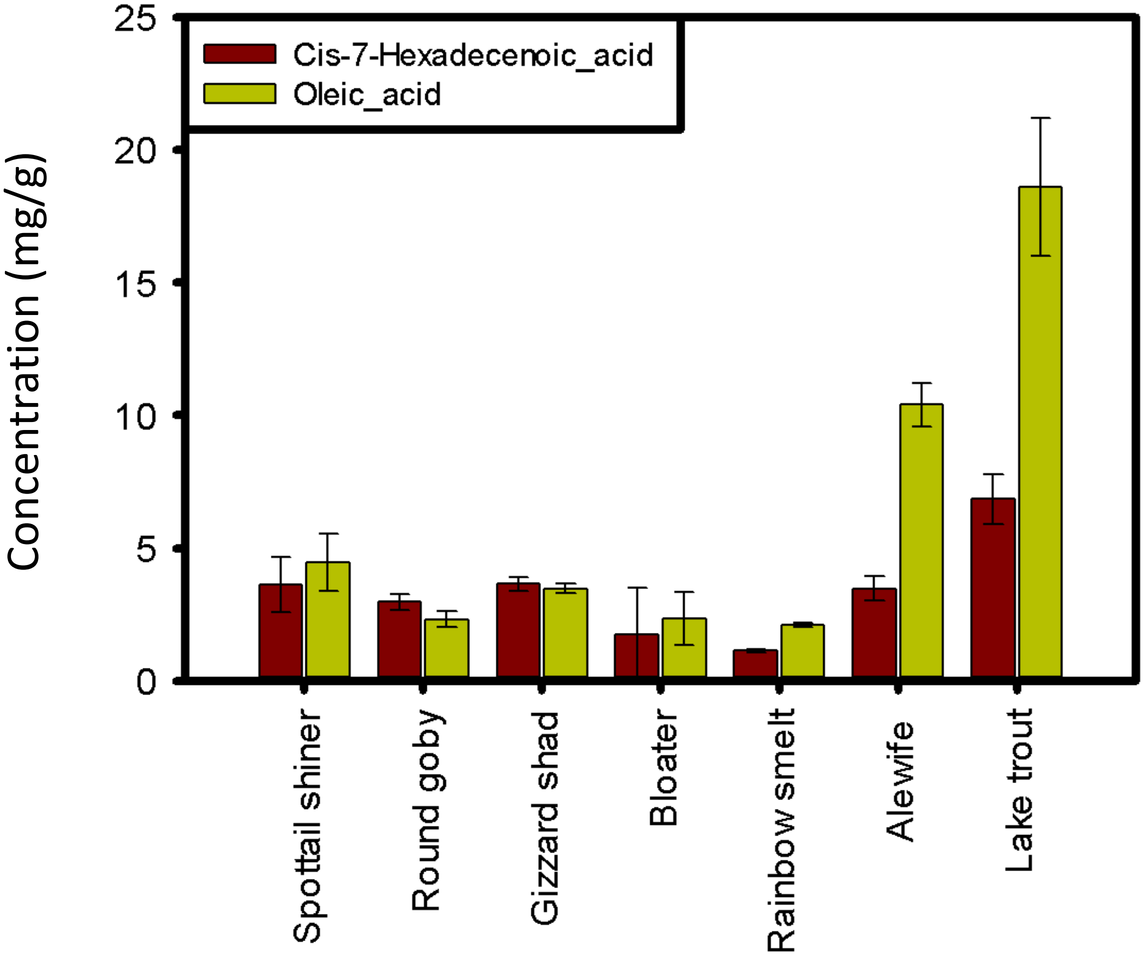

Figure 4. Summary of total PFAS concentrations in Lake Michigan sample types collected as part of the 2020 CSMI sampling effort. Error bars represent standard deviation among replicates. This is based on one sampling site and should not be inferred to be representative of all of Lake Michigan.

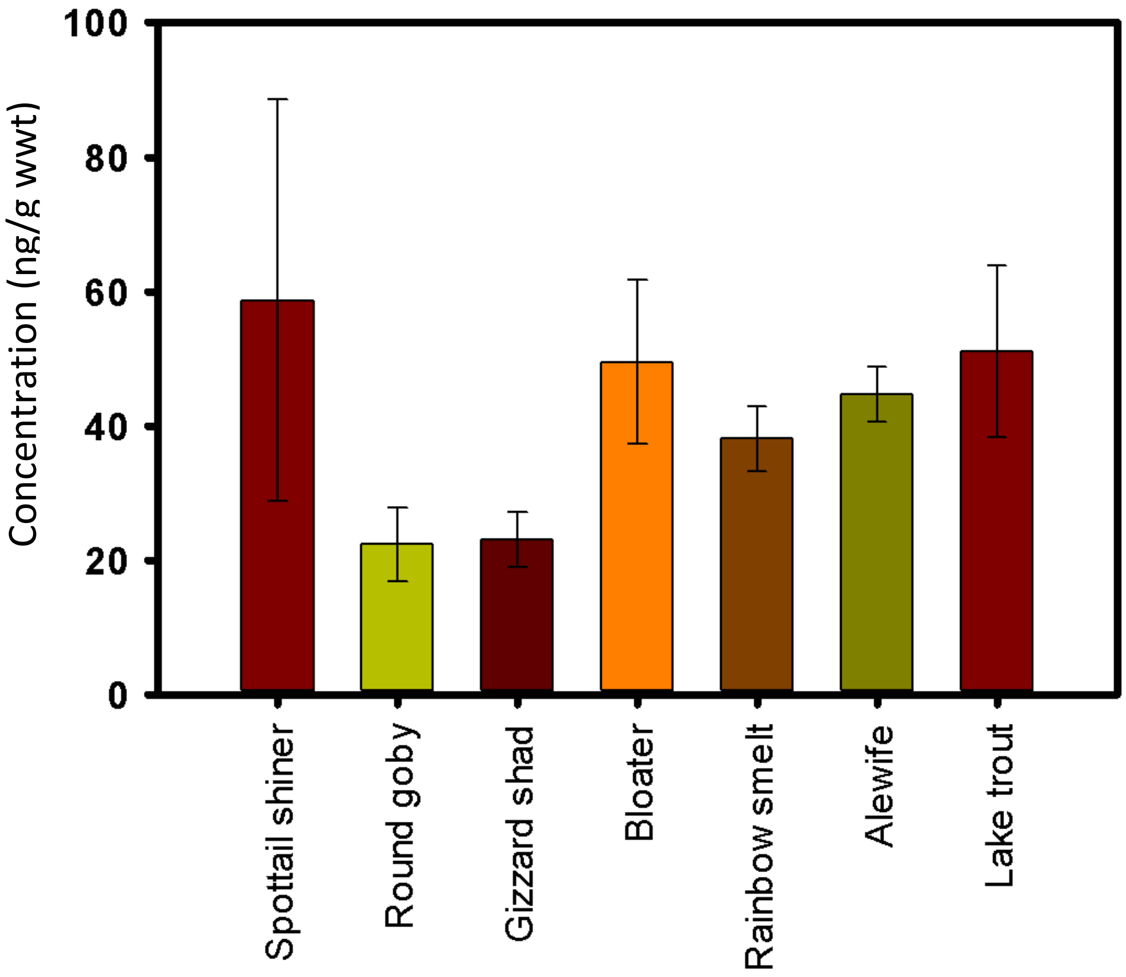

Figure 5. Summary of mercury concentrations in Lake Michigan sample types collected as part of the 2020 CSMI sampling effort. Error bars represent standard deviation among replicates. This is based on one sampling site and should not be inferred to be representative of all of Lake Michigan.